UNIVERSITY OF LONDON THESIS

Degree PhD Year 2006 Name of Author CIARAMELLA Konrad Mark

University College London

Department of Mechanical Engineering

PhD Thesis

The Potential for Matrix Conversion in Marine Electric Propulsion Systems

Konrad Mark Ciaramella

ProQuest LLC
789 East Eisenhower Parkway
P.O. Box 1346
Ann Arbor, MI 48106-1346

Statement of Originality

The accompanying thesis covers research work carried out by the author at the Department of Mechanical Engineering, University College London, between September 1999 and November 2005 and is duly submitted for consideration for the award of a PhD.

This research investigation reports on the feasibility of a future marine electric propulsion system based on the matrix converter. The matrix converter has been thoroughly examined and its performance investigated using computer and laboratory-based models. It is the author's belief that all the investigations, ideas and work in this thesis are original, unless otherwise acknowledged in the text by reference.

The author claims to have made the following contributions to the subject of marine electric propulsion and matrix converter variable speed drives:

1. A laboratory-sized model of a marine electric propulsion system employing a self built matrix converter and advanced control system driving an induction motor has been designed and constructed.

2. Custom software implementing two advanced control algorithms was designed and developed to allow safe and reliable operation of the laboratory matrix converter.

3. Computer models of the matrix converter have been designed, developed and verified to support and extend the matrix converter investigations.

4. Alternative matrix converter commutation sequences have been investigated. The effect of these strategies on the operation of the matrix converter has been considered.

5. A novel optimised switching technique, 'Opti-Soft', that maximises natural commutations in the matrix converter and equalises device commutation loss has been proposed, developed and its performance investigated.

6. The feasibility of a practical marine matrix converter drive has been investigated and considered for future ship propulsion.

Signed:

Konrad Ciaramella
UCL
11 September 2006

Abstract

The Potential for Matrix Conversion in Marine Electric Propulsion Systems

The growing interest in marine electric propulsion is driven by the need to improve ship performance. This thesis presents a review of existing marine electric propulsion technology and potential future variable speed drives. The matrix converter was found to be a promising alternative to existing technology and this thesis describes an investigation into its potential for marine electric propulsion. The matrix converter performs direct AC-AC conversion using a high switching frequency to produce high-quality converter waveforms. The investigations were carried out using a 10kVA laboratory matrix converter and a series of computer models.

The laboratory matrix converter employed IGBT bi-directional switches operated by a custom-built stand-alone control system employing various Venturini algorithms. The completed system was then used to investigate the performance of the matrix converter, examine the operational effect of different switch sequences on loss and converter input and output waveform harmonics. Computer models of the various control algorithms were developed and verified against results produced by the laboratory matrix converter and further developed for more detailed investigation.

An examination of switch commutation and the effect on loss is reported and this led to the development of a novel commutation strategy named 'Opti-Soft'. This strategy maximises 'natural' current commutation in the matrix converter and balances switching loss across devices without increasing total loss above existing switching strategies. The results from the computer models show the 'Opti-Soft' strategy to possess a similar harmonic characteristic to the conventional strategy allowing the use of existing filter designs.

The design of a conceptual marine matrix converter drive and ancillary equipment is also considered and its performance investigated. The problems of reduced supply utilisation, topology selection, cooling and protection are examined. A novel mode of operation that takes advantage of the matrix converter's unrestricted output frequency is proposed. The conclusions discuss the findings of the study and relate the practical issues that will need to be overcome before the matrix converter can be considered for marine use.

Table of Contents

List of Figures

List of Tables

List of Achievements

- September 1999 - Award of a three year scholarship and grant from the Engineering and Physical Sciences Research Council for this investigation.

- October 1999 - Award of a three year Stanley Gray Fellowship from the Institute of Marine Engineering, Science and Technology.

- December 2000 - Attended the Ship Propulsion Systems conference in Manchester in support of a presentation of research at UCL

- September 2001 - Attended the University Power Engineering Conference at Swansea University to present a paper on this research entitled 'Design, Construction & Performance Analysis of a Matrix Converter'.

- October 2001 - Attended a regional technical meeting for the IMechE and IEE held at the University of Sussex, Brighton, to give a joint presentation on 'Propelling Ships Electrically: 'Past, Present and Future'.

- February 2003 - Attended the All Electric Ship conference in Edinburgh to present a paper entitled 'Potential use of Matrix Converters in Marine Propulsion Applications'.

- April 2003 - Attended an IEE Matrix Conversion technical seminar held at the Austin Court, Birmingham.

- December 2003 - Attended the Ship Propulsion Systems conference at the Manchester conference centre.

Acknowledgements

The Author acknowledges with thanks the assistance given by the following:

- My family who have always supported me throughout University and have given me the extra motivation to succeed during difficult times.

- Dr R.W.G. Bucknall for undertaking the supervision of this project and for his invaluable help and advice throughout.

- The Engineering and Physical Sciences Research Council for their sponsorship in the form of a subsistence grant.

- The Institute of Marine Engineering, Science and Technology for their sponsorship in the form of a Stanley Gray Fellowship award.

- QinetiQ for the loan of equipment for the duration of this research study.

- I am also very grateful to Sophie Vaudolon for her immense patience and sacrifice during this research.

Nomenclature

Θ - Input to output phase transfer ratio (tan ϕ_i / tan ϕ_o)
α_1 & α_2 - Ratios of symmetric (α_1) and anti-symmetric (α_2) Venturini modulators
ω_i - Supply frequency (rads/s)
ϕ_i - Input displacement angle (radians)
ϕ_o - Load phase angle (radians)
ω_o - Output frequency (rads/s)
η_{prop} - Propulsor efficiency (%)
η_{trm} - Transmission efficiency (%)
E_{off} - IGBT Turn-off energy loss (Joules)
e_{off} - IGBT Turn-off energy loss (Joules) per unit voltage and current (J/V/I)
E_{on} - IGBT Turn-on energy loss (Joules)
e_{on} - IGBT Turn-on energy loss (Joules) per unit voltage and current (J/V/I)
E_{rec} - Diode recovery energy loss (Joules)
e_{rec} - Diode recovery energy loss per unit voltage and current (J/V/I)
F_{out} - Output frequency (Hz)
I_c - IGBT conducted current (I)
I_d - Diode conducted current (I)
I_i & I_o - Input & output currents (A)
I_L - Load Current (A)
I_{lim} - Maximum converter current (A)
$L_{\delta,r}$ - Motor rotor leakage inductance (H)
$L_{\delta,s}$ - Motor stator leakage inductance (H)
m(t) - Duty cycle
P_b - Motor brake power
P_{cond} - Instantaneous conduction loss (W)
P_e - Propulsive power (W)
q - Output amplitude (V_o/V_i)
r_{ce} - IGBT on-state resistance for the linearised characteristic (Ω)
r_d - Diode on-state resistance for the linearised characteristic (Ω)
$S_{'XY'}$ - Switch XY
SWF - Matrix converter switching frequency (Hz)
t - Time (s)
$T_{'XY'}$ - Period of conduction for switch XY (s)
T_{seq} - Matrix switching cycle = 1/SWF (s)
$v_{'n'}(t)$ - Instantaneous voltage for input phase 'n' (V)
V_{ce} - IGBT collector-emitter voltage (V)
V_{ce0} - IGBT collector-emitter voltage drop at zero current (V)
V_{co} - Initial clamp voltage (V)
V_d - Diode conducted voltage (V)
V_{env} - Measured maximum continuous supply phase voltage envelope (V)
V_{f0} - Diode forward voltage drop at zero current (V)
V_L - Load Voltage (V)
V_{max} - Maximum voltage (V)
V_o - Output voltage (RMS)
V_{pk} - Peak voltage (V)
V_r - Instantaneous target output voltage (V)
V_s - Vessel speed (m/s)

Abbreviations

AC - Alternating Current
ADC - Analogue-Digital-Converter
AFE - Active-Front-End : Pulse Width Modulated Converter
DAC - Digital-Analogue-Converter
DC - Direct Current
DOS - Disc Operating System
DSP - Digital Signal Processor
FFT - Fast Fourier Transform
GTO - Gate-Turn-Off
I/O - Input/Output
IC - Integrated Circuit
IDE - Integrated Development Environment
IGBT - Insulated Gate Bipolar Transistor
IGCT - Integrated Gate Commutated Thyristor
LCD - Liquid Crystal Display
LCI - Load Commutated Inverter
LNG - Liquefied Natural Gas
LPD - Landing Platform Dock
MBS - Monolithic Bi-directional Switch
MCU - Micro-Controller Unit
MOSFET - Metal Oxide Semiconducting Field Effect Transistor
PCA - Programmable Counter Array
PCB - Printed Circuit Board
PF - Power Factor
PP-IGBT - Press-Pack Insulating Gate Bipolar Transistor
PSB - Power System BlockSet
PWM - Pulse Width Modulation
RAM - Random Access Memory
RB-IGBT - Reverse Blocking Insulated Gate Bipolar Transistor
ROM - Read Only Memory
Ro-Ro - Roll-on-Roll-off
SCDC - Sequential Capacitive Discharge Converter
SCR - Silicon Controlled Rectifier
SOA - Safe Operating Area
SVM - Space Vector Modulator
THD - Total Harmonic Distortion
VSI - Voltage Source Inverter

Definitions

Control System - A system used to control the operating parameters of the matrix converter to meet the demanded speed and torque, e.g. in a propulsion system to meet ship speed.

Control Strategy - An algorithm that calculates the duration of conduction for each semiconductor switch in a power electric converter to achieve the desired output waveform.

Duty Cycle - Defines the ratio of the time a switch is closed to the switching period i.e. $T_{closed}/(T_{closed} + T_{open})$.

Switching/Sequencing Strategy - A strategy that defines the order in which the matrix converter input phases are connected to the output phase.

Standard Venturini - Alesina & Venturini's original control strategy for calculating the duration of conduction for each switch in a matrix converter, output voltage limited to 50% for a three-phase input, three-phase output converter.

Advanced Venturini - Alesina & Venturini's improved control strategy for calculating the duration of conduction for each switch in a matrix converter, output voltage limited to 86.6% for a three-phase input, three-phase output converter.

Hard Switch Commutation - Occurs when a single, independent, semiconductor switch is opened (or closed) with non-zero voltage or current conditions leading to commutation loss. The following example shows a simple resistive-inductive circuit with a conducting switch and the resulting device voltage and current when opened.

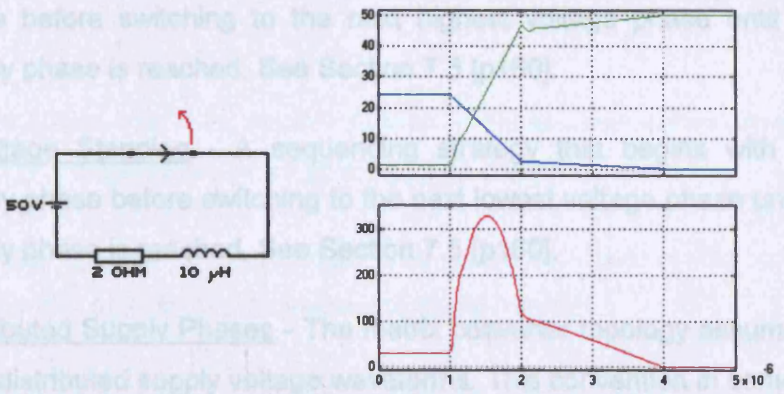

Figure 1 - Hard Switch Commutation (a) Voltage & Current Waveforms & (b) Energy Loss

Soft Switch Commutation - Occurs when a single, independent, semiconductor switch is opened (or closed) with either zero voltage or zero current conditions.

Natural Current Commutation - describes transfer of load current between two bi-directional switches in a matrix converter when the incoming switch is forward-biased. Example:

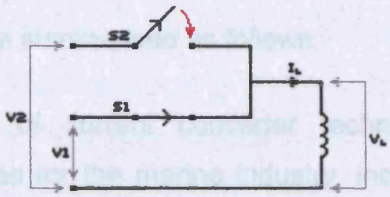

Figure 2 - Natural Current Commutation Example

With S1 closed, the load voltage $V_L \approx V1$, and the conducted current equals I_L. S2 is forward-biased and, when closed, induces a natural circulating current that drives the current conducted by S1 to zero. Once the current conducted by S2 equals I_L, S1 is reverse-biased and non-conducting and may be opened at zero current. See Section 2.4.3 [p46] and Section 7.2.1 [p151].

Forced Current Commutation - describes transfer of load current between two bi-directional switches in the matrix converter when the incoming switch is reverse-biased. Example:

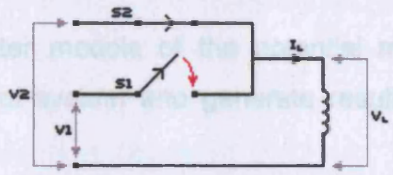

Figure 3 - Forced Current Commutation Example

The load current I_L is initially carried solely by switch S2 and the load voltage $V_L \approx V2$. S1 is reverse-biased and does not conduct when closed. The load current I_L is only commutated to S1 when S2 is opened, forcing V_L to approximately V1. See Section 2.4.3 [p46] and Section 7.2.2 [p152].

Positive Voltage Stepping - A sequencing strategy that begins with the lowest voltage supply phase before switching to the next highest voltage phase until the highest voltage supply phase is reached. See Section 7.5 [p160].

Negative Voltage Stepping - A sequencing strategy that begins with the highest voltage supply phase before switching to the next lowest voltage phase until the lowest voltage supply phase is reached. See Section 7.5 [p160].

Equally Distributed Supply Phases - The matrix converter topology assumes operation from equally distributed supply voltage waveforms. This convention in some cases may differ to those waveforms commonly generated by standard rotating machines. The required supply waveforms for multi-phase matrix converters are shown in Annex A2 [p249] including the type of electrical machine required to generate them.

Chapter One - Introduction

1.1 Aims & Objectives

The aims of the research are summarised as follows:

- To conduct a review of current converter technologies and establish the requirements of future drives for the marine industry, including existing technologies and likely future topologies.

- Use the results obtained from the converter and technology review to select a topology that most closely approaches the characteristics of the 'ideal' converter and has the potential to be the future of marine electric propulsion.

- Perform a literature review of the significant papers that investigate the selected drive to establish the state-of-the art and all issues relevant to a marine application. This will allow detailed analysis of the control, operation and physical characteristics of the selected drive, when considering marine electric propulsion.

- Create detailed computer models of the potential marine drive to gain further understanding of the control system and generate results to establish performance characteristics.

- Design and construct a scaled version of the potential marine drive for practical laboratory testing to drive a suitable motor and perform experiments under various operating conditions. This will highlight issues regarding matrix converter operation and allow verification of computer models.

- Use the laboratory converter to investigate the input and output harmonic behaviour and the influence that the converter control strategy has on these parameters.

- Investigate areas that may require further analysis when considering the design and operation of a large marine electric propulsion drive.

- Examine the causes of conduction and switching loss in the converter and investigate possible approaches to managing these losses.

With the experience gained to this point, consider the design and operation of a full-scale marine converter and make recommendations regarding the circuit topology, switch and semiconductor selection, control system design and predict the performance of this conceptual drive.

1.2 Marine Electric Propulsion

Electrical variable speed propulsion motor drives have been used in ships since the beginning of the 1970s [1]. Conventional turbo-electric and DC Ward Leonard drives had already gained a foothold in the marine industry at the beginning of the 20th Century but the unexpected rise in fuel costs during the early 1970s led to the demand for integrated electric propulsion and ship service systems to improve efficiency and reliability, thereby reducing vessel operating costs in an increasingly competitive shipping market. Furthermore, the offshore oil and gas industry developed rapidly during this period, giving rise to the demand for vessels with accurately controlled propulsion systems allowing dynamic positioning over the seabed for exploration, drilling and support [2]. In naval ships, there was a demand for very low noise propulsion systems to help detect submarines and also for propulsion systems that offered high reliability, flexibility and low cost in line with reduced military spending [3]. The variable speed electric motor drive provided propulsion solutions for all these vessel types. Electric power conversion equipment and electric motors originally developed for shore-based industrial applications were 'marinised' to provide the means of varying propulsion motor speed, thus allowing the prime-mover generator sets to operate at a constant speed. In a modern marine electrical propulsion system, the fixed frequency, fixed voltage generated power is used for ship services but is converted into a different voltage and frequency by a power converter to control propulsion motor speed and torque [4]. Figure 4 shows an electrical schematic of a typical integrated full electric propulsion system.

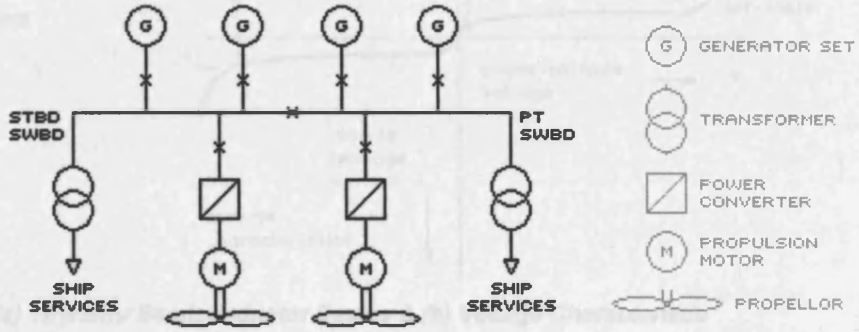

Figure 4 - Marine Propulsion System Line Diagram

1.3 Historical Review

The first solid-state electrical power conversion equipment to be used in a marine propulsion plant was the AC to DC rectifier, driving a DC motor at variable speed. Propulsion motor speed control was achieved by varying the DC output voltage controlled by the thyristor phase angle firing delay. The drawback with this type of propulsion is the limitation of DC motor design [5]. AC propulsion motors generally have much better power-to-weight and power-to-volume ratios, require much less maintenance [6] and can be built to potentially very high power levels as compared with

DC propulsion motors [7]. The two types of AC motor that are primarily found in electrical propulsion systems are the synchronous motor and the induction motor. The synchronous motor is popular in direct drives where high power and high torque are required at low speeds. In contrast, the induction motor is often operated at higher speeds in combination with a reduction gearbox. The synchronous motor allows for input displacement angle control and possesses an inherently wider air gap to give it a better shock capability. The induction motor, on the other hand, is somewhat lighter and does not require a separate excitation supply, although its power factor is relatively poor and it usually has a lower shock capability. However, a direct-drive Advanced Induction Motor design that meets shock requirements has recently been selected for the future Royal Navy Type 45 Destroyer [8]. To vary the speed of either types of AC propulsion motor, it is necessary to change both the voltage and the frequency of the electrical supply. There are several methods of achieving AC conversion using power electronic systems but the cycloconverter and the load commutated inverter have to date proved to be the most popular in marine applications.

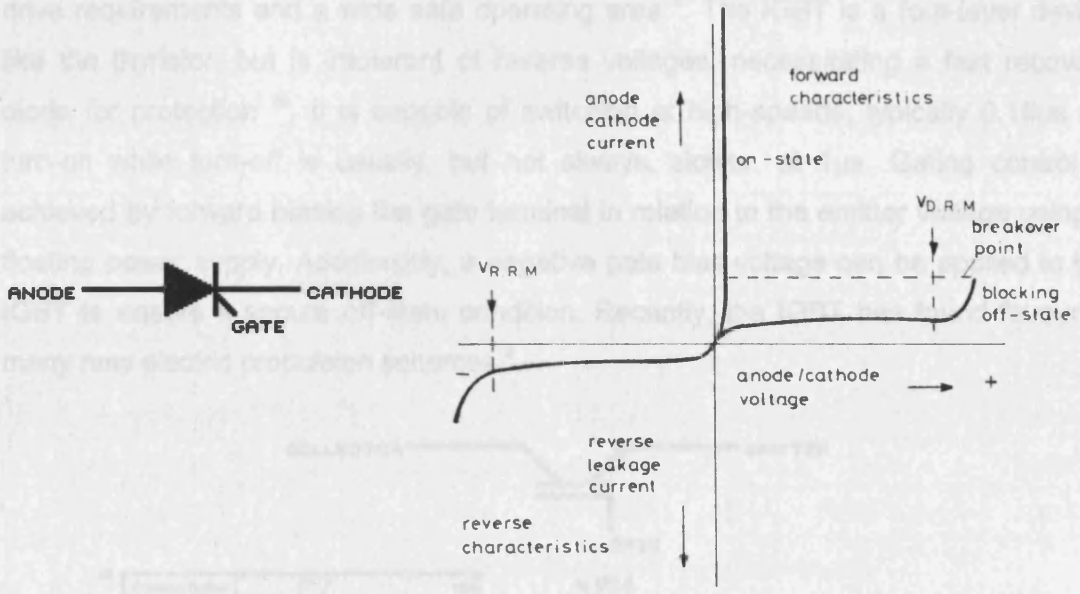

Figure 5 - (a) Thyristor Semiconductor Device & (b) Voltage Characteristic [9]

Early electric power conversion systems were based upon the thyristor (or Silicon Controlled Rectifier, SCR) semiconductor device. The thyristor remains the 'workhorse' of the majority of marine electrical propulsion systems in service today because ongoing development, since its discovery by Schottky in 1957, has resulted in a robust, reliable and very efficient switch capable of handling high currents and voltages. The thyristor is a four layered sandwich of semiconductor material constructed from alternate levels of 'n' and 'p' doped silicon and is designed to conduct current in only one direction. Conduction commences only on the application of a 'gating' signal and ceasing when current attempts to reverse through the device [9], as shown in Figure 5.

Such characteristics make the thyristor well suited for use with AC supplies as precise portions of the alternating current half cycles can be conducted, turning off naturally when the current reverses (natural commutation) [3]. Today, the main converter types employing thyristors in the marine industry are the cycloconverter, the load-commutated inverter and the DC rectifier bridge.

By the end of the 1970s large variable speed drive systems employing thyristors were commonplace. However, the limitations of these naturally commutated drives led to the development of new power electronic devices that allowed 'forced commutation'. Unlike the thyristor, which requires a zero current condition, forced commutation occurs when power electronic switches are turned off using a control signal at any time during conduction. Examples of such devices include the gate-turn-off thyristor (GTO), the integrated gate commutated thyristor (IGCT) and the insulated gate bipolar transistor (IGBT), as shown in Figure 6(a). The IGBT is a high-power semiconductor switch that combines the advantages of the power MOSFET and the bipolar power transistor and offers high forward conduction density, low voltage drop, simple gate drive requirements and a wide safe operating area [3]. The IGBT is a four-layer device like the thyristor, but is intolerant of reverse voltages, necessitating a fast recovery diode for protection [10]. It is capable of switching at high-speeds, typically 0.15μs for turn-on while turn-off is usually, but not always, slower, at 1μs. Gating control is achieved by forward biasing the gate terminal in relation to the emitter voltage using a floating power supply. Additionally, a negative gate bias voltage can be applied to the IGBT to ensure a secure off-state condition. Recently, the IGBT has found favour in many new electric propulsion schemes [3].

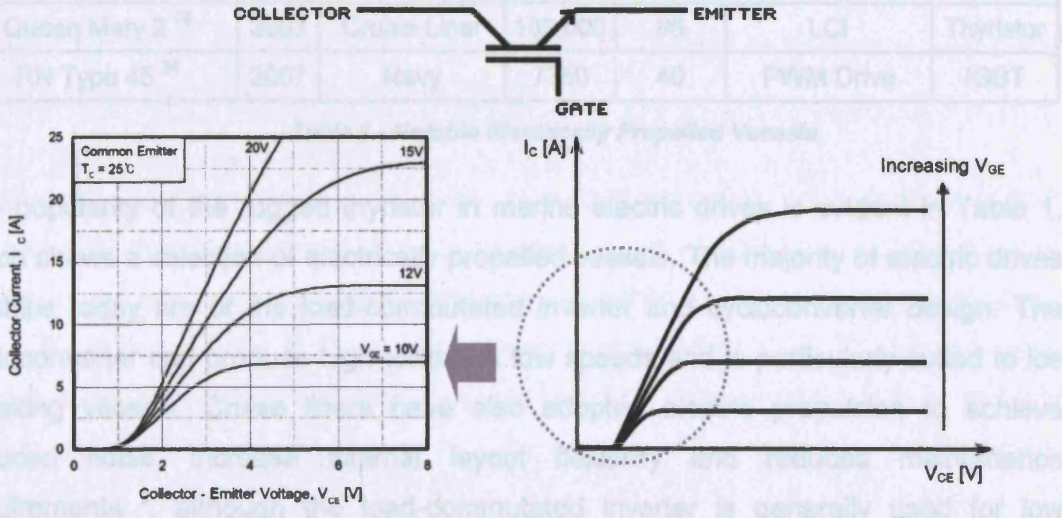

Figure 6 - (a) IGBT Semiconductor Device & (b) Static Characteristics [10]

The new generation of forced commutated devices switch at high frequencies rather than at line frequency, thereby introducing the concept of pulse width modulation

(PWM). Using PWM techniques allows the generation of higher quality output waveforms containing less harmonic distortion than that experienced with load-commutated inverters, cycloconverters and DC rectifiers, thus reducing harmonic filtering requirements. Converters using these new devices are able to produce pulses of power with continuously varying periods of conduction and are generally capable of generating output waveforms over considerable ranges of voltage and frequency. Higher switching speeds of power electronic devices have led to the widespread use of variable speed drives at low and medium powers in manufacturing and processing industries, facilitating precise control over production rates and thereby increasing production efficiency [9].

Ship	Year	Type	Size (G-T)	Power (MW)	Converter	Switch Type
Seaway Prince	1975	Ro-Ro Ferry	4,174	8.9	AC-DC Rectifier	Thyristor
Pacific Guardian [11]	1984	Cable Layer	6133	5.5	AC-DC Rectifier	Thyristor
CCGS Henry Larsen [12]	1987	Ice Breaker	6166	12.2	Cycloconverter	Thyristor
QE2 [13]	1987	Cruise Liner	70,327	88	LCI	Thyristor
RN Type 23 [14]	1989	Navy	3,500	1.5	AC-DC Rectifier	Thyristor
MV Fantasy [15]	1990	Cruise Liner	70,000	42	Cycloconverter	Thyristor
The Cable Innovator [16]	1994	Cable Layer	10,040	12.8	PWM Drive	GTO
USCGC Healy [17]	1997	Ice Breaker	16,000	22.4	Cycloconverter	Thyristor
The Grand Princess [18]	1998	Cruise Liner	108,806	35.3	LCI	Thyristor
MV Elation [19]	1998	Cruise Liner	70,400	47.5	Cycloconverter	Thyristor
The Aurora [20]	2000	Cruise Liner	76,000	46	LCI	Thyristor
Navion Munin [21]	2001	Shuttle Tanker	66,200	22.9	LCI	Thyristor
HMS Albion/Bulwark [22]	2003	Navy	18,000	12.2	LCI	Thyristor
Queen Mary 2 [23]	2003	Cruise Liner	150,000	86	LCI	Thyristor
RN Type 45 [24]	2007	Navy	7350	40	PWM Drive	IGBT

Table 1 - Notable Electrically Propelled Vessels

The popularity of the rugged thyristor in marine electric drives is evident in Table 1, which shows a selection of electrically propelled vessels. The majority of electric drives in ships today are of the load-commutated inverter and cycloconverter design. The cycloconverter can produce high torque at low speeds and is particularly suited to ice breaking vessels. Cruise liners have also adopted electric propulsion to achieve reduced noise, increase internal layout flexibility and reduced maintenance requirements [3], although the load-commutated inverter is generally used for low volume, for example the QE2 [25]. The PWM drive has yet to become fully established in the marine power propulsion drives market, although it is found in specialist vessels, e.g. the cable laying vessel Cable Innovator.

1.4 Advantages of Electric Propulsion

The key advantages of electric propulsion over mechanical propulsion systems are well described [1,26] but have been summarised here for completeness.

- Elimination of the heavy gearbox and long shaft lines that constrain location of machinery and internal ship layout [27]. The gearbox is also expensive to buy and maintain.

- Position of prime-mover generator sets may be optimised to maximise cargo carrying capacity and vessel stability [3,27].

- Multiple prime-mover generator sets may be operated at maximum efficiency, stepping in or stepping out to match demand and avoiding inefficient and costly part load operation [3].

- Increased electrification allows a reduction in the crew and associated accommodation requirements, leading to cost savings [27]. For example, due to reduced maintenance, the electrical propulsion system installed on HMS Albion (2003) allows a two-thirds reduction in marine engineering personnel compared to its predecessor [22].

- Reduction in vibration and noise, leading to improved passenger comfort. Noise reduction has also attracted naval interest, where noise signatures are a major concern: an electric ship is a quiet ship. Acoustically shielded diesel generators and very low noise DC motors have been used in the Type 23 Frigates to minimise interference with the towed sonar array. More recently, electric propulsion has been selected for the Royal Navy Type 45 Destroyer [28]. Electric propulsion is also being considered for the RN's Future Aircraft Carrier.

- Podded electric propulsion (motors in a pod mounted underneath the hull) considerably increases manoeuvrability and reduces machinery space inside the ship [2]. Elation, the world's first podded cruise ship, achieved an 8% increase in propulsion efficiency in comparison to Carnival's existing Fantasy class ships [19]. The full speed turning circle diameter of the vessel was reduced by approximately 30% [19] and it is able to dock without the aid of tugs in a third less time than previous Fantasy class vessels [29].

- Electric propulsion facilitates computer controlled dynamic vessel positional control [2]. This is useful in the oil and gas industries.

- Novel, more efficient hullforms, such as trimarans or pentamarans, become feasible with the use of electric propulsion, as electric propulsion increases the flexibility of internal layout and overcomes the problems associated with narrow hullforms [27,30,31].

1.5 Disadvantages of Electric Propulsion

The disadvantages associated with electric propulsion are as follows:

- Additional equipment is required to match the operating performance of the existing mechanical propulsion systems, such as electrical generators, power converters and electrical motors [3].

- Electrical propulsion systems are more expensive to purchase due to the additional equipment such as generators, motors and converters [27]. This is partially offset by the removal of the gearbox.

- The efficiency of an electrically propelled ship may be lower than a conventionally driven vessel at full speed and is therefore not a suitable propulsion plant for all vessels [27,32].

- The power converter(s) may pollute the power supply used by the ship services and (in warships) the weapons systems.

The marine industry is presently in a transitional period with new electrical technologies allowing greater flexibility in ship design. Figure 7 shows the current types of marine electrical propulsion systems and their typical applications.

Electric propulsion can be found in several different vessel applications, primarily where either high torque is required at low speeds or where noise and vibration must be kept at minimum levels.

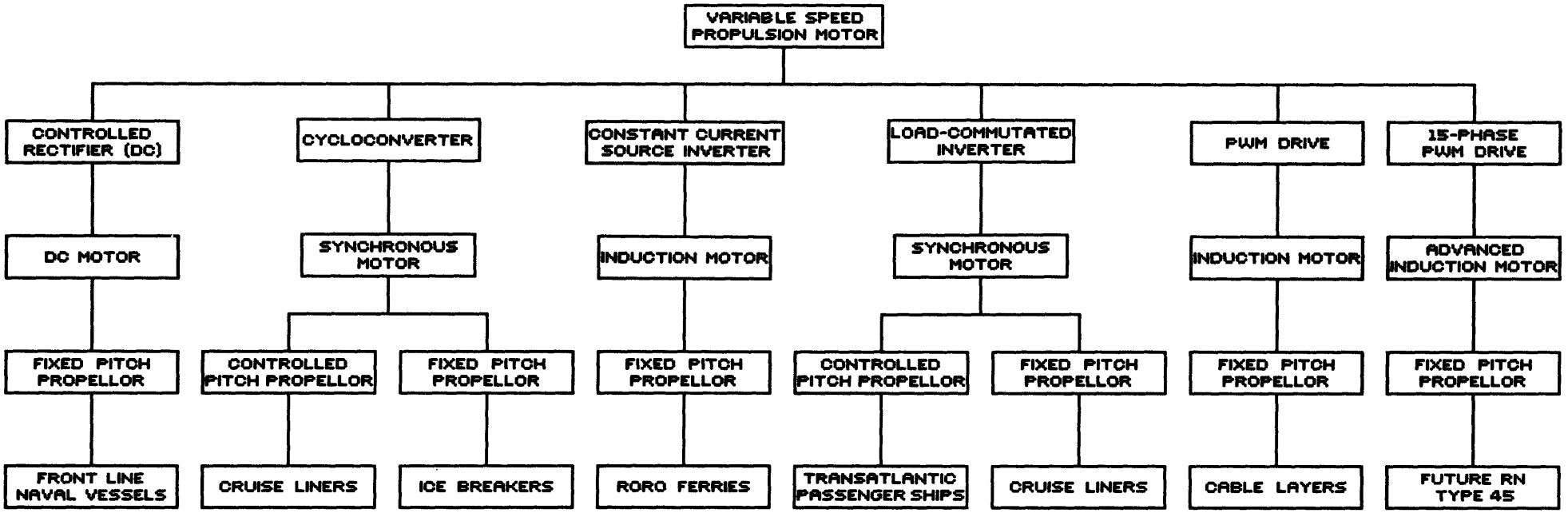

Figure 7 - Classification of Present Drive Topologies

1.6 Current Marine Converter Technology

1.6.1 Graetz Bridge

The first modern power conversion system to be used in marine electrical propulsion was the AC to DC converter. The Graetz Bridge rectifies the generated three-phase electrical power using thyristors to produce DC power suitable to drive a DC propulsion motor. The thyristor conducts only when forward-biased and a 'gating' signal is required to begin conduction with blocking occurring upon current reversal. This method of 'turning-off' the thyristor, known as 'natural commutation', is desirable as minimal switching loss results.

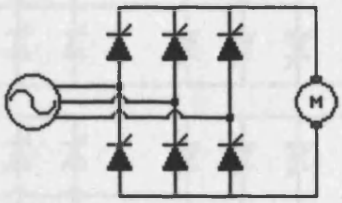

Figure 8 - Graetz Bridge

The mean value of the rectified DC output voltage depends on the periods of conduction during each half cycle of the supply waveform with motor speed control achieved by varying the DC output voltage. This type of propulsion has the advantage of providing maximum torque across the whole speed range and simplifying motor speed control. Continuous research and development of the DC motor over many decades (largely to meet the need of submarines) has resulted in the design of extremely low noise propulsion motors. Unfortunately, the DC motor has power-to-weight and power-to-volume ratios that are inferior to the equivalent rated AC motors, requires greater maintenance and has an inherent power limitation that effectively limits its size to around 8 MW at 200 rpm [33]. Beyond this power limitation, multiple shaft motors are needed. By the end of the 1970s, several vessels were using Graetz bridge-based DC propulsion. Examples include the roll-on-roll-off ferries Seaway Prince (1974) and Seaway Princess (1975) and the cable layer Pacific Guardian (1984) [11]. The low-noise aspect resulted in the Type 23 Frigate (1989 - 2001) employing two very quiet 1.5 MW DC motors with acoustically shielded generators, contributing to provide anti-submarine warfare capability.

1.6.2 Cycloconverter

The cycloconverter has been used in specialist applications since the 1920s but became more common following the development of the thyristor semiconductor switch [9]. Composed of a pair of back-to-back connected Graetz bridges for each output phase, the cycloconverter represents a variable speed drive capable of direct AC-AC conversion and is, therefore, highly efficient (>98%). The cycloconverter cascades sections of the constant frequency and constant voltage supply waveforms

to form a continuously variable voltage and variable frequency output waveform to drive either synchronous or induction motors.

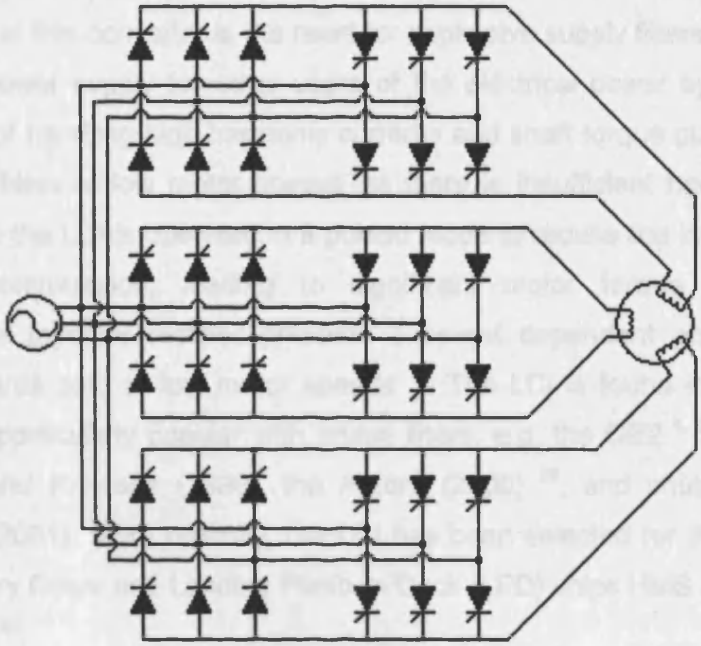

Figure 9 - Three-Phase Cycloconverter

The control of both the output amplitude and frequency makes this drive the preferred choice for heavy-duty icebreaker applications where high torque is required at low speed. Symmetry of the electrical path enables power to be regenerated from the load, allowing rapid braking of the shaft. Although switching at line frequency allows the thyristors to self-commutate for low loss, the cycloconverter produces non-integer supply harmonics down to dc and the output frequency is limited to approximately one-third of the supply frequency. The other main drawback is physical size; the cycloconverter contains 36 stacks of thyristors and requires either isolated motor phases or supply transformers for each anti-parallel bridge pair. This drive is found primarily in icebreakers, CCGS Henry Larsen (1987) [12] and USCG vessel Healy (1997) [17] and some cruise liners, including MV Fantasy (1990) [15].

1.6.3 Load-Commutated Inverter

An alternative to the cycloconverter is the load-commutated inverter (LCI - also known as the auto-synchronous converter or synchro-converter). This is a physically smaller drive than the cycloconverter, requiring only two back-to-back Graetz bridges, as shown in Figure 10.

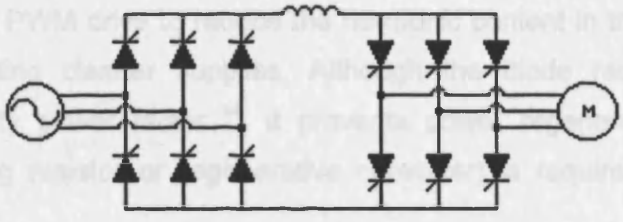

Figure 10 - Typical Load-Commutated Inverter Drive

The first Graetz bridge rectifies the generated three-phase AC power into a variable DC level and this is inverted by the second bridge into a variable frequency and variable current three-phase supply to drive a synchronous propulsion motor [3]. The main drawback of this converter is the need for expensive supply filters to preserve the quality of the power supply for other users of the electrical power system and for a motor capable of handling high harmonic currents and shaft torque pulsations. This is a particular problem at low motor speeds as there is insufficient back EMF for self commutation so the LCI is operated in a pulsed mode to reduce the inverter current to zero during commutation, leading to significant motor torque fluctuations [34]. Additionally, the thyristor rectifier presents a speed dependent power factor that decreases towards zero at low motor speeds [34]. The LCI is found in many different vessels and is particularly popular with cruise liners, e.g. the QE2 [1, 25] (re-engined in 1987), the Grand Princess (1998), the Aurora (2000) [20], and shuttle tankers e.g. Navion Munin (2001). More recently, the LCI has been selected for the Royal Navy's two new Auxiliary Oilers and Landing Platform Dock (LPD) ships HMS Albion and HMS Bulwark (2003) [22].

1.6.4 Pulse Width Modulated Drive

The Pulse Width Modulation (PWM) drive exploits a new generation of high-speed semiconductor switch that allows the point at which conduction begins and ends to be controlled. The PWM drive works on the principle of switching at high frequencies to produce pulses of power with continuously varying periods of conduction and, therefore, does not exhibit any output frequency limitation.

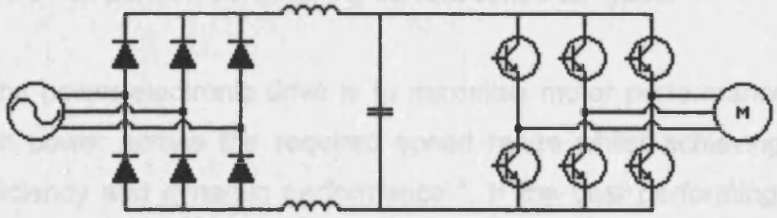

Figure 11 - Typical PWM Drive Configuration

The PWM drive first converts the three-phase AC generated power into positive and negative DC voltage levels using a rectifier which is then 'chopped' to form a modulated output voltage waveform at the required frequency to drive either an induction or synchronous motor [2]. The high-speed switching possible with the IGBT devices allows the PWM drive to reduce the harmonic content in the input and output waveforms, providing cleaner supplies. Although the diode rectifier results in a constant near unity power factor [34], it prevents power regeneration so additional equipment (braking resistor or regenerative converter) is required for ship braking duties [2].

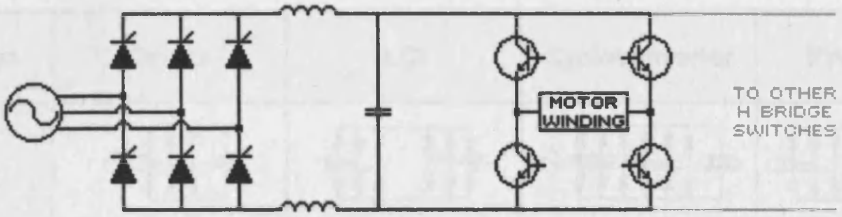

Figure 12 - Single-Phase Output 'H'-Bridge Configuration

Recently, PWM drives in an 'H'-bridge configuration, as shown in Figure 12, have been developed at high powers and is the chosen topology for the 15-phase Advanced Induction Motor drive for the Royal Navy Type 45 Destroyer [8,35]. The converter allows the voltage applied to each phase of the motor to be rapidly switched between the positive and negative DC levels, allowing a pulse width modulated output waveform to be generated.

1.7 Converter Comparison

The previously described converters represent the present generation of electrical drives found in marine applications. It has been shown that electrical propulsion is popular in many different types of vessels because of the advantages it offers over mechanical propulsion systems. The choice of electrical drive is extensive, with many different systems available. Cycloconverter propulsion is popular in vessels requiring high torque at low speed, such as icebreakers. The LCI is popular in cruise ships due to reduced physical size and lower cost. The PWM drive is popular in applications where high dynamic performance is needed. Indeed, a PWM converter driving an Advanced Induction Motor has been chosen for the Royal Navy's Type 45 Destroyer [8]. Table 2 shows a comparison between the current converter types.

The aim of the power electronic drive is to maximise motor performance and extract the maximum power across the required speed range whilst achieving the highest operating efficiency and dynamic performance [9]. If the best performing converter in each category is highlighted, this shows that there is no universally superior drive suitable for all applications. None satisfies all of the requirements and selection is therefore based on design compromises and the ship propulsion requirements.

Converter	Graetz	LCI	Cycloconverter	PWM Drive
Circuit	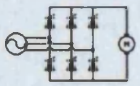	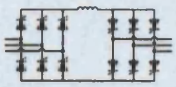		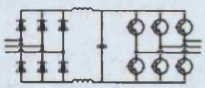
Device No.	Thyristor (6)	Thyristor (12)	Thyristor (36)	Diode (6) GTO/IGBT (6)
Conversion Process	AC - DC	AC - DC - AC	AC - AC	AC - DC - AC
DC-Link Required	N/A	Yes	No	Yes
Voltage/Current Source	Voltage	Current	Voltage	Voltage
Slow Speed Controllability	Good	Poor and complex to achieve	Good	Good
Output Voltage	$\frac{3\sqrt{2}}{\pi} V_{line}$	-	$\frac{3\sqrt{2}}{\pi} V_{line}$	$\sqrt{2}\, V_{line}$
Output Frequency	N/A	Wide Range	40% Supply	Wide Range
Commutation	Natural	Natural	Natural	Rectifier - Natural Inverter - Forced
Regeneration	No	Yes	Yes	No
Dynamic Performance	Good	Fair, but problems at low speeds	Good	Very Good
Converter Complexity	Low	Medium	Medium	High
Converter Losses	Low	Low	Very Low	Medium
Converter Dimensions	Small	Medium	Large	Medium
Input Current Waveform Quality	Poor	Poor	Poor	Poor
Simulated Output Waveforms	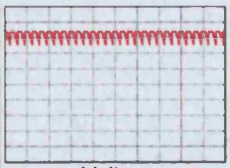 *Voltage*	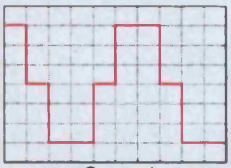 *Current*	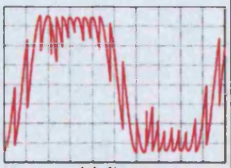 *Voltage*	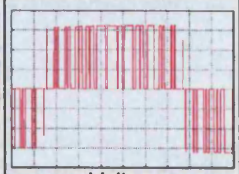 *Voltage*
Output Wave-form Quality	Good	Fair	Fair - Medium	Good

Table 2 - Comparison of Existing Marine Drives

1.8 Developing Converter Technology for Marine Applications

In the following section, converters representing the most promising future marine variable speed drive topologies are discussed and compared in Table 3.

1.8.1 Multilevel PWM Drive

The Multilevel PWM drive is a development of the standard PWM drive design that addresses the problem of loss at high switching frequencies [36]. Whereas the PWM drive switches between two voltage levels and varies the duty cycle to control the mean output voltage, multilevel converters switch between several voltage levels to generate a high quality output waveform [37]. Three main types exist: The diode-clamped multilevel converter is easily scaled but capacitor-balancing issues have limited it to three level configurations that are now widely used in industry [38,39]. Problems are also encountered when the output phase voltage exceeds 65% of the maximum value [40]. The Capacitor Clamped multilevel inverter (also known as the flying-capacitor) requires no clamping diodes, the capacitor voltages are balanced and can operate from a single DC source [38], see Figure 13(a). However high-voltage rated capacitors are required to withstand the DC link voltage [40]. The multilevel 'H'-bridge converter is also easily scaled but requires a high number of isolated voltages, derived using separate transformer windings and rectifiers, to supply each cell [38,40].

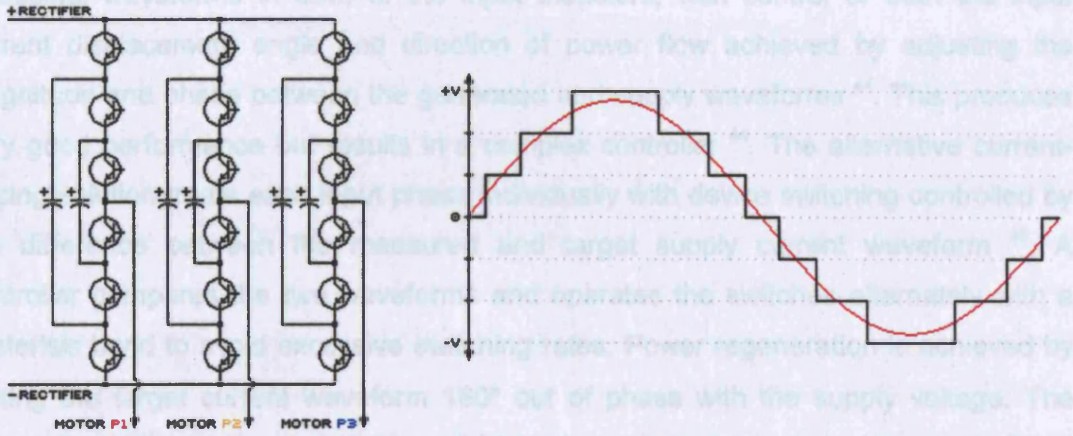

Figure 13 - (a) 4 Level Capacitor-Clamped Converter [38] (b) Output Voltage & Current Waveform

The output waveform is constructed using a sequence of pulses of different periods and mean voltages with each switch operating at the fundamental output frequency, thereby considerably reducing switching loss [41]. The lower voltage step change (per device) promotes a reduced rate of change of voltage, which improves insulation reliability that can become a problem at high switching frequencies [37]. The resolution of the output waveform can be further improved by adding more discrete DC levels but at the cost of a considerably increased component count. Various configurations are being actively researched, most prominently, the US Navy's 15 Phase, 17 level, 'H'-bridge integrated propulsion system converter [35].

1.8.2 Active-Front-End PWM Drive

The Active-Front-End (AFE) PWM converter replaces the uncontrolled diodes of the standard PWM drive with an active rectification stage to improve the input current waveforms. Although a thyristor rectifier is one solution, it produces input current harmonics and ripple on the output voltage and operates with a lagging displacement angle that worsens as the output voltage is reduced [42,43]. An IGBT front-end is therefore more desirable as it can produce a variable ripple free DC output while drawing sinusoidal input current at a unity displacement angle [42]. As a consequence, the generator set can be operated more efficiently. The active rectifier also allows certain harmonic components to be reduced with optimisation of switching patterns [34].

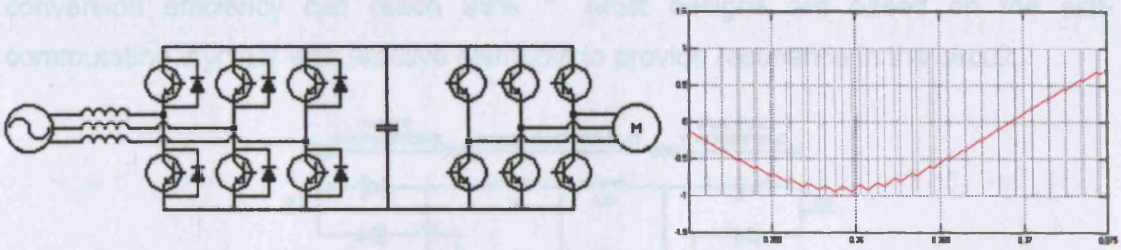

Figure 14 - (a) AFE PWM Drive & (b) Simulated Output Voltage & Current Waveforms

There are two principal methods of controlling the AFE rectifier, voltage-forcing and current-forcing. The voltage-forced approach requires generation of three-phase sinusoidal waveforms in front of the input inductors, with control of both the input current displacement angle and direction of power flow achieved by adjusting the magnitude and phase between the generated and supply waveforms [44]. This produces very good performance but results in a complex controller [44]. The alternative current-forcing solution treats each input phase individually with device switching controlled by the difference between the measured and target supply current waveform [45]. A controller compares the two waveforms and operates the switches alternately with a hysterisis band to avoid excessive switching rates. Power regeneration is achieved by setting the target current waveform 180° out of phase with the supply voltage. The current-forced provides superior transient performance, quieter operation and allows use of simpler control hardware [44].

Inverter operation is unchanged with the AFE rectifier and it retains all of the advantages associated with high-speed switching. However, when using an AFE-PWM inverter, the dc-link capacitors need to be pre-charged to their rated operating voltage during the inverter start-up phase to avoid excessive inrush currents. These occur when the dc-link is uncharged or at a lower voltage than the peak line voltage, causing uncontrolled operation of the AFE rectifier [46]. Pre-charging at start-up is therefore necessary for safe operation and is achieved using a dedicated circuit such as the one described by Koellner et al [47]. The topology of the AFE-PWM inverter with its greater

number of controlled switching devices and pre-charging needs suggests that it will be a more complex and hence more expensive drive when compared to the LCI or conventional PWM drives, however, the AFE-PWM does offer improved dynamic performance and good waveform quality [48].

1.8.3 Resonant Converters

Using resonance to self-commutate devices and virtually eliminate switching loss is another approach being considered [32,49]. Most modern electric drives are 'force-commutated' and require a gating signal to control both the beginning and end of conduction. Resonance is used to optimise device switching to reduce loss, allowing conduction to begin at zero voltage and end at zero current. Under these conditions, conversion efficiency can reach 98% [49]. Most designs are based on the self-commutating thyristor with reactive elements to provide resonance in the circuit.

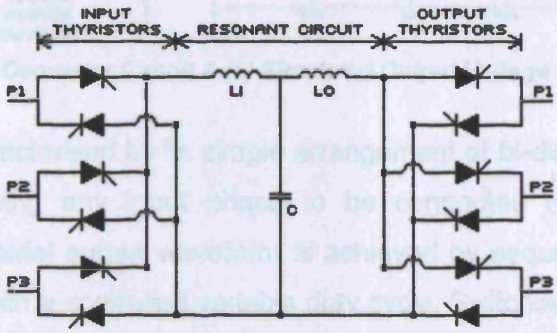

Figure 15 - Sequential Capacitive Discharge Converter

Several different resonant converter topologies have been proposed and are being researched, aiming to achieve high efficiency operation across the output frequency and voltage ranges. The sequential capacitive discharge converter (SCDC) is an example of one such drive. A central capacitor is alternately charged from the power supply and discharged to the converter load using twelve thyristor devices [50]. The output waveform is a series of discrete voltage pulses [32], as shown in Figure 16 where the simulated output waveform is shown and uses an operational scheme similar to that of the PWM drive. Instead of a square voltage output, the drive provides a much more rounded pulse of energy that reduces insulation shock loading and harmonic noise [32,49,50].

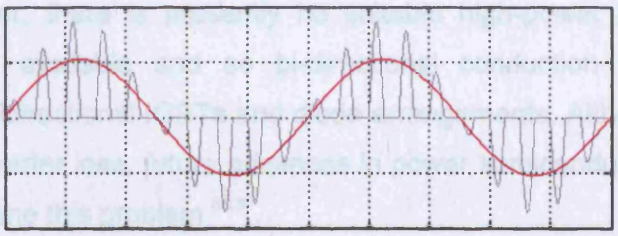

Figure 16 - Simulated SCDC Output Voltage & Current Waveforms

Although the SCDC offers reduced switching loss, the circuit is electrically complex with a demanding control algorithm that requires a capable control system [51].

1.8.4 Matrix Converter

The matrix converter is another promising drive topology. It performs direct AC-AC conversion, like the cycloconverter, but without an upper output frequency limitation. The matrix converter ideally requires only nine bi-directional semiconductor switches and has the potential to be an all-silicon drive.

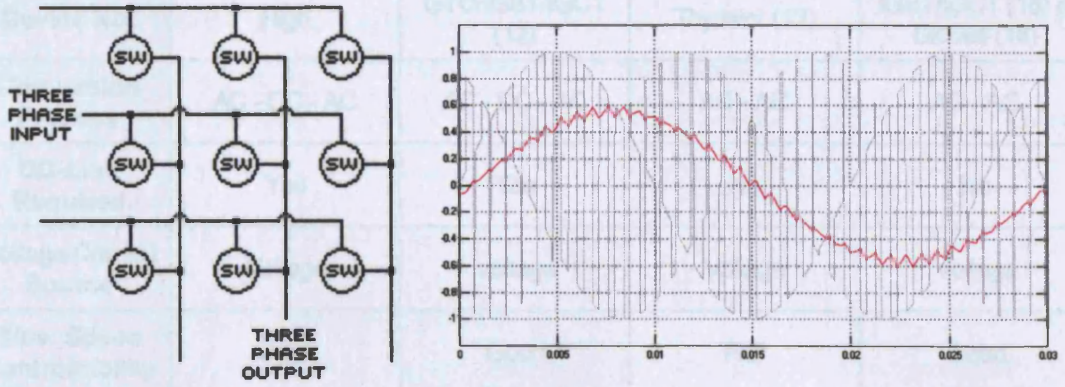

Figure 17 - (a) Matrix Converter Circuit & (b) Simulated Output Voltage & Current Waveforms

The converter is characterised by its simple arrangement of bi-directional switches in a grid formation, allowing any input phase to be connected to any output phase. Synthesis of a sinusoidal output waveform is achieved by sequential sampling of the three-phase supply with a controlled variable duty cycle. Switching is performed at high frequencies (>1kHz) with, on average, each switch conducting for one-third of the time. High-speed switching of modern semiconductor switches means that removal of generated harmonics can be performed with a more compact (and therefore inexpensive) supply filter. Although there are several different strategies that can control the semi-conducting switches, all exhibit the same fundamental voltage transfer limitation of 0.866 for a three input phase, three output phase configuration [52,53,54]. This is only a problem when replacing an existing converter, since new motor installations can be optimised for the reduced operating voltage [55]. The matrix converter is also able to vary the input displacement angle through appropriate control of the devices [6].

For current to flow in both directions the semi-conducting switches must be bi-directional. However, there is presently no suitable high-power bi-directional semi-conducting device available and so bi-directional conduction is achieved using combinations of unidirectional IGBTs and diode arrangements. Although this increases drive size and converter loss, future advances in power semiconductor technology are expected to overcome this problem [56,57].

Converter	Multilevel PWM	AFE PWM Drive	Resonant Converters	Matrix Converter
Circuit	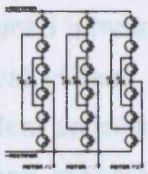	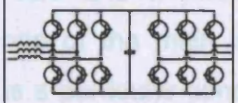	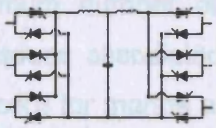	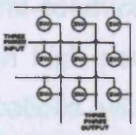
Device No.	High	GTO/IGBT/IGCT (12)	Thyristor (12)	IGBT/IGCT (18) & Diodes (18)
Conversion Process	AC - DC - AC	AC - DC - AC	AC - AC	AC - AC
DC-Link Required	Yes	Yes	No	No
Voltage/Current Source	Voltage	Voltage	Voltage	Voltage
Slow Speed Controllability	Good	Good	Fair	Good
Maximum Output Voltage	$\sqrt{2}\ V_{line}$	$\sqrt{2}\ V_{line}$	$2\ V_{line}$	$3\phi : 0.866V_{in}$ $6\phi : 0.972V_{in}$
Output Frequency	Wide Range	Wide Range	Wide Range	Wide Range
Commutation	Rectifier - Forced Inverter - Forced	Rectifier - Forced Inverter - Forced	Natural	Standard = 50% Natural 'Opti-Soft' = 67% Natural
Regeneration	No	Yes	Yes	Yes
Dynamic Performance	Very Good	Very Good	Average	Very Good
Converter Complexity	Very High	Medium	High	Medium
Converter Losses	Low	Medium	Very Low	Medium
Converter Dimensions	Large	Small	Medium	Medium-Small
Displacement Angle Control?	No	Yes	No	Yes
Input Current Waveform Quality	Depends on front end	Good	Good	Good
Output Wave-form Quality	Excellent	Good	Good	Very Good
Simulated Output Voltage Waveforms	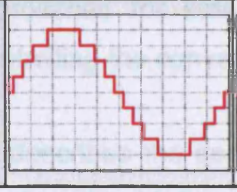	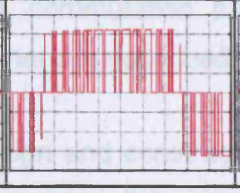	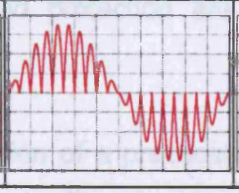	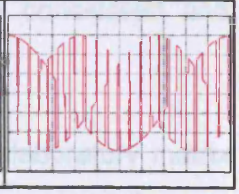

Table 3 - Comparison of Developing Variable Speed Drives

1.9 Converter Developments and Future Marine Demands

A future ship propulsion converter will need to be highly efficient and provide improved performance, reduced physical size and a minimum number of semi-conducting devices, as removal of heat is one of the main issues associated with high power marine drives [26]. Heat sensitivity is a particular concern for marine applications, where enclosed spaces can concentrate heat that can prove damaging to capacitors [58]. The 'ideal' drive would be free of capacitors in the electrical circuit, so an all-silicon solution would be a step towards the 'ideal' drive [58]. Of the present marine drives, only the cycloconverter is capacitor free but it suffers from limited output frequency, poor quality voltage waveforms and a high device count that make it unsuited to some marine applications.

The matrix converter has the potential to become the future of marine electric propulsion by harnessing high-speed switching semiconductors to improve on the performance of the cycloconverter. The symmetrical electrically path allows power regeneration from the propulsion motor, while displacement angle control reduces the loading on the generator sets. High-speed switching reduces harmonic content in the output waveform, which in turn reduces torque fluctuations that can lead to a noisy signature and increased shaft stresses [7]. Supply filtering requirements are subsequently reduced due to the high switching frequency. A converter composed of only silicon components will be able to exploit improvements in semiconductor technology and even fully integrated drives are already possible for low power applications.

Although the competing AFE and multilevel PWM converters are receiving considerable attention [35], the matrix converter has not yet been investigated for marine application despite it appearing to possess the necessary attributes for such a role and the potential to be a very compact variable speed drive.

1.10 Structure of Thesis

A review of related work carried out in each area supporting the investigation has been presented in the appropriate chapter. The historic development of the matrix converter and its performance is presented in Chapter Two. Bi-directional switch topologies are discussed, approaches for safe commutation and protection are considered and methods for controlling the converter are described.

Chapter Three describes the design and construction of a practical laboratory matrix converter, including the bi-directional switch, supply filter design, supply reference system and protection.

Chapter Four details the development of the custom written control system software, designed to implement both standard and advanced Venturini modulation strategies. Also detailed are the techniques adopted to reduce real-time computation and allow higher operating frequencies.

Chapter Five investigates the performance of the matrix converter using the developed laboratory model. This shows that both output frequency and output voltage are independently controllable and that the matrix converter draws and produces high-quality waveforms that are dependent on the switching frequency. Input displacement angle control is also demonstrated. Spectral analysis of the converter waveforms show that harmonics are produced at sidebands of multiples of the switching frequency.

In Chapter Six, sources of loss in the laboratory matrix converter are analysed. Methods of reducing switching loss are investigated, including modification of the commutation sequence and the semi-symmetrical PWM strategy. The effect on the converter input and output waveforms are compared with the use of spectral analysis. Semi-symmetrical PWM has been found to produce significantly increased low frequency harmonics that impact on the supply filter performance, making this approach unfeasible for practical application in the marine environment.

A novel commutation sequencing strategy for the Venturini controlled matrix converter is presented in Chapter Seven. An increase in natural commutations has been achieved by optimising the switching order according to the supply voltage levels and load currents to achieve 66.67% natural switching for a three-phase input converter. An increase to 83.3% natural commutation is possible for a six-phase input configuration. Commutation reliability is increased and the distribution of loss in the semiconductor switches is equalised. Analysis of the output current harmonics produced by the proposed strategy suggests that these do not differ significantly from those of standard sequential commutation, allowing use of existing filter designs.

Chapter Eight discusses the matrix converter and assesses its potential as a marine electric drive. A novel mode of operation is proposed that takes advantage of the matrix converter's unlimited output frequency to allow direct connection between generator and propulsion motors. A conceptual marine matrix converter drive that meets the requirements of the Royal Navy's Type 45 Destroyer has been considered and its performance investigated using computer based models.

Finally, the conclusions discuss the findings of the study and relate the practical issues that need to be overcome for commercialisation of the matrix converter. Also presented are recommendations for the continuation of this research.

2. Chapter Two - Matrix Conversion

2.1 Introduction

The matrix converter concept was first proposed in 1976 to represent the 'ideal' power converter topology and is characterised by the arrangement of bi-directional switches in a three by three grid formation [59], allowing any input phase to be connected directly to any output phase, as shown in Figure 17(a) [p37]. The absence of energy storage elements and the electrically symmetrical circuit of the converter allow four-quadrant operation when driving an AC motor. A literature review revealed the solutions employed to overcome the lack of a high-power bi-directional switch with unidirectional devices and future advances in semiconductor technology that may in future entirely solve this problem. Safe current commutation between switches emerged as a problem although several solutions have been proposed including numerous staggered strategies that facilitate loss reduction in the matrix converter.

Sampling of the supply at high frequency under the control of an advanced control strategy allows the matrix converter to produce high-quality waveforms with reduced filtering requirements. A complex control system is required to calculate the switching periods and avoid combinations that short-circuit the supply. An attractive feature is the ability of the converter to vary the input displacement angle without additional equipment, allowing a lagging load to appear as unity or even leading angle to the supply. Although there are several different regimes for controlling the switches, most exhibit the same fundamental input-output voltage limitation of 86.6% for a three-phase input, three-phase output converter [52,53,54]. Certain modulation schemes claim to achieve a greater transfer ratio but do so at the cost of increased input and output harmonic distortion [60]. Additional input phases may also be used to raise the maximum possible output voltage, however most motors can be redesigned for operation at reduced voltage.

2.2 Literature Review

A literature review was undertaken to establish the current state of the art and to assess matrix converter research undertaken elsewhere. Several key papers were obtained and milestones in development are summarised in Appendix A1 [p234].

The review of papers published on the matrix converter has shown it to be an active area of research. The drive has attracted considerable attention and many of the initial challenges have been solved over the past two decades. Earlier efforts focused primarily on the formulation of an optimum control strategy, with the Venturini and Space Vector Modulator algorithms emerging as the main options for matrix converter control, having comparable performance whilst achieving the maximum voltage

transfer ratio and input displacement angle control. The literature review revealed that there were four major technical problems associated with the matrix converter concept that have slowed its introduction into the variable speed drive market. These were:

- Lack of a bi-directional semiconductor switch
- Safe current commutation
- Reduced voltage transfer ratio
- High converter loss

These are discussed further in the following sections.

2.3 Bi-directional Switch

The matrix converter requires a high-speed semiconductor switch that can block voltage and conduct current in both directions. The lack of such a switch has been one of the main limiting factors in the development of the matrix converter. The established solution to this problem has been to synthesise bi-directional operation using unidirectional semiconductor devices in topologies such as those described below.

2.3.1 Diode-bridge

The diode-bridge arrangement is the most straightforward method of using unidirectional semiconductor devices to produce a bi-directional switch. A single semiconductor switch is connected to four diodes in a 'bridge' arrangement, as shown in Figure 18. A single gate drive circuit is required for each switch and consequently only one control signal operates the bi-directional switch. Unfortunately, losses are high due to the conduction path being a semiconductor switch and two diodes, with all commutations hard-switched.

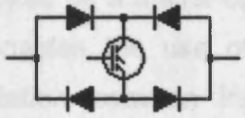

Figure 18 - Diode-Bridge Switch Topology

For a three-phase input, three-phase output matrix converter, the drive density is compromised by the requirement for 36 diodes and nine unidirectional switches.

2.3.2 Common-Collector and Common-Emitter

The common-collector and common-emitter switches, collectively known as anti-parallel arrangements. These are very similar circuits that represent more advanced bi-directional switches as each switch has two diodes and two unidirectional switching devices. Each individual switching device controls conduction in a single direction and therefore full bi-directional control requires two unidirectional switches operating together. Although this requires a more complex gate drive and control system, research has shown that it is possible to reduce the number of isolated power supplies required by the gate drivers to only nine for the common-emitter and six for the

common-collector [61], thus offsetting the need for increased complexity in small drives. However isolated supply sharing is of little interest in a marine application where series connected devices already require isolated gate drives.

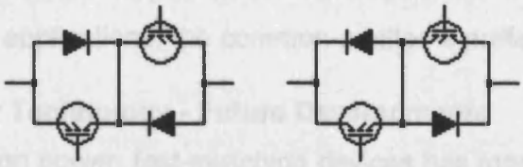

Figure 19 - Common-Collector & Common-Emitter Switch Topologies

The devices can be arranged with either a common-collector or a common-emitter, as shown in Figure 19, to achieve similar switching speeds. The benefit of using this type of bi-directional switch is that only a single diode and unidirectional switch are conducting at any point, reducing conduction loss in comparison with the diode-bridge. Both switch configurations can be operated without the central link that creates the collector or emitter commonality but the link does provide some transient benefits during commutation [55]. Although the requirement for additional gate drive and control circuitry initially appears to be a disadvantage, the ability to control the direction of current as well as the conduction period facilitates staggered commutation strategies that halves switching loss. This is discussed in greater detail in Section 2.4 [p45].

2.3.3 Switch Topology Discussion

Table 4 summarises the key attributes of the three bi-directional switches constructed from discrete unidirectional semiconductor devices. It shows that the anti-parallel configurations are more desirable due to the reduction in conduction loss and in the total number of components required by a matrix converter. The ability to control the direction of current flow also enables the use of staggered commutation, which facilitates safe current commutation between input phases and allows natural commutation.

	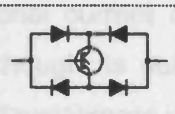	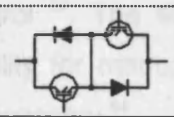	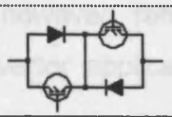
Topology	**Diode-Bridge**	**Common-Emitter**	**Common-Collector**
Active Switches	9	18	18
Passive Devices	36	18	18
Total Components	45	36	36
Gate Drives	9	18	18
Control Signals	9	18	18
Isolated PSU	9	9	6
Conduction Path	Switch + 2 Diodes	Switch + Diode	Switch + Diode
Commutation Type	100% Hard	50% Soft	50% Soft

Table 4 - Comparison of Switch Topologies

The choice of which anti-parallel switch topology to use is largely dictated by the size of converter being designed, as loss is equal for both. Although the common-collector configuration allows a reduction in the number of gate drive components, this is often unfeasible in larger drives as stray inductance between commutating cells can cause problems, so for these applications, the common-emitter is preferred [55].

2.3.4 Semiconductor Technology - Future Developments

The requirement for high power, fast-switching devices has made the IGBT well suited to matrix converter applications. Continuous development of the IGBT for PWM drive applications over a twenty-year period has resulted in a rugged, low-loss, high-speed switching device. Virtually all matrix converters employ the IGBT together with combinations of high-speed diodes in the switch topologies previously discussed. However, alternatives to the IGBT exist, including the MOS controlled thyristor, which has the potential for reduced conduction loss and increase converter efficiency [62,63].

More recently there have been several advances in semiconductor device technology that show promise for matrix conversion. This includes the development of the reverse-blocking IGBT [56] and the Monolithic Bi-directional Switch [57]. The RB-IGBT integrates a high-speed blocking diode in the same package as a standard IGBT. Although still a unidirectional device, when paired with an identical device the resulting bi-directional switch has the same characteristics as the existing anti-parallel configurations. An additional benefit of the RB-IGBT is that conduction loss is reduced due to the saturation voltage of the combined part being less than the sum of a conventional IGBT saturation voltage and series connected diode forward voltage [56].

The Monolithic Bi-directional Switch (MBS) is a novel power device that achieves true switch bi-directionality with similar gate drive characteristics to an IGBT but with two gate inputs to allow directional current control [57]. The MBS, however, remains an experimental device and although its suitability for matrix converter application has been demonstrated, further development is necessary [64].

Looking further into the future, silicon may eventually be replaced entirely in power electronic devices. Silicon Carbide has been proposed as a viable alternative with the potential for a greatly increased operating temperature of 300°C compared with 125°C for silicon, ideal for the power dense matrix converter [60]. Diamond based devices are also being researched with indications that loss could be reduced to less than 5% of those experienced with silicon [65]. These future advances should have a significant impact on matrix converter performance [63].

2.3.5 Integrated Modules

With the increase in effort to encourage matrix converter adoption, research is focused on the design of integrated modules. Examining the VSI market shows that many years of semiconductor development has resulted in power modules that integrate a large proportion of the power electronic devices into a single module [66]. This is advantageous as external wiring is simplified with consequential reductions in leakage inductance within a more compact drive. Additional components such as gate drives and voltage or current transducers can also be integrated to optimise converter dimensions even further.

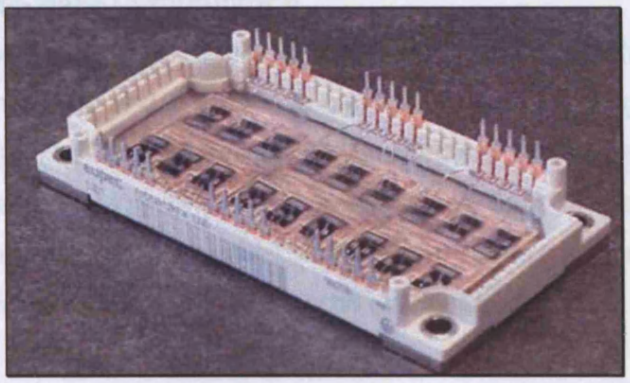

Figure 20 - Eupec Integrated Matrix Converter Module

Very recently, results have been published from the first integrated 7.5kW matrix converter module that utilises the common-collector switch topology [58]. The module, shown in Figure 20, integrates nine bi-directional switches with simplified connections and requires only six isolated power supplies for operation. The module design and manufacture is based on existing process technology and therefore full-scale production should not pose a problem [58].

Ultimately, development will focus on reducing conduction and switching loss to increase competitiveness with existing drive topologies. Although multiple step commutation strategies, as discussed later in Section 2.4, reduce switching loss significantly with increased reliability, advances in bi-directional switch design and performance appear possible.

The IGBT presently appears to be most suitable semiconductor switch for the matrix converter, although recent developments of reverse blocking capability and the MBS have promise for increases in power density and efficiency.

2.4 Switch Commutation

In a theoretical matrix converter, commutation from one switch to the next switch occurs instantaneously with perfect synchronisation, to maintain continuous input

voltage and continuous output current. In practice, however, this is difficult to achieve due to finite device switching times and the practical constraints of drive circuitry, with potentially damaging consequences when driving large inductive loads [67]. Reliable commutation is more difficult than in conventional voltage source inverters as there is no natural freewheeling path [60]. Two possible solutions are to operate using break-before-make or make-before-break commutation employing additional hardware to protect the converter switches for each mode of operation. However, reliable commutation can also be achieved using staggered strategies that reduce the need for such protective components.

2.4.1 Break-Before-Make Commutation

The break-before-make regime results in an open circuit when the outgoing switch opens before the incoming phase begins to conduct, as shown in Figure 21(a). Voltage transients caused by high di/dt at turn-off can exceed the blocking voltage capabilities of the IGBT or other switching device and cause failure, so a snubber circuit is usually required to limit the damaging transient voltage and protect the switching device by diverting the load current for the duration of the dwell period.

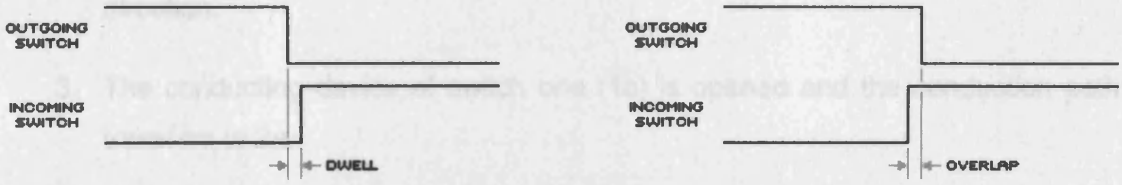

Figure 21 - (a) Break-before Make & (b) Make-before-Break Commutation

2.4.2 Make-Before-Break Commutation

Make-before-break commutation requires a brief overlap between switch conduction periods, as shown in Figure 21(b). As a consequence, the two supply lines are connected together during the overlap period causing a short circuit. Additional inductance can be added to the supply lines to limit the surge current that occurs during the overlap period.

2.4.3 Four-Step Commutation

The previous commutation techniques require additional passive components that both increase loss and prevent the matrix converter from being an ideal all-silicon system. A reliable solution to the commutation method has been proposed when employing the common emitter/collector switch topologies, where it is possible to control the direction of current flow [68]. The commutation is staggered between each set of bi-directional switches to maintain a continuous flow of current to the load while facilitating a safe transfer of operation [67].

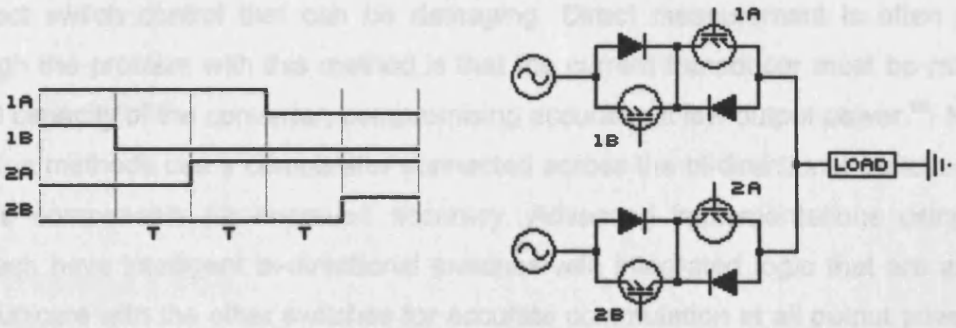

Figure 22 - Semi-soft current commutation sequence for Positive Load Current

Figure 22 shows two sets of anti-parallel bi-directional switches with switch one closed and switch two open. During switch commutation, the four unidirectional devices are operated independently with a fixed transition period between each commutation until the final state is reached [68]. The four-step sequence is as follows:

1. Commutation begins with the reverse-biased device of switch one (1b) opened as it carries no current.

2. The incoming forward-biased device of switch two (2a) is closed: no phase-to-phase short-circuit exists as both 1a and 2a are conducting in the same direction.

3. The conducting device of switch one (1a) is opened and the conduction path transfers to 2a.

4. The second device of switch two (2b) is then closed to complete the commutation.

With the staggered commutation strategy, each commutation involves either a hard turn-on and soft turn-off or a soft turn-on and hard turn-off, rather than a hard turn-on and hard turn-off, thus halving converter switching loss [60,67,68].

2.4.4 Two-Step Commutation

The two-step commutation strategy is very similar to the four-step version but eliminates the first and final commutations that serve no electrical purpose due to being reverse-biased and non-conducting [60]. In Figure 22 [p47], it is evident that both switch 1a and 2b are reverse-biased and therefore only the second and third steps are necessary. The result is that the commutation process is halved in length in addition to the reduction in gate drive activity.

The main requirement with these staggered commutation techniques is to select the appropriate switching sequence correctly, particularly during a current reversal. Accurate detection of the current direction is required to prevent errors leading to

incorrect switch control that can be damaging. Direct measurement is often used, although the problem with this method is that the current transducer must be rated to the full capacity of the converter, compromising accuracy at low output power [69]. Newer detection methods use a comparator connected across the bi-directional switches with passive components for improved accuracy. Advanced implementations using this approach have intelligent bi-directional switches with integrated logic that are able to communicate with the other switches for accurate commutation at all output powers [69]. An alternative detection technique tracks the relative magnitude of the supply voltages to select the appropriate staggered commutation sequence [70].

2.4.5 Three-Step Commutation

A recent development in staggered commutation has been the realisation that semiconductor devices generally turn-on more quickly than turn-off. This implies that the dwell time between the second and third commutations of the four-step strategy can be safely reduced to zero to create a three-step commutation strategy [62], see Figure 23. The intrinsic device switching characteristic reliably prevents a supply open-circuit. The same technique is equally valid with the two-step commutation strategy and leads to safe single step operation.

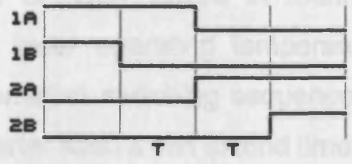

Figure 23 - Three-Step Commutation Strategy

The advantage of shortening the middle commutation step is a significant reduction in output current distortion. This is particularly evident with short device switching periods that approach the dwell duration, creating distortion similar to uncompensated dead-time in an inverter [62]. Eliminating the middle step yields an improvement in output current quality and this is particularly evident at low power levels [62,63].

2.4.6 Resonant Switching

Attempts have also been made to apply resonance to the matrix converter to achieve zero voltage switching and eliminate switching loss entirely. Various topologies have been proposed, with most requiring complex and limiting control strategies with an increased number of components that increase overall conduction loss [71]. Two main categories of resonant matrix converters exist: the soft switched cell that includes resonant elements in each bi-directional switch with greatly increased component count and conduction loss and the auxiliary resonant circuit that adds resonant components to each converter output phase to induce zero voltage or current commutation. The auxiliary resonant circuits do not incur as great a component penalty

as the soft-switched cells and the resonant components are only active during commutation, limiting the impact on conduction loss. Since commutation loss occurs primarily at high converter power outputs, efforts are currently focused on auxiliary circuits to allow standard operation at low power and then reduced loss at peak output. Recent efforts are reporting a potential reduction of commutation loss in excess of 30% [71].

2.5 Protection Issues

Power electronic devices are the vital component of any converter, so adequate protection against excessive voltage, current, temperature and rapid rates of change of these parameters must be provided to avoid permanent damage to the converter.

2.5.1 Device Over-Temperature Protection

Each conducting device in a circuit poses some degree of resistance to the flow of current. This loss is evident as heat generated in the device and, therefore, an adequate means of maintaining a safe operating temperature is necessary. When attached to the semiconductor device firmly using thermal compound, a heat-sink can passively dissipate heat to the surrounding air. In larger applications it is usually necessary to use forced convection rather than natural convection over the heat-sink to remove sufficient quantities of heat, with modern marine drives using seawater for cooling [72]. The main cause of IGBT failure in marine drives is thermal cycling. Overcoming this requires a lower operating temperature to ensure an acceptable component life, although alternative switching sequences that share the thermal load more evenly across the converter IGBTs can extend time between failures.

2.5.2 Device Protection

During commutation, the voltage and current across a semiconductor switch changes very quickly and this can sometimes exceed the safe parameters of the device. This situation can occur when using IGBT devices in a matrix converter, so it is usual to include some form of protection against this. A capacitor-resistor network can be used to protect a semiconductor switch against excessive rates of change of voltage (dv/dt), whereas inline saturable inductors can provide similar protection against excessive rates of change of current (di/dt) [72,73].

2.5.3 Over-Current Protection

Semiconductor switches typically fail in the on-state, leading to a risk of supply short-circuit at the next scheduled commutation. It is important for any supply short-circuit to be quickly interrupted, otherwise the entire converter could be irrevocably damaged. One solution is to install fast-acting fusible links on each input phase ahead of the converter so that in the event of an on-state failure, supply to the converter will be promptly interrupted. However, in a marine converter, it is more common to commutate the short in a failed device using the incoming switch.

2.5.4 Circuit Protection

A unique aspect of the matrix converter is that in the event of a fault the drive cannot be turned-off as the current still flowing in the load will cause a damagingly high-voltage transient. A common solution to this problem is to connect a diode-bridge across the converter input and output lines with an appropriately sized capacitor to absorb the energy stored in the load while protecting the maximum voltage rating of the devices. The capacitor is sized according to the leakage inductance in the electric motor, the hardware current and clamp voltage limits [74]. Bernet et al showed the matrix converter clamp capacitor to be approximately one-sixth of the size of the dc-link capacitor of a similar rated PWM drive [74]. A complete diode clamp protection system can now be inexpensively realised using a reconfigured standard dual three-phase diode-bridge module [75].

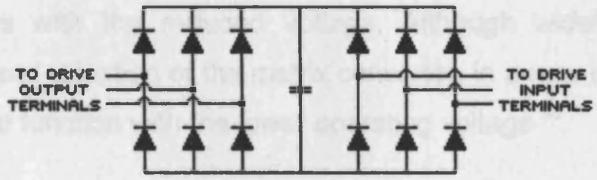

Figure 24 - Matrix Converter Clamp Protection

A rationalisation of the voltage clamp design allows only six diodes to provide the same level of protection by implementing a configuration that makes use of some of the bi-directional switch diodes as part of the clamp protection [76]. Although this proposed protection is valid for both diode-bridge and anti-parallel based matrix converters, it is more easily accommodated with the diode-bridge type drive as no alteration to the electrical circuit is necessary, as shown in Figure 25.

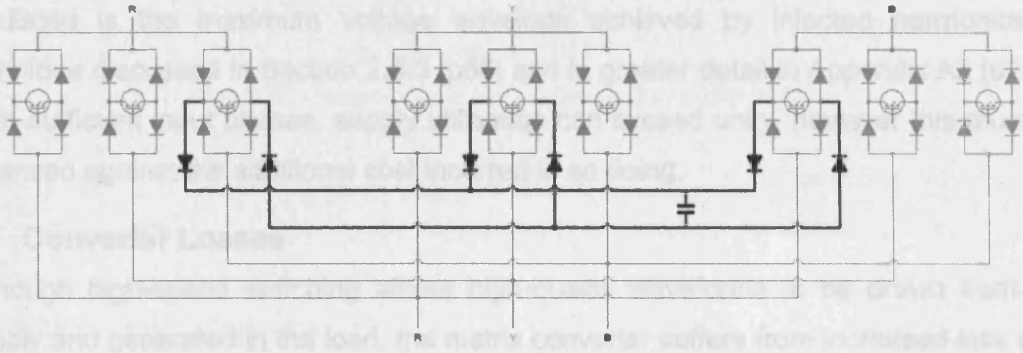

Figure 25 - Diode-Bridge Reduced Clamp Circuit

For the more advanced anti-parallel based topologies, it has been shown that a hybrid of both bi-directional switches could also use the reduced diode clamp topology [76]. The circuit requires three common-emitter type switches with the remainder being common-collector switches, although the drawback is the minimum number of isolated power supplies for gate drivers is increased from six to nine.

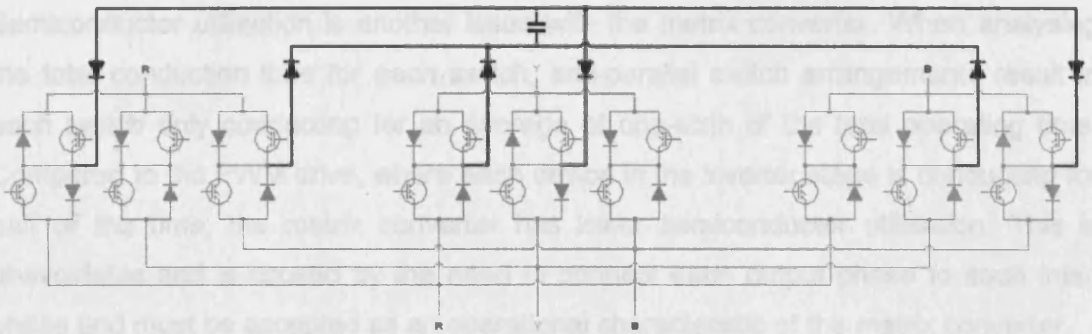

Figure 26 - Reduced Clamp Circuit for Anti-Parallel Switches

2.6 Voltage Transfer Limitation

The intrinsic maximum voltage transfer ratio for a three-phase input, three-phase output matrix converter is 86.6% irrespective of modulation strategy [52]. The matrix converter cannot therefore directly replace an existing drive unless the motor is modified to operate with the reduced voltage. Although widely perceived as an obstacle to widespread adoption of the matrix converter, in a new installation the motor could be designed to function with the lower operating voltage [55].

Input Phases	3	4	5	6
Unaltered Voltage Envelope	0.5	0.707	0.809	0.866
Enhanced Voltage Envelope	0.866	0.816	1.044	1.000

Table 5 - Variation in Matrix Converter Voltage Utilisation with Increasing Input Phases

In applications where this is unacceptable, installing extra input phases to the matrix converter, e.g. by using phase shifting or step-up transformers, can improve supply voltage utilisation. Table 5 illustrates the increase in the voltage envelope as the number of input phases to a three-phase output matrix converter is increased. Also tabulated is the maximum voltage envelope achieved by injected harmonics, a technique discussed in Section 2.8.3 [p56] and in greater detail in Appendix A2 [p249]. With sufficient input phases, supply utilisation can exceed unity, however this must be balanced against the additional cost incurred in so doing.

2.7 Converter Losses

Although high-speed switching allows high-quality waveforms to be drawn from the supply and generated in the load, the matrix converter suffers from increased loss over existing variable speed drives. Losses at a similar switching frequency may be higher due to the converter requiring three device commutations (one for each input phase) for each output phase, compared with only two commutations for the equivalent PWM drive. As the number of input phases increases, it is evident that drive commutation loss will increase at the same rate. The diode rectifier of the PWM drive contributes little towards total loss and the PWM drive may, therefore, be more efficient than the matrix converter [77].

Semiconductor utilisation is another issue with the matrix converter. When analysing the total conduction time for each switch, anti-parallel switch arrangements result in each switch only conducting for an average of one-sixth of the total operating time. Compared to the PWM drive, where each device in the inverter stage is conducting for half of the time, the matrix converter has lower semiconductor utilisation. This is unavoidable and is caused by the need to connect each output phase to each input phase and must be accepted as an operational characteristic of the matrix converter.

The various approaches to realising the bi-directional switch also contribute to increased conduction loss as the combined voltage drop of multiple devices becomes significant. Future developments in semiconductor technology may yield a lower loss integrated device more suited to matrix converter application.

2.8 Matrix Converter Modulation Theory

2.8.1 Waveform Synthesis

The matrix converter is based upon a set of bi-directional switches that can be configured to connect any input phase to any output line. The following theoretical analysis assumes the switches to operate instantaneously with no resistance when closed and infinite resistance when open. Although any number of input and output phases can be accommodated, it is clearer to demonstrate the operation of the matrix converter considering a three-phase input, single-phase output converter as shown in Figure 27.

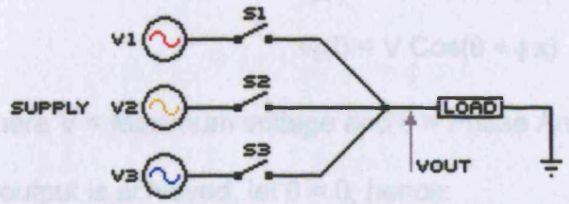

Figure 27 - Single-Phase Output Matrix Converter Diagram

Each of the three switches S_1, S_2, S_3 can be closed to conduct each supply phase to the load for periods of T_1, T_2, T_3 respectively. To satisfy the following relationship, where SWF is the switching frequency of the converter and T_{seq} is the sum of the conducting period sequence:

$$T_1 + T_2 + T_3 = T_{seq} = \frac{1}{SWF}$$

Figure 28 - Matrix Converter Switching Sequence

An important condition is that only one switch per output phase can be closed at any time to prevent supply short-circuits. The matrix converter is connected to an equally

spaced, fixed-frequency and amplitude, three-phase balanced AC supply. This can be represented as a phasor diagram, shown in Figure 29.

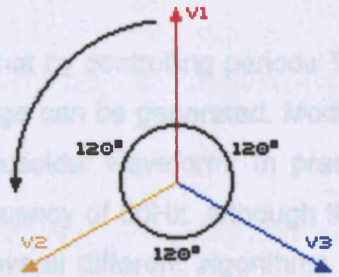

Figure 29 - Three-Phase Supply Phasor Representation Diagram

The length of each phasor represents the amplitude of the input phase voltage. The angle between each phasor is fixed at 120°. The phasors rotate together fifty times a second for a 50Hz supply. In a sufficiently short period of time, T_{seq}, the phasors can be considered to be stationary. The converter output voltage is the average of the three input segments multiplied by the conduction period of each switch:

$$V_o(t) = \frac{\nu_1(t)T_1 + \nu_2(t)T_2 + \nu_3(t)T_3}{T_{seq}}$$

Equation 1

The instantaneous amplitude of the supply voltages may be described as:

$$\nu_1(t) = V\,\mathrm{Cos}(\theta)$$

$$\nu_2(t) = V\,\mathrm{Cos}(\theta + \tfrac{2}{3}\pi)$$

$$\nu_3(t) = V\,\mathrm{Cos}(\theta + \tfrac{4}{3}\pi)$$

Where V = Maximum voltage and θ = Phase Angle

To illustrate how the output is achieved, let θ = 0, hence:

$$\nu_1(t) = V$$

$$\nu_2(t) = -½V$$

$$\nu_3(t) = -½V$$

Assuming the switches are closed for an equal period ($T_1 = T_2 = T_3$), the resultant mean output is:

$$V_{O\,AVE} = (V)⅓ - (½V)⅓ - (½V)⅓ = 0$$

The output is zero because the contributions of each phase are equal and over the period T_{seq}, they will sum to cancel each other out. If T_1 is increased to ½ and T_2 and T_3 are reduced to ¼, the mean output voltage becomes:

$$V_o(t) = (V)½ - (½V)¼ - (½V)¼ = ½V$$

Similarly, if T_2 and T_3 are increased to $\frac{3}{8}$ and T_1 is reduced to $\frac{1}{4}$, the mean output becomes:

$$V_o(t) = (V)\frac{1}{4} - (\frac{1}{2}V)\frac{3}{8} - (\frac{1}{2}V)\frac{3}{8} = -\frac{1}{8}V$$

It has therefore been shown that by controlling periods T_1, T_2 & T_3, both a positive and negative average output voltage can be generated. Modulation of the output voltage is then used to generate a sinusoidal waveform. In practice, the supply amplitude is continually changing at a frequency of 50Hz. Although this complicates the calculation of the conduction periods, several different algorithms have been formulated for the correct calculation of these values.

2.8.2 Original Venturini Control Strategy

Venturini & Alesina proposed their control strategy in 1980 [6]. Their strategy allows the synthesis of three output waveforms by sequential piecewise sampling of a fixed frequency & amplitude supply. Equation 2 describes the input voltage (V_I) and current (I_I) and the output voltage (V_o) and current (I_o) relationship. These are:

$$[V_I] = V_I \begin{bmatrix} \cos(\omega_i t) \\ \cos(\omega_i t - \frac{2}{3}\pi) \\ \cos(\omega_i t - \frac{4}{3}\pi) \end{bmatrix} \qquad [I_I] = I_I \begin{bmatrix} \cos(\omega_i t - \phi_i) \\ \cos(\omega_i t - \phi_i - \frac{2}{3}\pi) \\ \cos(\omega_i t - \phi_i - \frac{4}{3}\pi) \end{bmatrix}$$

$$[V_o] = V_o \begin{bmatrix} \cos(\omega_o t) \\ \cos(\omega_o t - \frac{2}{3}\pi) \\ \cos(\omega_o t - \frac{4}{3}\pi) \end{bmatrix} \qquad [I_o] = I_o \begin{bmatrix} \cos(\omega_o t - \phi_o) \\ \cos(\omega_o t - \phi_o - \frac{2}{3}\pi) \\ \cos(\omega_o t - \phi_o - \frac{4}{3}\pi) \end{bmatrix}$$

Equation 2

V_I & V_o = Input & output voltages

I_I & I_o = Input & output currents

ϕ_I & ϕ_o = input & output displacement angles

ω_i & ω_o = input & output frequencies

The general relationships between input and output voltage and input and output current are described by [6]:

$$[V_o] = [M_{(t)}]\,[V_I] \quad \& \quad [I_I] = [M_{(t)}]^T\,[I_o]$$

$[M_{(t)}]^T$ represents the transpose of the modulation matrix and these statements remain true only if the matrix identity below holds true [78,79]:

$$[M_{(t)}] \cdot 1 = 1 \quad \& \quad 0 < M_{(t)} < 1$$

Equation 3

Assuming a lossless converter, the power entering the converter must equal that leaving, thus:

$$V_I\, I_I \cos\phi_I = V_o\, I_o \cos\phi_o$$

Equation 4

Substituting Equation 2 into Equation 4 allows the two modulation matrices to be derived. The first solution to the modulation matrix, known as the symmetric modulator, operates the matrix converter with a lagging input displacement angle equal to the power factor of the load [6]. The second solution is known as the anti-symmetric modulator and operates the converter with a leading displacement angle to the power factor of the load [6].

Combining the two solutions together, the following modulation matrix $[M_{(t)}]$, Equation 5, is developed to allow control of the input displacement angle [6].

$$[M_{(t)}] = \left(\frac{\alpha_1}{3}\right)\begin{Bmatrix} 1+2qCS(0) & 1+2qCS(-\frac{2}{3}\pi) & 1+2qCS(-\frac{4}{3}\pi) \\ 1+2qCS(-\frac{4}{3}\pi) & 1+2qCS(0) & 1+2qCS(-\frac{2}{3}\pi) \\ 1+2qCS(-\frac{2}{3}\pi) & 1+2qCS(-\frac{4}{3}\pi) & 1+2qCS(0) \end{Bmatrix} +$$

$$\left(\frac{\alpha_2}{3}\right)\begin{Bmatrix} 1+2qCA(0) & 1+2qCA(-\frac{2}{3}\pi) & 1+2qCA(-\frac{4}{3}\pi) \\ 1+2qCA(-\frac{2}{3}\pi) & 1+2qCA(-\frac{4}{3}\pi) & 1+2qCA(0) \\ 1+2qCA(-\frac{4}{3}\pi) & 1+2qCA(0) & 1+2qCA(-\frac{2}{3}\pi) \end{Bmatrix}$$

Equation 5

Where:

$CS(x) = Cos(\omega_m t + x)$ $\quad CA(x) = Cos[-(\omega_m + 2\omega_I)t + x]$ $\quad \omega_m = \omega_o - \omega_I$

$\alpha_1 = ½ (1 + Tan\ \phi_I\ Cot\ \phi_o)$ $\quad \alpha_2 = 1 - \alpha_1$ $\quad \alpha_1 , \alpha_2 \geq 0$

$q = V_o / V_I$ $\quad 0 \leq q \leq ½$ = output amplitude

The modulation matrix $[M_{(t)}]$ is used to calculate the period each switch is closed. This modulation technique exhibits an input-output voltage gain of 50%, as shown in Figure 30. The red line shows the maximum possible amplitude of the output waveform when constrained by the shaded fully bound region. The fully bound region is limited to 50% of the three-phase supply, shown in grey, resulting in the converter load receiving a lower waveform amplitude than is usual with existing drives.

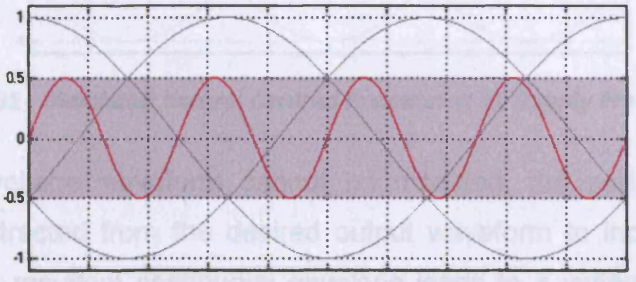

Figure 30 - Simulated Three-Phase Matrix Converter 50% Output Voltage Envelope

2.8.3 Advanced Venturini Control Strategy

Later work by Venturini & Alesina found that the theoretical maximum output voltage of a three-phase matrix converter could be increased to 86.6% of the supply and subsequently developed their advanced control strategy in 1988 [52]. Two techniques were used to increase the voltage transfer ratio.

The entire area bounded by the three-phase supply waveform is shown in Figure 31. For an odd phased system, the maximum and minimum voltages that constrain the fully bound region do not occur simultaneously, indicating that the available voltage range is not optimised.

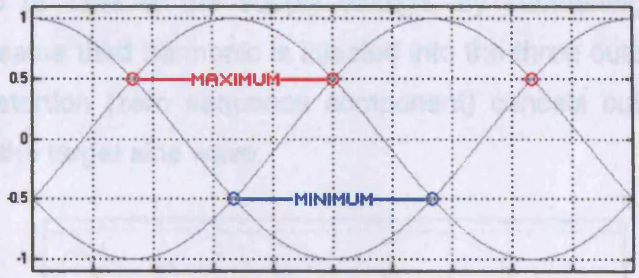

Figure 31 - Simulated Maximum & Minimum Voltage Constraints

The available voltage envelope can therefore be increased by referencing the load to a neutral centred function at three times the supply frequency, i.e. 3rd harmonic as shown in Figure 32. The amplitude of this harmonic is equal to the input range offset at maximum and minimum voltage, this being 25% of the supply voltage. Its form is:

$$F(t) = -(¼)V_i\cos(3\omega_i t)$$

Equation 6

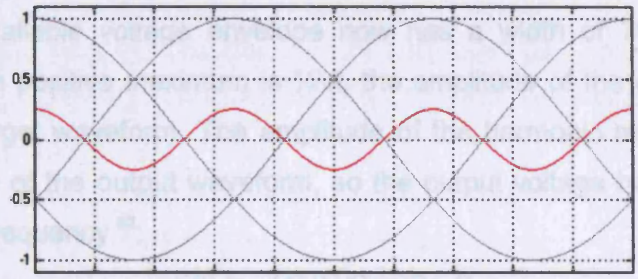

Figure 32 - Simulated Neutral Centred Function at 3X Supply Frequency

Since the input voltage waveform cannot be modified, the periodic waveform of Equation 6 is subtracted from the desired output waveform to increase the voltage transfer ratio. The resultant continuous envelope leads to a voltage transfer ratio of 75% and is shown in Figure 33 as the shaded region.

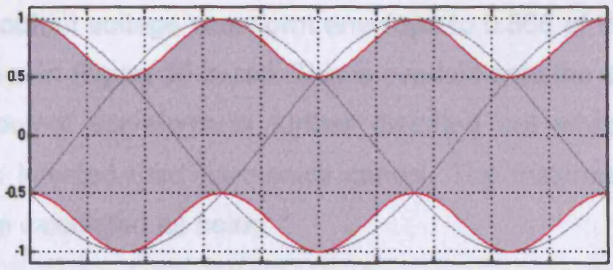

Figure 33 - Simulated Converter Output Voltage Envelope Increased to 75%

The shaded region shows the increased available output voltage range overlaid on the three-phase supply waveforms. The addition of the third harmonic allows the maximum and minimum input voltage to be reached thus increasing the continuously available output voltage range to 75%. Figure 34 shows how the target output waveform (in red) can be increased to 75% of the supply voltage, by subtracting the supply third harmonic. As the same third harmonic is injected into the three output waveforms, the common-mode distortion (zero sequence component) cancels out in a three-phase load to leave only the target sine wave.

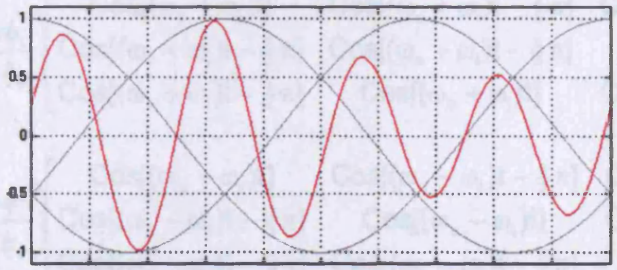

Figure 34 - Simulated Target Waveform Increased to 75% with Added Supply 3rd Harmonic

When this technique of third harmonic modulation is applied to the output waveform, the maximum and minimum bound points are not coincident, proving the voltage range is not optimised. A common mode at three times the target frequency is added to allow for greater amplitude output phase-to-phase differences to fit into the available input range. As the available voltage envelope now has a width of 75%, 25% remains unused. Since the positive maximum is ¾Vi, the amplitude of the output harmonic is 16.67% of the target waveform. The amplitude of the harmonic must be negative to lower the maxima of the output waveform, so the output voltage harmonic is at three times the output frequency [52]:

$$F(t) = -(\tfrac{1}{6})V_o\cos(3\omega_o t)$$

Equation 7

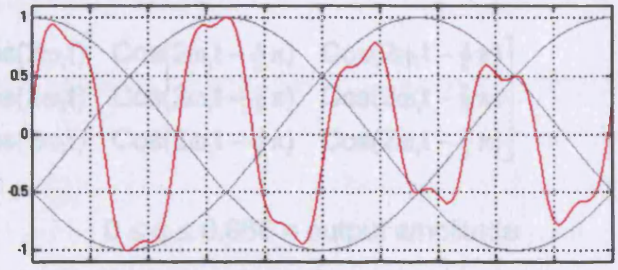

Figure 35 - Simulated Target Waveform Maximised using Supply & Output 3rd Harmonics

This increases the output voltage waveform envelope to 0.866 of the maximum output phase voltage, shown in Figure 35 in red. This is overlaid onto the supply waveforms in grey. The target output waveform is further distorted but when combined in the converter load, the injected third harmonics cancel. The maximum possible voltage transfer ratio can be calculated as being:

$$\frac{V_o}{V_i} = \frac{0.75}{0.866} = 0.866$$

The target output waveform can now be described by:

$$[V_o] = \begin{bmatrix} V_o\text{Cos}(\omega_o t) + \frac{1}{4}V_i\text{Cos}(3\omega_i t) - \frac{1}{6}V_o\text{Cos}(3\omega_o t) \\ V_o\text{Cos}(\omega_o t - \frac{2}{3}\pi) + \frac{1}{4}V_i\text{Cos}(3\omega_i t) - \frac{1}{6}V_o\text{Cos}(3\omega_o t) \\ V_o\text{Cos}(\omega_o t - \frac{4}{3}\pi) + \frac{1}{4}V_i\text{Cos}(3\omega_i t) - \frac{1}{6}V_o\text{Cos}(3\omega_o t) \end{bmatrix}$$

Equation 8

The solution of the resultant modulation matrix $[M_{(t)}]$ is found as [52]:

$$[M_{(t)}] = \frac{1}{3} + \frac{q}{3}\left(1 - \frac{\tan\phi_i}{\tan\phi_o}\right)\begin{bmatrix} \text{Cos}[(\omega_o + \omega_i)t] & \text{Cos}[(\omega_o + \omega_i)t - \frac{2}{3}\pi] & \text{Cos}[(\omega_o + \omega_i)t - \frac{4}{3}\pi] \\ \text{Cos}[(\omega_o + \omega_i)t - \frac{2}{3}\pi] & \text{Cos}[(\omega_o + \omega_i)t - \frac{4}{3}\pi] & \text{Cos}[(\omega_o + \omega_i)t] \\ \text{Cos}[(\omega_o + \omega_i)t - \frac{4}{3}\pi] & \text{Cos}[(\omega_o + \omega_i)t] & \text{Cos}[(\omega_o + \omega_i)t - \frac{2}{3}\pi] \end{bmatrix}$$

$$+ \frac{q}{3}\left(1 + \frac{\tan\phi_i}{\tan\phi_o}\right)\begin{bmatrix} \text{Cos}[(\omega_o - \omega_i)t] & \text{Cos}[(\omega_o - \omega_i)t - \frac{4}{3}\pi] & \text{Cos}[(\omega_o - \omega_i)t - \frac{2}{3}\pi] \\ \text{Cos}[(\omega_o - \omega_i)t - \frac{2}{3}\pi] & \text{Cos}[(\omega_o - \omega_i)t] & \text{Cos}[(\omega_o - \omega_i)t - \frac{4}{3}\pi] \\ \text{Cos}[(\omega_o - \omega_i)t - \frac{4}{3}\pi] & \text{Cos}[(\omega_o - \omega_i)t - \frac{2}{3}\pi] & \text{Cos}[(\omega_o - \omega_i)t] \end{bmatrix}$$

$$- \frac{q}{18}\begin{bmatrix} \text{Cos}[(3\omega_o + \omega_i)t] & \text{Cos}[(3\omega_o + \omega_i)t - \frac{2}{3}\pi] & \text{Cos}[(3\omega_o + \omega_i)t - \frac{4}{3}\pi] \\ \text{Cos}[(3\omega_o + \omega_i)t] & \text{Cos}[(3\omega_o + \omega_i)t - \frac{2}{3}\pi] & \text{Cos}[(3\omega_o + \omega_i)t - \frac{4}{3}\pi] \\ \text{Cos}[(3\omega_o + \omega_i)t] & \text{Cos}[(3\omega_o + \omega_i)t - \frac{2}{3}\pi] & \text{Cos}[(3\omega_o + \omega_i)t - \frac{4}{3}\pi] \end{bmatrix}$$

$$- \frac{q}{18}\begin{bmatrix} \text{Cos}[(3\omega_o - \omega_i)t] & \text{Cos}[(3\omega_o - \omega_i)t - \frac{4}{3}\pi] & \text{Cos}[(3\omega_o - \omega_i)t - \frac{2}{3}\pi] \\ \text{Cos}[(3\omega_o - \omega_i)t] & \text{Cos}[(3\omega_o - \omega_i)t - \frac{4}{3}\pi] & \text{Cos}[(3\omega_o - \omega_i)t - \frac{2}{3}\pi] \\ \text{Cos}[(3\omega_o - \omega_i)t] & \text{Cos}[(3\omega_o - \omega_i)t - \frac{4}{3}\pi] & \text{Cos}[(3\omega_o - \omega_i)t - \frac{2}{3}\pi] \end{bmatrix}$$

$$- \frac{q}{18\sqrt{3}}\begin{bmatrix} \text{Cos}(4\omega_i t) & \text{Cos}(4\omega_i t - \frac{2}{3}\pi) & \text{Cos}(4\omega_i t - \frac{4}{3}\pi) \\ \text{Cos}(4\omega_i t) & \text{Cos}(4\omega_i t - \frac{2}{3}\pi) & \text{Cos}(4\omega_i t - \frac{4}{3}\pi) \\ \text{Cos}(4\omega_i t) & \text{Cos}(4\omega_i t - \frac{2}{3}\pi) & \text{Cos}(4\omega_i t - \frac{4}{3}\pi) \end{bmatrix}$$

$$+ \frac{7q}{18\sqrt{3}}\begin{bmatrix} \text{Cos}(2\omega_i t) & \text{Cos}(2\omega_i t - \frac{4}{3}\pi) & \text{Cos}(2\omega_i t - \frac{2}{3}\pi) \\ \text{Cos}(2\omega_i t) & \text{Cos}(2\omega_i t - \frac{4}{3}\pi) & \text{Cos}(2\omega_i t - \frac{2}{3}\pi) \\ \text{Cos}(2\omega_i t) & \text{Cos}(2\omega_i t - \frac{4}{3}\pi) & \text{Cos}(2\omega_i t - \frac{2}{3}\pi) \end{bmatrix}$$

Equation 9

$0 \le q \le 0.866$ = output amplitude

The advanced Venturini control strategy achieves the maximum converter voltage transfer ratio of 86.6%. However, due to the greater number of cosine functions, computation of the switching periods is lengthened, requiring three times as many cosine function calls compared to the original strategy.

2.8.4 Input Displacement Angle Control

When using the advanced Venturini control strategy, displacement angle control is dependent on the output amplitude 'q'. When altering the converter input displacement angle, it is important to avoid invalid switching conditions from taking place by reducing the converter output amplitude 'q' to ensure that each switching period respects the following constraint [52]:

$$0 \le T_{'XY'} \le 1$$

Equation 10

Equation 11 governs the maximum converter amplitude when implementing the advanced Venturini control algorithm, and is shown graphically in Figure 36.

$$2q\left[|\Theta|\left(1-\frac{\text{sgn}(p)}{\sqrt{3}}\right)+\left(\frac{\text{sgn}(p)}{\sqrt{3}}\right)\right] \le 1$$

Equation 11

where

$$p=\frac{2q}{\sqrt{3}}\left(1-|\Theta|\right) \quad , \quad \text{sgn}(p)=\{1 \text{ if } p \ge 0 \text{ or } -1 \text{ if } p<0\} \quad \& \quad \Theta=\frac{\tan\phi_i}{\tan\phi_o}$$

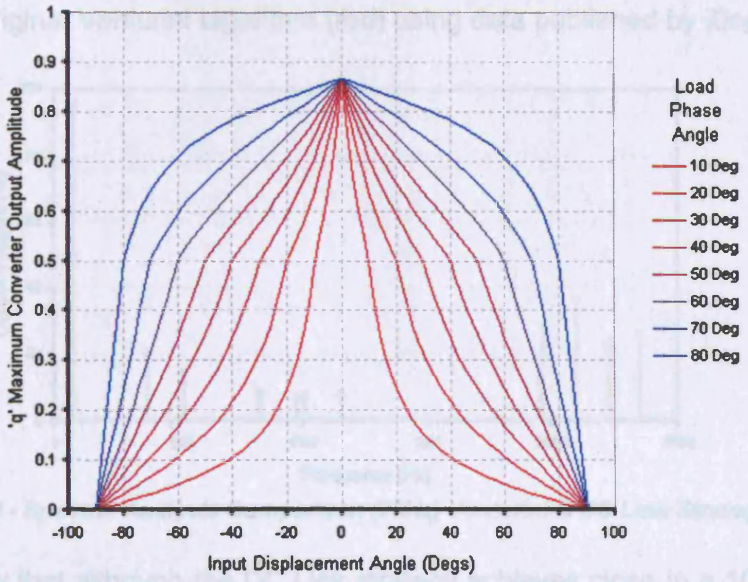

Figure 36 - Maximum Venturini Amplitude vs. Input Displacement & Load Phase Angles

Figure 36 shows the necessary reduction in 'q' as the input displacement or load phase angles change. Maximum supply utilisation is always achieved when operating with a desirable unity input displacement angle, irrespective of the load phase angle. The advanced Venturini control algorithm can therefore be simplified to provide a unity input displacement angle to maximise supply utilisation under all operating conditions.

2.8.5 Virtual DC-Link Strategy

The virtual DC-link strategy is an alternative control scheme for the matrix converter that imitates the rectification and inversion process of the PWM drive [80,81]. The first step is to continuously identify the input phases with the highest and lowest voltage amplitudes, effectively 'rectifying' the sinusoidal input to a quasi DC level, comparable to a six-pulse rectifier, as shown in Figure 37.

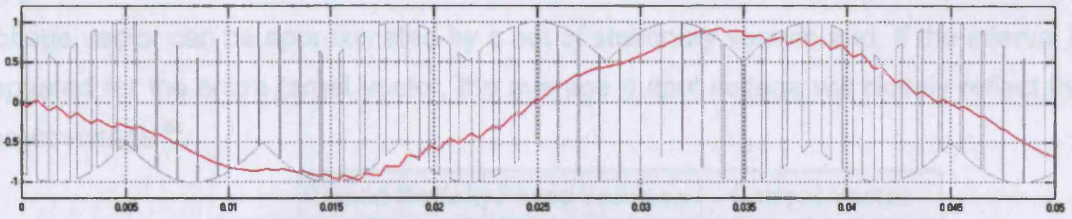

Figure 37 - Simulated Virtual DC-Link Rectification, Output Voltage & Current Waveforms

The second 'inversion' step employs standard PWM techniques to modulate the switch duty cycle and generate the target output waveform by switching between the instantaneous maximum and minimum input phases. Although the virtual DC-link strategy has the advantage of considerably reduced computational demands and can achieve a voltage transfer ratio in excess of unity (107%) with square output waveforms [81], it produces increased input and output waveform harmonics and continuous voltage and frequency control is difficult to achieve [82]. This is illustrated by Figure 38, that compares the output voltage frequency spectra of the DC link strategy (blue) with the original Venturini algorithm (red) using data published by Ziogas et al [80].

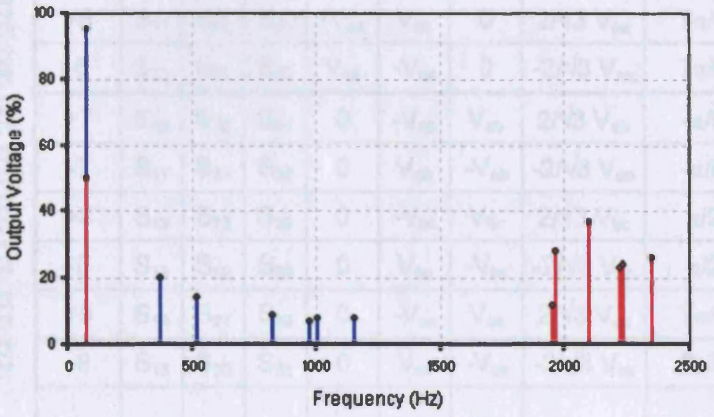

Figure 38 - Spectral Analysis Comparison (75Hz) Venturini & DC Link Strategies

The results show that although the DC Link strategy achieves close to a 100% voltage transfer ratio at the target output frequency of 75Hz, harmonics are produced close to this frequency, making filtering difficult. However, the Venturini strategy produces a large gap between the target frequency and the switching harmonics, and therefore the DC Link strategy is now seldom used where importance is placed on waveform quality. Furthermore, the output frequency with this control strategy is limited to under 200Hz [80].

2.8.6 Space Vector Modulation

Space Vector Modulation (SVM) offers comparable performance to the advanced Venturini strategy with an identical voltage transfer ratio of 86.6% and input displacement angle control but with reduced computation requirements [83]. Similar to the virtual DC-link PWM strategy, SVM identifies the maximum instantaneous phase voltage but then applies an innovative modulation strategy to generate the desired output waveform. The method assumes that, for a suitable short interval, the target voltage vector can be approximated by a set of stationary vectors and, if the interval is repeated for the entire target vector, the average output voltage will closely reflect the target voltage [84].

	Closed Switch			Phase Voltages			Current Vector	
Name	**P1**	**P2**	**P3**	**V_{AB}**	**V_{BC}**	**V_{CA}**	**Magnitude**	**Angle**
+1	S_{11}	S_{22}	S_{32}	V_{ab}	0	$-V_{ab}$	$2/\sqrt{3}\ V_{ab}$	$-\pi/6$
-1	S_{12}	S_{21}	S_{31}	$-V_{ab}$	0	V_{ab}	$-2/\sqrt{3}\ V_{ab}$	$-\pi/6$
+2	S_{12}	S_{23}	S_{33}	V_{bc}	0	$-V_{bc}$	$2/\sqrt{3}\ V_{bc}$	$\pi/2$
-2	S_{13}	S_{22}	S_{32}	$-V_{bc}$	0	V_{bc}	$-2/\sqrt{3}\ V_{bc}$	$\pi/2$
+3	S_{13}	S_{21}	S_{31}	V_{ca}	0	$-V_{ca}$	$2/\sqrt{3}\ V_{ca}$	$7\pi/6$
-3	S_{11}	S_{23}	S_{33}	$-V_{ca}$	0	V_{ca}	$-2/\sqrt{3}\ V_{ca}$	$7\pi/6$
+4	S_{12}	S_{21}	S_{32}	$-V_{ab}$	V_{ab}	0	$2/\sqrt{3}\ V_{ab}$	$-\pi/6$
-4	S_{11}	S_{22}	S_{31}	V_{ab}	$-V_{ab}$	0	$-2/\sqrt{3}\ V_{ab}$	$-\pi/6$
+5	S_{13}	S_{22}	S_{33}	$-V_{bc}$	V_{bc}	0	$2/\sqrt{3}\ V_{bc}$	$\pi/2$
-5	S_{12}	S_{23}	S_{32}	V_{bc}	$-V_{bc}$	0	$-2/\sqrt{3}\ V_{bc}$	$\pi/2$
+6	S_{11}	S_{23}	S_{31}	$-V_{ca}$	V_{ca}	0	$2/\sqrt{3}\ V_{ca}$	$7\pi/6$
-6	S_{13}	S_{21}	S_{33}	V_{ca}	$-V_{ca}$	0	$-2/\sqrt{3}\ V_{ca}$	$7\pi/6$
+7	S_{12}	S_{22}	S_{31}	0	$-V_{ab}$	V_{ab}	$2/\sqrt{3}\ V_{ab}$	$-\pi/6$
-7	S_{11}	S_{21}	S_{32}	0	V_{ab}	$-V_{ab}$	$-2/\sqrt{3}\ V_{ab}$	$-\pi/6$
+8	S_{13}	S_{23}	S_{32}	0	$-V_{bc}$	V_{bc}	$2/\sqrt{3}\ V_{bc}$	$\pi/2$
-8	S_{12}	S_{22}	S_{33}	0	V_{bc}	$-V_{bc}$	$-2/\sqrt{3}\ V_{bc}$	$\pi/2$
+9	S_{11}	S_{21}	S_{33}	0	$-V_{ca}$	V_{ca}	$2/\sqrt{3}\ V_{ca}$	$7\pi/6$
-9	S_{13}	S_{23}	S_{31}	0	V_{ca}	$-V_{ca}$	$-2/\sqrt{3}\ V_{ca}$	$7\pi/6$
0A	S_{11}	S_{21}	S_{31}	0	0	0	0	0
0B	S_{12}	S_{22}	S_{32}	0	0	0	0	0
0C	S_{13}	S_{23}	S_{33}	0	0	0	0	0

Table 6 - SVM Valid Switch Combinations

Figure 17 [p37] shows a three-phase input, three-phase output matrix converter comprised of nine bi-directional switches. These allow connection of any input phase to any of the output phases. If only one switch per output phase is closed to avoid both

supply short-circuit and load open circuit conditions, there are 27 valid switch combinations. The first six of these combinations, each connecting a different input phase to each output phase, are not used as they produce non-zero output line voltages and variable voltage vector phase angles. The remaining 21 combinations can be divided into two groups, 18 with a single zero output line voltage and three that connect the output lines together. Table 6 shows the 21 valid switching combinations used by the SVM strategy as they provide a fixed voltage vector and phase angle. The first 18 switch combinations can be subdivided into three groups of six, each containing a zero voltage value at the same output phase. Although these vectors possess a constant phase angle and are known as stationary vectors, their magnitude varies with the input line-to-line voltage. The final three switch combinations result in zero line-to-line voltage and are therefore known as zero voltage vectors.

The switch combinations can assume one of seven discrete positions upon the complex plane. These are called the switching state vectors and are shown in the FCC hexagon diagram.

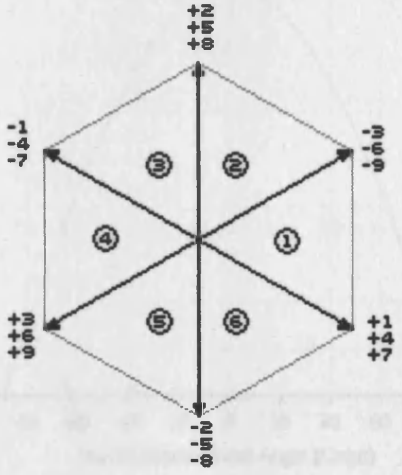

Figure 39 - FCC Hexagon Diagram

Each switching state vector can be reached using any one of six switch combinations. The two correct switching combinations are selected with knowledge of the highest instantaneous line voltage and the position of the reference vector in the FCC hexagon. The period of conduction for the selected switch combinations are calculated using Equation 12:

$$T_\alpha = \frac{2}{\sqrt{3}} \frac{V_r}{V_{env}} T_{seq} \sin(60° - \theta) \qquad T_\beta = \frac{2}{\sqrt{3}} \frac{V_r}{V_{env}} T_{seq} \sin(\theta) \qquad T_o = T_{seq} - T_\alpha - T_\beta$$

Equation 12

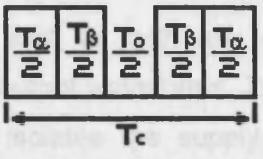

Figure 40 - SVM Switching Sequence

The first stage of the SVM is to determine the instantaneous maximum line voltage and the position of the reference vector within the FCC hexagon. This information is used to obtain two valid switch combinations. The switching periods are then calculated using measured values for the instantaneous voltage envelope.

When compared with the advanced Venturini modulation strategy, SVM offers a more simplified control of the converter input displacement angle, as only the desired input angle governs the maximum allowable output amplitude. The governing equation is:

$$0 \leq q_{max} \leq (\sqrt{3}/2 \text{ Cos } \phi_i)$$

Equation 13

Figure 41 shows the safe operating area for the SVM as the input displacement angle varies and demonstrates the independence of the load phase angle, unlike the Venturini [83].

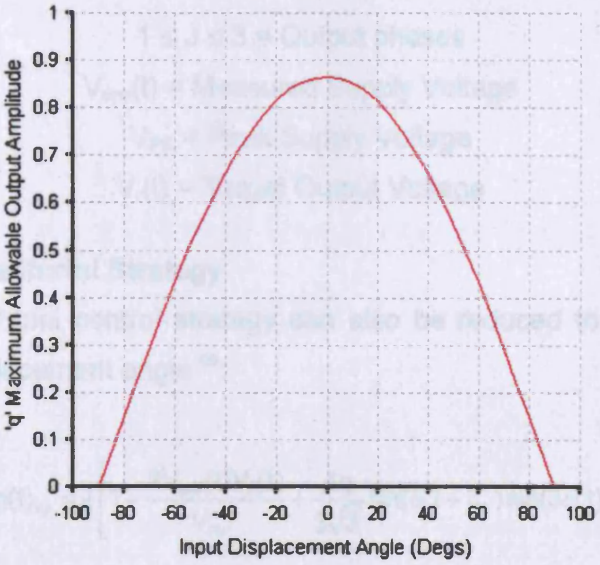

Figure 41 - SVM Maximum Amplitude vs. Input Displacement Angle

Several different versions of the SVM strategy have been developed that improve performance by reducing switching loss (by modelling the converter as two independent stages performing rectification and inversion) [85,86], increasing supply unbalance immunity [87,88] or allowing displacement angle control.

2.9 Closed Loop Control Implementation

The modulation algorithms described previously assume an ideal sinusoidal supply waveform. In practice this is unlikely to be the case since local electrical demand may degrade the supply waveform and, as with any direct AC-AC converter, supply distortion will be reflected in the output waveforms. The PWM drive has an advantage in this respect as the rectifier isolates the supply and eliminates synchronisation

requirements. However, the matrix converter is particularly susceptible to supply distortion and it is therefore desirable to implement a control strategy that can compensate for supply inadequacies and maintain the target output waveform.

2.9.1 Standard Venturini Strategy

The above Venturini regimes are unsuited to feedback implementation as they assume ideal sinusoidal supply waveforms, however alternative versions that track the supply voltage are available. In this case the matrix converter modulation may be described as [89]:

$$m(t)_{KJ} = \frac{1}{3}\left[1+\frac{2V_{env}(t)V_r(t)}{V_{PK}^{\ 2}}\right]$$

Equation 14

Where

m(t) = duty cycle

$1 \leq K \leq 3$ = Input phases

$1 \leq J \leq 3$ = Output phases

$V_{env}(t)$ = Measured Supply Voltage

V_{PK} = Peak Supply Voltage

$V_r(t)$ = Target Output Voltage

2.9.2 Advanced Venturini Strategy

The advanced Venturini control strategy can also be reduced to a similar algorithm with fixed unity displacement angle [89]:

$$m(t)_{KJ} = \frac{1}{3}\left[1+\frac{2V_{env}(t)V_r(t)}{V_{PK}^{\ 2}}+\frac{4q}{3\sqrt{3}}\sin(\omega_i t+\beta_K)\sin(3\omega_i t)\right]$$

Equation 15

Where

m(t) = duty cycle

$1 \leq K \leq 3$ = Input phases

$1 \leq J \leq 3$ = Output phases

$\beta_K = 0, 2\pi/3, 4\pi/3$ for K=1,2,3 respectively

The target output voltages are:

$$[V_o](t) = qV_{im}\begin{bmatrix} \cos(\omega_o t)+\frac{1}{2\sqrt{3}}\cos(3\omega_i t)-\frac{1}{6}\cos(3\omega_o t) \\ \cos(\omega_o t-\frac{2}{3}\pi)+\frac{1}{2\sqrt{3}}\cos(3\omega_i t)-\frac{1}{6}\cos(3\omega_o t) \\ \cos(\omega_o t-\frac{4}{3}\pi)+\frac{1}{2\sqrt{3}}\cos(3\omega_i t)-\frac{1}{6}\cos(3\omega_o t) \end{bmatrix}$$

Equation 16

Both these versions of the Venturini algorithms allow simplified operation of the matrix converter with a fixed unity displacement angle, whilst exhibiting the same supply utilisation. Although the target waveform must be generated externally from the modulation equation, this also allows modified output waveforms to be generated: for example a trapezoidal waveform for increased power transfer. The performance of these strategies was investigated using a computer model of the matrix converter. The results are shown in Figure 42 and Figure 43 below.

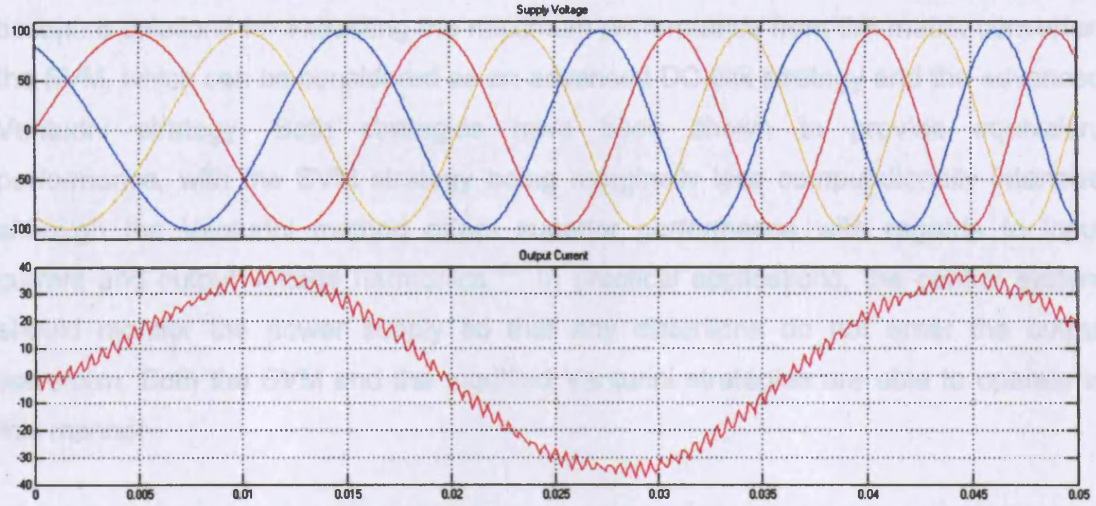

Figure 42 - The Effect of Supply Frequency Variation

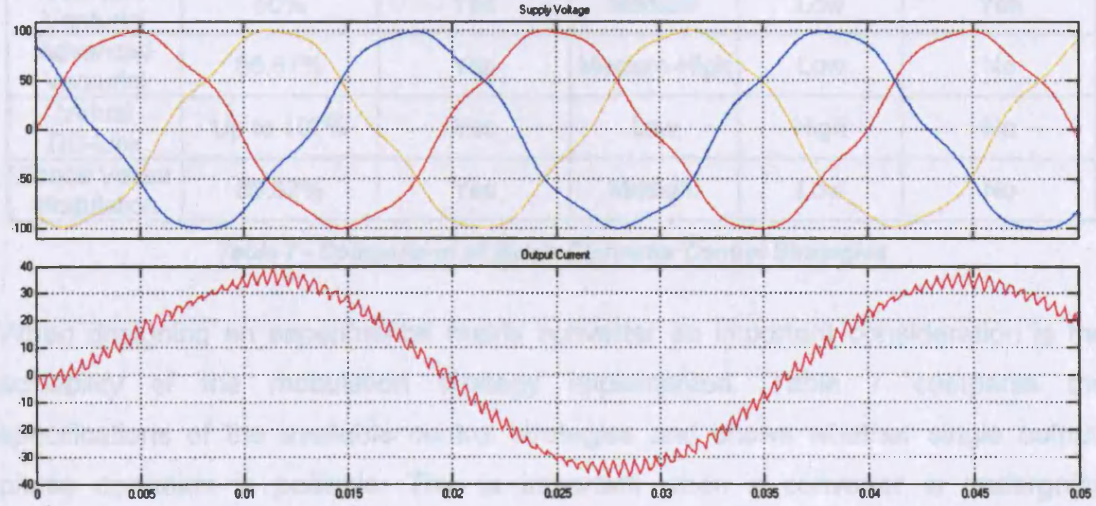

Figure 43 - The Effect of Supply Waveform Distortion

Figure 42 shows the effect of supply frequency variation and Figure 43 shows the result of supply distortion. The results demonstrate that by continuously tracking the instantaneous phase voltages, the control modulator can compensate for any distortion and maintain accurate synthesis of the target waveform. However, this supply voltage distortion correction is achieved at the cost of the input current waveform.

2.10 Conclusions

The literature survey demonstrated the matrix converter to be a very flexible topology, as demonstrated by the range of control regimes allowing safe operation. The virtual DC-link method suffers in comparison with the established Venturini and SVM control strategies by failing to fully exploit the potential of the matrix converter topology due to poor input and output waveform quality. The standard Venturini strategy allows full displacement angle correction in addition to sinusoidal input and output currents but suffers from an inferior voltage transfer ratio. Two control regimes have become accepted solutions for extracting the maximum performance from the matrix converter: the SVM, which can be considered as an advanced DC-link strategy and the advanced Venturini strategy. Both strategies have been shown to provide equivalent performance, with the SVM strategy being marginally less computationally intensive although the Venturini method offers superior performance with regards to input current and output voltage harmonics [83]. In practical applications, the control system should monitor the power supply so that any distortions do not enter the output waveform. Both the SVM and the modified Venturini strategies are able to operate in this manner.

Strategy	Voltage Transfer Ratio	Displacement Angle Control	Control Complexity	Harmonic Generation	Single Output Phase?
Standard Venturini	50%	Yes	Medium	Low	Yes
Advanced Venturini	86.67%	Yes	Medium-High	Low	No
Virtual DC-Link	Up to 107%	Yes	Low	High	No
Space Vector Modulation	86.67%	Yes	Medium	Low	No

Table 7 - Comparison of Matrix Converter Control Strategies

When designing an experimental matrix converter an important consideration is the scalability of the modulation strategy implemented. Table 7 compares the specifications of the available control strategies and shows whether single output-phase operation is possible. This is important when a converter is undergoing sustained design and development, where the electrical circuit is being assembled and tested. An additional problem is the development of the actual control system hardware and software: a complex control programme is easier to analyse and problems easier to trace and rectify when operating with a reduced number of semiconductor switches. In consideration of this, the Venturini control strategy represented the logical solution for the laboratory matrix converter. The standard strategy allows single-phase output operation during the initial development stage using the simplest algorithm without input displacement angle control. The anti-

symmetric modulator could subsequently be added to provide displacement angle control. Once development of the single-phase output system had been completed, testing would verify the design of the control system and hardware before completing the construction of the final two output phases. The working control strategy would then be extended to allow full three-phase output operation. At this point in development, the experience accumulated would allow addition of the third harmonics to the existing Venturini control strategy to increase the voltage transfer ratio from 50% to 87%. This solution, as shown in Figure 44, provides a clear and logical development path with design goals that facilitate construction of the electrical circuit.

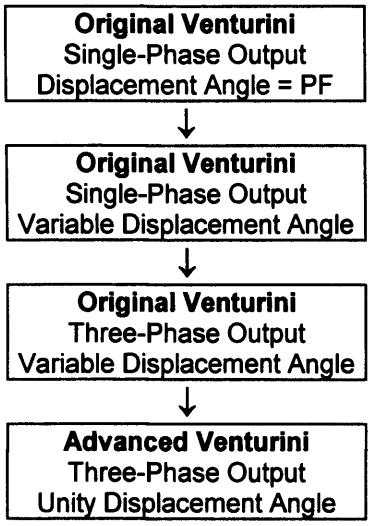

Figure 44 - Proposed Control System Development Path

Current commutation between input phases is a problem that requires careful consideration when designing a high power matrix converter, as additional hardware may be required to protect against over-current or short-circuit conditions. If the common-collector/emitter topology is used, advanced staggered commutation techniques allow safe and reliable commutation, a halving of switching loss and reduced conduction loss, as shown in Table 4 [p43]. This method of creating a bi-directional switch using unidirectional devices can be further refined with reverse-blocking devices, such as the RB-IGBT or IGCT, which reduce conduction loss and halve the total number of components. At present, this form of bi-directional switch appears to be the best solution until future refinement of the monolithic bi-directional switch (MBS) occurs. The MBS has the potential to represent the ideal bi-directional switch but should the development period be excessively lengthy, the conventional discrete solutions may have become established in the matrix converter market. This may be exacerbated by the present thrust to reduce drive dimensions by integrating an entire matrix converter into a single compact module for the low power drives market.

Unfortunately, the increased gate drive and control requirements make the anti-parallel switch configurations more complex and costly to implement for an initial experimental converter. A converter implementing anti-parallel bi-directional configurations requires double the number of gate control systems in addition to the complexity required to safely and reliably sequence each set of staggered commutations. It was therefore necessary to select the more rugged diode-bridge bi-directional switch configuration. Each switch has only one controllable device with a single gate drive circuit but, most importantly, this eliminates the need to develop a complex staggered commutation controller for each output phase. The diode-bridge effectively protects the semiconductor switch and an IGBT semiconductor switch results in a more rugged solution for development of the laboratory converter.

In summary, the design and assembly of a laboratory matrix converter would give a useful insight into matrix converter behaviour. The selection of the Venturini control strategies and the IGBT diode-bridge based circuit will minimise control system design costs and complexity and result in a rugged platform suitable for laboratory experimentation.

3. Chapter Three - Converter Hardware Design

3.1 Introduction

While several manufacturers, including Siemens, Rockwell & Yaskawa [60], have expressed their intent to launch low-power commercial drives, the matrix converter remains experimental. It was therefore necessary to design and construct a laboratory converter for practical testing and verification of computer models, as no off the shelf solution existed. A review of earlier matrix converter designs aided in the development of the laboratory drive, which emphasised ease of operation and repair. Although, the diode-bridge topology emerged as a suitable solution in the previous chapter, additional problems, including choice of semiconductor switch type, specification and protection issues required further consideration. Operation of the semiconductor switches also represented a challenge with the need to maximise switching speeds without compromising the reliability of the electronic circuits. Also considered was the design of an input filter to limit pollution of the supply with high frequency switching harmonics and to enable input current measurement. Control of the resulting power electronics required a high performance system to accurately implement an advanced modulation algorithm with a suitable user interface.

3.2 Power Circuit Considerations and Design

The matrix converter is composed of a number of switches that allow any input phase to be connected to any output phase. High-speed switching between input phases allows synthesis of a variable voltage and frequency output waveform. High numbers of input or output phases were therefore undesirable, as the additional complexity would present unnecessary obstacles to both power electronics and control system design. In view of the available electrical resources and control algorithm practicalities, a three-phase input, three-phase output configuration was selected with an emphasis on simplicity of design.

3.2.1 Requirements

The practical nature of the matrix converter necessitated a rationalisation of the electrical circuit to allow ease of assembly, maintenance and operation. A modular approach allowed incremental construction and testing of the power electronic circuits, the control system and associated software. During initial testing, the matrix converter may be operated incorrectly, so a rugged design that is easy to maintain would save considerable time in the event of a device failure. High-speed operation of the bi-directional switches would shorten the commutation time, reduce power loss and facilitate high frequency operation. The laboratory matrix converter has been designed with the following requirements:

- Rugged, reliable and modular design
- High-speed semiconductor devices
- Suitable protection of the electrical circuit
- Supply filter for quieter operation

3.2.2 Converter Specification

The main design requirement was to develop a matrix converter capable of driving a laboratory 10kVA induction machine, without excessive complexity. A review of prior investigations showed that although the anti-parallel bi-directional switch offers improved performance, it has a considerable cost and complexity penalty. Each bi-directional switch contains two active devices with independent gate drive circuits and control system supervision. The intended three-phase input, three-phase output configuration would require eighteen independent gate drivers, unnecessary complexity that could be avoided with the diode-bridge switch topology. Each bi-directional switch employs one semiconductor switch, halving converter complexity and was therefore selected for the laboratory matrix converter.

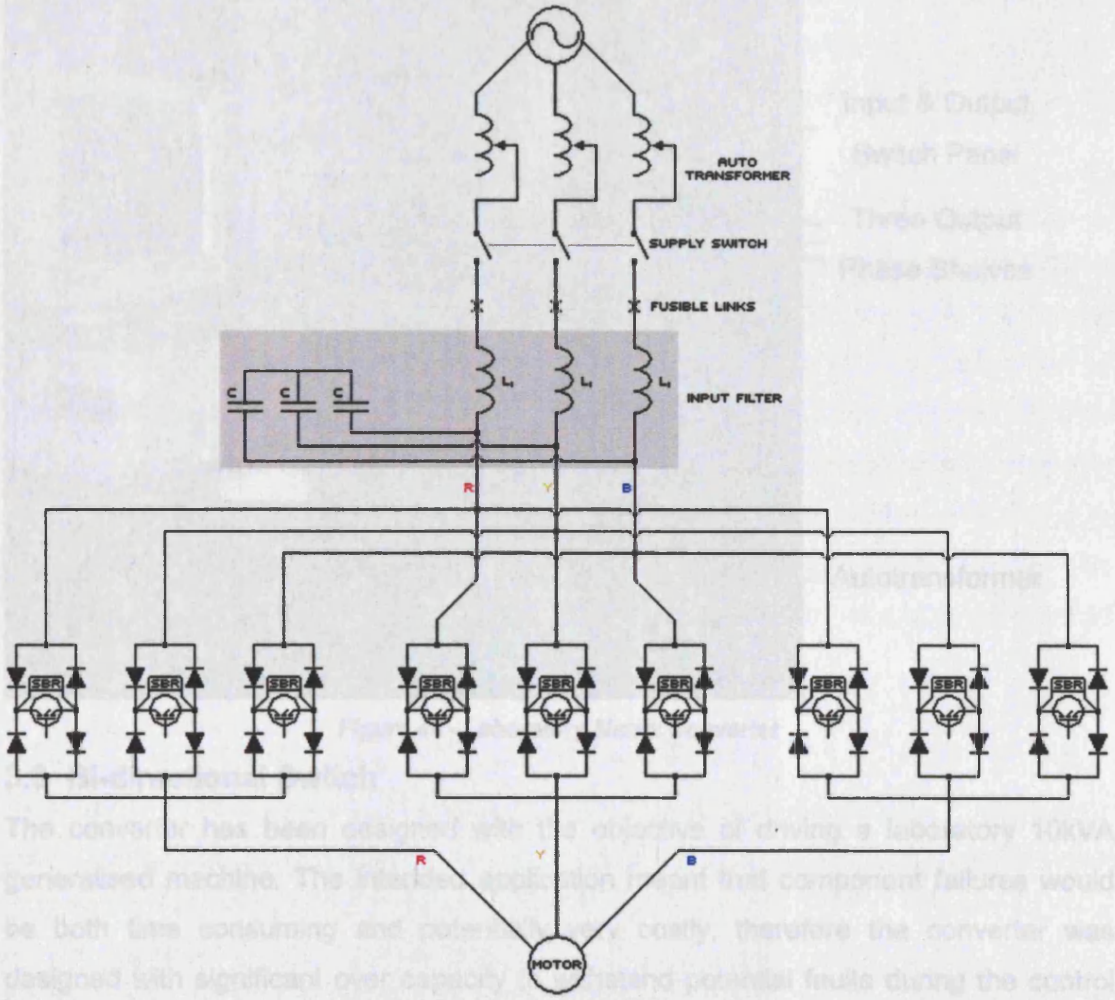

Figure 45 - Laboratory Matrix Converter Power Circuit

The matrix converter was designed so that each set of bi-directional switches was grouped together in banks of three. This simplified design and allowed individual banks to be tested in initial single-phase output matrix converter configurations. The layout is shown in Figure 45.

3.2.3 Converter Housing

The matrix converter has been assembled in a standard rack unit to facilitate transportation within the laboratory. A distribution block provides electricity to the independent converter power and control circuits. Converter instrumentation is described in Appendix A3 [p254].

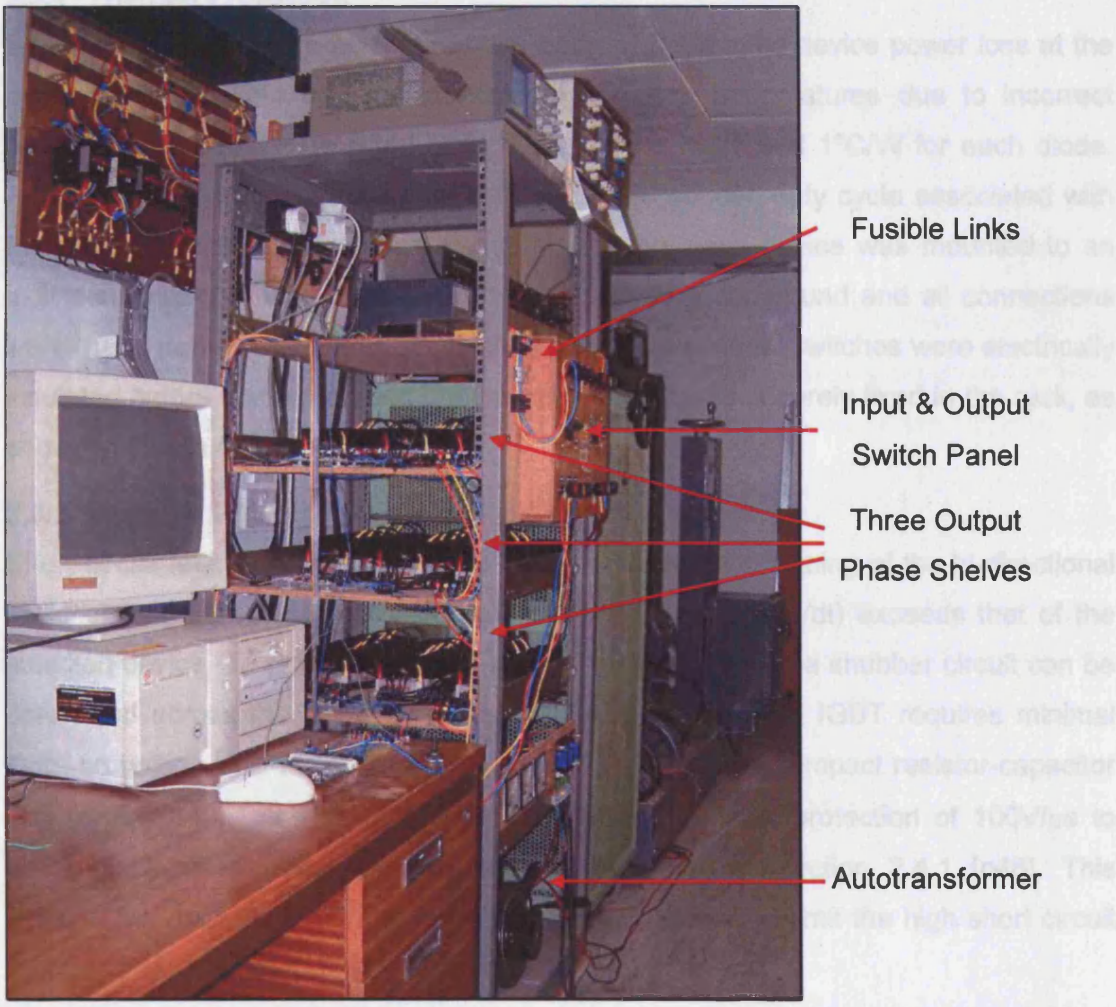

Figure 46 - Laboratory Matrix Converter

3.3 Bi-directional Switch

The converter has been designed with the objective of driving a laboratory 10kVA generalised machine. The intended application meant that component failures would be both time consuming and potentially very costly, therefore the converter was designed with significant over capacity to withstand potential faults during the control system development cycle. The diode-bridge bi-directional switch topology was selected in preference to the alternatives to simplify both hardware and control system

3.3.3 Gate Drive

To correctly operate an IGBT, the gate drive signal must be positively biased with respect to the IGBT emitter voltage, necessitating isolated or 'floating' supplies. The power supply provides a voltage above that at the IGBT emitter terminal. For the IGBT employed, a positive drive voltage of 15V was derived using isolated DC-DC converter modules (NMF0515s). The drive circuit uses the high-speed HCPL-3120 IGBT integrated circuit that also provides integral opto-isolation of the control signals [94], see Appendix A6 [p257] for datasheet. Additionally, to ensure the IGBT remained reliably off, the gate driver circuit applied a negative biased voltage, requiring a second DC-DC converter (NMF0505s) floating at 5V below the IGBT emitter terminal voltage.

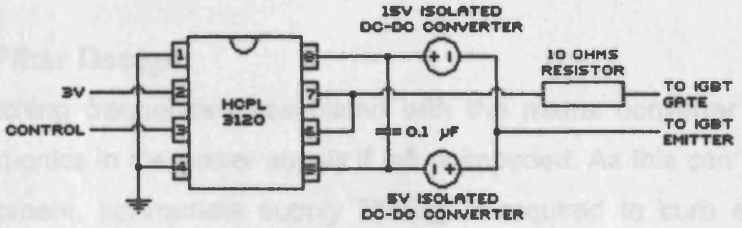

Figure 48 - IGBT Opto-Isolated Gate Driver Circuit

The gating circuit, shown in Figure 48, drives the IGBT at 15V above the emitter terminal voltage when closed and 5V below when opened. Suitable electrical isolation of the less robust low-voltage control system allowed direct connection between the control system and the gate drive circuit.

3.4 Power Supply

A three-phase 440V laboratory supply provided power for the matrix converter. Throughout the development process, an autotransformer was connected between the power supply and the matrix converter to provide reduced voltage for experimentation.

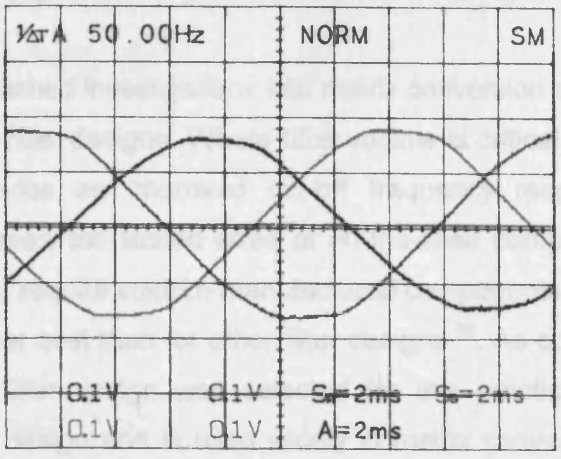

Figure 49 - Laboratory Three-phase Supply Waveform Unbalance & Distortion

During experimentation moderate distortion was evident in the power supply, visible as a flattening of the peaks and troughs of the waveform. This phenomenon was found to

be time related, being worst during standard working hours and attributed due to increased local computer usage. To counter this, a significant proportion of all investigations was performed during off-peak periods to limit outside influences. The visible supply offset was attributed to slight imperfections in the autotransformer.

3.4.1 Power Supply Protection

The risk of a switching device failure or wiring error necessitated suitable short-circuit protection for the power supply. A fusible link was inserted between each set of bi-directional switches and the supply autotransformer using quick-acting ceramic fuses, rated at 3.3 Amperes (i.e. de-rating for experimental procedures). This was found to sufficiently protected the power electronic devices during the investigation.

3.5 Supply Filter Design

The high switching frequencies associated with the matrix converter produce high frequency harmonics in the power supply if left unimpeded. As this can be detrimental for local equipment, appropriate supply filtering is required to curb excessive high frequency noise and maintain the quality of supply.

The main requirement for the practical supply filter was to allow safe operation of the laboratory matrix converter at switching frequencies of 4kHz and 6kHz. A filter resonant frequency of around 1.5kHz was therefore considered as being a compromise between reducing the risk of resonant excitation while avoiding excessively large component values. The supply filter was required to:

- Allow the fundamental supply waveform frequency to pass unimpeded
- Attenuate harmful high frequency harmonics from entering the supply

A review of other published investigations into matrix conversion showed that there is a wide range of supply filter designs. Where filter volume is critical, a second-order two-stage filter can provide an improved cut-off frequency response using smaller components [93]. However, the limited sizes of off-the-shelf components means that a two-stage design may require custom manufactured components to satisfy the design, contributing to a higher cost than for other filter designs [93]. As consequence, a single-stage second-order filter design was selected for this practical investigation as it represents a proven design and is used widely in matrix converter research [95,96,97,98]. This filter configuration is also less sensitive to component tolerance [93] and the lack of a tuned diversion path allows a wider range of converter switching frequencies to be employed [98].

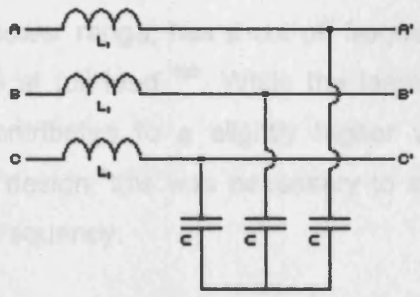

Figure 50 - Single-Stage Second-Order Low-Pass Filter

The equations governing the harmonic performance of a single-stage second-order filter were used to calculate the attenuation and the resonant frequency of various capacitor-inductor combinations [99]. Analysis of these equations showed that filter design is a series of compromises [100]:

- The filter voltage drop is proportional to the inductor value and must be minimised
- The capacitor value governs the filter power factor and must be carefully sized

With the resonant frequency known, the governing equations allowed a relationship between the inductor and capacitor values to be derived. The power factor of the proposed supply filter was then investigated. Maintaining a unity power factor was desirable to minimise converter disturbance and the capacitor was found to have a far greater influence on the filter power factor than the inductor. It was therefore necessary to minimise the capacitor size in relation to the inductor. However the voltage drop across the filter increases as the inductor grows, necessitating a trade off. An iterative design process, described in Appendix A7 [p258], was used to produce the following filter component values:

	Capacitor	Inductor
Author's Design	6μF	1.8mH
Huber et al [95]	5μF	2mH
Sunter et al [96]	8μF	-
Klumpner et al [97]	6μF	1.2mH
Casadei et al [100]	6μF	1mH

Table 8 - Proposed & Published Filter Component Values

The selected filter design is shown in Table 8 along with published filter specifications used by other matrix converter projects for comparison. In their design example of a supply filter, also for a 10kVA matrix converter switching at 5kHz, Casadei et al produced a very similar design [100]. The resulting filter maintains a power factor above

0.9 in 90% of the output power range, has a cut off frequency of approximately 2kHz and a voltage drop of 2% at full load [100]. While the larger inductor of the proposed laboratory supply filter contributes to a slightly higher voltage drop at full power compared to the Casadei design, this was necessary to allow operation at the lower 4kHz converter switching frequency.

To verify the design practically, the supply filter was bench tested to measure the voltage input-output characteristic across the frequency range when connected across a small 5Ω resistor. A high-power amplifier, driven by a function generator, provided sinusoidal excitation of the filter while measuring the output voltage to determine the voltage transfer ratio across the frequency range. The resulting filter response is shown in Figure 51, with the resonant frequency observed as 1.5kHz, as intended by the design.

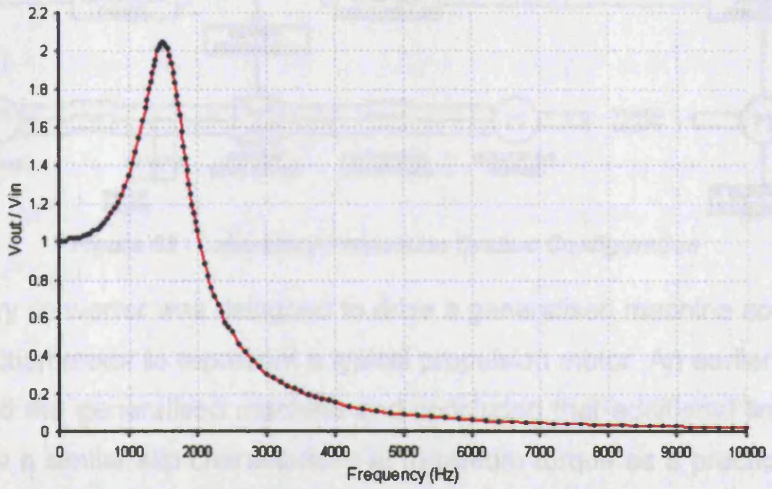

Figure 51 - Practical Supply Filter Measured Frequency Response

The supply filter was subsequently installed in the matrix converter rack and tested. The filter performed as expected and Figure 52 shows a comparison of the supply voltage and current waveforms before and after filter installation.

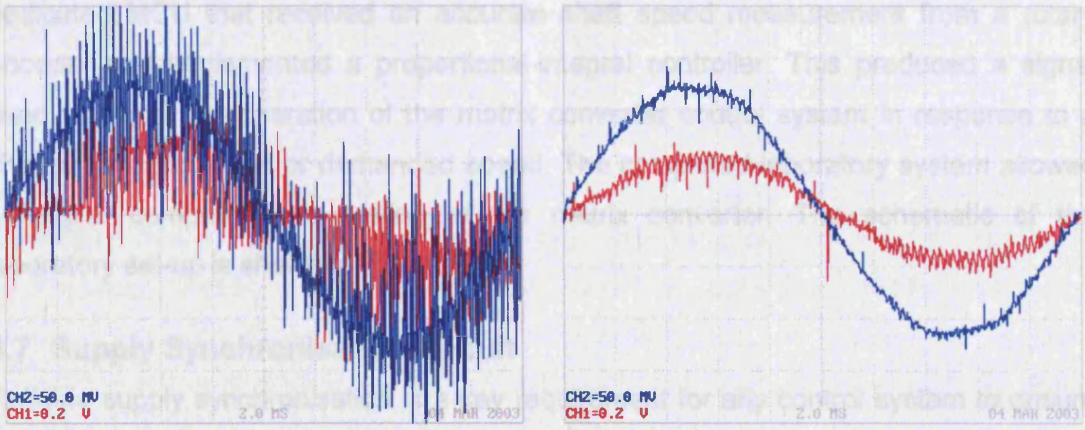

Figure 52 - Supply Voltage & Current (a) before & (b) after Installation of Filter

The supply current waveform, measured in front of the filter, was recognisably sinusoidal with greatly reduced harmonic content when compared to operation without the supply filter, although some ripple remained due to the design constraints of minimal power-factor variation and filter voltage drop. This allowed safe operation of the laboratory matrix converter and allowed measurement of the supply current waveforms.

3.6 Laboratory Propulsion System

The development of the laboratory matrix converter was performed using a simple static resistive/inductive load before progressing to a small induction motor. This eased the converter development process.

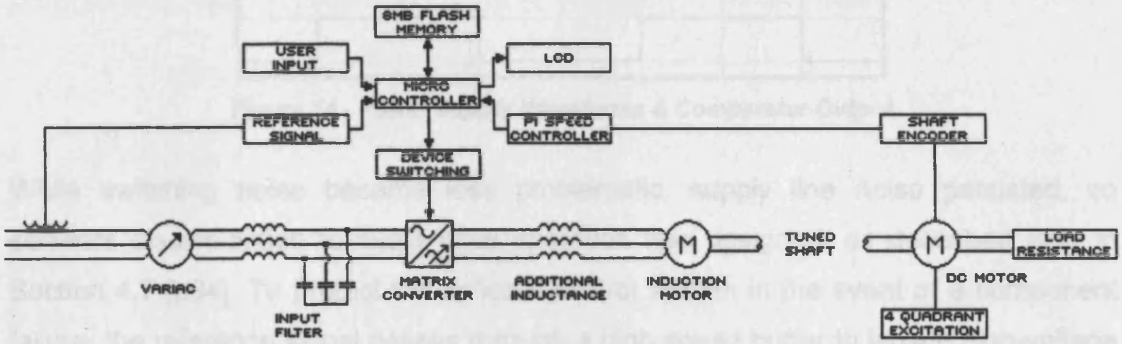

Figure 53 - Laboratory Propulsion System Configuration

The laboratory converter was designed to drive a generalised machine configured as a six-pole induction motor to represent a typical propulsion motor. An earlier investigation had examined the generalised machine and concluded that additional line inductance would provide a similar slip characteristic at maximum torque as a practical propulsion motor [7]. An aluminium shaft had also been designed and 'tuned' to provide realistic torsional characteristic of a practical system and connected the propulsion motor to a DC motor that acted as a 'load' to the propulsion motor [7]. The propulsion load could be varied by changing the static load on the DC motor, allowing simulation of a typical marine propulsion system. Motor speed control was achieved with the use of a dedicated MCU that received an accurate shaft speed measurement from a rotary encoder and implemented a proportional-integral controller. This produced a signal used to adjust the operation of the matrix converter control system in response to a change in shaft speed or demanded speed. The completed laboratory system allowed safe and comprehensive testing of the matrix converter. The schematic of the laboratory set-up is shown in Figure 53.

3.7 Supply Synchronisation Circuit

Reliable supply synchronisation is a key requirement for any control system to ensure correct operation of the power electronic devices. Supply synchronisation was initially

achieved by determining the instant when the Red input phase crossed the zero voltage threshold using a high-speed differential comparator (KA311) connected to the 'Red' phase. Although this proved adequate during initial testing, subsequent experiments found switching noise interfering with the threshold detection and resulted in unstable controller operation. The solution was to detect the crossing point between the 'Yellow' and 'Blue' input phases, see Figure 54.

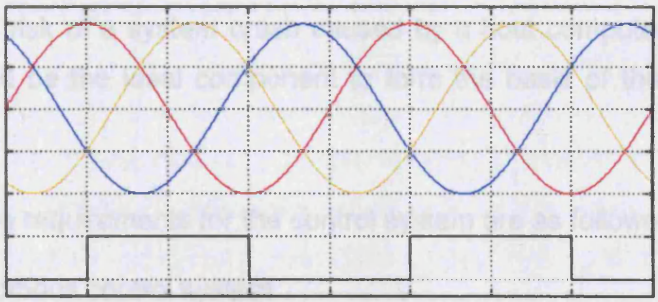

Figure 54 - Power Supply Waveforms & Comparator Output

While switching noise became less problematic, supply line noise persisted, so software discrimination to avoid false operation was designed, as described later in Section 4.7 [p94]. To protect the delicate control system in the event of a component failure, the reference signal passes through a high-speed buffer to isolate high-voltage and low-voltage circuits.

3.8 Control System

The control system is perhaps the key element of any power converter. Considerable effort was therefore focused on the matrix converter control system design. A previous investigation at UCL had highlighted the need for flexibility in the control system architecture [84]. It was therefore decided to design and build a dedicated standalone MCU based control system with bespoke control software to implement an advanced control strategy.

3.8.1 Requirements

The control system was designed to maximise flexibility and provide sufficient processing power to allow implementation of any of the advanced control strategies for future research. Although previous research projects had explored the matrix converter using limited control systems that operated at fixed frequencies with pre-calculated modulator results, this was entirely unsuited to driving an active load, such as a synchronous motor where shaft speed must be continually varied. Real-time computation was therefore crucial to this investigation. In addition to real-time operation, the control strategy should also allow fine user adjustment of the output frequency and voltage to allow smooth acceleration of the induction motor. Visual

feedback of the control system operating parameters would also be useful during operation. Additional protection against supply short-circuits, independent from the processor software, would prevent dangerous switching combinations from occurring. A wide range of switching frequencies is important to allow exploration of the matrix converter harmonic characteristics and the effect on the load.

The control system must be able to operate autonomously and contain its own control software to avoid risk of a system crash caused by a host computer. This suggested that a MCU would be the ideal component to form the basis of the matrix converter control system.

To summarise, the requirements for the control system are as follows:

- Autonomous control system
- Real-time operation
- Wide range of operating frequencies, 1 - 6kHz
- High switching resolution, <250ns
- Fine output frequency and amplitude control, <1Hz & q=1% of V_{in}
- Adaptive & selective supply synchronisation
- User interface to facilitate standalone operation

3.8.2 Microcontroller Unit

A MCU is essentially a microprocessor with onboard RAM, ROM and I/O ports and various additional components on a single integrated circuit. The processor executes the programme that resides in the ROM, making it a very powerful tool for embedded applications and an ideal solution for control system implementation. Several competing manufacturers offer different architectures of MCU, each with differing programming requirements, onboard peripherals and speed. After reviewing the processor market, the Cygnal C8051F020 was chosen because of its high performance, flexibility and class leading processor power [101]. Further Information is available in Appendix A8 [p261]. The MCU was obtained directly from the manufacturer; the device was supplied soldered to a PCB with all I/O pins accessible via a standard 96-way connector. This prevented the need to design a custom PCB and solder a very fine pitch chip without damage but allowed an external daughter board to be plugged directly to the development board. This provided a degree of redundancy, as a fault in one board would not require the entire system to be replaced. The auxiliary components were designed and tested on prototyping board before being soldered to the daughter board.

The integrated development environment software allowed Assembly or 'C' code to be written and downloaded to the target processor for execution. Programme code can be 'stepped through' one line at a time with the ability to examine and modify processor internal registers and memory to aid in the debugging of the code. This feature makes the development kit particularly desirable as the code is always executed in silicon and not a software simulator that could be less accurate with time critical applications.

3.8.3 Switch Commutation Control

As described in Chapter Two, only one switch per output phase should be closed at any time to avoid destructive supply short-circuits in the matrix converter. Although the control software was developed and tested rigorously, it was still possible for an unanticipated software fault to cause erroneous switch commutation. It was therefore necessary to implement hardware protection against potential incorrect switching combinations during any stage of the development process. The solution was a high-speed 2-bit binary decoder (74AC139) for each converter output phase [102]. See Appendix A9 [p263].

In 1	In 2		Out 1	Out 2	Out 3	Out 4
0	0		1	0	0	0
1	0		0	1	0	0
0	1		0	0	1	0
1	1		0	0	0	1

Table 9 - Binary Decoder Truth Table

Each binary decoder is controlled via a 2-bit signal, reducing the number of MCU I/O pins required to control the converter and reliably preventing more than one switch from each output phase from being closed. Two 74AC139 IC's were soldered to the daughter board and operate at the same voltage (3.3V) as the MCU board. The output for each is an inverted signal used to directly control the gate drivers via a ribbon cable.

3.8.4 External Lookup Table

With the need to streamline the software to maximise the potential switching frequency of the matrix converter, a large external memory device was required to store a high-resolution cosine lookup table. The other consideration was the access time required to retrieve data from the table. Serial flash memory devices were investigated initially but later rejected due to poor data access time and availability. Instead, a standard (parallel interface) 8MB Smartmedia memory card was adopted [103], with future potential for up to 128MB if required [104], see also Appendix A10 [p264]. This allowed very large optimised cosine lookup tables to be generated and stored for reduced real-

time computation. A total of 16 I/O pins were required to operate the Smartmedia memory card and the low operating voltage allowed direct power sharing with the MCU.

3.8.5 User Interface

While some matrix converter implementations have used simplified control strategies that only operate at certain fixed frequencies, often with pre-calculated data, such a limited control system was not practical when driving an active load like a motor. A full user interface was therefore implemented to allow control of the matrix converter. This took the form of an alphanumeric LCD module (16 character by 2 line) interfaced with the MCU to provide visual feedback of the operating parameters of the converter. In operation, the LCD shows the current switching frequency, output amplitude and frequency, switch dwell and other user selected sequencing options. The LCD communicates using an 8-bit data-bus with three additional control lines. Although an additional DC-DC charge pump converter was required to increase the control board voltage from 3.3V to the 5V required to power the LCD module, the output voltage swing of the MCU was sufficiently high for direct connection of the I/O pins.

Figure 55 - LCD Module

Figure 56 - Rotary Encoder

The second part of the user interface was an indexed rotary encoder. Since rotating a dial is more natural than an array of push buttons, all aspects of the matrix converter operation are controlled using the encoder. A compact Bourns 24-detent incremental encoder was connected to the MCU via an additional signal conditioner (Motorola MC 14490) to eliminate switch contact bounce. Two data lines provide a square wave output 90° offset to each other, allowing both the number of steps and the direction to be obtained from the encoder. A push button on the MCU motherboard confirms the selection made using the rotary encoder.

3.9 Conclusions

The lack of a commercial matrix converter made it necessary to design and build a practical 10kVA laboratory converter to allow verification of developed computer models and testing of novel modes of operation. The hardware was designed with simplicity and reliability as the main objectives. The converter implements diode-bridge bi-directional switches that were found to reduce not only the number of gate drive and snubber devices but also control system complexity. This approach also limited the risk

factor of designing and building an advanced converter without prior experience of the practical issues and demands. The high-speed switching IGBT complimented the diode bridge topology to produce a robust platform to aid in the development process. Maintenance was further assisted with the use of screw terminals for all electrical connections, including the semiconductor devices that were mounted to suitably sized heat-sinks with thermal compound to aid cooling. Additional snubber elements were installed to protect the IGBT from excessive rates of change of voltage and avoid costly and lengthy component replacement. Each identical output phase was assembled with independent gate driver circuits on an insulated board and stacked in the rack-mounted converter, to complete the modular design. Although a strict testing methodology was implemented, it was not viable or safe to begin experimentation at the full supply voltage and an autotransformer was installed to enable reduced voltage testing. Supply isolating switches, located on the front panel, provided quick access in the event of a fault, in addition to three inline high-speed fuses that protect the electrical power supply against potential short-circuit conditions. The completed converter design is rated to 10kVA and designed to drive a generalised machine configured as a six-pole induction motor.

A filter was designed and installed in the laboratory matrix converter to limit pollution of the electrical supply with the high-frequency switching harmonics. Optimised for a switching frequency of 4kHz and above, the filter implemented an economical single-stage, second-order design to allow a wide range of operating frequencies. Component sizing was an exercise in compromise between maximum allowed filter voltage drop, the variation in power factor across the anticipated operating range and the desired attenuation. When tested, the final filter design closely matched the frequency response predicted by numerical analysis and reduced switching noise to acceptable levels.

The interface between the high-voltage power electronics and the delicate low-voltage control system required additional isolation. The gate driver circuit already included optical isolation so no further precautions were necessary but the supply reference comparator output required an additional circuit both to reduce the voltage and fully buffer the signal. The supply reference signal was obtained with the use of a voltage comparator connected to the 'Blue' and 'Yellow' phases with the crossover point defining the peak of the 'Red' phase supply voltage.

The matrix converter operates at high frequency in order to improve output waveform quality and therefore requires an equally capable control system. Although other

investigations had implemented PC based control systems, a custom designed and assembled control system was chosen to increase reliability and be more representative of a marine system.

The system was designed in two parts to future proof the control boards and used the latest in MCU technology. The system consists of a Cygnal 8052 based MCU board, sourced from the manufacturer, connected to a secondary 'daughter' board that contains the added peripherals necessary to control the matrix converter. The final configuration is shown in Figure 57.

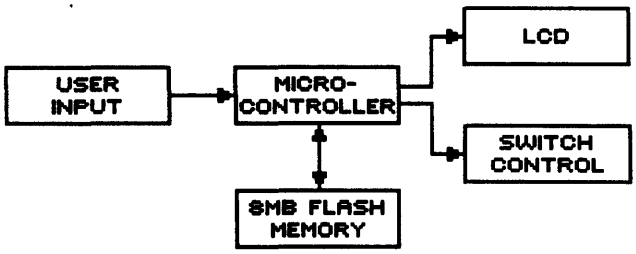

Figure 57 - Completed Control System

A user interface was designed to facilitate autonomous control and allows the user to vary the operating parameters in real-time using a rotary encoder and push-button with visual feedback provided on an alphanumeric LCD module. Protection against supply short-circuits is provided by a set of high-speed binary decoders that prevents more than one switch in each output phase from being closed at once and also reduce MCU I/O usage.

The target of real-time Venturini control required extensive use of pre-calculated cosine data stored in large external lookup tables, and is described in detail in Chapter Four. This has been achieved by interfacing the MCU to an 8 MB Smartmedia parallel flash memory card. The external memory stores parameters at high resolution allowing the control system to operate with increased output resolution and a wider frequency range. The complete control system represents a powerful yet flexible platform for software implementation of the most complex Venturini control strategies.

4. Chapter Four - Matrix Converter Software

4.1 Introduction

This chapter describes the original control system software created for the laboratory matrix converter. The complex algorithms and the 8-bit processor architecture require very efficient software to be written that minimises real-time computation to allow increased switching frequencies to be explored. Original control codes implementing both Venturini strategies have been written in Assembler language for high performance and real-time operation, despite the numerous cosine calls. Also described is the user interface to ease converter operation and a method to reliably synchronise the laboratory converter and the supply.

Software Version	Venturini Strategy	Output Phases	Output Frequency Increment	Converter Input Displacement Angle
V.1	Original	1	1	As Load
V.2	Original	1	1	Variable
V.3	Original	3	1	Variable
V.4	Advanced	3	0.1	Unity

Table 10 - Control Software Development Progression

With the laboratory matrix converter hardware being developed in logical stages, it was necessary to implement a control strategy suited to an incrementally expanding hardware and software platform. Although the advanced Venturini is superior to its predecessor, the process by which it achieves increased supply utilisation cannot be realised with a single-phase output converter, as the injected third harmonics do not cancel out in a single-phase load. Therefore, the first version of the control software employed the original Venturini strategy that is more easily adapted to a wide range of converter configurations. Initial revisions of the control software were designed for single-phase output operation and later expanded to allow full three-phase operation once the software design philosophy was verified. Later features included input displacement angle control, wider output frequency range and motor control optimisations. The development cycle is summarised in Table 10. The complete software listing for both standard and advanced Venturini control algorithms described in this chapter is available as a separate document.

4.2 Programming Language

As with most microcontrollers, the selected 8052 MCU is most commonly programmed using 'C', a high-level language, or Assembly (machine) code. Although 'C' programming offers simplified syntax and allows lengthy processes to be accomplished with few lines of software, the compiled code is not as efficient as the

Assembly code equivalent and requires expensive compilers to produce efficient code. With Assembly language, each line of code directly corresponds to a single processor instruction, allowing development of highly optimised code to maximise the performance and operation of onboard peripherals. For this reason and the intended time critical application where the switches must be controlled with high precision, the MCU was programmed exclusively in Assembly language.

Operation	8-bit Duration (Clock Cycles)	16-bit Duration (Clock Cycles)
Addition	1	9
Subtraction	1	11
Multiply	4	74
Divide	8	596

Table 11 - Comparison of Function Execution Time

The 8051 MCU is an 8-bit device and is capable of performing 8-bit multiplication, division, addition and subtraction operations. Manipulation of larger numbers, e.g. 16, 24 or 32-bit, requires routines that call the native 8-bit calculation several times. Extending these calculations is not difficult; there are widely published standard routines available in numerous books and on the Internet [105,106,107]. However, the constraint is increased execution time for each routine. Although extended addition and subtraction routines are short, multiplication and, particularly, division operations are processor intensive, as shown in Table 11. It was therefore important to minimise use of extended multiplication and division operations to enable higher switching frequencies.

4.3 Cosine Generation

Analysis of the Venturini control algorithms highlighted the extensive use of the cosine function in each switching cycle. Several methods of generating the cosine function in real-time using the MCU were investigated, including Goertzal, Cordic and various arithmetic progression techniques [108] but were found to be excessively processor intensive when operating with the minimum of one hertz output resolution required for this application. As operational speed was the most important factor, the only solution was to minimise real-time computation with the use of large cosine lookup tables.

4.4 Testing and Validation

The operation of each control strategy required careful testing to avoid the risk of supply short-circuits that could catastrophically damage the matrix converter. Although the system was designed with hardware protection against this, see Section 3.8.3 [p80], the following two approaches to offline software verification were implemented prior to live testing.

4.4.1 Output Signal Observation

An initial verification of the software was to examine the output firing signals generated by the control system using a high-speed oscilloscope. Any software glitches could be seen very clearly and this facilitated offline debugging. The control software was tested offline until the oscilloscope presented a clear and steady output pulse train that oscillated smoothly across the screen in accordance with the output frequency.

4.4.2 Numerical Verification

The second approach to software verification was to examine the calculated output switching periods at the end of each cycle. The control software was configured to halt at the end of each calculation and display the results on the LCD module. These results were then verified against a computer spreadsheet of either the original or advanced Venturini algorithm at the same output frequency and voltage setting. This was performed at various output frequencies and amplitudes for further confirmation and was particularly useful when checking the advanced Venturini software where the output period does not vary sinusoidally and could not, therefore, be checked with an oscilloscope.

4.5 Original Venturini Software

The first stage of the control software development was to design and implement the original Venturini control strategy, as described in Section 2.8.2 [p54]. Although restricted to a maximum voltage transfer ratio of 50%, it allows control of the input displacement angle.

4.5.1 Version 1

The first version of the original Venturini algorithm, Equation 5 [p55], represented the most basic control software written and operated the matrix converter with an input displacement angle (ϕ_i) equal to the power factor demanded by the load (ϕ_o) and, therefore, required only the symmetrical modulator. This initial version was also limited to single-phase output operation.

$$\text{If:} \quad \phi_i = \phi_o \quad \therefore \quad \alpha_1 = \tfrac{1}{2}(1 + \text{Tan}\,\phi_i\,\text{Cot}\,\phi_o) = 1 \quad \& \quad \alpha_2 = 0$$

Hence

$$[M_{(t)}] = \left(\frac{1}{3}\right)\begin{Bmatrix} 1+2q\text{Cos}(\omega_m t) & 1+2q\text{Cos}(\omega_m t-\frac{2}{3}\pi) & 1+2q\text{Cos}(\omega_m t-\frac{4}{3}\pi) \\ 1+2q\text{Cos}(\omega_m t-\frac{4}{3}\pi) & 1+2q\text{Cos}(\omega_m t) & 1+2q\text{Cos}(\omega_m t-\frac{2}{3}\pi) \\ 1+2q\text{Cos}(\omega_m t-\frac{2}{3}\pi) & 1+2q\text{Cos}(\omega_m t-\frac{4}{3}\pi) & 1+2q\text{Cos}(\omega_m t) \end{Bmatrix}$$

Equation 17

Symmetry of Equation 17 allowed the calculation to be reduced by a further two-thirds without compromising accuracy. The calculation becomes:

$$T_1, T_5, T_9 = \frac{T_{seq}}{3} [1 + 2\,q\,\mathrm{Cos}\,(K\,T_{seq}\,\omega_m)]$$

$$T_2, T_6, T_7 = \frac{T_{seq}}{3} [1 + 2\,q\,\mathrm{Cos}\,(K\,T_{seq}\,\omega_m - \tfrac{4}{3}\pi)]$$

$$T_3, T_4, T_8 = \frac{T_{seq}}{3} [1 + 2\,q\,\mathrm{Cos}\,(K\,T_{seq}\,\omega_m - \tfrac{2}{3}\pi)]$$

Equation 18

The 'K' term represents an integer number that is incremented each switching cycle. The '$K\,T_{seq}\,\omega_m$' term can, therefore, be simplified to a number that increases by a predetermined increment each cycle before overflowing when 360 (°) is passed. The increment is calculated with knowledge of the supply frequency (ω_i), the target output frequency (ω_o) and the desired switching period (T_{seq}) using the following relationship:

$$\text{Symmetric Step Value} = 360\,T_{seq}\,(\omega_o - \omega_i)$$

Equation 19

For T_1, the cosine term starts at zero and increments (or decrements) by the value defined by Equation 19. Values T_2 and T_3 are also incremented by the same amount but start with an offset of 120 and 240 respectively to accommodate the phase angle delays.

To further reduce real-time computation, the step value for each output frequency over a range of 0 to 99Hz was pre-calculated and stored in a series of small lookup tables, one for each switching frequency. The updated step value is retrieved from the corresponding lookup table each time the output frequency is adjusted. The above step value relationship indicates that the cosine lookup table would need a resolution of 0.01° to achieve the desired integer output frequency for the original Venturini control software. A comparison of the relative accuracy of using 8, 16, 24, or 32-bit resolution showed that 24-bit resolution would provide sufficient accuracy. Storage of the resultant cosine lookup table was then considered. Although a full lookup table for 360° (360*100*3 = 108,000 bytes) was larger than the available 64kB ROM, symmetry of the cosine function allowed this to be reduced by a factor of four and allow internal storage for maximum retrieval speed.

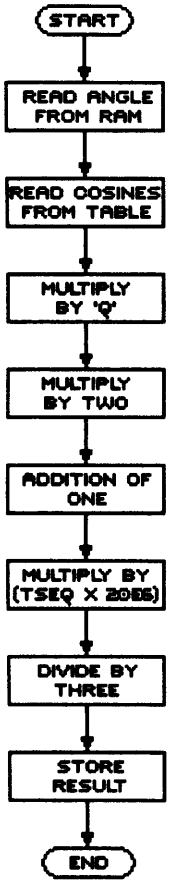

Figure 58 - Venturini Algorithm Code V.1 Flowchart

The Venturini calculation multiplies the cosine value by 'q', the desired output amplitude and this result is then doubled according to the Venturini algorithm. A notional '1' is added to this result, since the cosine was normalised to 24-bit, adding 1 becomes 1 * ((2^24) -1), before multiplication by the switching period and division by three. The calculated time values, T_1, T_2 and T_3, are then stored in a one-cycle buffer, ready for implementation. This operation is summarised in Figure 58 and is repeated for each switch.

The final divide by three routine was specifically developed for this application as the standard division method (16-bit divide by 8-bit) was too long. Mathematical repetitiveness of the result along with the fixed divisor (three) was used to write this quicker subroutine.

4.5.2 Version 2

The second version of the Venturini control software incorporated the ability to control the input displacement angle across the full range of leading and lagging positions. This software was approximately twice as complex as the previous version as both symmetrical and anti-symmetrical modulators required evaluation. The converter displacement angle is varied by changing the ratio of the modulators using α_1. This

version of the control strategy was limited to a single-phase output configuration to simplify the development process. The switch duration calculations became:

$$T_1 = T_{seq}\frac{\alpha_1}{3}[1 + 2q\,Cos((\omega_o - \omega_i)K\,T_{seq})] + T_{seq}\frac{1-\alpha_1}{3}[1 + 2q\,Cos((\omega_o + \omega_i)K\,T_{seq})]$$

$$T_2 = T_{seq}\frac{\alpha_1}{3}[1 + 2q\,Cos((\omega_o - \omega_i)K\,T_{seq} - \tfrac{4}{3}\pi)] + T_{seq}\frac{1-\alpha_1}{3}[1 + 2q\,Cos((\omega_o + \omega_i)K\,T_{seq} - \tfrac{2}{3}\pi)]$$

$$T_3 = T_{seq}\frac{\alpha_1}{3}[1 + 2q\,Cos((\omega_o - \omega_i)K\,T_{seq} - \tfrac{2}{3}\pi)] + T_{seq}\frac{1-\alpha_1}{3}[1 + 2q\,Cos((\omega_o + \omega_i)K\,T_{seq} - \tfrac{4}{3}\pi)]$$

$$T_4 = T_{seq}\frac{\alpha_1}{3}[1 + 2q\,Cos((\omega_o - \omega_i)K\,T_{seq} - \tfrac{2}{3}\pi)] + T_{seq}\frac{1-\alpha_1}{3}[1 + 2q\,Cos((\omega_o + \omega_i)K\,T_{seq} - \tfrac{2}{3}\pi)]$$

$$T_5 = T_{seq}\frac{\alpha_1}{3}[1 + 2q\,Cos((\omega_o - \omega_i)K\,T_{seq})] + T_{seq}\frac{1-\alpha_1}{3}[1 + 2q\,Cos((\omega_o + \omega_i)K\,T_{seq} - \tfrac{4}{3}\pi)]$$

$$T_6 = T_{seq}\frac{\alpha_1}{3}[1 + 2q\,Cos((\omega_o - \omega_i)K\,T_{seq} - \tfrac{4}{3}\pi)] + T_{seq}\frac{1-\alpha_1}{3}[1 + 2q\,Cos((\omega_o + \omega_i)K\,T_{seq})]$$

$$T_7 = T_{seq}\frac{\alpha_1}{3}[1 + 2q\,Cos((\omega_o - \omega_i)K\,T_{seq} - \tfrac{4}{3}\pi)] + T_{seq}\frac{1-\alpha_1}{3}[1 + 2q\,Cos((\omega_o + \omega_i)K\,T_{seq} - \tfrac{4}{3}\pi)]$$

$$T_8 = T_{seq}\frac{\alpha_1}{3}[1 + 2q\,Cos((\omega_o - \omega_i)K\,T_{seq} - \tfrac{2}{3}\pi)] + T_{seq}\frac{1-\alpha_1}{3}[1 + 2q\,Cos((\omega_o + \omega_i)K\,T_{seq})]$$

$$T_9 = T_{seq}\frac{\alpha_1}{3}[1 + 2q\,Cos((\omega_o - \omega_i)K\,T_{seq})] + T_{seq}\frac{1-\alpha_1}{3}[1 + 2q\,Cos((\omega_o + \omega_i)K\,T_{seq} - \tfrac{2}{3}\pi)]$$

Equation 20

Two sets of rotating vectors were now required to represent both the symmetric (α_1) and anti-symmetric (α_2) terms, see Section 2.8.2 [p54]. The anti-symmetric step was calculated for each output frequency and switching frequency and added to the program software as a second set of lookup tables, using the following relationship.

$$\text{Anti-symmetric Step Value} = 360\,T_{seq}\,(\omega_o + \omega_i)$$

Equation 21

The calculation was reduced to six cosine operations due to repetition in the equations:

$$T_1 = T_{seq}(a + x) \qquad T_4 = T_{seq}(b + y) \qquad T_7 = T_{seq}(c + z)$$

$$T_2 = T_{seq}(c + y) \qquad T_5 = T_{seq}(a + z) \qquad T_8 = T_{seq}(b + x)$$

$$T_3 = T_{seq}(b + z) \qquad T_6 = T_{seq}(c + x) \qquad T_9 = T_{seq}(a + y)$$

$$a = \frac{\alpha_1}{3}[1 + 2q\,Cos((\omega_o - \omega_i)K\,T_{seq})] \qquad x = \frac{1-\alpha_1}{3}[1 + 2q\,Cos((\omega_o + \omega_i)K\,T_{seq})]$$

$$b = \frac{\alpha_1}{3}[1 + 2q\,Cos((\omega_o - \omega_i)K\,T_{seq} - \tfrac{2}{3}\pi)] \qquad y = \frac{1-\alpha_1}{3}[1 + 2q\,Cos((\omega_o + \omega_i)K\,T_{seq} - \tfrac{2}{3}\pi)$$

$$c = \frac{\alpha_1}{3}[1 + 2q\,Cos((\omega_o - \omega_i)K\,T_{seq} - \tfrac{4}{3}\pi)] \qquad z = \frac{1-\alpha_1}{3}[1 + 2q\,Cos((\omega_o + \omega_i)K\,T_{seq} - \tfrac{4}{3}\pi)$$

Equation 22

The value α_1 is an 8-bit number that can be varied between 0 and 255, to provide 256 positions for the input displacement angle. Although this software revision evaluates twice as many cosine terms, with a further six alpha multiplications and nine additions, it is still sufficiently optimised to allow up to 6kHz operation. The calculation for each switch is shown in Figure 59.

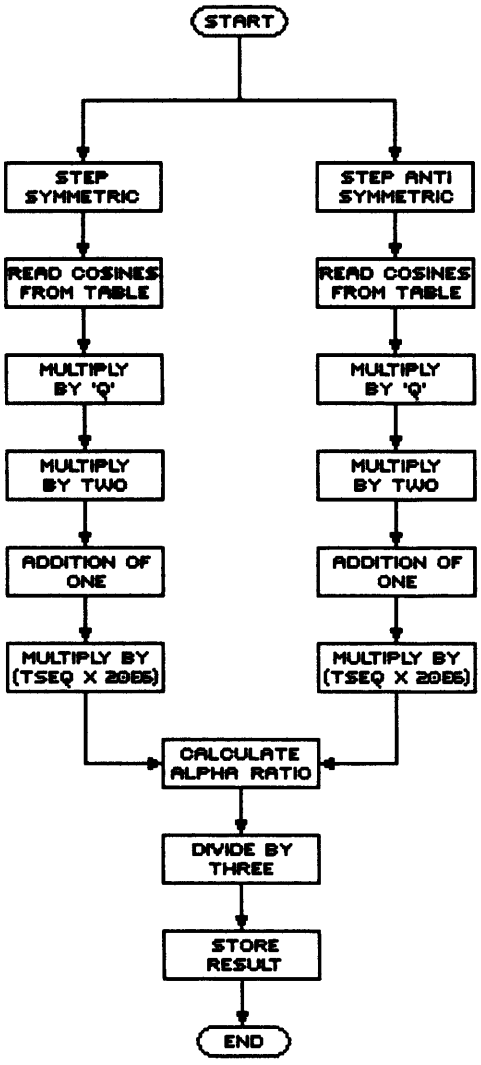

Figure 59 - Venturini Algorithm Code V.2 Flowchart

4.5.3 Version 3

The third version of the original Venturini control strategy expanded operation to allow full control of nine switches in addition to the input displacement angle. Symmetry of the modulation equations, as described in Section 4.5.2, enabled the additional switches to be operated with little increase in processor load.

4.6 Advanced Venturini Software

The advanced Venturini control strategy had been chosen to form the basis of further investigations and therefore required a more accurate implementation. While the previous software implementations of the standard strategy provided an integer output

frequency resolution, this was unsuited to fine motor speed control and therefore necessitated an increase in the output frequency resolution to 0.1Hz for this software version.

The advanced Venturini algorithm is considerably more complex than the standard version as the additional 3rd order harmonics greatly increase the number of cosine terms that require evaluation, see Section 2.8.3 [p56]. To simplify the calculation and maximise supply utilisation (see Section 2.8.4 [p59]), the control strategy was configured to provide unity input displacement angle ($\phi_i = 0$) at all times, resulting in the following modulation equation:

$$\text{If } \phi_i = 0 \quad \therefore \quad \tan \phi_i = 0$$

$$[M_{(t)}] = \frac{1}{3} + \frac{q}{3}\begin{bmatrix} \text{Cos}[(\omega_o + \omega_i)t] & \text{Cos}[(\omega_o + \omega_i)t - \frac{2}{3}\pi] & \text{Cos}[(\omega_o + \omega_i)t - \frac{4}{3}\pi] \\ \text{Cos}[(\omega_o + \omega_i)t - \frac{2}{3}\pi] & \text{Cos}[(\omega_o + \omega_i)t - \frac{4}{3}\pi] & \text{Cos}[(\omega_o + \omega_i)t] \\ \text{Cos}[(\omega_o + \omega_i)t - \frac{4}{3}\pi] & \text{Cos}[(\omega_o + \omega_i)t] & \text{Cos}[(\omega_o + \omega_i)t - \frac{2}{3}\pi] \end{bmatrix}$$

$$+ \frac{q}{3}\begin{bmatrix} \text{Cos}[(\omega_o - \omega_i)t] & \text{Cos}[(\omega_o - \omega_i)t - \frac{4}{3}\pi] & \text{Cos}[(\omega_o - \omega_i)t - \frac{2}{3}\pi] \\ \text{Cos}[(\omega_o - \omega_i)t - \frac{2}{3}\pi] & \text{Cos}[(\omega_o - \omega_i)t] & \text{Cos}[(\omega_o - \omega_i)t - \frac{4}{3}\pi] \\ \text{Cos}[(\omega_o - \omega_i)t - \frac{4}{3}\pi] & \text{Cos}[(\omega_o - \omega_i)t - \frac{2}{3}\pi] & \text{Cos}[(\omega_o - \omega_i)t] \end{bmatrix}$$

$$- \frac{q}{18}\begin{bmatrix} \text{Cos}[(3\omega_o + \omega_i)t] & \text{Cos}[(3\omega_o + \omega_i)t - \frac{2}{3}\pi] & \text{Cos}[(3\omega_o + \omega_i)t - \frac{4}{3}\pi] \\ \text{Cos}[(3\omega_o + \omega_i)t] & \text{Cos}[(3\omega_o + \omega_i)t - \frac{2}{3}\pi] & \text{Cos}[(3\omega_o + \omega_i)t - \frac{4}{3}\pi] \\ \text{Cos}[(3\omega_o + \omega_i)t] & \text{Cos}[(3\omega_o + \omega_i)t - \frac{2}{3}\pi] & \text{Cos}[(3\omega_o + \omega_i)t - \frac{4}{3}\pi] \end{bmatrix}$$

$$- \frac{q}{18}\begin{bmatrix} \text{Cos}[(3\omega_o - \omega_i)t] & \text{Cos}[(3\omega_o - \omega_i)t - \frac{4}{3}\pi] & \text{Cos}[(3\omega_o - \omega_i)t - \frac{2}{3}\pi] \\ \text{Cos}[(3\omega_o - \omega_i)t] & \text{Cos}[(3\omega_o - \omega_i)t - \frac{4}{3}\pi] & \text{Cos}[(3\omega_o - \omega_i)t - \frac{2}{3}\pi] \\ \text{Cos}[(3\omega_o - \omega_i)t] & \text{Cos}[(3\omega_o - \omega_i)t - \frac{4}{3}\pi] & \text{Cos}[(3\omega_o - \omega_i)t - \frac{2}{3}\pi] \end{bmatrix}$$

$$- \frac{q}{18\sqrt{3}}\begin{bmatrix} \text{Cos}(4\omega_i t) & \text{Cos}(4\omega_i t - \frac{2}{3}\pi) & \text{Cos}(4\omega_i t - \frac{4}{3}\pi) \\ \text{Cos}(4\omega_i t) & \text{Cos}(4\omega_i t - \frac{2}{3}\pi) & \text{Cos}(4\omega_i t - \frac{4}{3}\pi) \\ \text{Cos}(4\omega_i t) & \text{Cos}(4\omega_i t - \frac{2}{3}\pi) & \text{Cos}(4\omega_i t - \frac{4}{3}\pi) \end{bmatrix}$$

$$+ \frac{7q}{18\sqrt{3}}\begin{bmatrix} \text{Cos}(2\omega_i t) & \text{Cos}(2\omega_i t - \frac{4}{3}\pi) & \text{Cos}(2\omega_i t - \frac{2}{3}\pi) \\ \text{Cos}(2\omega_i t) & \text{Cos}(2\omega_i t - \frac{4}{3}\pi) & \text{Cos}(2\omega_i t - \frac{2}{3}\pi) \\ \text{Cos}(2\omega_i t) & \text{Cos}(2\omega_i t - \frac{4}{3}\pi) & \text{Cos}(2\omega_i t - \frac{2}{3}\pi) \end{bmatrix}$$

Equation 23

Although the increase in mathematical complexity is evident, a considerable reduction in the calculation was achieved by applying the same repetition technique used in the previous versions of the Venturini software. Instead of a single lookup table, four tables were created to reduce real-time calculation requirements.

Table	Data
1	$\cos\theta$
2	$\frac{1}{6}\cos\theta$
3	$\frac{1}{6\sqrt{3}}\cos\theta$
4	$\frac{7}{6\sqrt{3}}\cos\theta$

Table 12 - Advanced Venturini Lookup Tables

For the optimised version shown below, if the values in the curly brackets are pre-calculated and read from lookup tables the program code reduces to simple addition and subtraction, operations the MCU is capable of doing very quickly.

$$[M_{(t)}] = \frac{q}{3}[1 + \{\cos\}_1 + \{\cos\}_2 - \{\tfrac{1}{6}\cos\}_3 - \{\tfrac{1}{6}\cos\}_4 - \{\tfrac{1}{6\sqrt{3}}\cos\}_5 + \{\tfrac{7}{6\sqrt{3}}\cos\}_6]$$

Equation 24

Figure 60 shows the operation to calculate the switching duration for each switch of the matrix converter when implementing the advanced Venturini control strategy. At the beginning of each switching cycle, the six reference angles are updated with the increments appropriate for the switching frequency, supply and target frequency and the output amplitude. This data is stored in a separate small table that is accessed each time the output parameters are changed and provides the correct increments for the reference angles. The next step is to retrieve the six sets of cosine values from the lookup tables that correspond to the previously calculated reference angles. This is the most processor intensive aspect of the software due to the volume of data being accessed and the slight time delay for the memory to respond to a 'read' instruction. This problem was overcome by enabling the software to perform alternative operations whilst waiting for data from the external lookup table. Once all the cosine data is retrieved, a summation of these values is performed for each output phase with a subsequent addition of a notional '1' before the final divide-by-three subroutine. The completed calculated periods are then converted into the correct format and stored in RAM for implementation in the MCU timer.

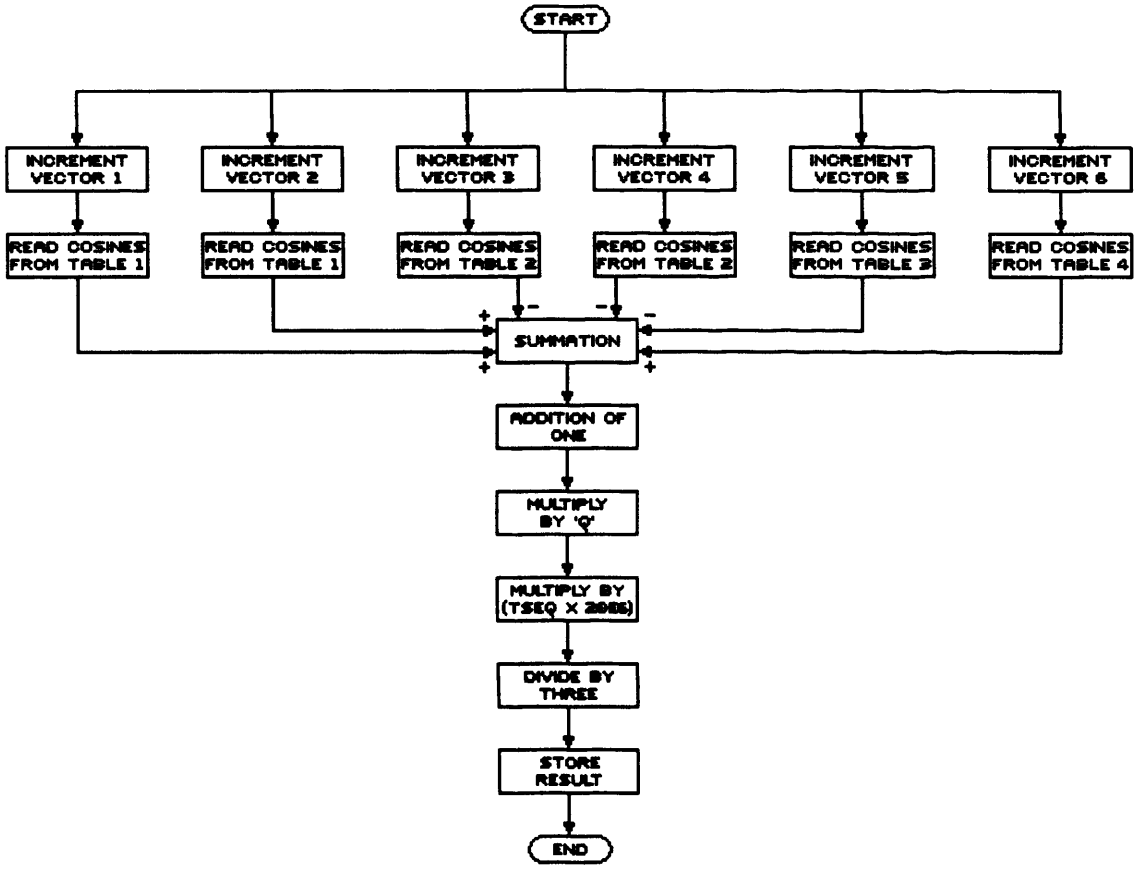

Figure 60 - Venturini Algorithm Code V.4 Flowchart

Further analysis of the step size and the cosine parameters showed that lookup Tables Three & Four could be safely reduced in size. Their step size does not vary with the output frequency but only with the supply and switching frequencies and consequently Tables Three & Four require a minimum increment of 12° and 6° respectively. This results in two very small lookup tables that were comfortably accommodated in internal memory for considerably increased throughput.

Switch Freq (kHz)	Table 3 Step (°)	Table 4 Step (°)
1	72	36
2	36	18
3	24	12
4	18	9
6	12	6

Table 13 - Lookup Tables Three & Four Step Values

Tables One and Two could not be further minimised without compromising accuracy, resulting in two large lookup tables that necessitated external storage. As adequate external memory was available, the two tables were generated for full 360° with interleaved data points to reduce the number of lookup operations by two-thirds. For

example, reading the value for θ=2.001° also provided sequential access to (2.001+120) 122.001° and (2.001+240) 242.001° with a further byte storing the sign for the three entries. Although the data interleaving increased the table size by a factor of three, the desired increase in data throughput was achieved. With 24-bit precision data, each table entry is 10 bytes in length and therefore each lookup table (1 & 2) is (360*1000*10) 3.6 megabytes in size.

θ	Cos θ			Cos θ + 120			Cos θ + 240			Sign
	Hi	Mid	Lo	Hi	Mid	Lo	Hi	Mid	Lo	
2.001	0FFh	0D8h	009h	087h	0A9h	0C2h	078h	02Eh	047h	006h
2.002	0FFh	0D7h	0FEh	087h	0AAh	0Bah	078h	02Dh	044h	006h
2.003	0FFh	0D7h	0F4h	087h	0ABh	0B2h	078h	02Ch	042h	006h
2.004	0FFh	0D7h	0EAh	087h	0ACh	0Abh	078h	02Bh	03Fh	006h

Table 14 - Interleaved Cosine Lookup Example in Hexadecimal Format

4.6.1 External Lookup Table

The storage and retrieval of the two large lookup tables presented a considerable problem as the MCU is limited to 64kBytes of internal storage. The initial solution of a pair of serial 4MB IC could not sustain adequate data throughput for this application, so a commonly available 8MB Smartmedia memory card was interfaced to the MCU, see Section 3.8.4 [p80]. The parallel interface allows high-speed access and due to the media's nature, future increases in storage requirements are easily accommodated with larger memory cards of up to 128MB. Custom hardware and software had to be developed to facilitate the use of this memory architecture and a library of subroutines was written to operate the memory card. The lookup table was loaded into the memory card using custom written software for the MCU that received the cosine data from a host computer via a serial interface.

4.7 Software 'Phase Lock Loop'

Although the mains supply is nominally rated at 50Hz, it exhibits both distortion and appreciable drift of up to ±1% depending on local demand and usage. As a consequence, reliable synchronisation of the control system with the electrical supply is essential for the Venturini algorithms to operate correctly, as non-synchronous operation produces erroneous input and output waveforms. As described in Section 3.7 [p77], a high-speed comparator had been connected to the 'Yellow' and 'Blue' input phases and provided a reference signal to the MCU defining the instant when the 'Red' phase is at its peak voltage. This triggers an internal software interrupt every 20ms (the period of the supply waveform) and resets an internal 16-bit timer. Since this timer cannot count for the entire 20ms (16-bits are filled in less than 3ms with an oscillator

frequency of 24MHz), the timer is configured to overflow at the rate of the converter switching frequency by loading an appropriate time value to the auto-reloading register. For a 1kHz switching frequency the timer overflows twenty times between each supply reference interrupt and, due to the timer always overflowing at the switching frequency, this point defines end/start of each cycle and commutates the switches ready for each new switching cycle.

To maintain synchronisation, the control software varies the duration of the timer to ensure that the final interrupt occurs as close as possible to the signal from the supply reference. For example, when operating at 1 kHz, correct synchronisation is assumed when the timer overflows for the 20th time at the same instant as the reference signal interrupt. No timer length modification occurs when this happens. If the reference signal is received before the 20th overflow, a manual timer reload is triggered and the auto-reload timer value is decremented by one cycle. Otherwise, if the reference signal is received after the 20th overflow, the auto-reload time value is incremented by one and the timer reloaded. This process requires the converter switching frequency to be a multiple of the supply frequency and a flowchart is shown in Figure 61.

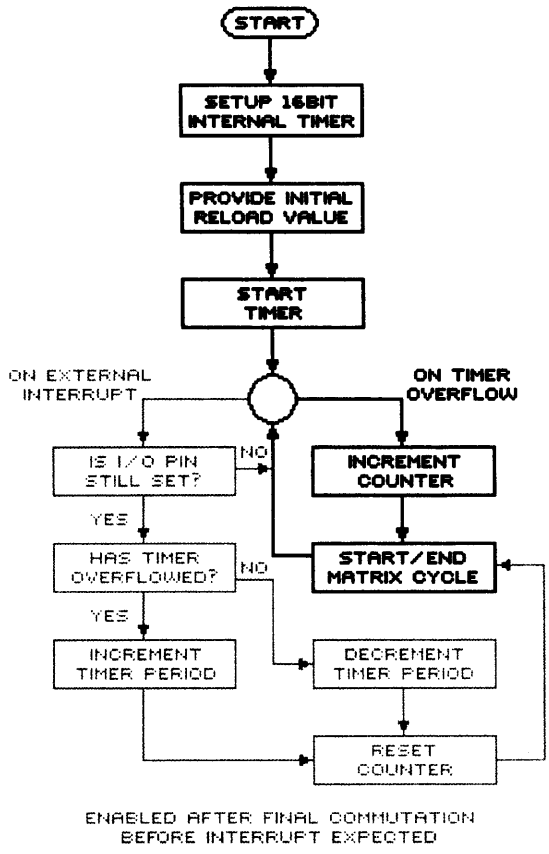

Figure 61 - Synchronisation Code Flowchart

A further feature of the software synchroniser is that a temporary loss of the supply reference signal will not disturb the timer but allows safe operation of the matrix

converter for several seconds until restoration of the signal. If the reference signal is permanently lost, the continued operation of the control hardware allows the converter to be safely shutdown.

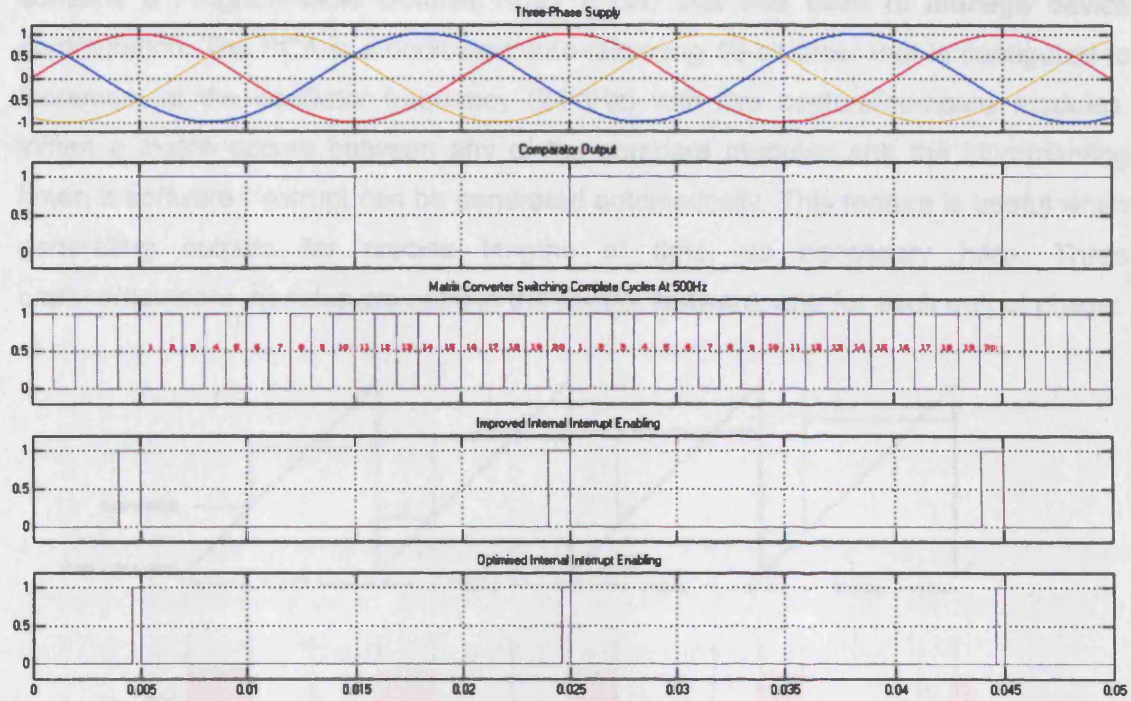

Figure 62 - Selective Reference Signal Enabling 1kHz Example

The effect of supply borne noise was found to influence the reference signal and occasionally cause false interrupts and incorrect synchronisation. Operation of the converter switches caused transients in the supply reference signal, resulting in unstable MCU interrupt operation. The first approach to resolving this issue was to enable the reference interrupt only during the last switching cycle before the signal was due and immediately disable the interrupt upon execution. In the 1kHz example in Figure 62, the interrupt has been enabled on the 19th switching cycle. A later enhancement of this method only enabled the interrupt once the final switch commutation of the 19th cycle has occurred, thus reliably preventing switch commutation noise from prematurely triggering an interrupt. The second approach was to monitor the reference signal, a square wave at the supply frequency. When triggered, the reference interrupt subroutine verifies that the supply reference is in the correct state and, if not, aborts the interrupt to avoid false operation.

By implementing the above precautions, the control system safely maintains synchronisation with the supply and is tolerant of supply borne noise and temporary interruption of the reference signal.

4.8 IGBT Control

High performance converter operation requires a high switching resolution to enable fine output frequency and amplitude control with low noise. The Cygnal 8052 derivative contains a Programmable Counter Array (PCA) that was used to manage device commutation. The PCA is a dedicated auto-reloading 16-bit timer that is configured to increment at the oscillator frequency (24MHz) with five capture/compare modules. When a match occurs between any of the compare modules and the incrementing timer, a software interrupt can be generated automatically. This feature is useful when generating outputs for precise lengths of time, as necessary here. Three capture/compare modules are used in the control software, one for each output phase:

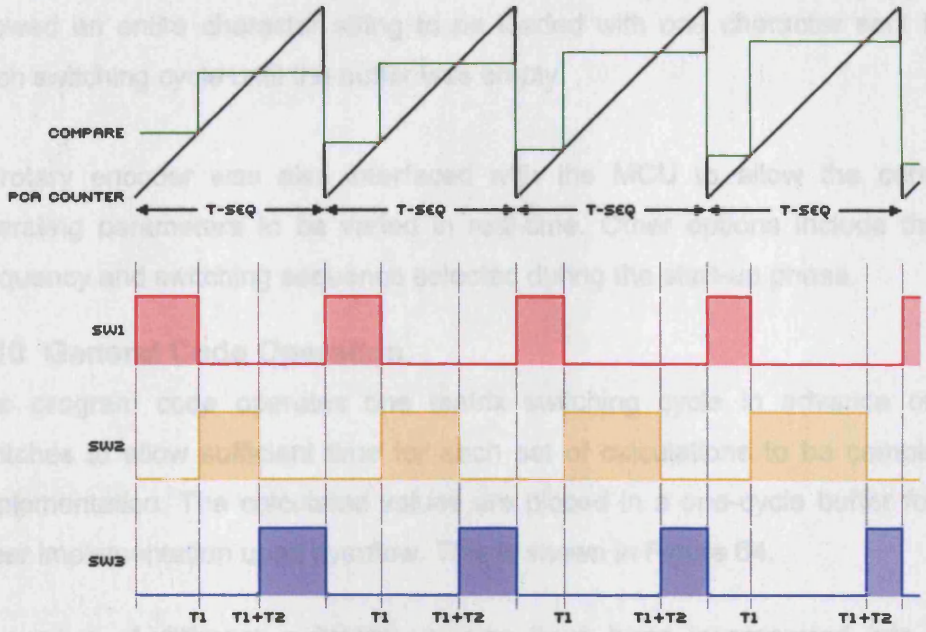

Figure 63 - PCA IGBT Control Technique

- The PCA counter is loaded with a value derived from the switching frequency
- The periods for the first set of switches are loaded into compare modules
- A match between the PCA timer and a module triggers an interrupt that commutates the correct switch and loads the duration for the following switch
- This continues until the third switch of each output phases is closed
- The process restarts when the PCA counter overflows

This is similar to the triangular waveform crossing technique often used in PWM drives and is shown in Figure 63. The resultant software provides a switching resolution of 41.67ns.

4.9 User Interface Operation

To facilitate feedback of the operating set-up, an alphanumeric LCD module was interfaced to the MCU, see Section 3.8.5 [p81]. The LCD communicates via an 8-bit data-bus with three additional control lines connected to the MCU. A library of subroutines has been written to correctly initialise, configure and operate the module. During tests at the higher switching frequencies, the relatively low speed of the LCD module was found to hinder the MCU when receiving long character strings. This was due to the relatively long time required by the LCD to execute each command, while the MCU waited to send the following character. The solution was to send a single character to the display during each switching cycle, the delay between successive characters being sufficient to remove the need to wait for the LCD. A software buffer allowed an entire character string to be loaded with one character sent to the LCD each switching cycle until the buffer was empty.

A rotary encoder was also interfaced with the MCU to allow the control system operating parameters to be varied in real-time. Other options include the switching frequency and switching sequence selected during the start-up phase.

4.10 General Code Operation

The program code operates one matrix switching cycle in advance of the IGBT switches to allow sufficient time for each set of calculations to be completed before implementation. The calculated values are placed in a one-cycle buffer for automatic timer implementation upon overflow. This is shown in Figure 64.

A number of different switching regimes have been incorporated into the control software for experimental analysis. The main software modifications allowed different switching sequences, both staggered and semi-symmetrical PWM and combinations of both. The control software prompts the user to select the appropriate commutation sequence at start-up. Table 15 lists the available converter operating modes:

Operating Mode	Switching Sequence		
	Output Phase 1	Output Phase 2	Output Phase 3
Standard	1-2-3	1-2-3	1-2-3
Positive Stagger	1-2-3	2-3-1	3-1-2
Negative Stagger	1-2-3	3-1-2	2-3-1
Sequence Offset 1	2-3-1	2-3-1	2-3-1
Sequence Offset 2	3-1-2	3-1-2	3-1-2
Semi-Sym	1-2-3 : 3-1-2 : 2-3-1	1-2-3 : 3-1-2 : 2-3-1	1-2-3 : 3-1-2 : 2-3-1
Semi-Sym + Stagger	1-2-3 : 3-1-2 : 2-3-1	2-3-1 : 1-2-3 : 3-1-2	3-1-2 : 2-3-1 : 1-2-3

Table 15 - Available Control System Operating Modes

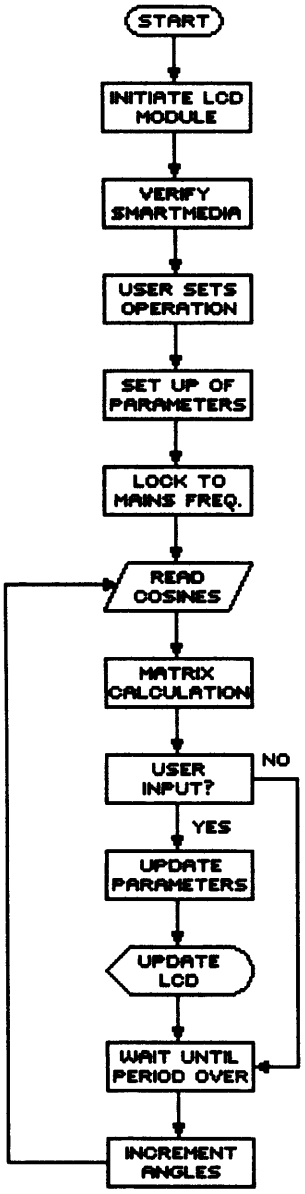

Figure 64 - Overview of Control Software Operation

4.10.1 Control System Initialisation

This section shows the contents of the LCD module during start-up of the laboratory matrix converter with explanation of the messages and options. All modes are selected by rotating the encoder until the desired option is displayed before pressing the MCU switch to confirm selection.

Select PWM Mode: Sequential	↔	Select PWM Mode: Semi-Symmetrical

1. At start-up, the user is prompted to select between sequential and semi-symmetrical PWM switching patterns, as described later in Section 6.7 [p145].

2. The desired stagger of the switching pattern is then selected. With no stagger, each output phase switches in the same sequence. Positive stagger applies a one input phase step offset to the switching sequence for each output phase. Negative stagger has the opposite effect.

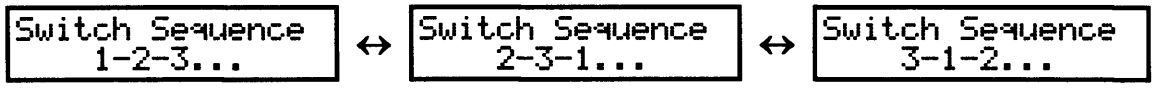

3. Assuming that 'sequential' PWM mode was selected previously without switch stagger, the above option allows the switch order to be altered. Commutation can start with any supply and increment upwards. Jump to step 5.

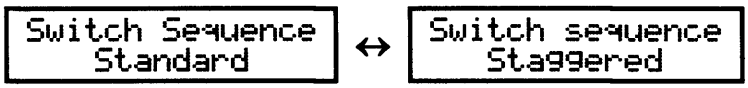

4. If semi-symmetrical PWM switching has been selected in step 1, the operator can select whether to have standard or staggered switching sequence for the semi-symmetrical PWM mode.

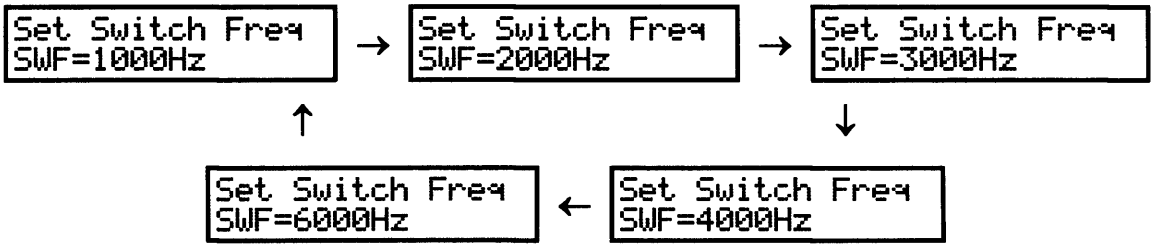

5. The switching frequency is finally selected from a set of five values, although operation at 4kHz or 6kHz is preferred.

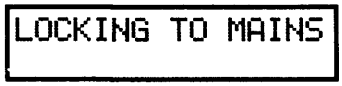

6. The control board then monitors the reference waveform and supply synchronisation begins.

7. Once supply synchronisation is achieved, the matrix converter begins operation

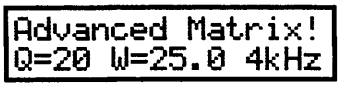

Figure 65 - Start-Up Sequence Diagram

4.10.2 Output Voltage & Frequency Control

As described in Section 3.8.5 [p81], all manipulation of the control system is performed using the rotary encoder. The output frequency or voltage is increased by rotating the encoder clockwise and anticlockwise to reduce the output parameters. Selection between the two values is via a small toggle switch soldered to the control system daughter board.

To accommodate both clockwise and anticlockwise propulsion motor rotation, the output frequency can be either positive or negative and is selected by reducing the output frequency to zero before reversing direction of rotation. The optimised motor control software incorporates a proportional relationship between the output frequency and amplitude, allowing only one parameter to control the motor across its full operating speed, both in forwards and reverse direction.

4.11 Conclusions

Although the Venturini control algorithms are generally regarded as complex to implement, this has been disproved with the flexible control software designed and developed for real-time operation of the laboratory matrix converter. The implementation of both original and advanced Venturini control regimes has been successfully accomplished using a low cost MCU while retaining the full range of features available with these strategies. This was realised by writing highly optimised control software that exploited the MCU architecture and minimised real-time computation through extensive use of lookup tables. The original Venturini control strategy allows full control of the input displacement angle while the advanced strategy operates with a unity displacement angle to maximise converter supply utilisation. The control software allows a number of different commutation sequences to be implemented for subsequent laboratory testing. Both control codes are fully autonomous and reside entirely within the MCU memory for standalone operation. The increased operating resolution of the advanced Venturini software necessitated

external storage of the large cosine lookup tables using a custom designed flash memory card solution. An increase in external cosine access speed was possible by interleaving the lookup table entries to allow sequential retrieval.

Reliable supply synchronisation has been achieved by sensing the supply voltage threshold to generate a reference signal for the control system. A software 'locking' algorithm was employed to synchronise the Venturini algorithm with the supply and provide additional noise immunity by selectively enabling the governing interrupt. This also allowed free running operation in the event of a momentary interruption of the reference signal. Reliable device commutation was ensured by implementing external logic that enabled only one switch to be closed at a time in each output phase. This also reduces MCU I/O resource usage and further accelerates the speed of the Venturini software implementations. The control software also allows alternative switching sequences to be investigated; these modes are selected during the converter start-up sequence.

The complete software listings of both original and advanced Venturini control algorithms described in this chapter are available as a separate document.

5. Chapter Five - Matrix Converter Performance

5.1 Introduction

Following a number of initial experiments conducted to verify the operation of the bi-directional switches, described in Appendix A11 [p265], the performance of the practical matrix converter was investigated in detail. This allowed the base performance of the matrix converter to be established and fully assess both the converter hardware and control software. At the initial lower switching frequencies, the practical converter output waveforms were observed and compared with a computer model that had been developed to aid familiarisation with the Venturini algorithms.

The performance of both the standard and advanced Venturini control algorithm implementations was examined using a static resistive-inductive load. The laboratory converter was tested across both the output amplitude and frequency range, with the results confirming that independent control of either variable is possible. The displacement-angle control feature of the original Venturini control software was investigated using a lagging load. The stability of this feature was further examined by varying the load inductance while maintaining a unity input displacement angle. These experiments were performed using both Venturini control strategies with a comparison highlighting the increase in supply utilisation possible with the advanced strategy. Harmonic analysis of the input and output current waveforms allowed comparison of the noise spectra produced by the matrix converter, showing that the harmonic noise profile for both control strategies were similar. Chapter Six considers motor operation.

5.2 Output Waveform Structure

The operating principle of the matrix converter has been described in Section 2.8 [p52] and showed that the output voltage waveform is composed of short samples of the supply waveforms. During a switching cycle, the output voltage waveform is synthesised by connecting each input phase to the converter load for a precise length of time. One switch per output phase is closed at a time to prevent supply short circuit with the switch periods calculated using one of a number of different modulation strategies that provide full control of both the output frequency and voltage and converter input displacement angle.

5.2.1 1kHz Waveforms

The following results have been obtained from the laboratory matrix converter when using the standard Venturini control strategy operating at a switching frequency of 1kHz with an AC supply voltage of 20V. They were recorded prior to the installation of the supply filter during the hardware verification phase.

Venturini	SWF	F_{out}	q	Load R (Ω)	Load L (H)
Original	1 kHz	See below	0.27	0.3	0.0018

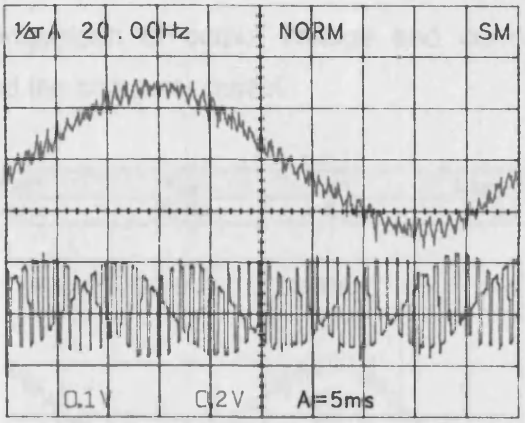

Figure 66 - Practical Output Current & Voltage Waveforms F_{out} = 20Hz

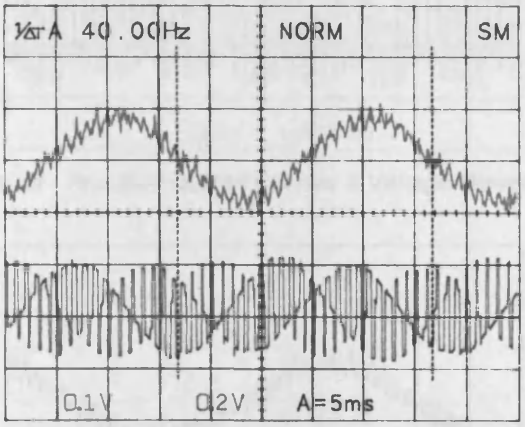

Figure 67 - Practical Output Current & Voltage Waveforms F_{out} = 40Hz

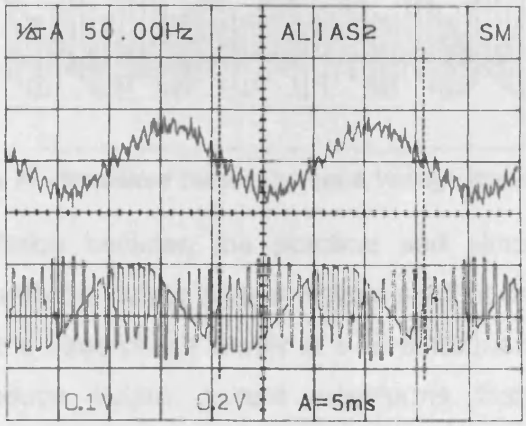

Figure 68 - Practical Output Current & Voltage Waveforms F_{out} = 50Hz

The output waveform results agree with those predicted by theory; the output voltage waveform is composed of short samples of the three-phase supply and its amplitude and frequency can be varied. The current waveform is recognisably sinusoidal and the low switching frequency, used here to allow capture of the output voltage waveform, results in the current waveform being moderately rippled.

Computer models of the matrix converter, as described in Appendix A12 [p267], were developed for initial experimentation with the Venturini control strategy. Figure 69 and Figure 70 show a comparison of output voltage and current waveforms for the laboratory converter and the computer model.

Venturini	SWF	F_{out}	q	Load R (Ω)	Load L (H)
Original	1 kHz	30 Hz	0.27	0.3	0.0018

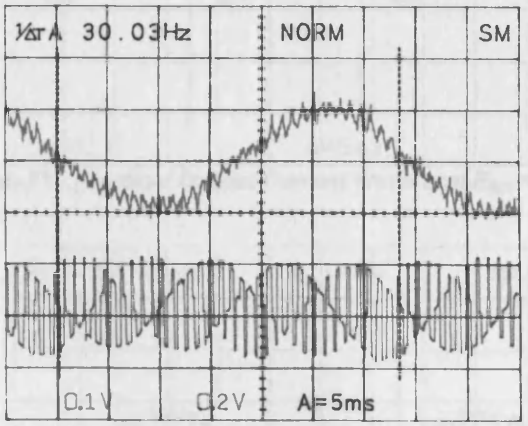

Figure 69 - Practical Output Current & Voltage Waveforms

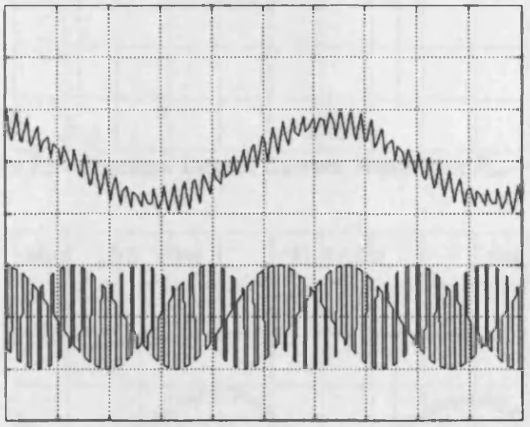

Figure 70 - Simulated Output Current & Voltage Waveforms

There is good correlation between the practical and simulated results. This is particularly noticeable with the output voltage waveforms that are virtually identical and show the sampling of the three-phase supply at a 1kHz frequency. The laboratory and computer model produce output current waveforms that also exhibit similar characteristics.

5.2.2 2kHz Waveforms

The switching frequency was subsequently increased to 2kHz in order to examine the effect on the input and output waveform ripple and to continue verification of the computer model. The supply voltage remained at 20V with the same resistive-inductive load as used previously.

Venturini	SWF	F_{out}	q	Load R (Ω)	Load L (H)
Original	2 kHz	See below	0.46	0.3	0.0018

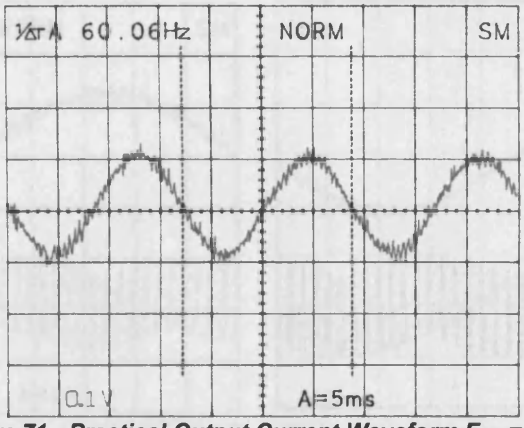

Figure 71 - Practical Output Current Waveform F_{out} = 60Hz

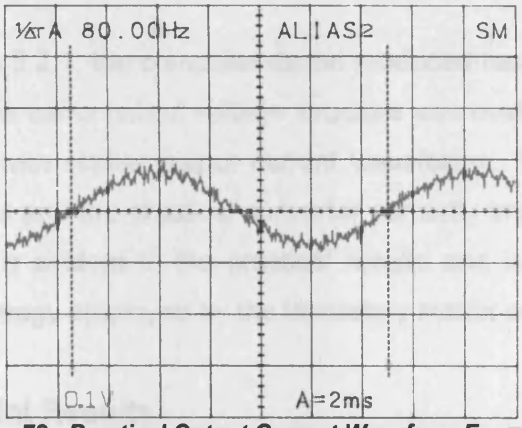

Figure 72 - Practical Output Current Waveform F_{out} = 80Hz

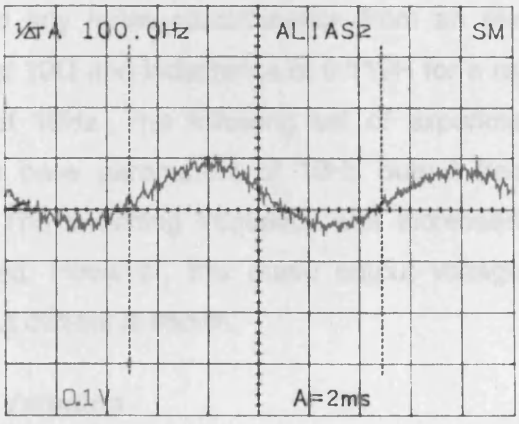

Figure 73 - Practical Output Current Waveform F_{out} = 100Hz

The wide operating range of the matrix converter is demonstrated by the ability to produce an output waveform at a frequency of 100Hz, as shown in Figure 73. The increase in switching frequency to 2kHz also reduces the output current waveform ripple as the higher switching rate allows synthesis of a higher quality waveform. A comparison between the practical laboratory converter and the computer model is shown in Figure 74 and Figure 75.

Venturini	SWF	F_{out}	q	Load R (Ω)	Load L (H)
Original	2 kHz	50 Hz	0.46	0.3	0.0018

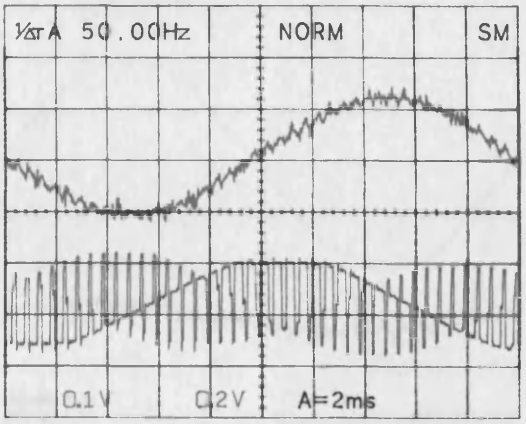

Figure 74 - Practical Output Current & Voltage Waveforms

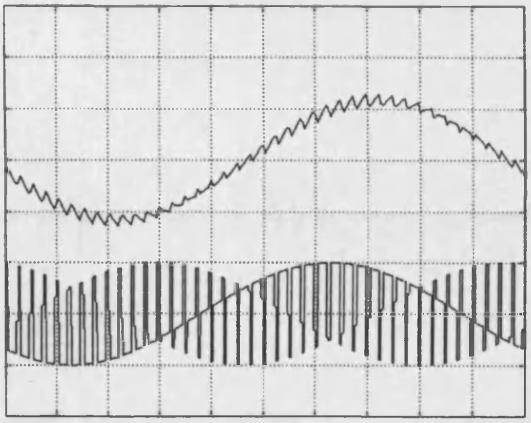

Figure 75 - Simulated Output Current & Voltage Waveforms

As observed in Section 5.2.1, the computer model produced results that closely match the practical results. The same output voltage structure was evident within the practical and simulated results with similar output current waveforms. This suggests that the computer model is valid and the practical converter correctly implements the Venturini strategy. Some noise is evident in the practical results and is due to break-before-make commutation strategy employed by the laboratory matrix converter.

5.3 Original Venturini Results

The performance of the matrix converter was investigated using a static resistive-inductive load to avoid any noise contamination from an electric motor. The load provided a resistance of 10Ω and inductance of 0.119H for a resultant power-factor of 0.80 at a frequency of 10Hz. The following set of experiments used the original Venturini strategy with base parameters of 10Hz output frequency and a voltage transfer ratio of 0.20. The switching frequency was increased to 4kHz to allow the supply filter to be used. However, this made output voltage capture difficult and therefore only the output current is shown.

5.3.1 Output Voltage Variation

The original Venturini control strategy allows independent control of the output amplitude and output frequency, much like a cycloconverter with particular relevance for applications where high power is required at low output frequencies. With a fixed output frequency of 10Hz, the original Venturini strategy was configured to provide a unity input displacement angle whilst the output voltage was tested across the available amplitude range. The following results show input voltage and current on the left with the corresponding output current on the right.

Venturini	SWF	F_{out}	q	Load R (Ω)	Load L (H)	Power Factor
Original	4 kHz	10 Hz	0	10	0.119	0.80

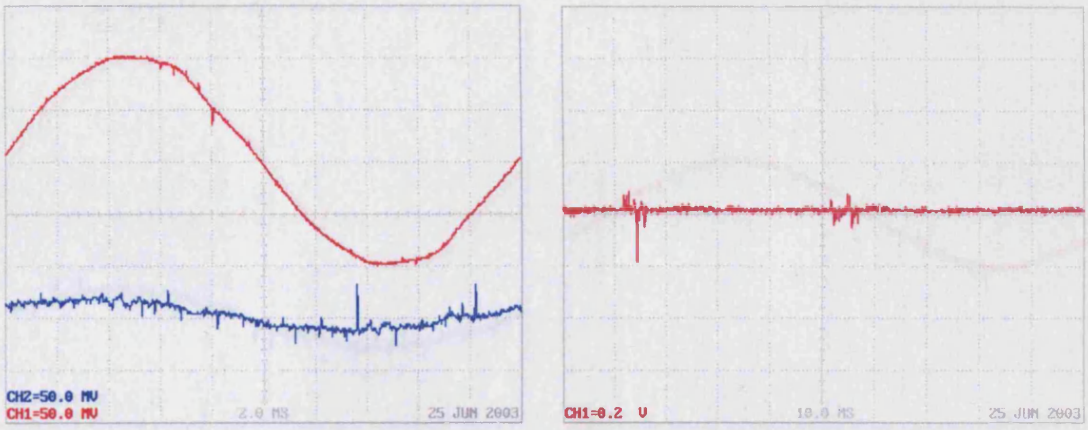

Figure 76 - q = 0.0 (a) Supply Voltage & Current & (b) Output Current

The converter is observed to effectively produce a DC output at zero volts when the output amplitude is reduced to zero. Analysis of the Venturini strategy in Equation 5 [p55] shows that when the voltage transfer ratio (q) is reduced to zero, each input phase is connected to the load for a third of the switching cycle. The supply vectors cancel each other to produce a zero mean output voltage with minimal drawn supply current.

Venturini	SWF	F_{out}	q	Load R (Ω)	Load L (H)	Power Factor
Original	4 kHz	10 Hz	0.10	10	0.119	0.80

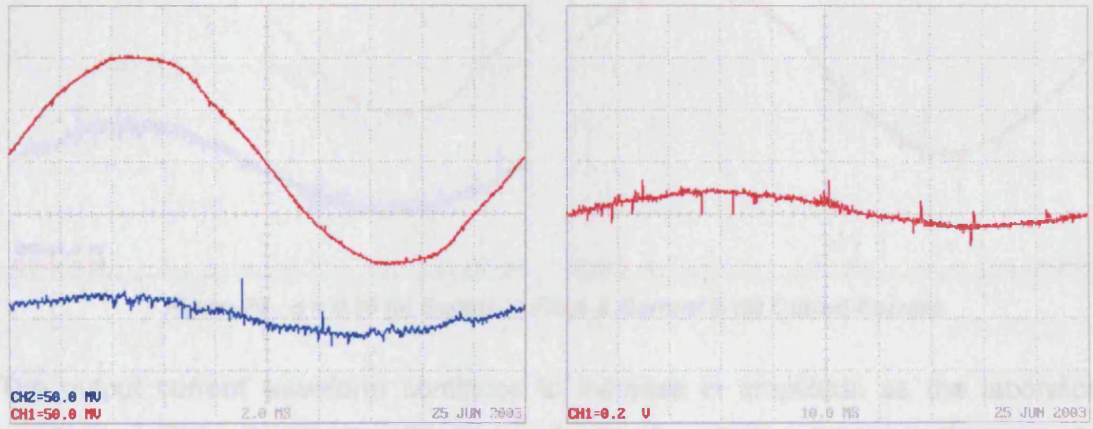

Figure 77 - q = 0.10 (a) Supply Voltage & Current & (b) Output Current

With a minimal voltage transfer ratio (q), the converter begins to produce a sinusoidal output waveform at the target frequency of 10Hz. Compared with the previous set of results in Figure 76, there is a slight increase in the demanded (also sinusoidal) supply current to satisfy the load.

Venturini	SWF	F_{out}	q	Load R (Ω)	Load L (H)	Power Factor
Original	4 kHz	10 Hz	0.20	10	0.119	0.80

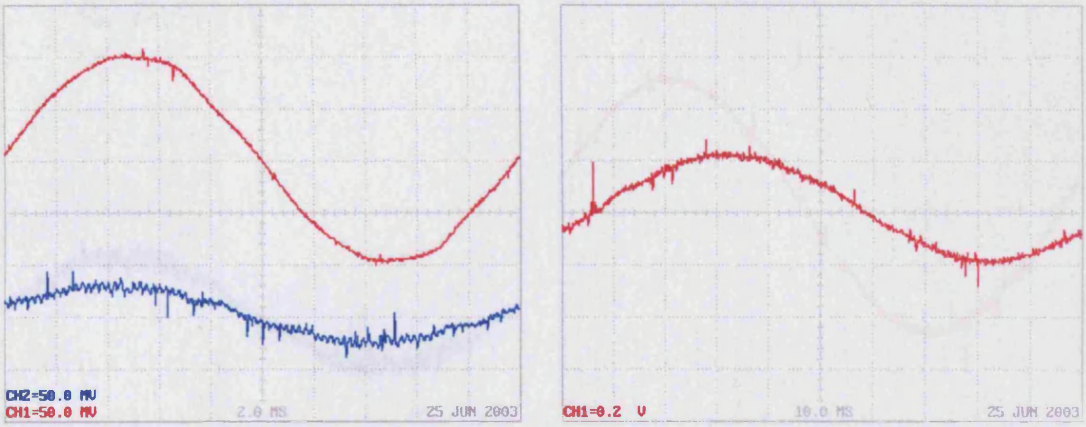

Figure 78 - q = 0.20 (a) Supply Voltage & Current & (b) Output Current

As the output amplitude (q) is increased, the output current waveform continues to increase in magnitude with a corresponding increase in the converter supply current amplitude.

Venturini	SWF	F_{out}	q	Load R (Ω)	Load L (H)	Power Factor
Original	4 kHz	10 Hz	0.30	10	0.119	0.80

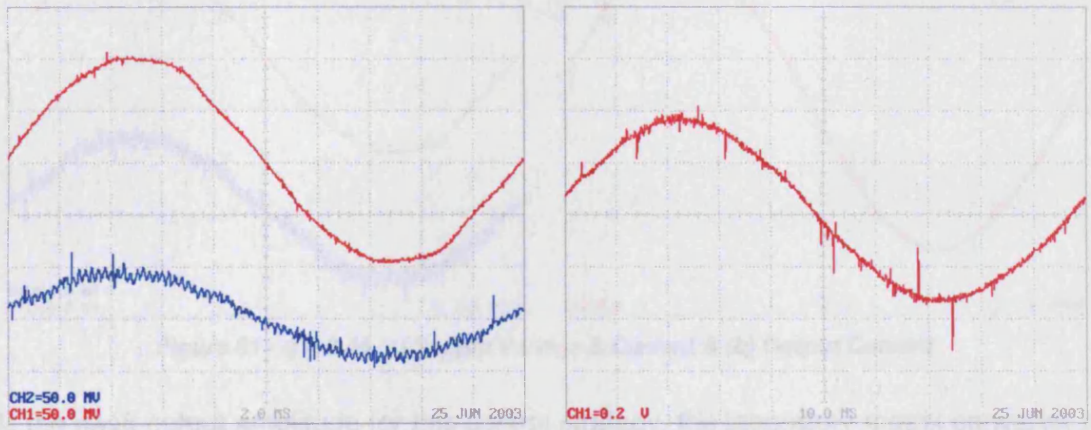

Figure 79 - q = 0.30 (a) Supply Voltage & Current & (b) Output Current

The output current waveform continues to increase in amplitude as the laboratory matrix converter output setting for (q) is raised with a similar change in the converter supply

Venturini	SWF	F_{out}	q	Load R (Ω)	Load L (H)	Power Factor
Original	4 kHz	10 Hz	0.40	10	0.119	0.80

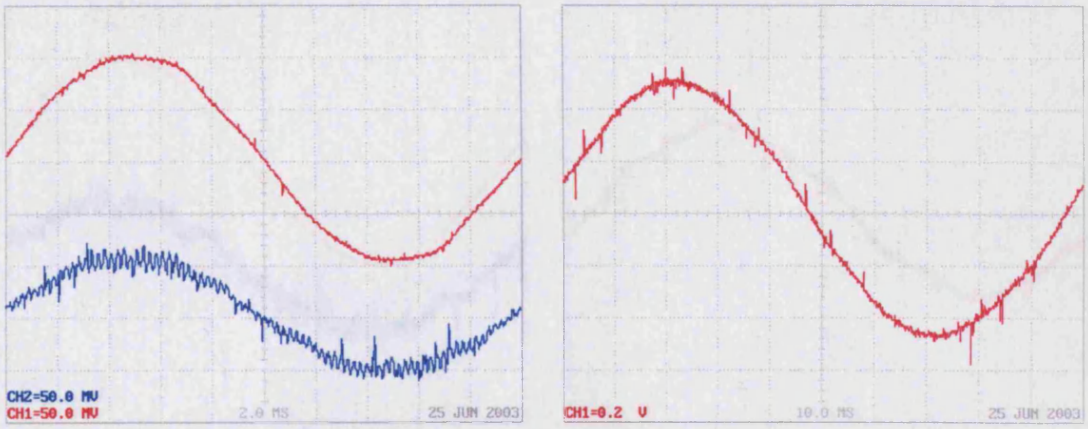

Figure 80 - q = 0.40 (a) Supply Voltage & Current & (b) Output Current

The same behaviour continues as the voltage transfer ratio (q) is increased to 0.40 and the supply voltage remaining unchanged.

Venturini	SWF	F_{out}	q	Load R (Ω)	Load L (H)	Power Factor
Original	4 kHz	10 Hz	0.46	10	0.119	0.80

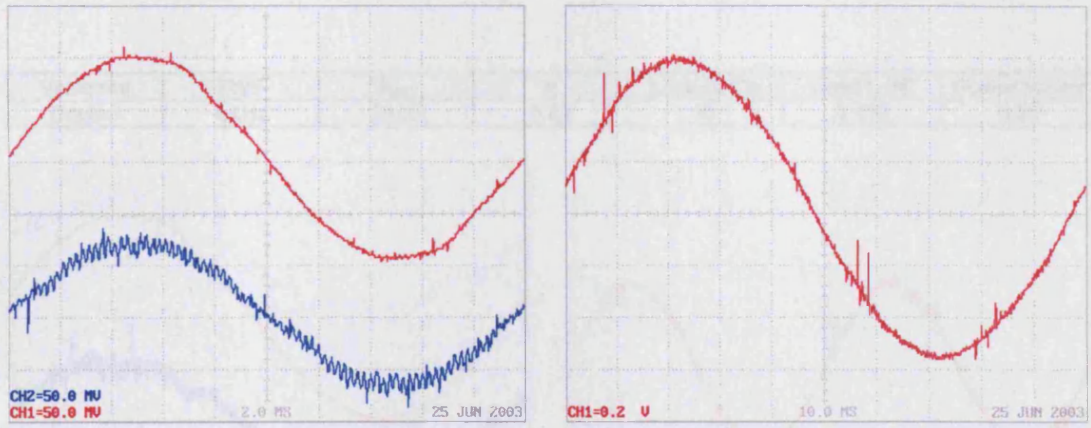

Figure 81 - q = 0.46 (a) Supply Voltage & Current & (b) Output Current

At the peak output amplitude for this control strategy, the laboratory matrix converter is observed to produce high-quality input and output waveforms. Although providing an inferior supply utilisation compared with later, more advanced techniques, the original Venturini strategy allows independent control of the output amplitude irrespective of the output frequency, whilst maintaining unity input displacement angle. The input current increases in response to the output current being drawn from the converter.

5.3.2 Output Frequency Variation

The total independence of the output amplitude and frequency has been verified in the following investigation using the original Venturini control strategy. With a fixed output amplitude of q=0.20, the input and output waveforms were examined as the output frequency was varied across a range of 5 - 50Hz.

Venturini	SWF	F_{out}	q	Load R (Ω)	Load L (H)	Power Factor
Original	4 kHz	5 Hz	0.20	10	0.119	0.94

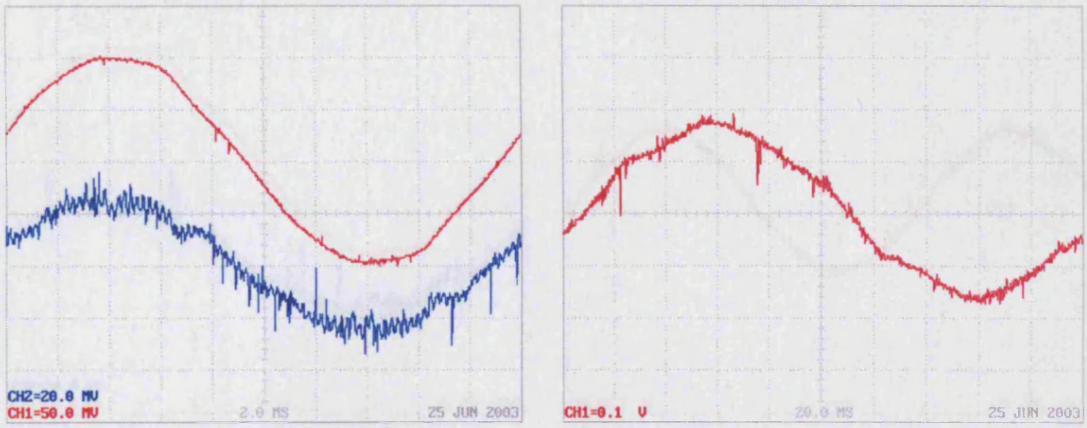

Figure 82 - F_{out} = 5Hz (a) Supply Voltage & Current & (b) Output Current

At this low frequency, the output current waveform is found to be slightly distorted, a result of the non-ideal power supply, as shown by the simulated results in Appendix A13 [p276].

Venturini	SWF	F_{out}	q	Load R (Ω)	Load L (H)	Power Factor
Original	4 kHz	10 Hz	0.20	10	0.119	0.80

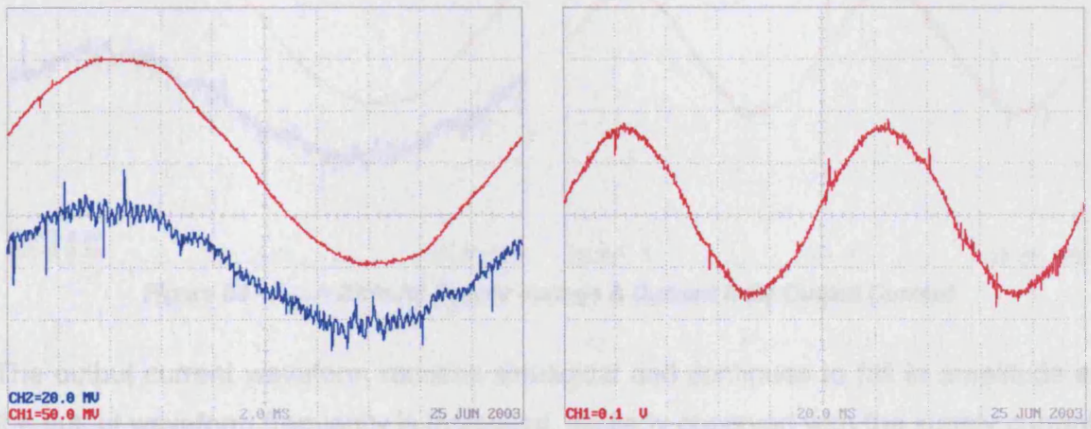

Figure 83 - F_{out} = 10Hz (a) Supply Voltage & Current & (b) Output Current

As the output frequency is increased to 10Hz, the output waveform distortion is almost eliminated as the effects of the imperfect supply waveform became less significant. Also visible is a fall in the input and output current waveform magnitudes, a result of the effective load impedance increasing with the output frequency.

Venturini	SWF	F_{out}	q	Load R (Ω)	Load L (H)	Power Factor
Original	4 kHz	15 Hz	0.20	10	0.119	0.67

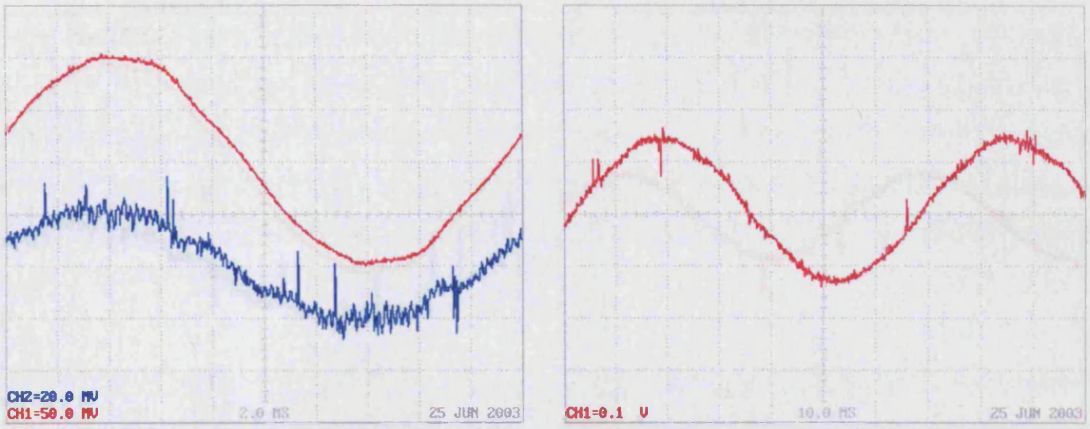

Figure 84 - F_{out} = 15Hz (a) Supply Voltage & Current & (b) Output Current

The same behaviour continues as the output frequency is increased.

Venturini	SWF	F_{out}	q	Load R (Ω)	Load L (H)	Power Factor
Original	4 kHz	20 Hz	0.20	10	0.119	0.56

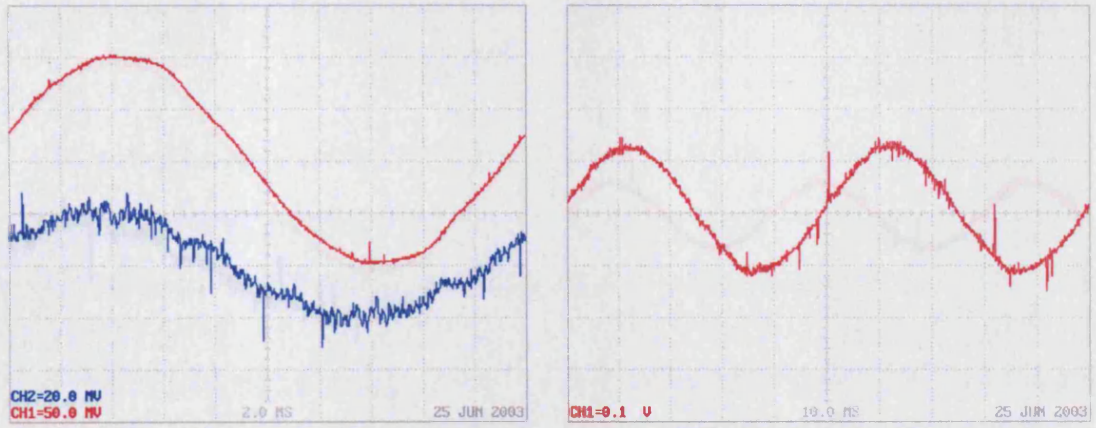

Figure 85 - F_{out} = 20Hz (a) Supply Voltage & Current & (b) Output Current

The output current waveform remains sinusoidal and continues to fall in amplitude as the output waveform frequency is increased, similarly observed with the supply current.

Venturini	SWF	F_{out}	q	Load R (Ω)	Load L (H)	Power Factor
Original	4 kHz	35 Hz	0.20	10	0.119	0.36

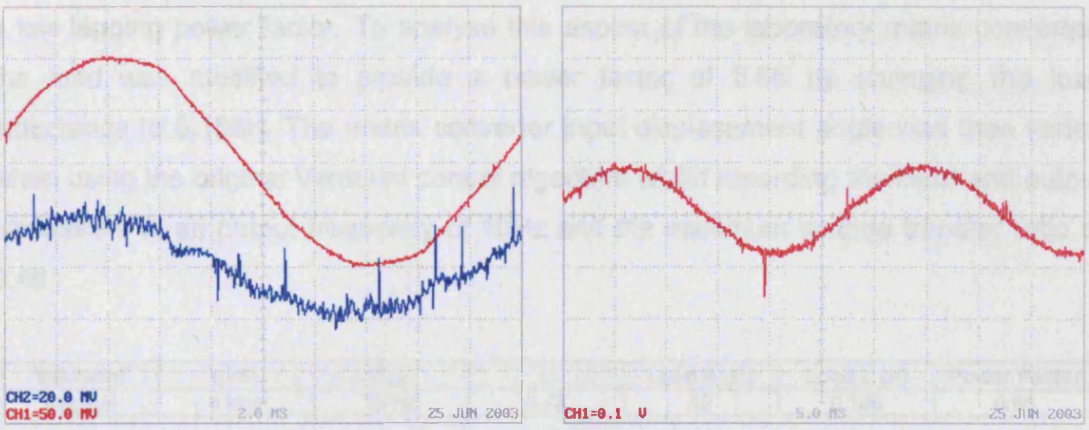

Figure 86 - F_{out} = 35Hz (a) Supply Voltage & Current & (b) Output Current

At a frequency of 35Hz, the waveforms are sinusoidal with unity displacement angle maintained in the supply.

Venturini	SWF	F_{out}	q	Load R (Ω)	Load L (H)	Power Factor
Original	4 kHz	50 Hz	0.20	10	0.119	0.26

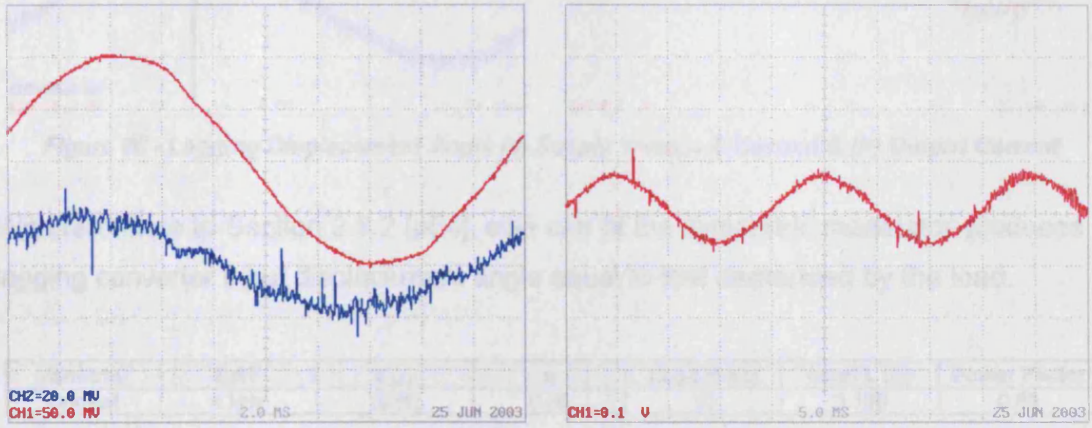

Figure 87 - F_{out} = 50Hz (a) Supply Voltage & Current & (b) Output Current

At the peak output frequency of 50Hz, synchronous with the power supply, the converter produces good quality sinusoidal waveforms in both the supply and load. As per theory, the output and, therefore, supply current falls as the output frequency is increased. Ignoring this natural effect, the original Venturini control strategy has been found capable of varying the output frequency independently of the amplitude whilst successfully maintaining a unity input displacement angle.

5.3.3 Input Displacement Angle Variation

A feature of both Venturini control strategies allows the input displacement angle to be varied irrespective of the load connected to the matrix converter. An electrically demanding load can be 'corrected' in order to reduce the strain on the generator and

limit interference with local electrical equipment. This is particularly valuable for marine applications where propulsion motors, such as an induction machine, may operate with a low lagging power factor. To analyse this aspect of the laboratory matrix converter, the load was modified to provide a power factor of 0.65 by changing the load inductance to 0.186H. The matrix converter input displacement angle was then varied when using the original Venturini control algorithm whilst recording the input and output waveforms at an output frequency of 10Hz and the maximum voltage transfer ratio of 0.46.

Venturini	SWF	F_{out}	q	Load R (Ω)	Load L (H)	Power Factor
Original	4 kHz	10 Hz	0.46	10	0.186	0.65

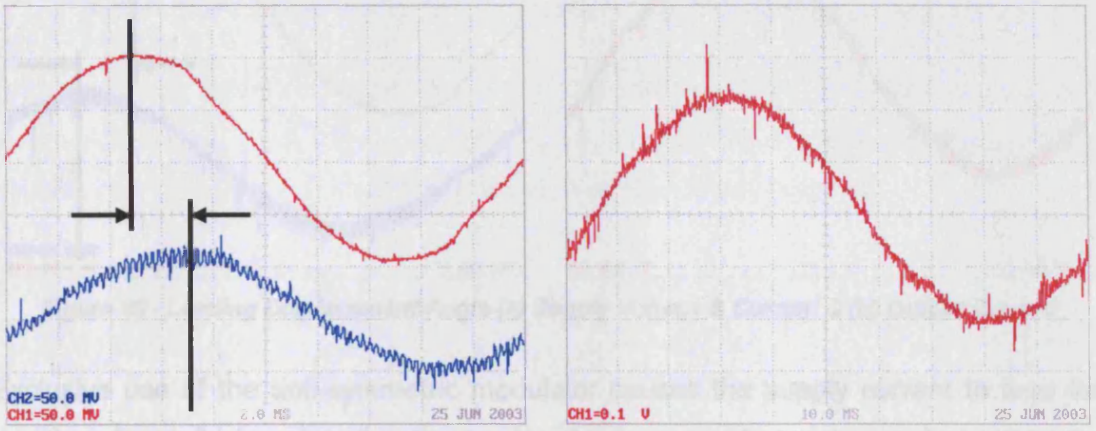

Figure 88 - Lagging Displacement Angle (a) Supply Voltage & Current & (b) Output Current

With reference to Section 2.8.2 [p54], sole use of the symmetric modulator produces a lagging converter input displacement angle equal to that demanded by the load.

Venturini	SWF	F_{out}	q	Load R (Ω)	Load L (H)	Power Factor
Original	4 kHz	10 Hz	0.46	10	0.186	0.65

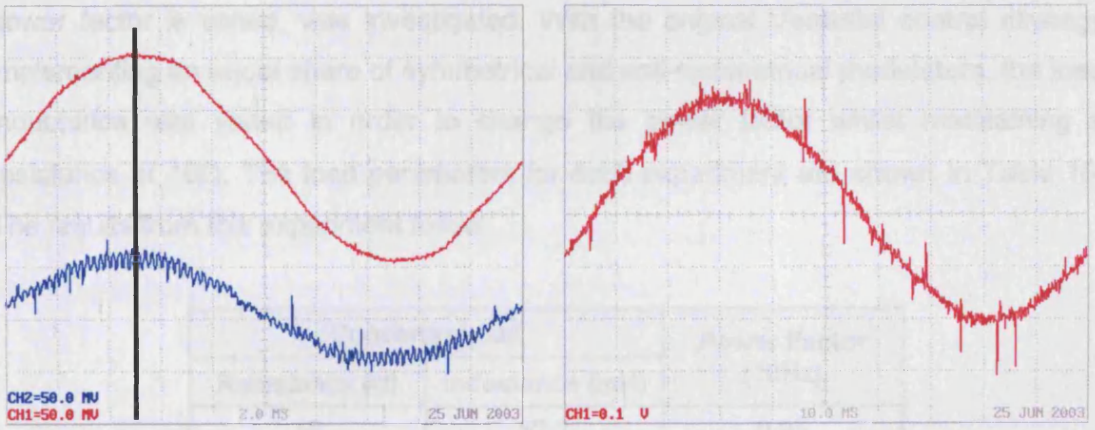

Figure 89 - Unity Displacement Angle (a) Supply Voltage & Current & (b) Output Current

With equal proportions of symmetric and anti-symmetric modulators, $\alpha_1 = \alpha_2 = ½$, the matrix converter produces an approximate unity input displacement angle. A slight time

lag in the supply voltage measurement, introduced by the necessity for the measurement to be initially captured using a powerscope before transferral to the storage oscilloscope, prevented the supply waveforms being precisely in phase. Both input and output waveform amplitudes are unaltered by the change in the converter input displacement angle.

Venturini	SWF	F_{out}	q	Load R (Ω)	Load L (Ω)	Power Factor
Original	4 kHz	10 Hz	0.46	10	0.186	0.65

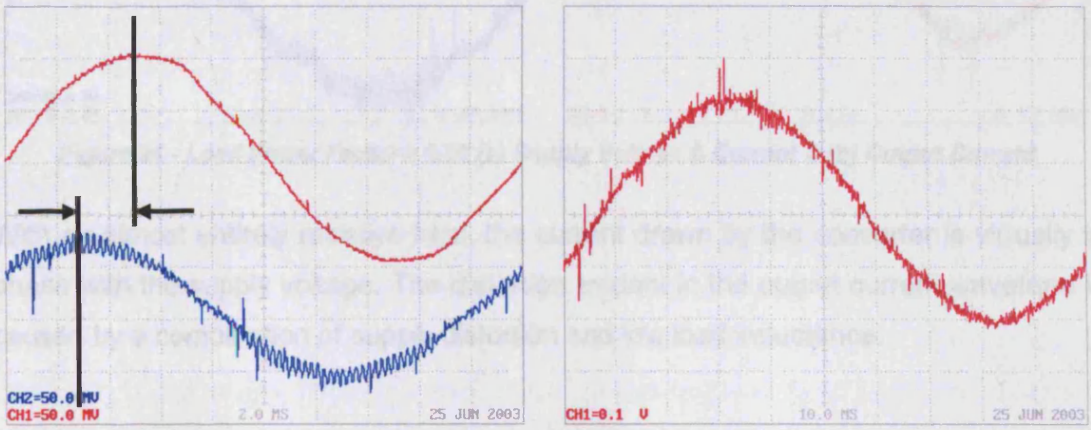

Figure 90 - Leading Displacement Angle (a) Supply Voltage & Current & (b) Output Current

Exclusive use of the anti-symmetric modulator causes the supply current to lead the supply voltage. As found earlier, the input and output waveforms are unchanged by the variation in displacement angle, confirming that this feature of the matrix converter can be safely used to reduce the impact of demanding loads on the generator set.

5.3.4 Load Power Factor Variation

As a unity input displacement angle is generally desirable in the majority of applications, the ability of the matrix converter to maintain this condition, as the load power factor is varied, was investigated. With the original Venturini control strategy implementing an equal share of symmetrical and anti-symmetrical modulators, the load inductance was varied in order to change the power factor whilst maintaining a resistance of 10Ω. The load parameters for each experiment are shown in Table 16. The results from this experiment follow:

Converter Load		Power Factor (10Hz)
Resistance (Ω)	Inductance (mH)	
10	52.3	0.95
10	119.5	0.80
10	186.1	0.65

Table 16 - Laboratory Converter R-I Load Parameters

Venturini	SWF	F_{out}	q	Load R (Ω)	Load L (H)	Power Factor
Original	4 kHz	10 Hz	0.20	10	0.052	0.95

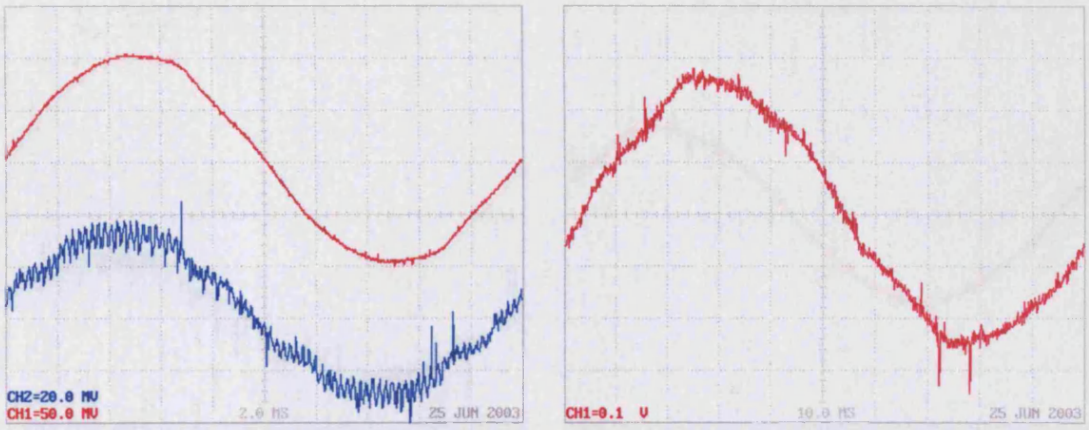

Figure 91 - Load Power Factor = 0.95 (a) Supply Voltage & Current & (b) Output Current

With an almost entirely resistive load, the current drawn by the converter is virtually in phase with the supply voltage. The distortion evident in the output current waveform is caused by a combination of supply distortion and low load inductance.

Venturini	SWF	F_{out}	q	Load R (Ω)	Load L (H)	Power Factor
Original	4 kHz	10 Hz	0.20	10	0.119	0.80

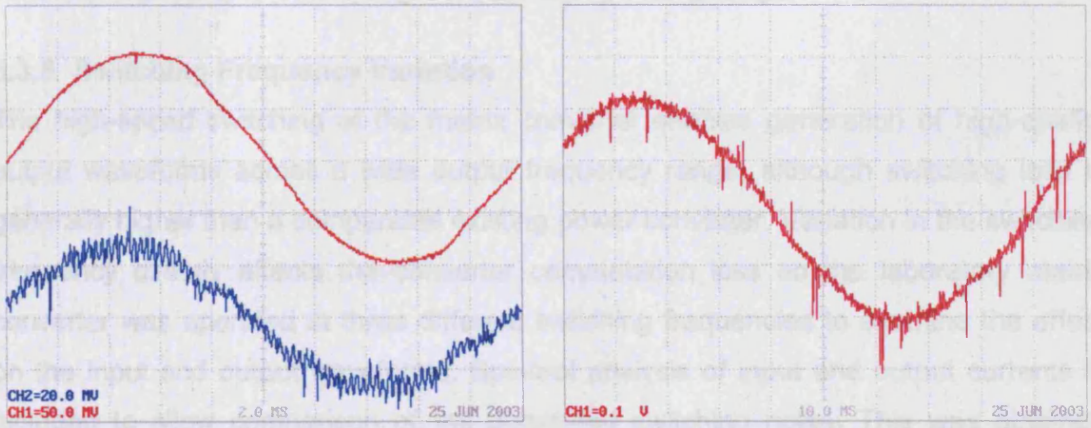

Figure 92 - Load Power Factor = 0.80 (a) Supply Voltage & Current & (b) Output Current

As the load power factor is reduced to 0.80, the converter maintains the same input displacement angle observed in the previous experiment. The input and output current amplitudes are reduced at this lower load power factor.

Venturini	SWF	F_{out}	q	Load R (Ω)	Load L (H)	Power Factor
Original	4 kHz	10 Hz	0.20	10	0.186	0.65

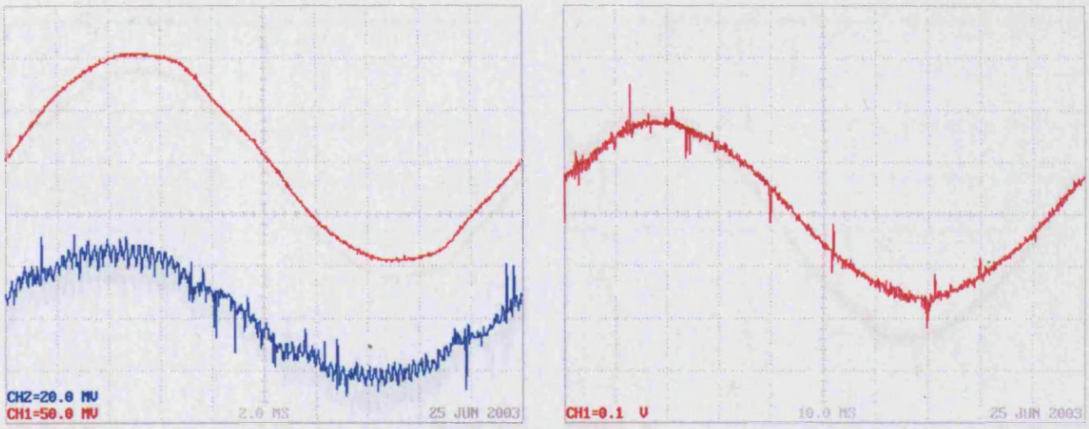

Figure 93 - Load Power Factor = 0.65 (a) Supply Voltage & Current & (b) Output Current

With the load power factor lowered to 0.65, unity input displacement angle is maintained, although both the input and output current waveform amplitudes are further reduced. Without modifying the ratio of symmetric to anti-symmetric modulators, the matrix converter succeeds in maintaining a fixed input displacement angle, irrespective of the load power factor. This characteristic allows a load with varying power factor to be connected to the generator set whilst maintaining a fixed converter input displacement angle across the operating range.

5.3.5 Switching Frequency Variation

The high-speed switching of the matrix converter enables generation of high-quality output waveforms across a wide output frequency range, although switching loss is generally higher than a comparable existing power converter. Variation in the switching frequency directly affects the converter commutation loss so the laboratory matrix converter was operated at three different switching frequencies to examine the effect on the input and output waveforms. Spectral analysis of input and output currents is included to allow comparison of the generated switching noise. This was obtained using a parallel port device connected to a host personal computer running the spectral analysis software. This was configured to sample at a frequency of 28kHz with a Blackman windowing function.

Venturini	SWF	F_{out}	q	Load R (Ω)	Load L (H)	Power Factor
Original	3 kHz	10 Hz	0.20	10	0.119	0.80

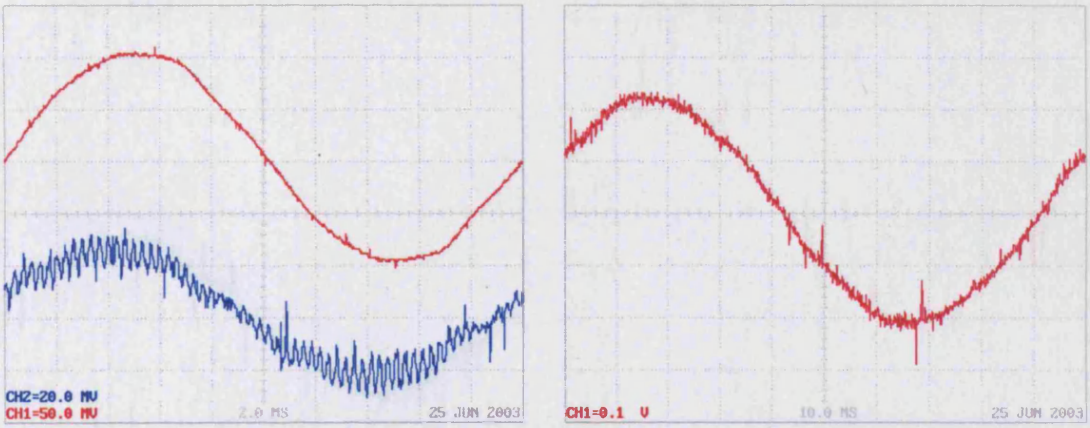

Figure 94 - SWF = 3kHz (a) Supply Voltage & Current & (b) Output Current

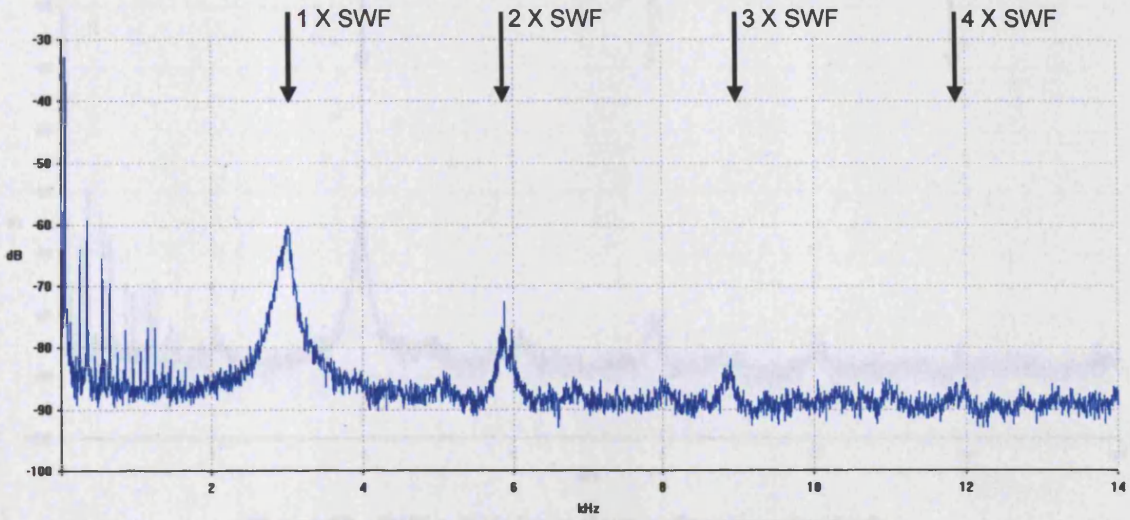

Figure 95 - SWF = 3kHz Input Current Spectrum Analysis

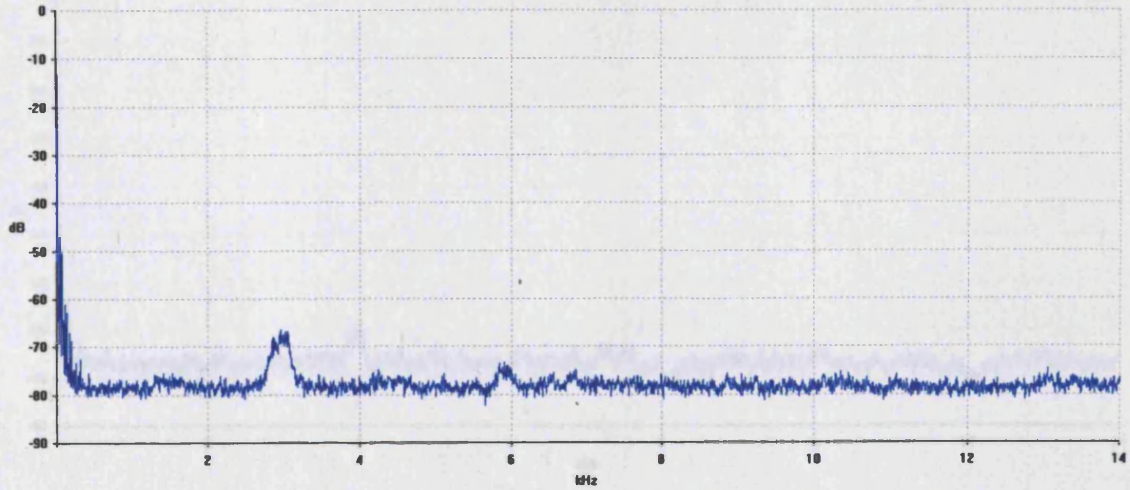

Figure 96 - SWF = 3kHz Output Current Spectrum Analysis

Venturini	SWF	F_{out}	q	Load R (Ω)	Load L (H)	Power Factor
Original	4 kHz	10 Hz	0.20	10	0.119	0.80

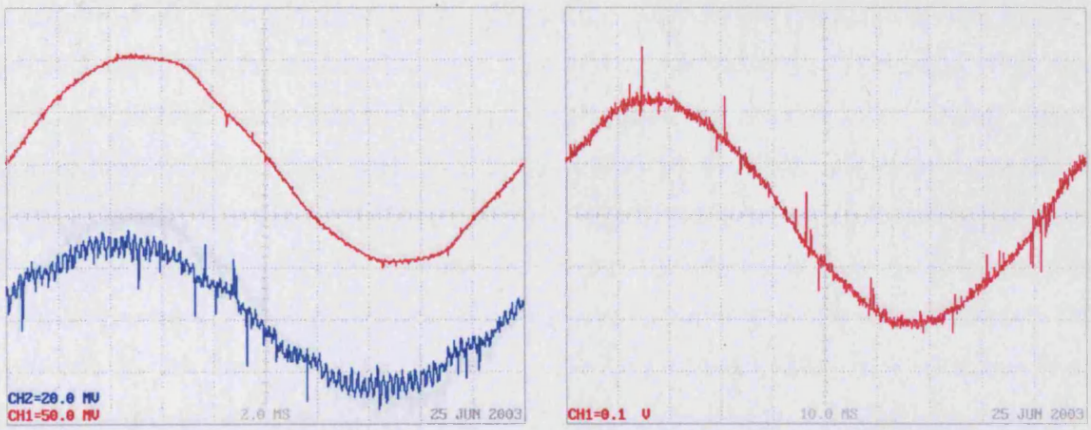

Figure 97 - SWF = 4kHz (a) Supply Voltage & Current & (b) Output Current

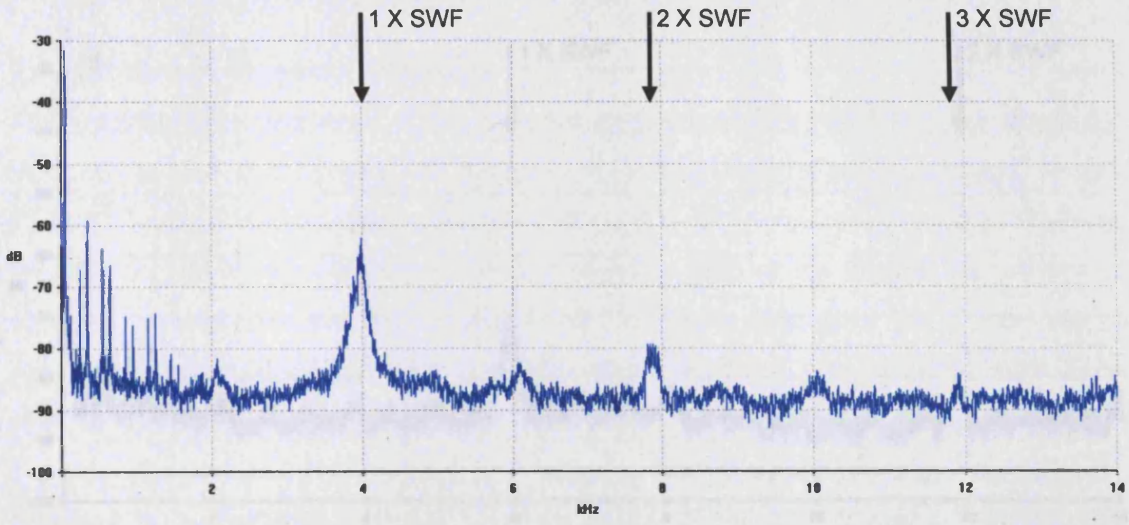

Figure 98 - SWF = 4kHz Input Current Spectrum Analysis

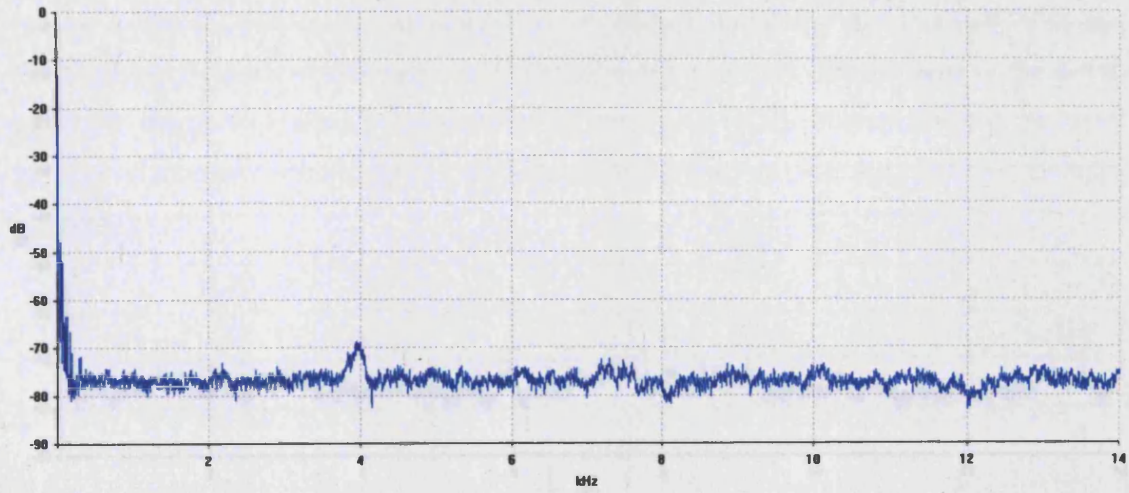

Figure 99 - SWF = 4kHz Output Current Spectrum Analysis

Venturini	SWF	F_{out}	q	Load R (Ω)	Load L (H)	Power Factor
Original	6 kHz	10 Hz	0.20	10	0.119	0.80

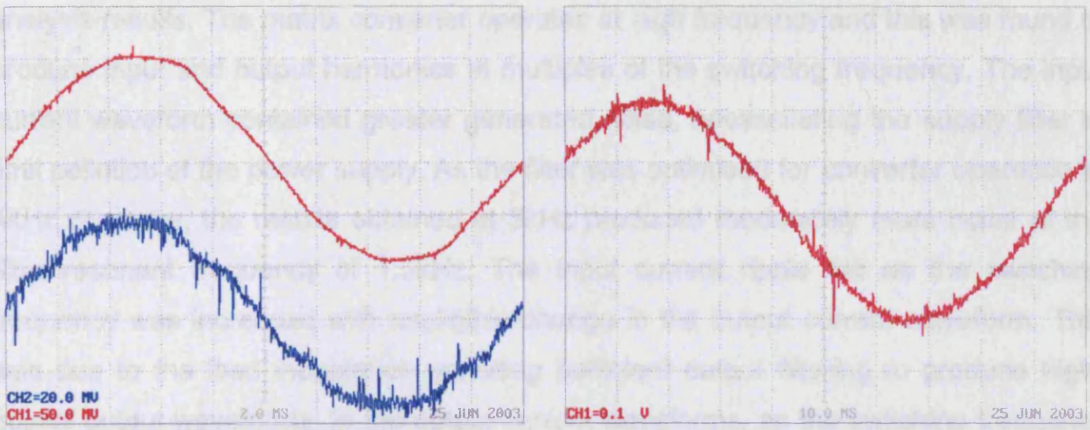

Figure 100 - SWF = 6kHz (a) Supply Voltage & Current & (b) Output Current

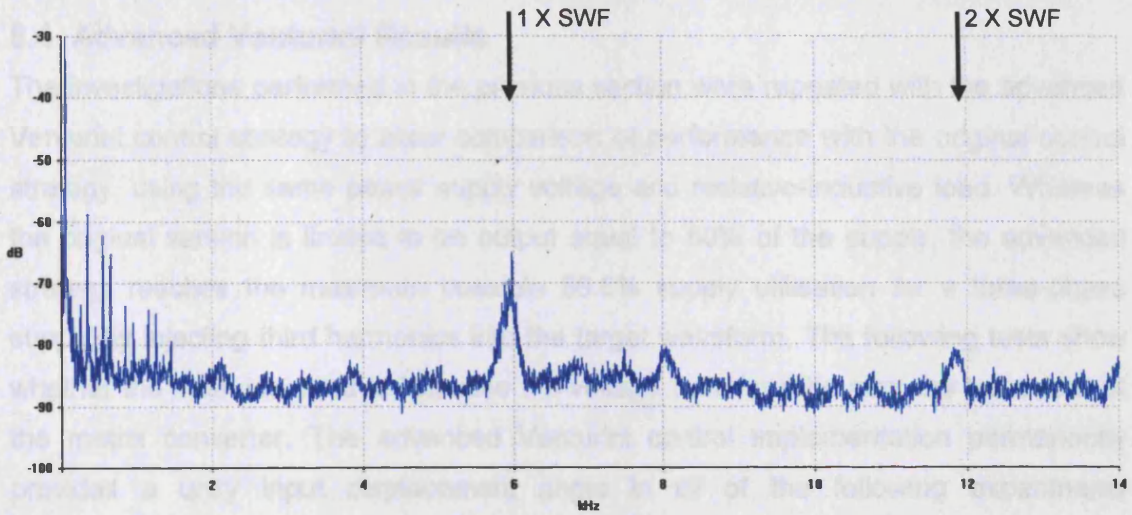

Figure 101 - SWF = 6kHz Input Current Spectrum Analysis

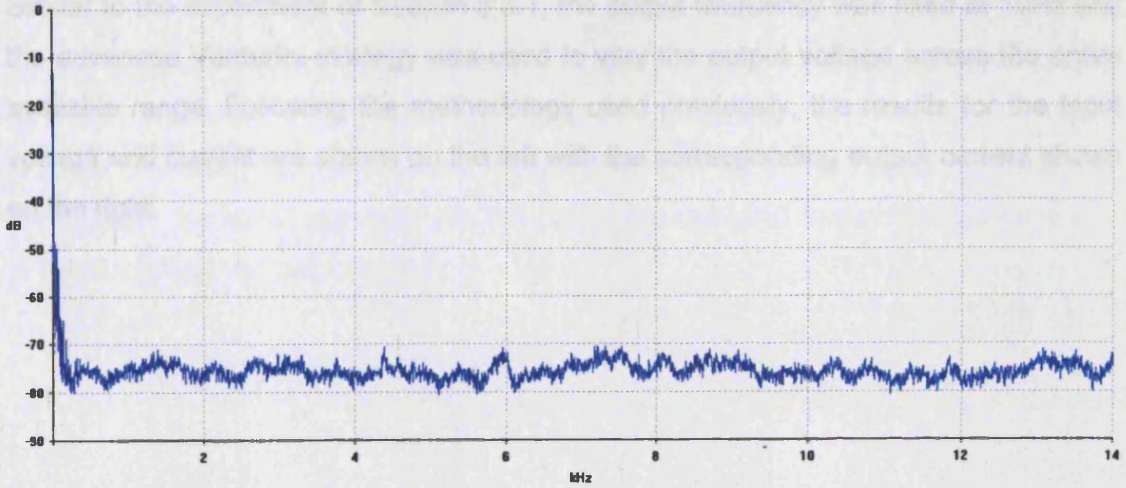

Figure 102 - SWF = 6kHz Output Current Spectrum Analysis

The input and output waveform quality was found to improve as the switching frequency was increased, as illustrated by the input and output current spectrum analysis results. The matrix converter operates at high frequency and this was found to produce input and output harmonics at multiples of the switching frequency. The input current waveform contained greater generated noise, necessitating the supply filter to limit pollution of the power supply. As the filter was optimised for converter operation at 4kHz or above, the results obtained at 3kHz produced moderately more noise at the filter resonant frequency of 1.5kHz. The input current ripple fell as the switching frequency was increased with negligible change in the output current waveform. This was due to the load inductance providing sufficient output filtering to produce high-quality output waveforms. In the output current waveforms, as the switching frequency was increased, the fundamental harmonics at this frequency were shifted further away from the output frequency with reduced magnitude.

5.4 Advanced Venturini Results

The investigations performed in the previous section were repeated with the advanced Venturini control strategy to allow comparison of performance with the original control strategy, using the same power supply voltage and resistive-inductive load. Whereas the original version is limited to an output equal to 50% of the supply, the advanced strategy reaches the maximum possible 86.6% supply utilisation for a three-phase supply by injecting third harmonics into the target waveform. The following tests show whether the methods used to increase the voltage transfer ratio alter the behaviour of the matrix converter. The advanced Venturini control implementation permanently provides a unity input displacement angle in all of the following experiments irrespective of the load.

5.4.1 Output Voltage Variation

Similar to the experiment of Section 5.3.1, the output frequency was fixed at 10Hz and the advanced Venturini strategy was used to vary the output voltage across the entire available range. Following the methodology used previously, the results for the input voltage and current are shown on the left with the corresponding output current shown on the right.

Venturini	SWF	F_{out}	q	Load R (Ω)	Load L (H)	Power Factor
Advanced	4 kHz	10 Hz	0	10	0.119	0.80

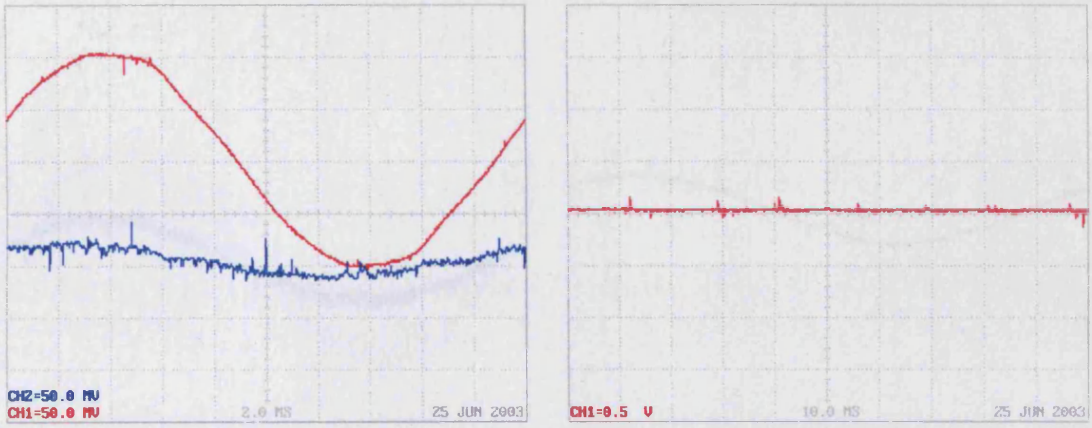

Figure 103 - q = 0.0 (a) Supply Voltage & Current & (b) Output Current

With the control system set for zero output amplitude (q=0), the converter produces a zero voltage DC output with minimal sinusoidal current drawn from the power supply.

Venturini	SWF	F_{out}	q	Load R (Ω)	Load L (H)	Power Factor
Advanced	4 kHz	10 Hz	0.15	10	0.119	0.80

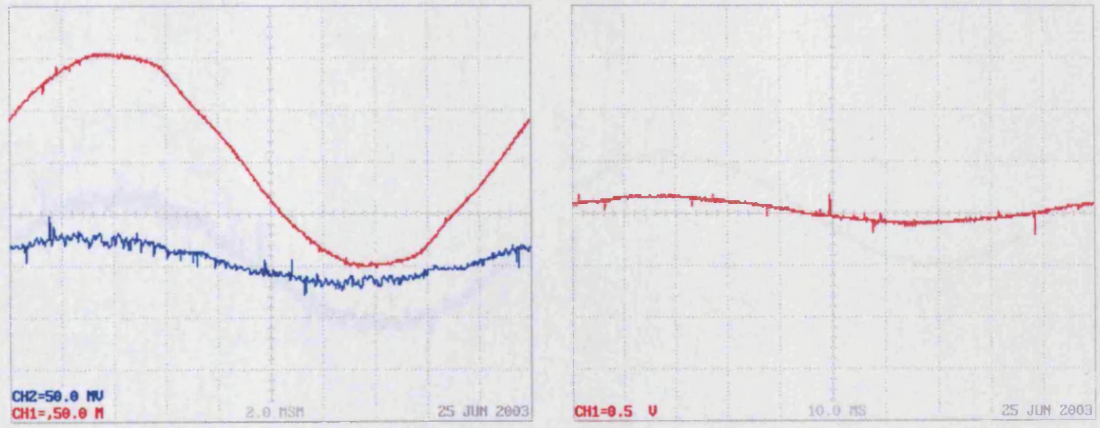

Figure 104 - q = 0.15 (a) Supply Voltage & Current & (b) Output Current

As the laboratory matrix converter output voltage transfer is increased from zero to q=0.15, the output current waveform assumes a sinusoidal form with the converter drawing increased current from the supply. The input current is largely in phase with the supply voltage, as expected with the laboratory controller system's implementation of the advanced Venturini strategy.

Venturini	SWF	F_{out}	q	Load R (Ω)	Load L (H)	Power Factor
Advanced	4 kHz	10 Hz	0.30	10	0.119	0.80

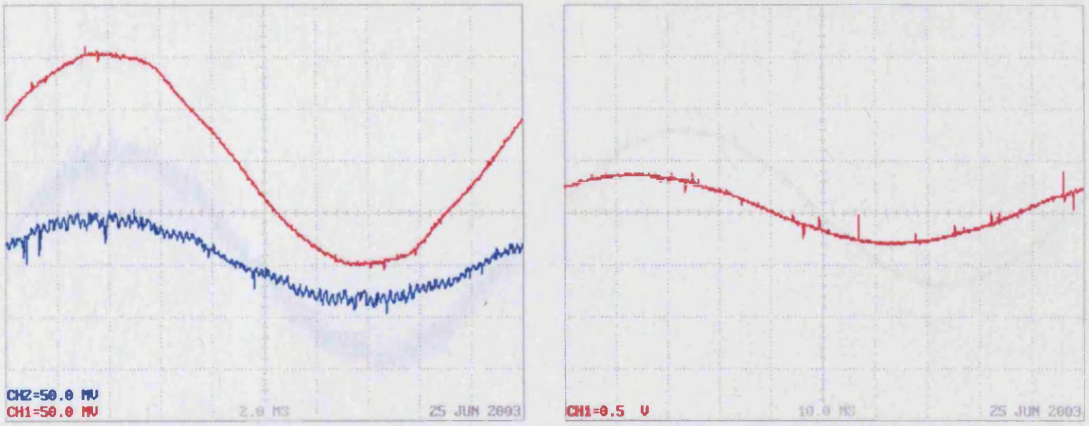

Figure 105 - q = 0.30 (a) Supply Voltage & Current & (b) Output Current

As the output amplitude increases, the supply current amplitude shows a corresponding rise.

Venturini	SWF	F_{out}	q	Load R (Ω)	Load L (H)	Power Factor
Advanced	4 kHz	10 Hz	0.45	10	0.119	0.80

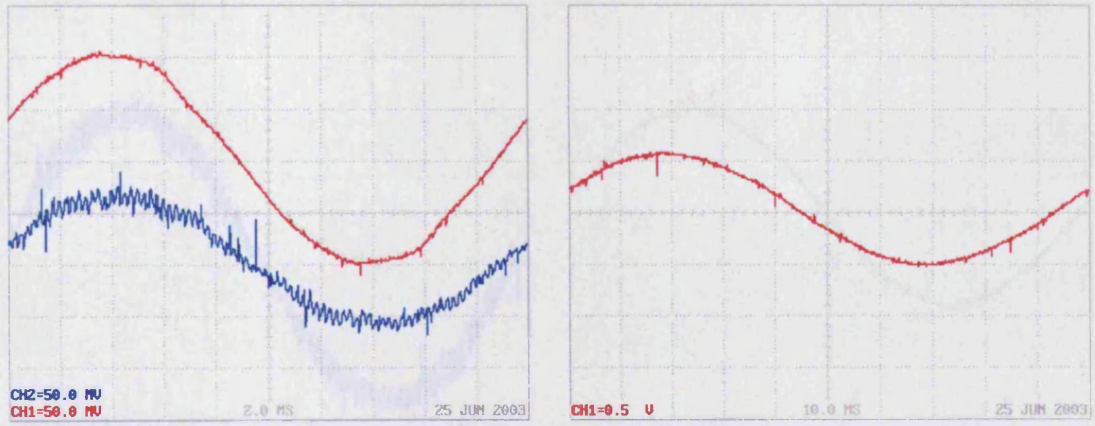

Figure 106 - q = 0.45 (a) Supply Voltage & Current & (b) Output Current

The sinusoidal input and output currents continue to increase together while the input current remains in phase with the supply voltage.

Venturini	SWF	F_{out}	q	Load R (Ω)	Load L (H)	Power Factor
Advanced	4 kHz	10 Hz	0.60	10	0.119	0.80

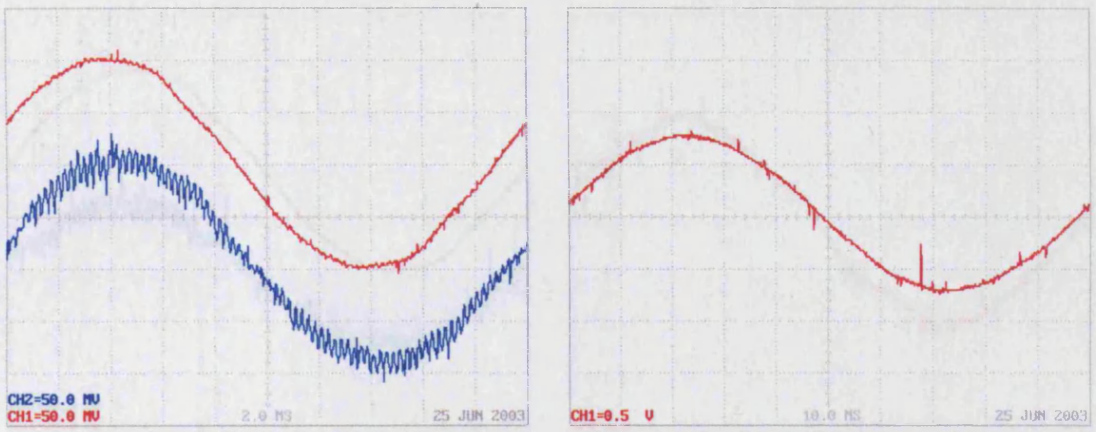

Figure 107 - q = 0.60 (a) Supply Voltage & Current & (b) Output Current

The same behaviour continues as the voltage transfer ratio (q) increases above that possible with the original Venturini control strategy.

Venturini	SWF	F_{out}	q	Load R (Ω)	Load L (H)	Power Factor
Advanced	4 kHz	10 Hz	0.76	10	0.119	0.80

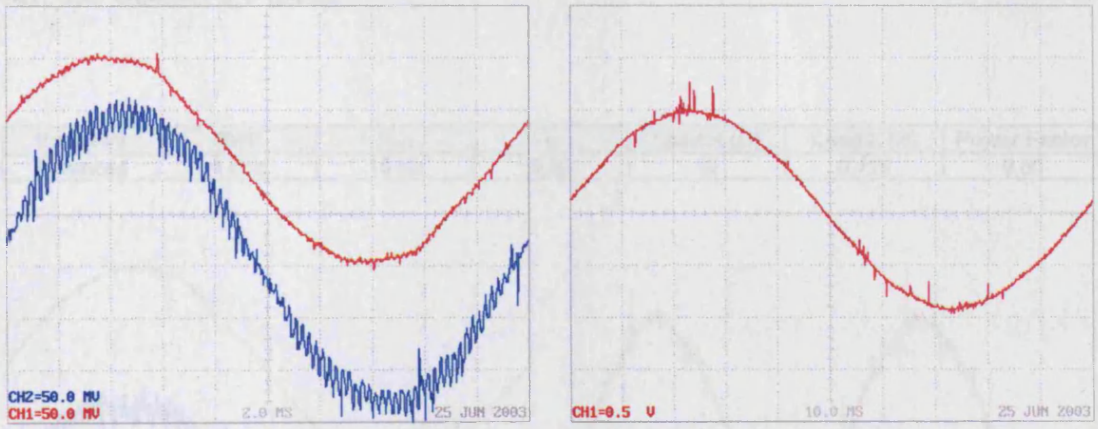

Figure 108 - q = 0.76 (a) Supply Voltage & Current & (b) Output Current

The advanced control strategy is found to produce sinusoidal input and output waveforms at higher voltage transfer ratios than possible with the original strategy. Input and output current waveforms are found to be high-quality sinusoids at all output amplitudes.

5.4.2 Output Frequency Variation

For completeness, Section 5.3.2 has been repeated for the advanced Venturini control strategy. With a fixed output amplitude of q=0.20, the input and output waveforms were captured as the output frequency was varied across a wide range.

Venturini	SWF	F_{out}	q	Load R (Ω)	Load L (H)	Power Factor
Advanced	4 kHz	5 Hz	0.20	10	0.119	0.94

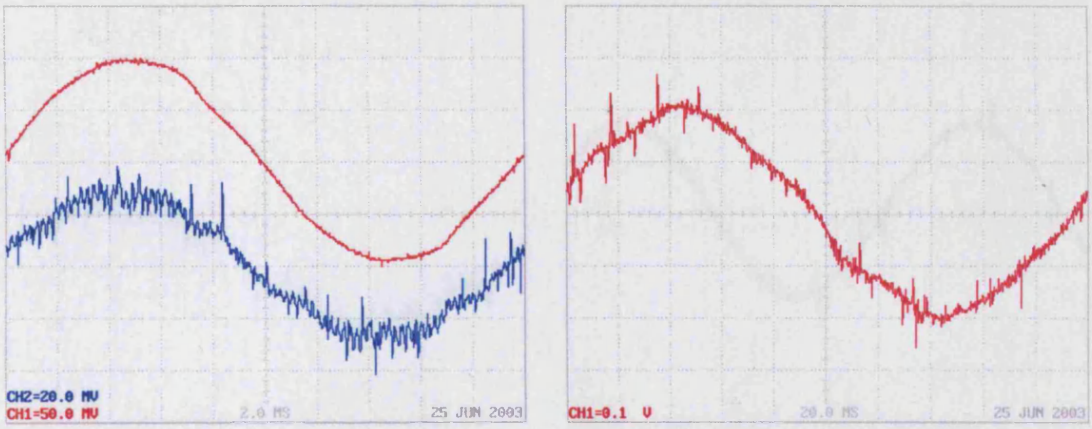

Figure 109 - F_{out} = 5Hz (a) Supply Voltage & Current & (b) Output Current

Similar to the original Venturini control strategy, the output current waveform is found to be distorted at such low output frequencies. The cause is slight supply voltage distortion that is transferred to the output waveform, an intrinsic problem for direct AC-AC converters, see Appendix A13 [p276]. A version of the Venturini strategy that tracks the supply voltages would avoid the output waveform from being distorted in this way, see Section 2.9 [p63].

Venturini	SWF	F_{out}	q	Load R (Ω)	Load L (H)	Power Factor
Advanced	4 kHz	10 Hz	0.20	10	0.119	0.80

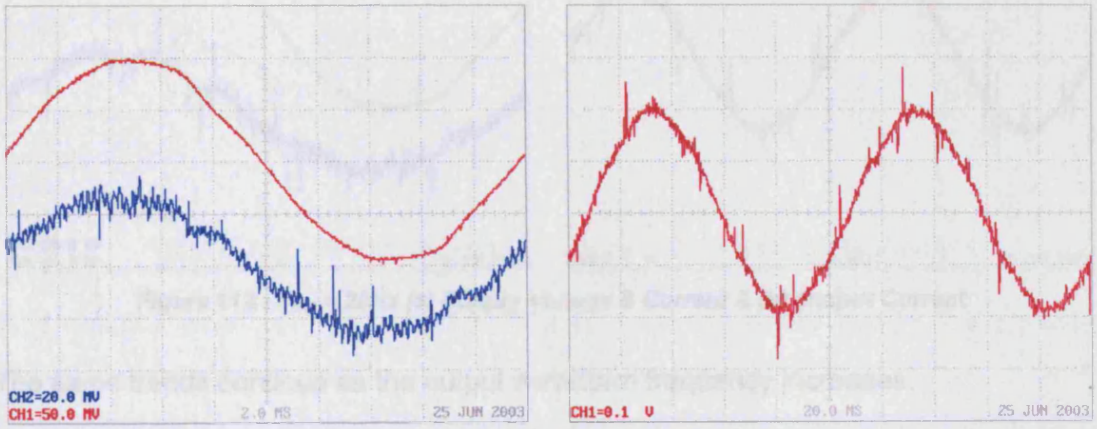

Figure 110 - F_{out} = 10Hz (a) Supply Voltage & Current & (b) Output Current

With the output frequency increased to 10Hz, the output current waveform distortion is no longer visible.

Venturini	SWF	F_{out}	q	Load R (Ω)	Load L (H)	Power Factor
Advanced	4 kHz	15 Hz	0.20	10	0.119	0.67

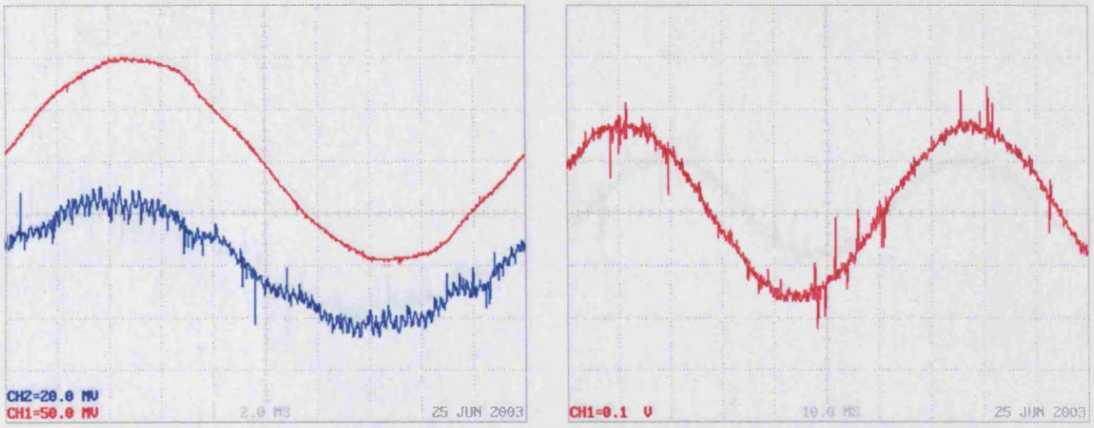

Figure 111 - F_{out} = 15Hz (a) Supply Voltage & Current & (b) Output Current

The input and output current amplitude falls as the output frequency increases, following inductive load theory as described previously. The input current remains in phase with the supply voltage.

Venturini	SWF	F_{out}	q	Load R (Ω)	Load L (H)	Power Factor
Advanced	4 kHz	20 Hz	0.20	10	0.119	0.56

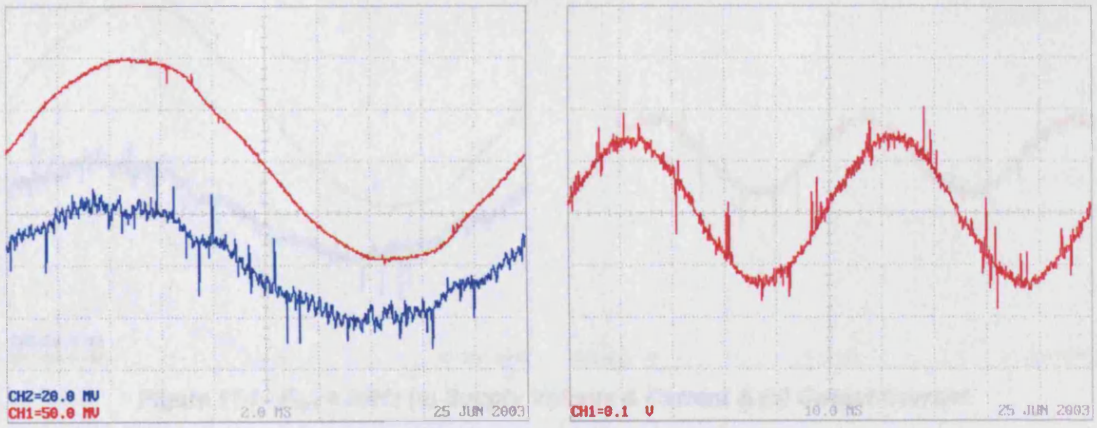

Figure 112 - F_{out} = 20Hz (a) Supply Voltage & Current & (b) Output Current

The same trends continue as the output waveform frequency increases.

Venturini	SWF	F_{out}	q	Load R (Ω)	Load L (H)	Power Factor
Advanced	4 kHz	35 Hz	0.20	10	0.119	0.36

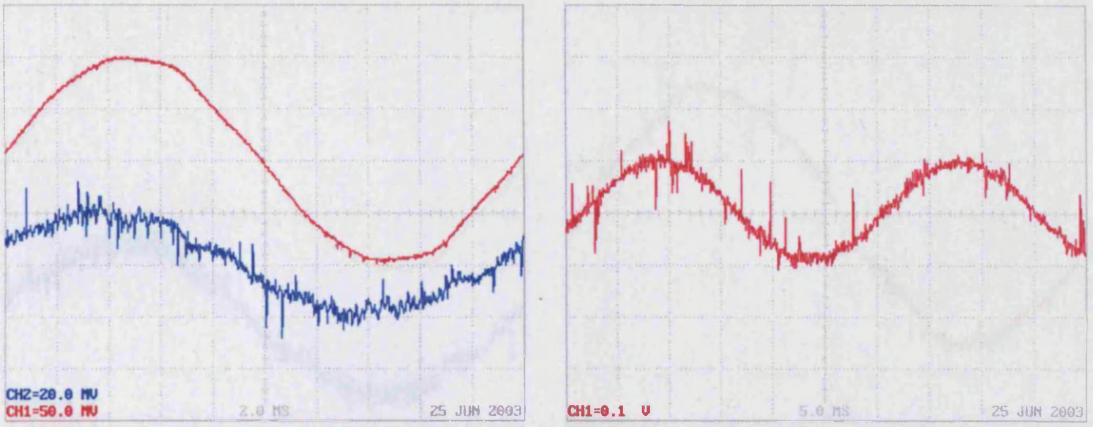

Figure 113 - F_{out} = 35Hz (a) Supply Voltage & Current & (b) Output Current

At an output frequency of 35Hz, the waveforms remain sinusoidal whilst continuing to fall in amplitude.

Venturini	SWF	F_{out}	q	Load R (Ω)	Load L (H)	Power Factor
Advanced	4 kHz	50 Hz	0.20	10	0.119	0.26

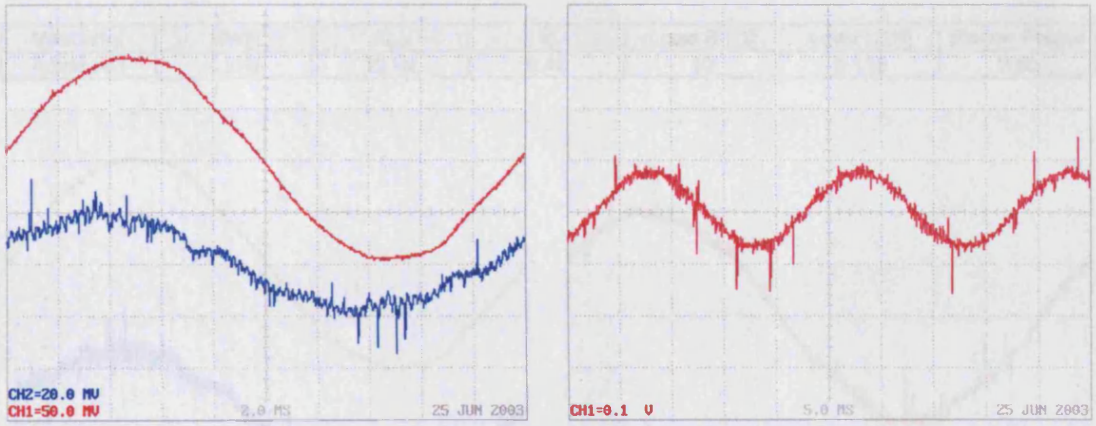

Figure 114 - F_{out} = 50Hz (a) Supply Voltage & Current & (b) Output Current

At an output waveform frequency synchronous with the power supply, the converter continues to maintain good quality sinusoidal waveforms. The advanced Venturini control strategy is found capable of varying the output frequency independently of the amplitude for more flexible control, whilst maintaining a fixed unity input displacement angle.

5.4.3 Load Power Factor Variation

To continue the investigation of Section 5.3.4, the ability of the advanced control strategy to maintain unity input displacement angle as the load power-factor was varied, was examined. The inductance in the load was varied in order to change the power factor, as in Table 16 [p115].

Venturini	SWF	F_{out}	q	Load R (Ω)	Load L (H)	Power Factor
Advanced	4 kHz	10 Hz	0.46	10	0.052	0.95

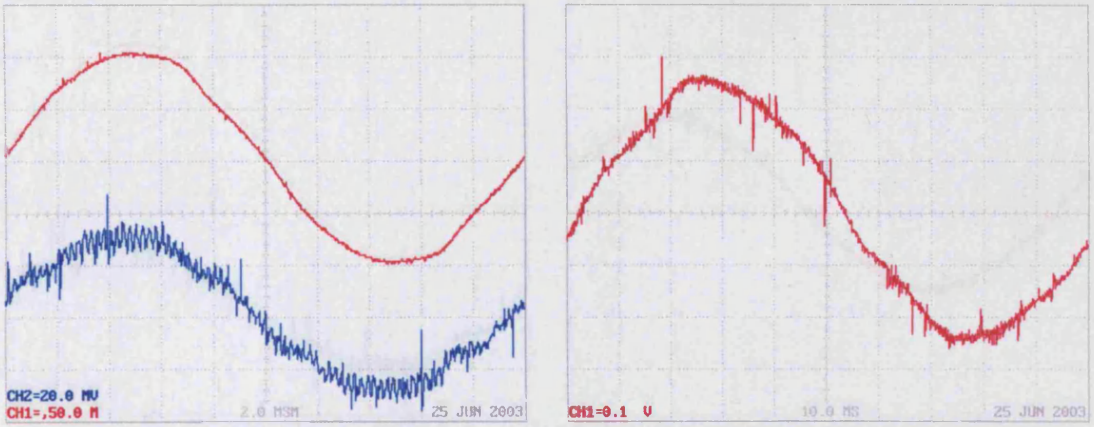

Figure 115 - Load Power Factor = 0.95 (a) Supply Voltage & Current & (b) Output Current

As with the original Venturini experiment, the output current waveform is somewhat distorted at this power factor. The almost entirely resistive load allows the converter to draw current virtually in phase with the supply voltage resulting in the desired unity input displacement angle.

Venturini	SWF	F_{out}	q	Load R (Ω)	Load L (H)	Power Factor
Advanced	4 kHz	10 Hz	0.46	10	0.119	0.80

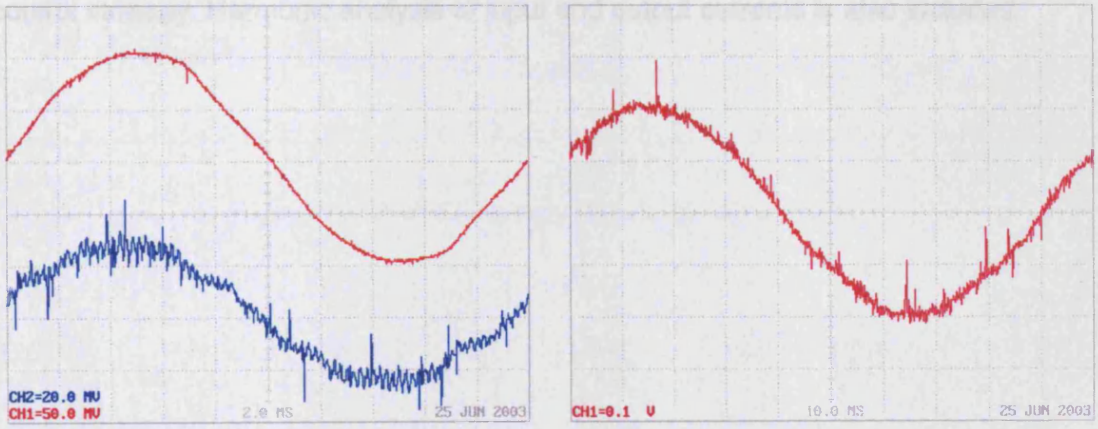

Figure 116 - Load Power Factor = 0.80 (a) Supply Voltage & Current & (b) Output Current

With a load power factor of 0.80, the converter maintains a unity input displacement angle as observed in the above experiment. The input and output current magnitudes are also reduced.

Venturini	SWF	F_{out}	q	Load R (Ω)	Load L (H)	Power Factor
Advanced	4 kHz	10 Hz	0.46	10	0.186	0.65

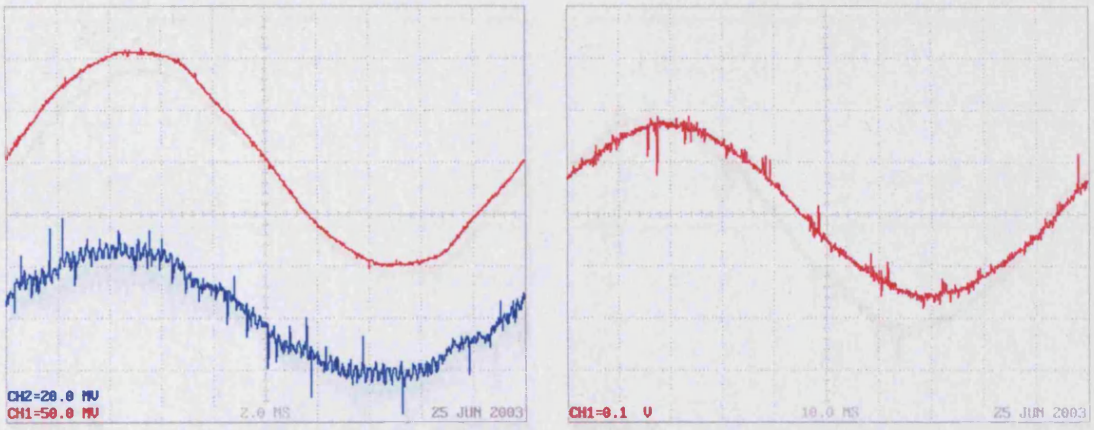

Figure 117 - Load Power Factor = 0.65 (a) Supply Voltage & Current & (b) Output Current

With a load power factor of 0.65, the same input displacement angle is retained with both the input and output current waveform amplitudes falling further. The advanced Venturini control strategy maintains a fixed displacement angle irrespective of the power factor demanded by the load.

5.4.4 Switching Frequency Variation

The matrix converter was operated at three different switching frequencies to examine the effect on the input and output waveforms generated by the advanced Venturini control strategy. Harmonic analysis of input and output currents is also included.

Venturini	SWF	F_{out}	q	Load R (Ω)	Load L (H)	Power Factor
Advanced	3 kHz	10 Hz	0.20	10	0.119	0.80

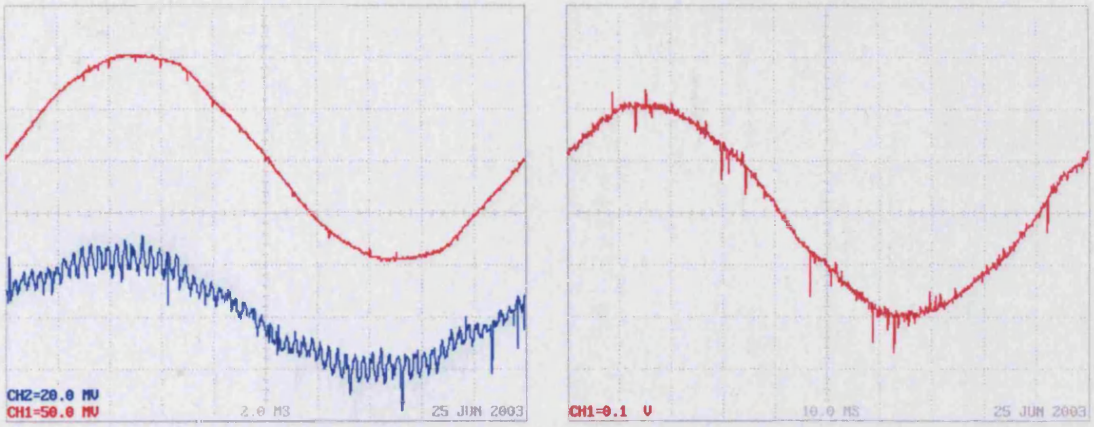

Figure 118 - SWF = 3kHz (a) Supply Voltage & Current & (b) Output Current

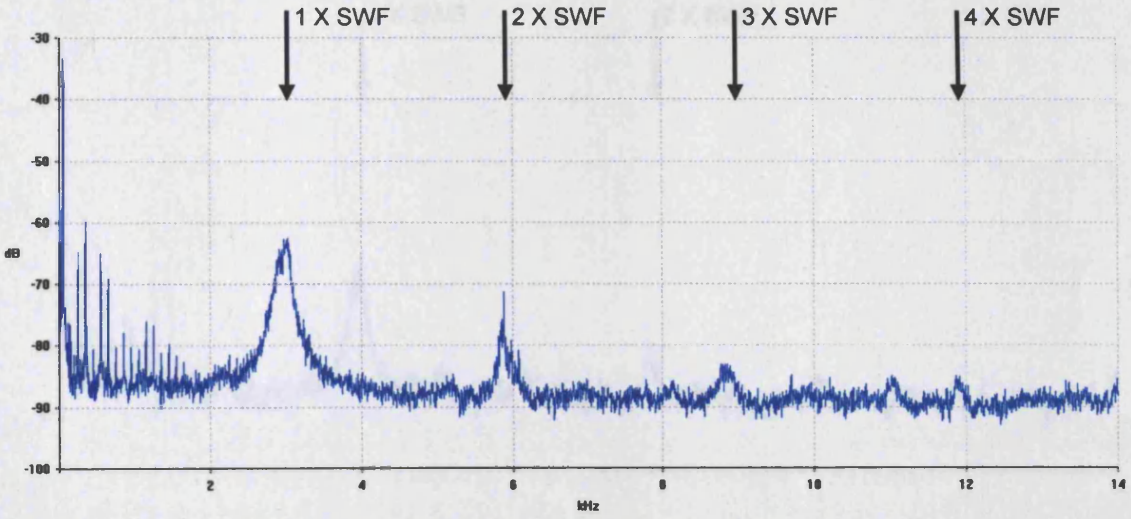

Figure 119 - SWF = 3kHz Input Current Spectrum Analysis

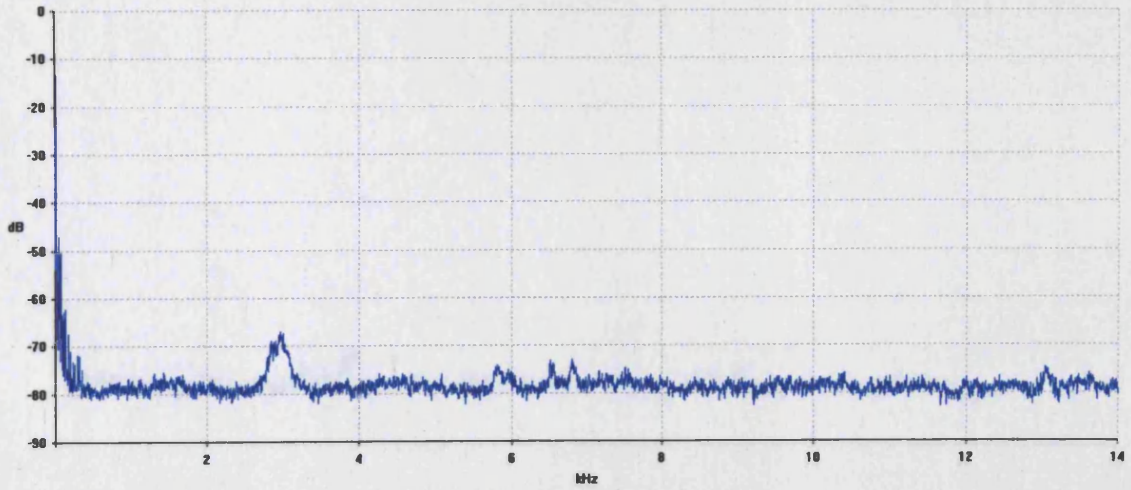

Figure 120 - SWF = 3kHz Output Current Spectrum Analysis

Venturini	SWF	F_{out}	q	Load R (Ω)	Load L (H)	Power Factor
Advanced	4 kHz	10 Hz	0.20	10	0.119	0.80

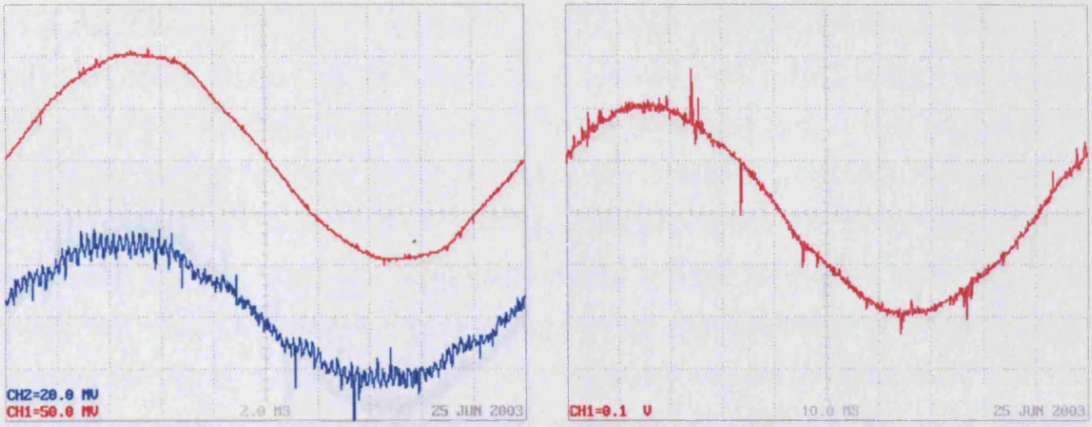

Figure 121 - SWF = 4kHz (a) Supply Voltage & Current & (b) Output Current

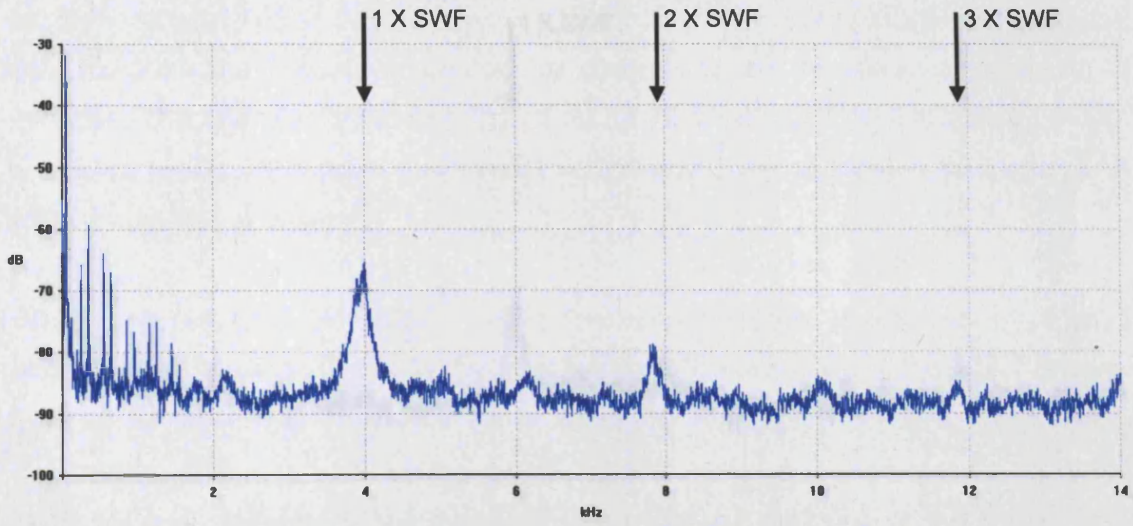

Figure 122 - SWF = 4kHz Input Current Spectrum Analysis

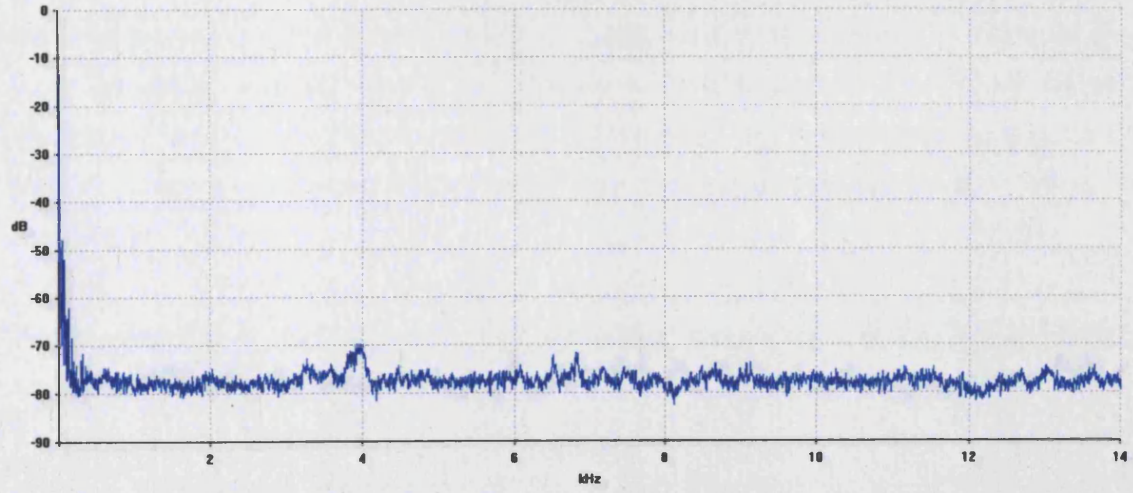

Figure 123 - SWF = 4kHz Output Current Spectrum Analysis

Venturini	SWF	F_{out}	q	Load R (Ω)	Load L (H)	Power Factor
Advanced	6 kHz	10 Hz	0.20	10	0.119	0.80

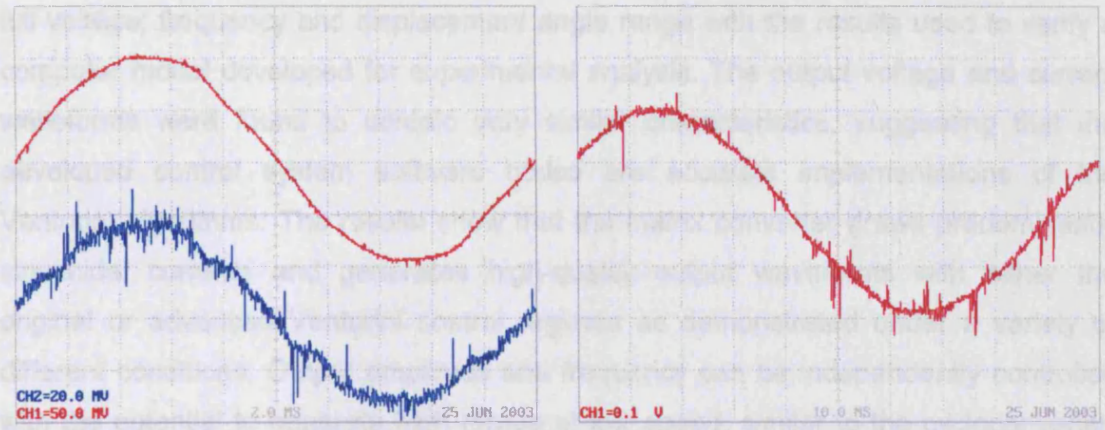

Figure 124 - SWF = 6kHz (a) Supply Voltage & Current & (b) Output Current

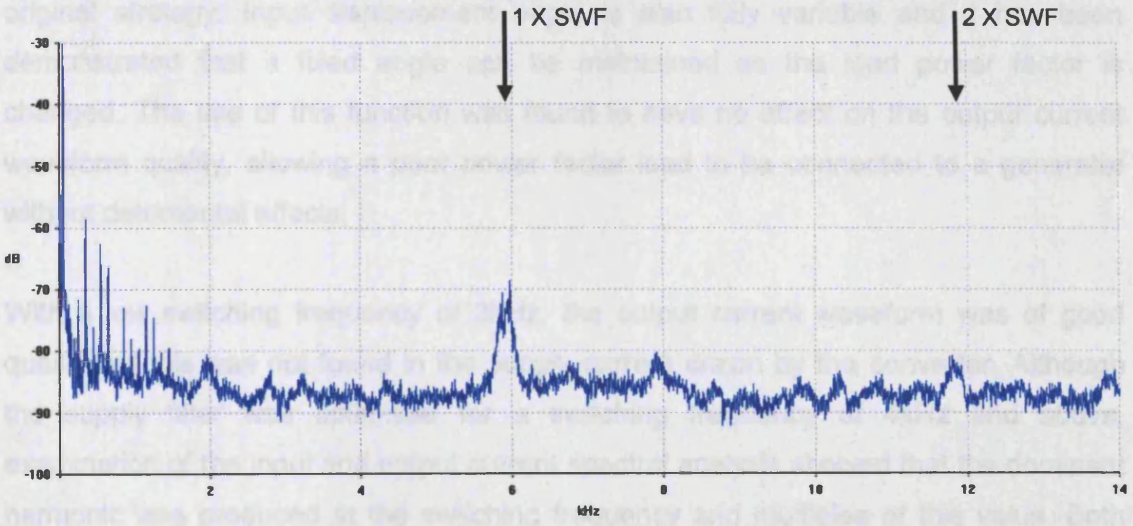

Figure 125 - SWF = 6kHz Input Current Spectrum Analysis

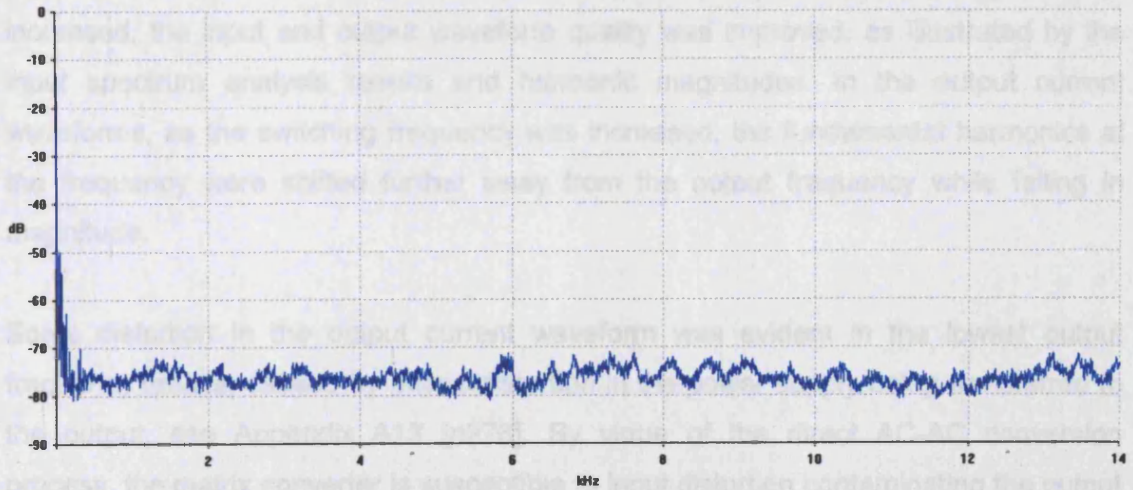

Figure 126 - SWF = 6kHz Output Current Spectrum Analysis

5.5 Conclusions

The performance of the laboratory matrix converter has been demonstrated across the full voltage, frequency and displacement angle range with the results used to verify a computer model developed for experimental analysis. The output voltage and current waveforms were found to contain very similar characteristics, suggesting that the developed control system software codes are accurate implementations of the Venturini algorithms. The results show that the matrix converter draws predominantly sinusoidal currents and generates high-quality output waveforms with either the original or advanced Venturini control regimes as demonstrated under a variety of different conditions. Output amplitude and frequency can be independently controlled with the potential to generate high torque at low speed, similar to the cycloconverter. The increase in supply utilisation possible with the advanced Venturini control strategy is also demonstrated and allows more efficient operation when compared with the original strategy. Input displacement angle is also fully variable and it has been demonstrated that a fixed angle can be maintained as the load power factor is changed. The use of this function was found to have no effect on the output current waveform quality, allowing a poor power factor load to be connected to a generator without detrimental effects.

With a low switching frequency of 3kHz, the output current waveform was of good quality but this was not found in the supply current drawn by the converter. Although the supply filter was optimised for a switching frequency of 4kHz and above, examination of the input and output current spectral analysis showed that the dominant harmonic was produced at the switching frequency and multiples of this value. Both standard and advanced Venturini control strategies were found to produce similar harmonic characteristics, suggesting that there is no reason to use the standard strategy ahead of the more advanced strategy. As the switching frequency was increased, the input and output waveform quality was improved, as illustrated by the input spectrum analysis results and harmonic magnitudes. In the output current waveforms, as the switching frequency was increased, the fundamental harmonics at the frequency were shifted further away from the output frequency while falling in magnitude.

Some distortion in the output current waveform was evident in the lowest output frequency results, caused by phase distortion in the power supply being transferred to the output, see Appendix A13 [p276]. By virtue of the direct AC-AC conversion process, the matrix converter is susceptible to input distortion contaminating the output waveforms but this can be minimised with closed loop control schemes that are

capable of compensating for supply imbalance and distortion, as described in Section 2.9 [p63]. A practical drive should therefore implement supply tracking for improved distortion immunity.

Higher switching frequencies are desirable because harmonics are produced at sidebands of multiples of the switching frequency, leading to converter waveforms containing less noise [60]. The ripple will also be lower in magnitude, allowing the use of a smaller supply filter whose size is inversely proportional to the switching frequency. However, operation at higher switching frequencies causes greater commutation loss and this must be balanced against the required waveform quality and filtering regulations. This problem is further exacerbated when multiphase matrix converter applications are considered. Consequently, alternative approaches to reduce commutation loss in the matrix converter must be explored with the aim of making this drive more competitive with existing and alternative marine variable speed drives.

6. Chapter Six - Matrix Converter Losses and Harmonics

6.1 Introduction

The general performance of the laboratory matrix converter has been investigated in the previous chapter using various passive loads. The results obtained demonstrated that high switching frequencies generated high-quality input and output current waveforms. However, it was also found that high switching frequencies contributed to increased switching loss, reducing the efficiency of the matrix converter [77]. Furthermore, converter switching loss increases in proportion to the number of output phases, suggesting that the multiphase converter configurations typical in marine applications would suffer from higher switching loss. In this chapter, energy loss in a matrix converter is investigated, including the problem of increased switching loss using a computer based model.

Venturini et al proposed a matrix converter switching sequence that requires each input phase to be connected to the load in a set order in every switching cycle [6]. However, as it has been shown that any switching order can be safely adopted [109], but the performance of the matrix converter needs to be investigated under alternative switching regimes. This chapter therefore describes a series of practical experiments that have been conducted using the laboratory matrix converter to verify computer models and explore the practical behaviour of the laboratory converter when alternative switching strategies are implemented.

6.2 Power Loss in the Matrix Converter

Three main types of power loss are known to exist in the matrix converter [93]; these are conduction loss, switching loss and harmonic loss.

6.2.1 Conduction Loss

Conduction loss is associated with devices conducting in their saturated on-state resulting in a voltage drop across each device in the converter [77]. Conduction loss in the matrix converter is also dependent on the circuit topology e.g. the number of supply and output phases. As conduction loss is independent of the switching frequency, only design improvements in the converter topology or device characteristics can help reduce conduction loss [77].

An example of circuit optimisation is the shortened conduction path that results by using an anti-parallel bi-directional switch instead of a diode-bridge arrangement; see Table 4 [p43]. The diode-bridge has a conduction path of two diodes and an IGBT, whereas the anti-parallel configuration has a shorter conduction path of a single diode and IGBT. This will improve converter efficiency and reduce cooling requirements. The

anti-parallel bi-directional switch represents the lowest loss configuration possible using available device technology allowing the direction of current flow to be controlled in both the forward and reverse directions and facilitating switching loss reduction by employing staggered commutation strategies [110], as described in Section 2.4.3 [p46].

6.2.2 Switching Loss

Switching, or commutation, loss occurs when a device changes from a conducting state to a blocking state or vice versa [3]. Switching loss is a consequence of the inability of the semiconductor device to instantaneously block or conduct current. Switching loss, therefore, occurs at device turn-on and turn-off. Additionally, stray circuit inductance contributes towards increased switching loss [72].

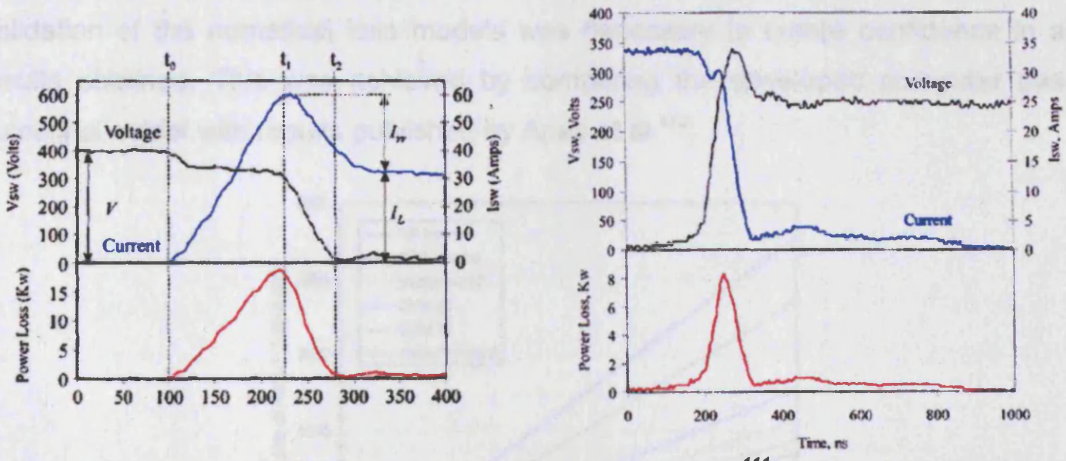

Figure 127 - Practical Matrix Converter Hard IGBT Commutations[111] (a) Turn-on & (b) Turn-off

During device commutation, the energy loss is proportional to the product of the conducted current, the device voltage drop and the time required to complete the commutation process [3]. Figure 127(a) shows a typical waveform for a bi-directional switch undergoing hard turn-on. At t_0, the load current begins to increase almost linearly causing a voltage drop across the parasitic inductance of the IGBT [111]. The current reaches a peak value at t_1, and then falls to I_L as the voltage across the opposing reverse blocking diode reaches ΔV. The hard turn-off, Figure 127(b), displays a current plateau caused by a change in voltage gradient across the parasitic capacitance in the non-conducting IGBT and the anti-parallel diode of the incoming switch [111].

A reduction in switching loss is most readily accomplished by reducing the switching frequency, however, this adversely affects the converter input and output waveform quality, as seen in Chapter Four. A trade-off between waveform quality and converter switching loss is therefore necessary. Attempts have also been made to reduce the total number of commutations that occur in the converter [67] and these are investigated

further in Section 6.7 [p145]. Switching loss can be eliminated altogether by either closing the switch at zero voltage or opening the switch at zero current [50].

6.2.3 Matrix Converter Conduction and Switching Loss Model

A computer-based numerical model of the matrix converter was developed following the methodology described by Apap et al [112], see Section 7.9 [p172] and Appendix A14 [p277]. The model considered both converter switching and conduction loss allowing comparisons to be made of the total loss incurred using different switching strategies and operating conditions. The first computer model simulated an anti-parallel IGBT based bi-directional switch to represent a state-of-the-art matrix converter. The second loss model employing a diode-bridge switch configuration, see Appendix A15 [p286].

6.2.4 Loss Model Verification

Validation of the numerical loss models was necessary to create confidence in any results obtained. This was achieved by comparing the developed computer based numerical model with results published by Apap et al [112].

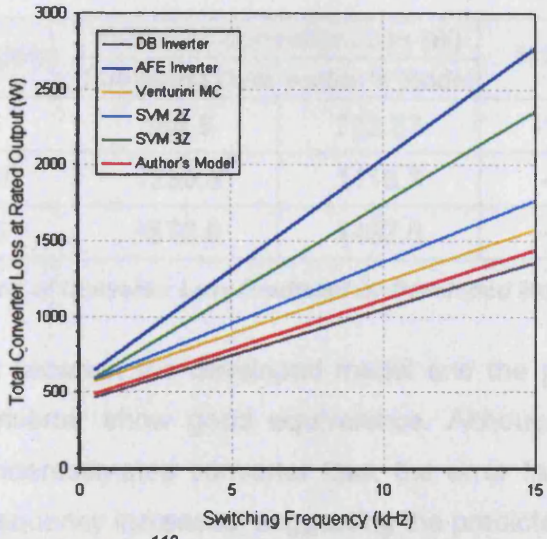

Figure 128 - Published Loss Data [112] Compared with the Developed Computer Model (Red)

Figure 128 shows converter loss for a diode-bridge-inverter, an AFE-inverter and three different operating modes of an equivalent sized matrix converter with different converter switching frequencies [112]. By employing the same IGBT device conduction and switching loss characteristics and an assumed motor load and output frequency of 25Hz, the results from the developed numerical model produced the matrix converter loss (shown in red). Although the published results for the 'Venturini' loss produced slightly higher loss, reasonable equivalence was found.

Further results obtained from the numerical loss model are shown in Figure 129. This figure demonstrates the variation in converter loss with the converter switching frequency and load current and compares this with published results [112].

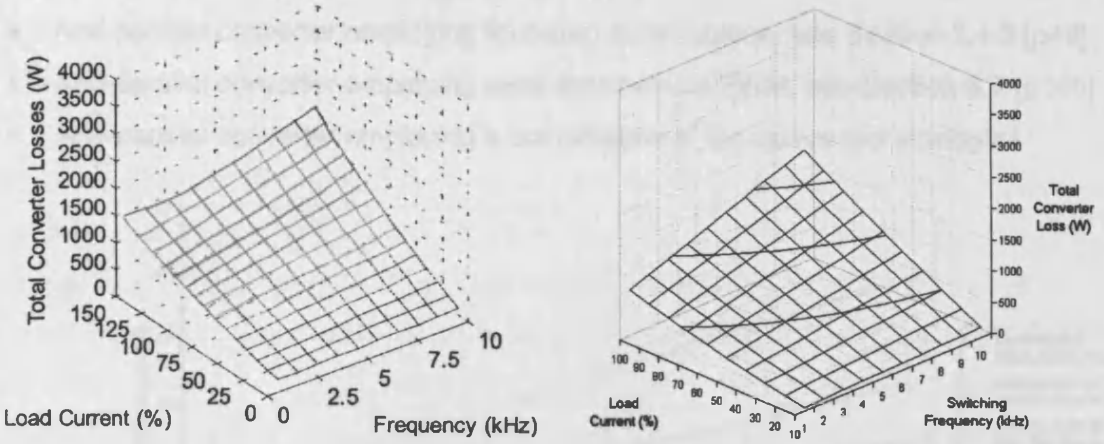

Figure 129 - Matrix Converter Loss Surfaces for (a) Published [112] & (b) Loss Models

Consider only the results for a load current within the range 0-100% in Figure 129(a) and (b). The numerical loss model is found to produce results comparable to published results. Table 17 compares the total loss predicted by the developed matrix converter model and the results presented in Figure 128 published by Apap et al [112].

SWF (kHz)	Predicted Converter Loss (W)		% Error
	Published Data	Author's Model	
5	884.6	782.87	-11.5
10	1230.8	1110.3	-9.8
15	1576.9	1437.8	-8.8

Table 17 - Comparison of Converter Loss Predicted by Developed Model & Published Data

The percentage error between the developed model and the published results for a (Venturini) Matrix converter show good equivalence. Although the developed loss model consistently underestimates converter loss, the error falls only slightly as the converter switching frequency increases, suggesting the predicted commutation loss to be very similar to the published data. The main difference appears to be in the conduction loss where motor load assumptions have reduced accuracy. The validated results of Figure 128 & Figure 129 demonstrate the numerical loss model is an acceptable model and suitable for further investigation.

6.2.5 Simulated Converter Loss Study

The verified converter numerical loss model, described in Section 6.2.4, was then used to perform a comparison of alternative commutation strategies for the matrix converter, see Appendix A16 [p290]. The loss in a matrix converter having the following modes of operation were compared:

- Diode-Bridge converter employing break-before-make commutation
- Anti-parallel converter employing break-before-make commutation

- Anti-parallel converter employing four-step commutation, see Section 2.4.3 [p46]
- Anti-parallel converter employing semi-symmetrical PWM, see Section 6.7 [p145]
- Anti-parallel converter employing a combination of the above two strategies

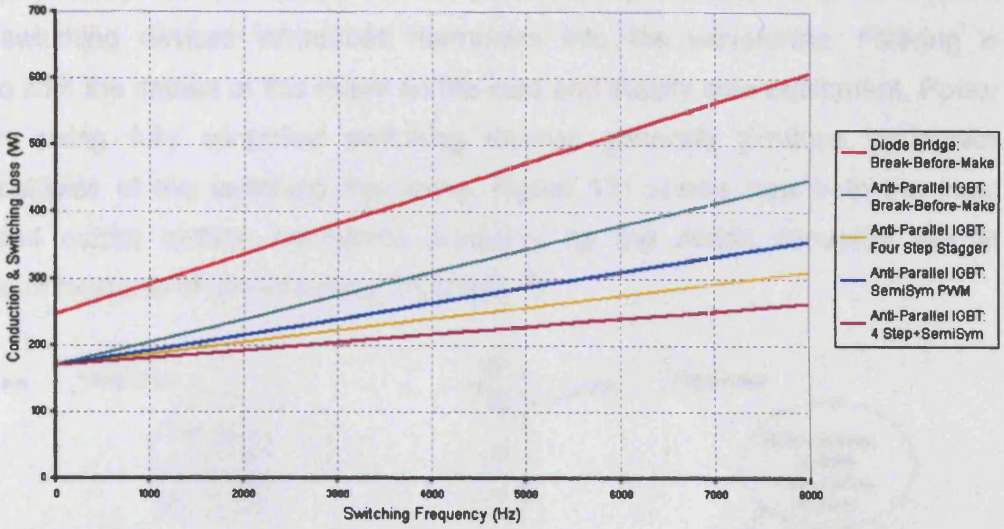

Figure 130 - Loss Analysis of Various Converter Commutation Strategies

The results shown in Figure 130 demonstrate that the diode-bridge configuration incurs approximately a third more conduction loss than the anti-parallel bi-directional switch. This is due to the longer conduction path in the diode bridge arrangement. Switching loss, however, increases at the same rate for both switch topologies when employing break-before-make commutation. The four-step staggered strategy was found to halve switching loss, while semi-symmetrical PWM reduces commutation loss by a third, confirming observations by Wheeler et al [93]. A combination of both previous techniques is shown by the results to reduce switching loss by a total of two-thirds compared with standard matrix converter operation thereby improving converter efficiency.

6.2.6 Harmonic Loss

Whereas conduction and switching loss are the main sources of loss, harmonic loss also contributes towards overall inefficiency of a drive system. Harmonics give rise to energy losses that cannot be recovered 'as useful energy' in the electrical system although it remains within it creating additional loss in transmission cables, transformers, motors and other electrical equipment. [73]. Matrix converter harmonics are observed as high frequency ripple on the fundamental input and output converter current waveforms. In Chapter Five, low switching frequencies were shown to increase current harmonic levels, necessitating a larger and more expensive input filter to maintain the quality of supply. High converter switching frequencies help to reduce converter harmonic loss but increase switching loss, so a compromise must always therefore be made.

6.3 Spectral Analysis

The power converter, in many texts, is often described as an ideal amplifier, producing a perfect amplified version of the reference signal [9]. However, this simplification is not true for practical power converters as the process of power electronic conversion through switching devices introduces harmonics into the waveforms. Filtering is needed to limit the impact of this noise on the load and supply side equipment. Power converters using fully controlled switching devices generally produce harmonics around multiples of the switching frequency. Figure 131 shows how both the input current and output voltage harmonics produced by the matrix converter are at sidebands of multiples of the switching frequency [82].

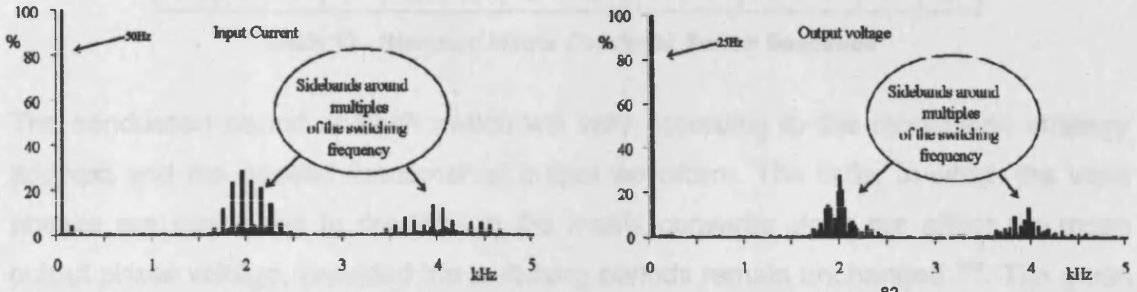

Figure 131 - Matrix Converter Input & Output Harmonics [82]

Although, high frequency harmonics are more easily and economically removed, harmonics caused by low switching frequencies or line-switched converters are far more difficult to manage as filters become large and expensive. Spectral analysis is used to investigate the harmonic performance of variable speed drives to allow the magnitude and frequency of each harmonic to be determined and compared against the fundamental.

To compare the harmonic noise profiles produced by alternative switching strategies, a high-resolution 100kSample/s Pico Technology ADC-100 unit was used to measure the harmonic noise present in both the input current and output current waveforms of the laboratory matrix converter. The parallel port unit sampled the circuit current at a frequency of 28kHz with the Picoscope PC software performing FFT spectrum analysis. Supply and output currents were analysed using Blackman windowing with an averaging display to minimise interference from transient phenomena. This equipment was used to investigate the following aspects:

- Performance of the standard sequential switching Venturini strategy
- Uniformity in supply and load current spectral waveforms
- Performance of alternative switching strategies
- Effect of novel loss reducing switching strategies

6.4 Venturini Strategy Spectral Analysis

When Venturini et al proposed their modulation algorithms for the matrix converter, a piecewise sampling technique was proposed. This strategy connects each input phase to the output line in the same sequential order for every switching cycle [6]. For a three-phase input, three-phase output converter, each switching cycle contains nine switch commutations (three per output phase), as shown in Table 18.

Output Phase	Cycle 'n'			Cycle 'n+1'			Cycle 'n+2'			Cycle 'n+3'		
a_o	1	2	3	1	2	3	1	2	3	1	2	3
b_o	1	2	3	1	2	3	1	2	3	1	2	3
c_o	1	2	3	1	2	3	1	2	3	1	2	3

Table 18 - Standard Matrix Converter Switch Sequence

The conduction period of each switch will vary according to the modulation strategy adopted and the desired fundamental output waveform. The order in which the input phases are connected to the load in the matrix converter does not affect the mean output phase voltage, provided the switching periods remain unchanged [109]. The mean output voltage is therefore equal to the sum of the instantaneous supply voltages multiplied by the period each switch is closed; see Equation 1 [p53].

If the supply voltages are assumed to be stationary during each switching cycle, i.e. cycle 'n', by assuming a sufficiently high converter switching frequency, the fundamental output voltage can be achieved using any switching sequence, e.g. 1-2-3 or 2-1-3 etc [109]. For a three-phase input, single-phase output converter, there are six possible sequences in which the three input phases can be connected to the load, as shown in Table 19:

Sequence	#1	#2	#3	#4	#5	#6
Switching Order	1 - 2 - 3	1 - 3 - 2	2 - 1 - 3	2 - 3 - 1	3 - 1 - 2	3 - 2 - 1

Table 19 - Possible Switching Sequences for a Single-Phase Output Converter

With six possible switching sequences for each output phase, a three-phase output matrix converter can adopt any one of 216 (6 x 6 x 6) possible switching sequences. Although the switching sequence has negligible effect on the load current, the supply current waveforms are influenced by the switching sequence adopted [109]. In order to explore this phenomenon further, the laboratory matrix converter control software, discussed in Chapter Four, was modified to allow virtually any commutation sequence to be implemented and then used to investigate different arrangements.

The laboratory matrix converter employing the standard 1-2-3 switching sequence was investigated to establish the 'base values' for comparative purposes. Converter operation was observed at two different switching frequencies (4kHz and 6kHz) and the harmonic spectrum of the three supply currents were analysed to establish the harmonics in each phase current. Appendix A17 [p291] contains the spectral waveforms for the 4kHz and 6kHz supply current spectra. Table 20 shows the harmonic magnitudes at SWF and 2xSWF.

	SWF = 4kHz (-dB)				SWF = 6kHz (-dB)		
	50Hz	4kHz	8kHz		50Hz	6kHz	12kHz
a_i	-15.4	-51.9	-66.8		-15.2	-57.2	-60.7
b_i	-15.2	**-48.2**	-65		-14.1	**-53.6**	-61.1
c_i	-15.2	-52.9	-66.8		-14.1	-57.8	-59.9

Table 20 - Supply Current Spectral Analysis Results

6.4.1 Observations

Moderate levels of harmonics were observed at the filter resonant frequency when operating at 4kHz. Additional harmonics were observed at 8kHz and 12kHz, which agrees with other published work [82]. Increasing the converter switching frequency to 6kHz was found to reduce overall input current noise across the frequency range, and reduce supply filter excitation.

Differences in the supply current spectra is evident in both the 4kHz and 6kHz results. The 'Yellow', or middle, input phase contains increased harmonic noise around the converter switching frequency as compared to the 'Red' and 'Blue' input phases. This was considered due to the first and final input phases having fixed start and end points during each switching cycle respectively. This is a problem inherent with the standard (1-2-3) sequence proposed by Venturini [6] and repeated by Bernet [109]. An investigation with a reordered switching sequence was the next step to confirm this observation.

6.5 Commutation Sequence Effect on Converter Harmonics

The cause of the non-uniform supply current spectra observed in Section 6.4 was examined further. The hypothesis was the middle input phase always contains increased noise at the switching frequency when employing the standard (1-2-3) switching sequence.

Two alternative commutation sequences were implemented using 'Blue' and then 'Red' as the middle input phase. This was achieved by reconfiguring the control software in the laboratory matrix converter to modify the switching order of each switching cycle. The following two commutation sequences result:

Output Phase	Cycle 'n'			Cycle 'n+1'			Cycle 'n+2'			Cycle 'n+3'		
a_o	2	3	1	2	3	1	2	3	1	2	3	1
b_o	2	3	1	2	3	1	2	3	1	2	3	1
c_o	2	3	1	2	3	1	2	3	1	2	3	1

Table 21 - Matrix Converter Commutation Sequence: b_I-c_I-a_I

Table 21 shows the switching sequence where the yellow input phase was expected to display increased harmonic noise at the switching frequency. The supply current spectra for 4kHz and 6kHz switching frequencies operation are shown in Appendix A18 [p293].

Output Phase	Cycle 'n'			Cycle 'n+1'			Cycle 'n+2'			Cycle 'n+3'		
a_o	3	1	2	3	1	2	3	1	2	3	1	2
b_o	3	1	2	3	1	2	3	1	2	3	1	2
c_o	3	1	2	3	1	2	3	1	2	3	1	2

Table 22 - Matrix Converter Commutation Sequence: c_I-a_I-b_I

Table 22 shows the third sequence tested that was expected to increase harmonic noise in the 'Red' input phase. The supply current spectra for 4kHz and 6kHz switching frequencies operation are shown in Appendix A19 [p295], with the harmonic magnitudes at SWF and 2xSWF shown in Table 23.

	SWF = 4kHz (-dB)				SWF = 6kHz (-dB)		
	50Hz	4kHz	8kHz		50Hz	6kHz	12kHz
a_I	-15.2	-51.3	-65.2		-13.9	-56.6	-60.7
b_I	-15.2	-52.9	-68.9		-14	-58.2	-60.3
c_I	-15.2	**-48**	-65.6		-14.8	**-54.5**	-60.9

Table 23 - Supply Current Spectral Analysis Results: b_I-c_I-a_I

	SWF = 4kHz (-dB)				SWF = 6kHz (-dB)		
	50Hz	4kHz	8kHz		50Hz	6kHz	12kHz
a_I	-15.2	**-48.4**	-65.6		-13.9	**-54.5**	-59.7
b_I	-15.4	-52.9	-66.8		-14.1	-57.4	-60.1
c_I	-15.2	-52.1	-68.5		-14.8	-57.4	-62.6

Table 24 - Supply Current Spectral Analysis Results: c_I-a_I-b_I

6.5.1 Observations

The results in Table 23 and Table 24 demonstrate increased harmonic noise, for the middle connected input phase, centred at the converter switching frequency, confirming the observations of Section 6.4 and elsewhere [109]. The reordered switching sequences were investigated at both 4kHz and 6kHz switching frequencies and were found to contain the same harmonic non-uniformity phenomenon.

The increase in harmonic noise in the middle connected phase over the other two, localised at the switching frequency, introduces an imbalance that prevents the matrix converter from drawing identical currents from the three-phase power supply. The standard Venturini sequence does not allow ideal performance of a matrix converter [109] so an alternative sequence that balances the supply currents is desirable.

6.6 Switch Sequence Stagger Spectral Analysis

As discussed in Section 6.4, alternative matrix converter switching strategies can be employed. The switching sequences investigated in Sections 6.4 and 6.5 operate the matrix converter with identical input phase orders. As these have been found to produce non-uniform supply currents, methods of limiting this effect have been explored. The switching sequences investigated in Section 6.5 were applied equally to each converter output phase, so an alternative approach was therefore examined.

A staggered strategy was investigated in an attempt to distribute the load more evenly across the supply lines. Instead of starting with the first switch of each converter output phase, a positive stagger was introduced; see Table 25.

Output Phase	Cycle 'n'			Cycle 'n+1'			Cycle 'n+2'			Cycle 'n+3'		
a_o	1	2	3	1	2	3	1	2	3	1	2	3
b_o	2	3	1	2	3	1	2	3	1	2	3	1
c_o	3	1	2	3	1	2	3	1	2	3	1	2

Table 25 - Staggered Matrix Converter Commutation Sequence

The supply and load current spectra for a 4kHz converter switching frequency are shown in Appendix A20 [p297]. The effect of increasing the switching frequency to 6kHz is shown in Appendix A21 [p299]. The harmonic magnitudes at SWF and 2xSWF are shown in Table 26 and Table 27.

	SWF = 4kHz (-dB)				SWF = 6kHz (-dB)		
	50Hz	4kHz	8kHz		50Hz	6kHz	12kHz
a_i	-14.5	-44.5	-61.3		-14.1	-50.8	-59.1
b_i	-14.4	-44.1	-62.7		-13.5	-50.4	-60.1
c_i	-14.4	-43.9	-63.1		-13.3	-51.3	-61.3

Table 26 - Supply Current Spectral Analysis Results with Stagger

	SWF = 4kHz (-dB)				SWF = 6kHz (-dB)		
	50Hz	4kHz	8kHz		50Hz	6kHz	12kHz
a_i	5.66	-52.5	-68.9		5.3	-57.2	-66
b_i	5.66	-50.8	-66.6		5.3	-55	-64.4
c_i	5.66	-52.7	-67.3		5.3	-56	-65.2

Table 27 - Output Current Spectral Analysis Results with Stagger

6.6.1 Observations

The staggered strategy succeeds in equalising input and output current harmonic profiles for both 4kHz and 6kHz converter operation, confirming observations by Bernet et al [109]. Although harmonics produced at the switching frequency are uniform across both supply and output phases, there is an overall increase in harmonic noise when compared to results found in Section 6.4.

Use of output staggered switching was found to have little effect on the output current noise aside from a minor increase in the harmonics produced at the switching frequency. The effect was consistently found in each output phase and at both 4kHz and 6kHz switching frequencies, demonstrating that output harmonics do not change with the commutation sequence employed [109]. Conversely, the harmonic magnitude at double the converter switching frequency fell when employing the staggered switching sequence.

6.7 Semi-symmetrical PWM Spectral Analysis

Wheeler et al proposed a switching strategy to reduce the number of commutations necessary in each switching cycle and thereby reducing switching loss [67]. This approach eliminates the final commutation of each switching cycle and maintains this switch into the following cycle, as shown in Table 28. Semi-symmetrical PWM requires no modification of the Venturini modulation strategy and reduces switching loss by a third for a three-phase matrix converter [67].

Output Phase	Cycle 'n'			Cycle 'n+1'			Cycle 'n+2'			Cycle 'n+3'		
a_o	1	2	3	1	2	3	1	2	3			
b_o	1	2	3	1	2	3	1	2	3			
c_o	1	2	3	1	2	3	1	2	3			

Table 28 - Semi-symmetrical PWM Commutation Sequence

The switching duty cycle for a matrix converter employing semi-symmetrical PWM is very different to the standard sequential sequence and is compared with the standard duty cycle, as shown by Figure 132.

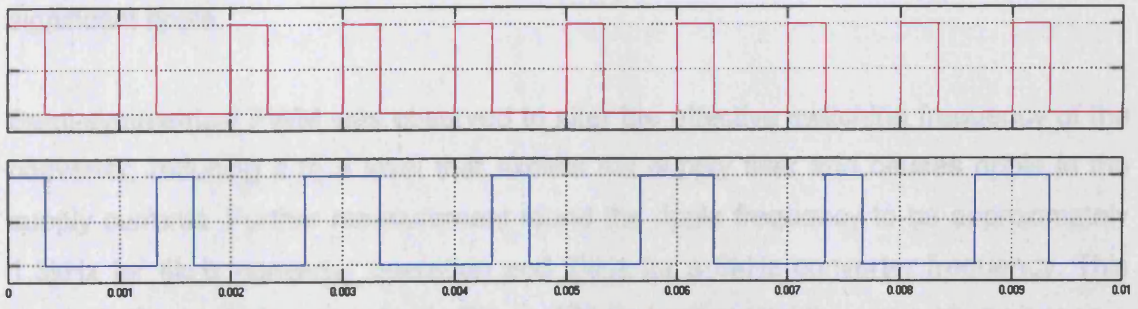

Figure 132 - Standard & Semi-symmetrical PWM Switch Duty Cycle Comparison

The upper graph (in red) shows the standard switching duty cycle for one switch, the frequency clearly matches the switching frequency (in this case 1kHz). The lower graph (in blue) shows the duty cycle for a semi-symmetrical PWM switched converter; the period is found to be 3ms, or 333.3kHz, a third of the switching frequency. The practical converter implementing semi-symmetrical PWM can therefore be expected to exhibit increased harmonic noise at a third of the switching frequency.

6.7.1 Supply and Load Current Waveforms

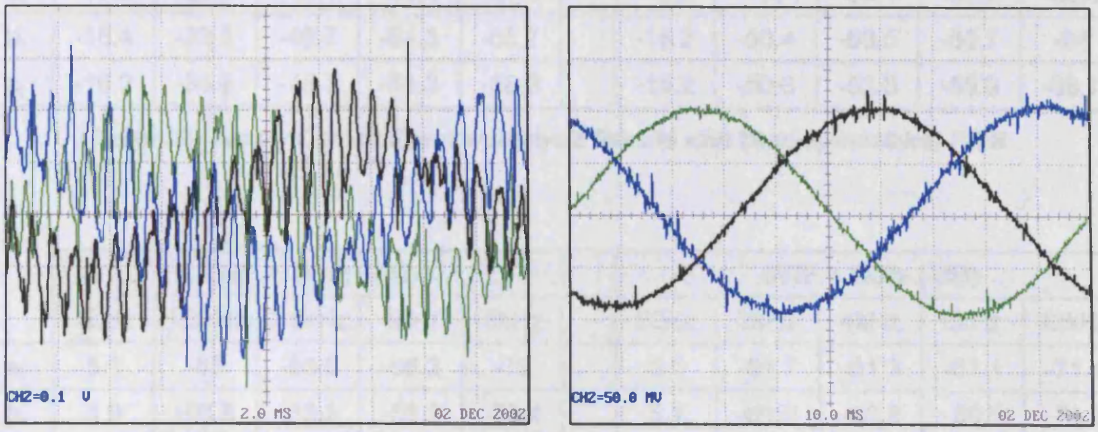

Figure 133 - 4kHz Semi-symmetrical PWM 3ϕ (a) Supply & (b) Output Currents

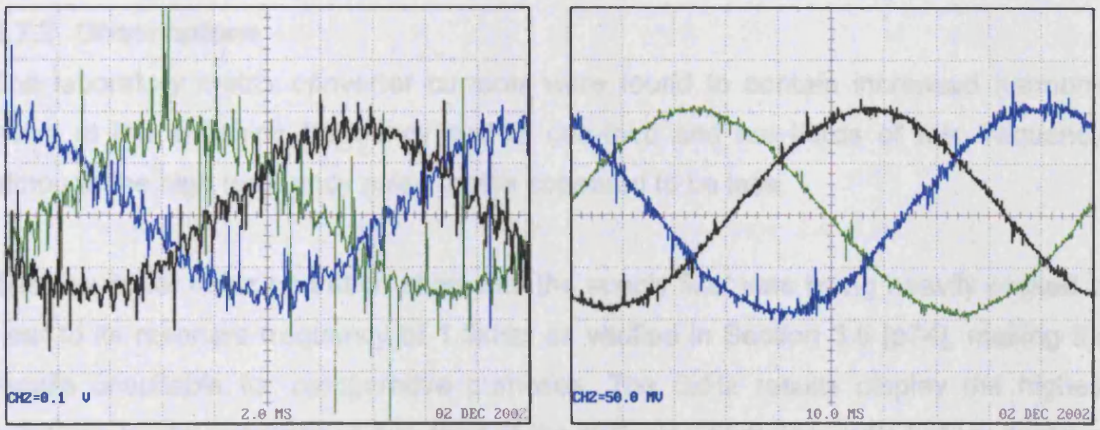

Figure 134 - 6kHz Semi-symmetrical PWM 3ϕ (a) Supply & (b) Output Currents

The output current waveforms remain unchanged from those observed using the standard commutation sequence, but the supply current is much inferior to the standard sequence. This is particularly true for operation at 4kHz which exhibits significant ripple.

Semi-symmetrical PWM was observed to alter the effective switching frequency of the converter, reducing it to a level that excites the supply filter and causes ripple in the supply currents. Further measurement found the ripple frequency to be approximately 1.3kHz for 4kHz converter operation and 2kHz for a 6kHz converter frequency. This supports the analysis presented in Figure 132 that suggested the same phenomenon.

The supply and load current spectra for a 4kHz switching frequency when employing a semi-symmetrical PWM sequence are shown in Appendix A22 [p301]. The effect of increasing the switching frequency to 6kHz is shown in Appendix A23 [p303]. The harmonic magnitudes at SWF and 2xSWF are shown in Table 29 and Table 30.

	SWF = 4kHz (-dB)						SWF = 6kHz (-dB)				
	50Hz	1.3kHz	2.6kHz	4kHz	8kHz		50Hz	2kHz	4kHz	6kHz	12kHz
a_i	-16.2	-32.2	-46.1	-55.4	-67.9		-15.2	-48	-53.1	-60.5	-65.4
b_i	-16.4	-33.8	-46.7	-54.3	-68.7		-15.2	-50.4	-53.5	-60.7	-64
c_i	-16.2	-33.8	-45.7	-54.3	-68.3		-15.2	-50.6	-53.5	-59.9	-68.7

Table 29 - Supply Current Spectral Analysis Results with Semi-symmetrical PWM

	SWF = 4kHz (-dB)						SWF = 6kHz (-dB)				
	50Hz	1.3kHz	2.6kHz	4kHz	8kHz		50Hz	2kHz	4kHz	6kHz	12kHz
a_i	5.1	-57	-58.8	-56.2	-72		5.1	-61.7	-61.3	-61.1	-71.4
b_i	4.9	-56.8	-60.3	-56.2	-73.4		5.1	-61.3	-62.9	-59.1	-71.3
c_i	4.9	-56	-59.9	-56.6	-73.4		4.9	-61.5	-61.3	-59.7	-71.4

Table 30 - Output Current Spectral Analysis Results with Semi-symmetrical PWM

6.7.2 Observations

The laboratory matrix converter currents were found to contain increased harmonic noise at the switching frequency and at one-third and two-thirds of this frequency, although the high frequency noise profile appeared to be less.

The results for 4kHz operation show that the supply filter was being heavily excited at near to its resonant frequency of 1.5kHz, as verified in Section 3.5 [p74], making the results unsuitable for comparative purposes. The 6kHz results display the highest harmonic peaks occurring at one-third of the switching frequency with further peaks at two-thirds and at the switching frequency, although reduced filter excitation was experienced. The results imply that attempts at reducing commutation loss in a matrix converter by employing the semi-symmetrical PWM strategy must be accompanied with an appropriately designed supply filter to avoid the effective reduction in switching frequency from causing input current problems. The filter is likely to be larger and more expensive.

Comparison shows the 6kHz semi-symmetrical results to be considerably inferior to the standard 4kHz results that incur similar commutation loss, see Section 6.4 [p141]. Semi-symmetrical PWM produces substantial harmonic noise at frequencies below

those produced by the standard 4kHz results, suggesting that it is better to reduce the matrix converter switching frequency instead of employing semi-symmetrical PWM.

6.8 Semi-symmetrical PWM with Switch Sequence Stagger

For completeness, semi-symmetrical PWM operation was combined with switch sequence staggering to create the following commutation sequence.

Output Phase	Cycle 'n'			Cycle 'n+1'			Cycle 'n+2'			Cycle 'n+3'	
a_o	1	2	3	1	2	3	1	2	3		
b_o	2	3	1	2	3	1	2	3	1		
c_o	3	1	2	3	1	2	3	1	2		

Table 31 - Semi-symmetrical PWM Switch Sequence With Positive Stagger

The supply and load current spectra for a 4kHz switching frequency when combining semi-symmetrical PWM with switch stagger are shown in Appendix A24 [p305]. The effect of increasing the switching frequency to 6kHz is shown in Appendix A25 [p307]. The harmonic magnitudes at SWF and 2xSWF are shown in Table 32 and Table 33.

	SWF = 4kHz (-dB)						SWF = 6kHz (-dB)				
	50Hz	1.3kHz	2.6kHz	4kHz	8kHz		50Hz	2kHz	4kHz	6kHz	12kHz
a_i	-15	-13.1	-40	-47	-62.3		-14.6	-32	-43.7	-59	-66.2
b_i	-14.8	-16.2	-41.2	-49.6	-65.4		-14.8	-33.4	-44.9	-59.3	-66.2
c_i	-15.6	-11.5	-41.2	-43.1	-60.9		-14.6	-32.8	-44.3	-61.1	-69.3

Table 32 - Supply Current Spectral Analysis for Semi-symmetrical PWM & Stagger

	SWF = 4kHz (-dB)						SWF = 6kHz (-dB)				
	50Hz	1.3kHz	2.6kHz	4kHz	8kHz		50Hz	2kHz	4kHz	6kHz	12kHz
a_i	4.7	-40.8	-47	-52.7	-68.5		5.3	-53.7	-52.3	-60.1	-72.4
b_i	4.7	-40.2	-46.9	-51.5	-67.2		5.1	-53.1	-51.2	-56.2	-71.8
c_i	4.5	-40	-46.7	-52.7	-69.5		5.1	-53.3	-51.3	-593	-71.1

Table 33 - Output Current Spectral Analysis for Semi-symmetrical PWM & Stagger

6.8.1 Observations

The practical results of employing a combined semi-symmetrical PWM and staggered switching strategy show an overall increase in harmonic noise at all frequencies. Semi-symmetrical PWM signature harmonics at one-third and two-thirds of the switching frequency are considerably larger than when not employing stagger. Converter operation at 4kHz excited the supply filter and generated audible filter noise.

Although the magnitude of the harmonic noise at the switching frequency is unchanged compared with the results in Section 6.7 of semi-symmetrical PWM, the two-thirds and one-third harmonics were found to increase in size. Nevertheless, the input and output currents were balanced with an almost equal harmonic profile, as found in Section 6.6.

6.9 Conclusions

This chapter has described the three types of loss that can occur in a matrix converter and has compared the conduction and switching loss of a number of commutation strategies using a verified computer loss model. The performance of a number of alternative commutation sequences including a strategy to reduce switching loss have been investigated using the practical laboratory matrix converter.

Three sources of loss are conduction, switching and harmonic loss. Conduction loss is dependent on the converter circuit topology and the switching device employed and its characteristics. Switching loss is directly proportional to the converter switching frequency and is dependent on whether commutations are soft or hard. Harmonic loss is additional lost energy that is generated by the converter and contained within the electrical system but which cannot be extracted from it for useful work. Harmonics are visible as ripple on the converter waveforms. Due to the number of commutations in the matrix converter it is important to focus on reducing loss.

The order in which the input phases are connected to the load was defined by Venturini et al as 1-2-3 when reporting their matrix converter control algorithms [6]. However, Bernet et al later showed that the switching order could be reordered safely without affecting the converter fundamental output waveform [109]. Such novel switching sequences were investigated using the practical laboratory matrix converter. The standard commutation sequence was examined by measuring the current harmonic content in each input phase. Although largely similar, the results did show an imbalance in the converter supply currents; with the middle phase containing increased harmonic noise at the switching frequency. A further two staggered commutation sequences where implemented to verify that a circuit electrical characteristic was not the cause of this effect but the above observation was indeed confirmed as postulated by others. This phenomenon is probably caused by the first and final input phases having fixed start and end times during each switching cycle, whereas the middle phase is variable between the two 'outer' phases. In an effort to eliminate this unbalance, an alternative staggered switching sequence was investigated. Although this succeeded in equalising the harmonic noise generated in the input phases, an

overall increase in the generated noise was observed in both input and output current waveforms.

The semi-symmetrical PWM switching strategy is a method of reducing commutation loss so it too has been investigated as a possible solution to improve matrix converter efficiency. However, while the semi-symmetrical PWM succeeded in reducing commutation loss by a third, it has been found to increase harmonic noise in both input and output current waveforms. The switching frequency was no longer the dominant harmonic and considerable noise was generated at one-third and two-thirds of this frequency, resulting in increased supply filter excitation. Although the filter in a practical system could be upgraded to avoid being adversely excited, the material cost and increased dimensions could be significant. Additionally, the 6kHz semi-symmetrical PWM results are considerably inferior than the standard sequence at 4kHz that offers similar commutation loss. This suggests that the semi-symmetrical PWM strategy is less desirable than simply reducing the converter switching frequency to reduce loss. In the interest of completeness, a staggered semi-symmetrical PWM strategy was also investigated but was found to produce the same undesirable effects as the standard staggered switching strategy.

From the investigations undertaken in this chapter, it was concluded that although imbalance can be reduced with staggered switching, it is preferable to switch each output phase in the same supply order for reduced harmonic noise overall. Furthermore, there remains a requirement for an approach to reduce commutation loss in a matrix converter that does not alter the characteristic harmonic noise generated during operation but maintains uniform input and output current waveforms.

7. Chapter Seven - Commutation Sequence Optimisation

7.1 Introduction

High-speed switching in a matrix converter produces high-quality input and output waveforms containing low levels of harmonic distortion. The increased switching loss associated with high frequency operation is one of the important reasons that has made this converter uncompetitive and hindered its commercial development and application [60]. Although a technique for reducing the number of converter commutations has been proposed (e.g. semi-symmetrical PWM) [67], modelling and experimental evidence reported on in Chapter Six has shown this technique to produce increased harmonic distortion that significantly impairs waveform quality and complicates the design of the supply filter.

In this chapter, the results of an investigation into switching loss are reported. This led to the development of a new commutation strategy by the author as a means to reduce switching loss. This novel strategy, named 'Opti-Soft' by the author, maximises 'natural' current commutations between switches, equalises switch commutation loss and is suited to multiphase inputs. Additionally, further computer modelling work shows that while a reduction in converter switching loss is not realised, the harmonic characteristics match those of the conventional commutation strategy, thus allowing use of standard supply filter designs. This chapter also compares the performance of 'Opti-Soft' with other strategies and finally discusses its practical implementation.

7.2 Device Commutations

Device commutation in the ideal matrix converter assumes idealised and instantaneous synchronised operation, something that is difficult to achieve in practice. As damagingly high load voltages result from open circuit conditions, matrix converters usually employ some form of staggered switching strategy with overlap or make-before-break commutation, as described in Section 2.4 [p45]. In the next sections, switch commutations are considered.

7.2.1 Natural Current Commutation

Consider two unidirectional semiconductor switches connected in parallel to a common load with different supplies as shown in Figure 135, i.e. from two switches in a matrix converter. Current can commutate naturally from the switch at a lower voltage (V_1) to a higher voltage (V_2) when the load current I_L is positive [110].

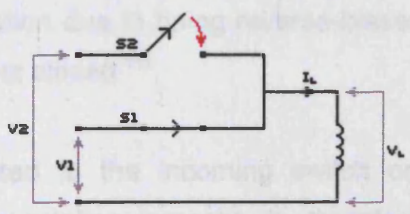

Figure 135 - Natural Current Commutation Example

With switch S1 closed, the load voltage V_L will be near equal to V1, and the current will be I_L. If switch S2 is forward-biased with V2 being greater than V1, then when S2 is closed, the current conducted by switch S1 will decay to zero and the current in switch S2 will increase to I_L. Switch S1 will then be reverse-biased and non-conducting and so may be opened at zero current to complete the commutation process [113].

The outgoing switch S1 is opened when it is no longer conducting current, therefore experiencing no switching loss. The turn-off commutation of S1 is deemed lossless since it has been soft switched [110]. However, the incoming switch S2 is hard turn-on switched because it was forward-biased when it was closed to initiate current transfer from S1 to S2 [112].

Natural commutation is generally desirable as the transfer of current between switches begins as soon as the incoming switch is closed. Similarly, a negative load current can be commutated naturally when switching from a higher voltage switch to a lower voltage switch [110].

7.2.2 Forced Current Commutation

Consider the same circuit when commutation occurs from the higher switch voltage S2 to the lower switch voltage S1, with a positive load current as illustrated in Figure 136. In this example, soft turn-on and hard turn-off commutations takes place.

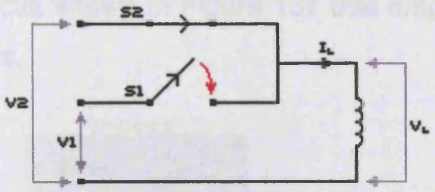

Figure 136 - Forced Current Commutation Example

The load current I_L is initially carried by switch S2 only and the load voltage V_L is near equal to V2. Switch S1 is reverse-biased by V1-V2 and does not conduct current when first closed. The load current I_L is only commutated to switch S1 when switch S2 is opened, i.e. forcing V_L to V1 [113].

The outgoing switch S2 is opened whilst still conducting the full load current and is therefore hard switched with some switching energy loss. The incoming switch undergoes a soft commutation due to being reverse-biased and does not conduct any of the load current when first closed [112].

Current is only commutated to the incoming switch once the outgoing switch is opened. The forced commutation process is therefore longer than the natural

commutation process. Forced commutation can also occur for negative load currents with a higher incoming voltage [110].

7.2.3 Staggered Commutation

The examples in Sections 7.2.1 & 7.2.2 of current commutation in a matrix converter are simplified, employing unidirectional switches that do not satisfy the requirement for bi-directional conduction. In a practical matrix converter, the supply voltages and load currents are changing continuously and the switch voltage polarity can change during conduction. For this reason, the bi-directional switch design must accommodate voltage reversal during conduction to ensure a continuous and seamless current path to the load.

7.3 Matrix Converter Device Commutation

The state-of-the-art approach for realising a bi-directional switch for the matrix converter using uni-directional devices is the anti-parallel topology, see Section 2.3.3 [p43]. When combined with staggered commutation strategies, these configurations maintain a continuous current path to the load and avoid potentially damaging open circuit conditions from arising [60].

The four-step staggered strategy orders the commutation sequence according to the load current polarity, as described in Section 2.4.3 [p46]. This allows half of all device commutations to be soft-switched to reduce converter loss [67]. This was investigated in greater detail using the circuit shown in Figure 137 that employs a pair of anti-parallel IGBT bi-directional switches.

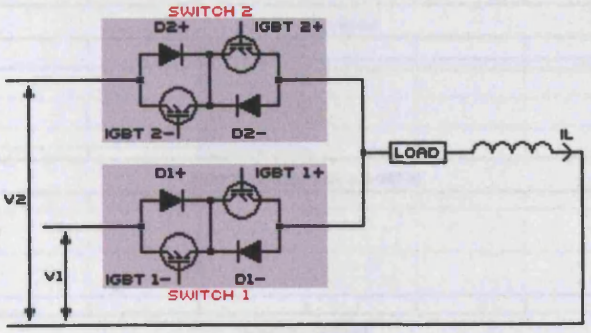

Figure 137 - Generalised Bi-directional Switch Test Circuit

A Matlab Simulink PSB model of the two bi-directional switch circuit shown in Figure 137 is described in Appendix A26 [p309], and has been used to analyse the conditions required for natural current commutations.

7.3.1 Four-step Commutation: Higher Incoming Voltage & Positive Load Current

Figure 138 shows the simulated circuit commutation analysis when the incoming switch S2 has a higher voltage than the outgoing switch S1 and there is a positive load current. The commutation sequence is as follows, referring to Figure 137 [p153]:

S1+ & S1- are initially closed with only S1+ conducting the (positive) load current. There is a small voltage drop across the conducting switch due to on-state resistance.

- At Com 1: S1- is opened first as it is reverse-biased and non-conducting with D1- also reverse-biased and non-conducting
- At Com 2: S2+ is closed and a circulating current begins to flow, reducing the current through S1+ to zero. S2+ undergoes a hard turn-on commutation and D2+ experiences turn-on loss
- At Com 3: S1+ is opened at zero current for a soft turn-off commutation while D1+ is reverse-biased and experiences reverse-recovery loss.
- At Com 4: S2- is closed to complete the commutation sequence but is reverse-biased and non-conducting with D2- also reverse-biased and non-conducting

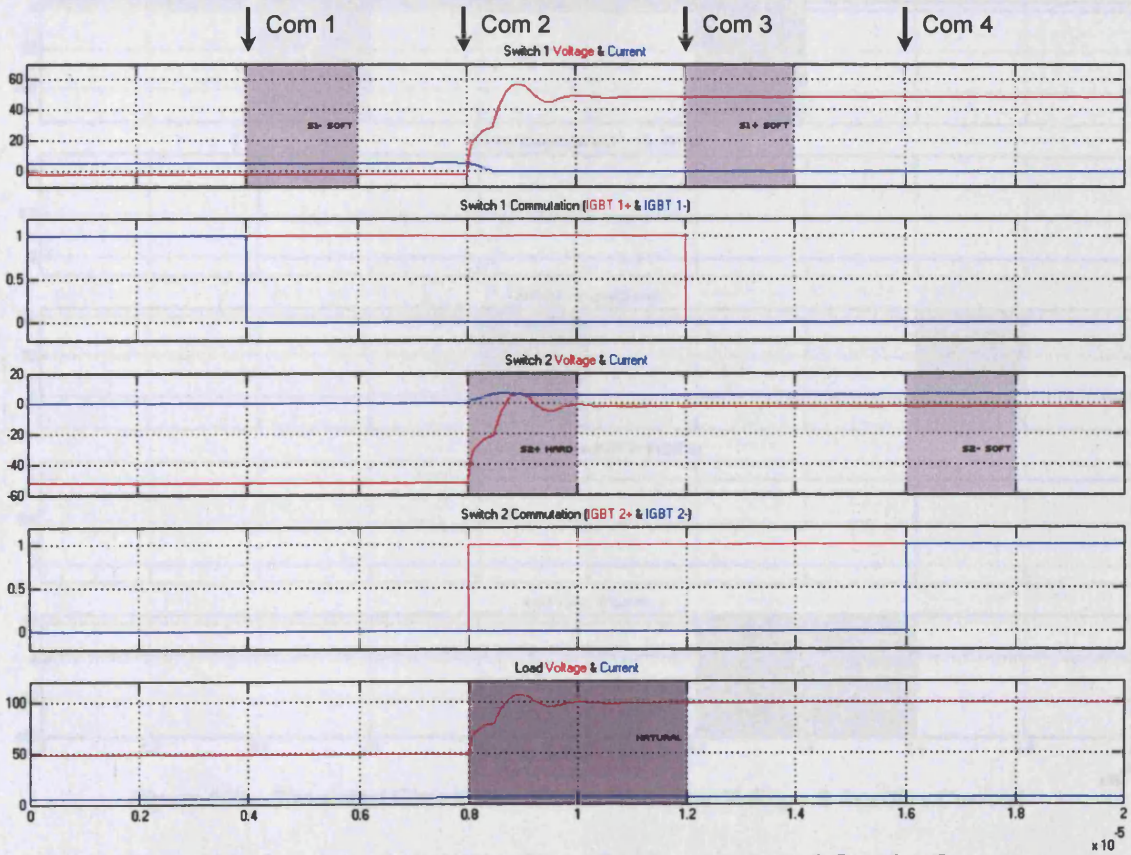

Figure 138 - Simulated Circuit Waveforms for Higher Voltage & Positive Current

The higher incoming switch voltage induces a circulating current that reduces the current flowing through the outgoing switch to zero for natural current commutation between the bi-directional switches. These results show that this process is natural.

7.3.2 Four-step Commutation: Lower Incoming Voltage & Positive Load Current

Figure 139 shows the simulated circuit commutation analysis when the incoming switch S2 has a lower voltage than the outgoing switch S1 and there is a positive load current. The commutation sequence is as follows, referring to Figure 137 [p153]:

S1+ & S1- are initially closed with only S1+ conducting the (positive) load current

- At Com 1: S1- is opened first as it is reverse-biased and non-conducting with D1- also reverse-biased and non-conducting
- At Com 2: S2+ is closed but cannot conduct as device is reverse-biased for soft turn-on commutation with D2+ also reverse-biased and non-conducting
- At Com 3: S1+ is opened to force load voltage below V1 and allow S2+ to conduct load current. S1+ experiences a hard turn-off commutation whereas D1+ does not become reverse-biased and therefore experiences no loss
- At Com 4: S2- is closed to complete the commutation sequence but is reverse-biased and non-conducting with D2- also reverse-biased and non-conducting

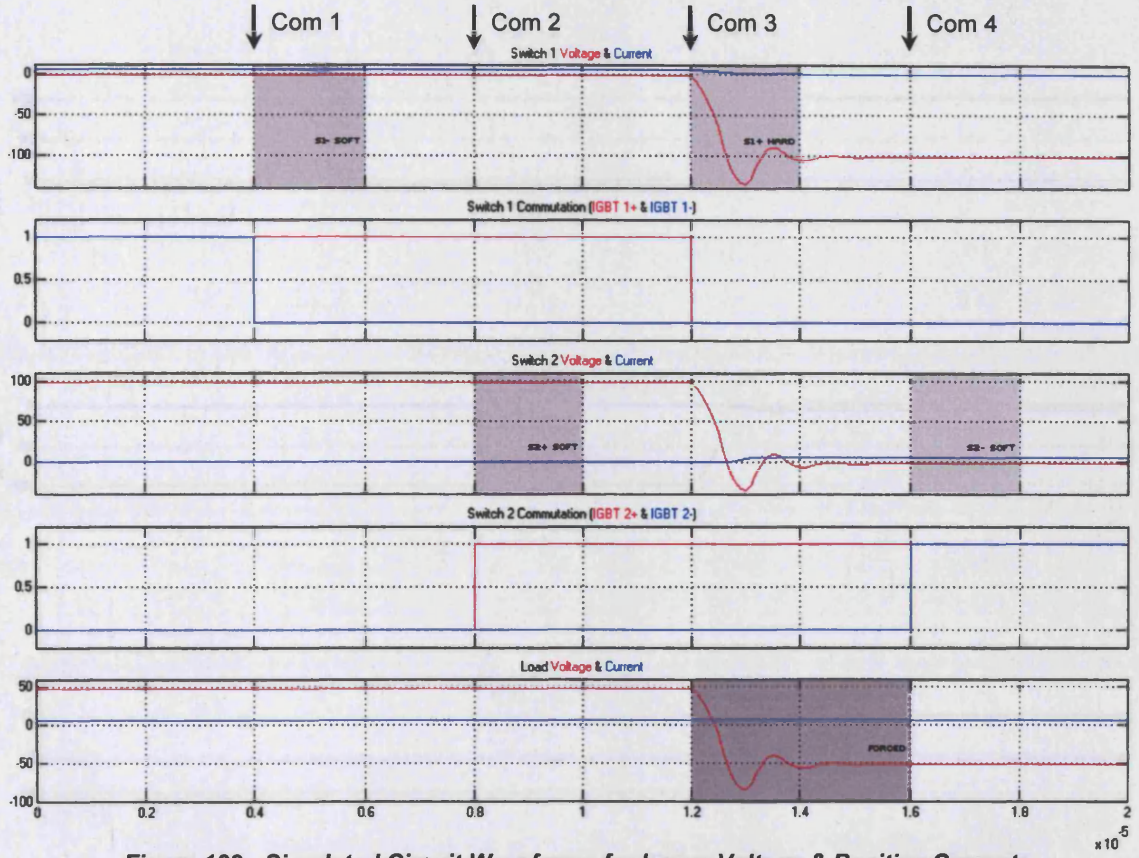

Figure 139 - Simulated Circuit Waveforms for Lower Voltage & Positive Current

The positive load current and lower incoming switch voltage means that a circulating current cannot flow and therefore current commutation between switches is forced since S1+ is turned off whilst current is flowing through it. Under these circumstances, the commutation is forced.

7.3.3 Four-step Commutation: Higher Incoming Voltage & Negative Load Current

Figure 140 shows the simulated circuit commutation analysis when the incoming switch S2 has a higher voltage than the outgoing switch S1 and there is a negative load current. The commutation sequence is as follows, referring to Figure 137 [p153]:

S1+ & S1- are initially closed with only S1- conducting the (negative) load current

- At Com 1: S1+ is opened first as it is reverse-biased and non-conducting with D1+ also reverse-biased and non-conducting
- At Com 2: S2- is closed but cannot conduct as device is reverse-biased for soft turn-on commutation with D2- also reverse-biased and non-conducting
- At Com 3: S1- is opened to force load voltage above V1 and allow S2- to conduct load current. S1- experiences a hard turn-off commutation whereas D1- does not become reverse-biased and therefore experiences no loss
- At Com 4: S2+ is closed to complete the commutation sequence but is reverse-biased and non-conducting with D2+ also reverse-biased and non-conducting

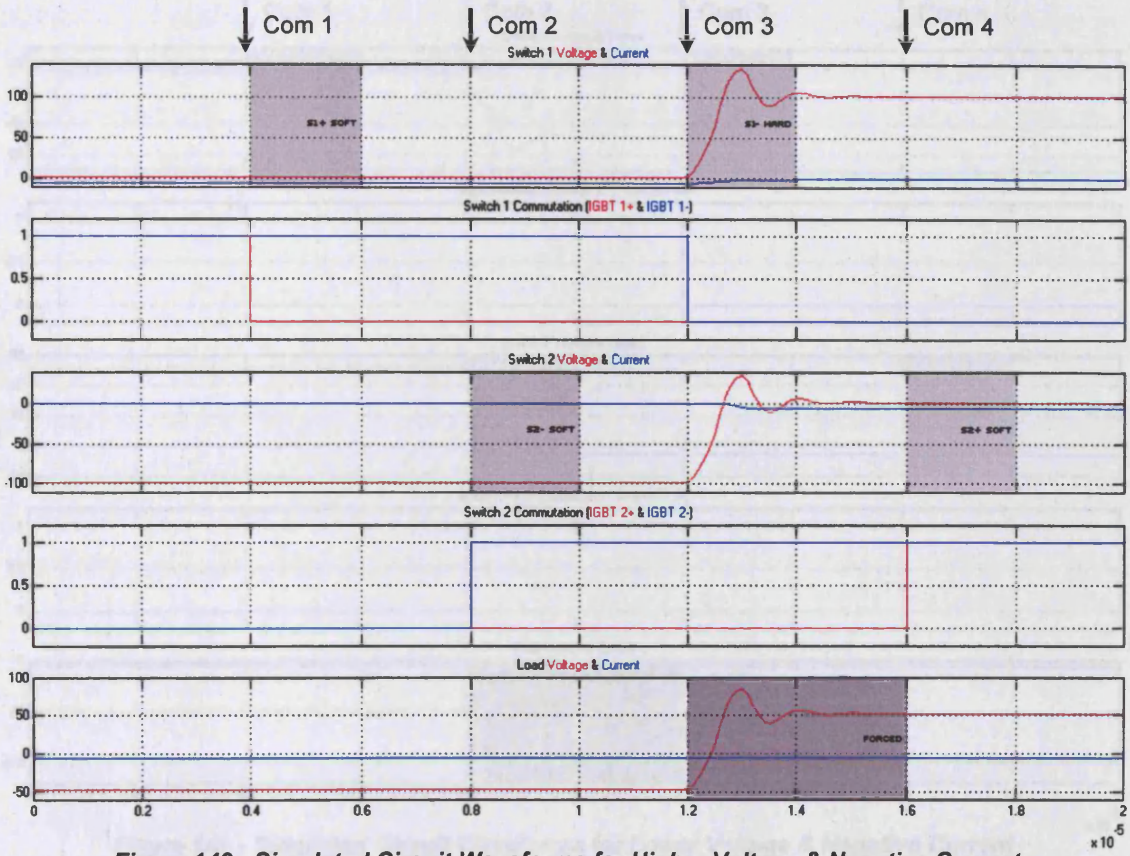

Figure 140 - Simulated Circuit Waveforms for Higher Voltage & Negative Current

The negative load current and higher incoming switch voltage means that a circulating current cannot flow and therefore commutation between switches is forced since S1- is turned off whilst current is flowing through it. Under these circumstances, the commutation is forced.

7.3.4 Four-step Commutation: Lower Incoming Voltage & Negative Load Current

Figure 141 shows the simulated circuit commutation analysis when the incoming switch S2 has a lower voltage than the outgoing switch S1 and there is a negative load current. The commutation sequence is as follows, referring to Figure 137 [p153]:

S1+ & S1- are initially closed with only S1- conducting the (negative) load current

- At Com 1: S1+ is opened first as it is reverse-biased and non-conducting with D1+ also reverse-biased and non-conducting
- At Com 2: S2- is closed and a circulating current begins to flow, reducing the current through S1- to zero. S2- undergoes a hard turn-on commutation and D2- experiences turn-on loss
- At Com 3: S1- is opened at zero current for a soft turn-off commutation while D1- is reverse-biased and experiences reverse-recovery loss.
- At Com 4: S2+ is closed to complete the commutation sequence but is reverse-biased and non- conducting with D2+ also reverse-biased and non-conducting

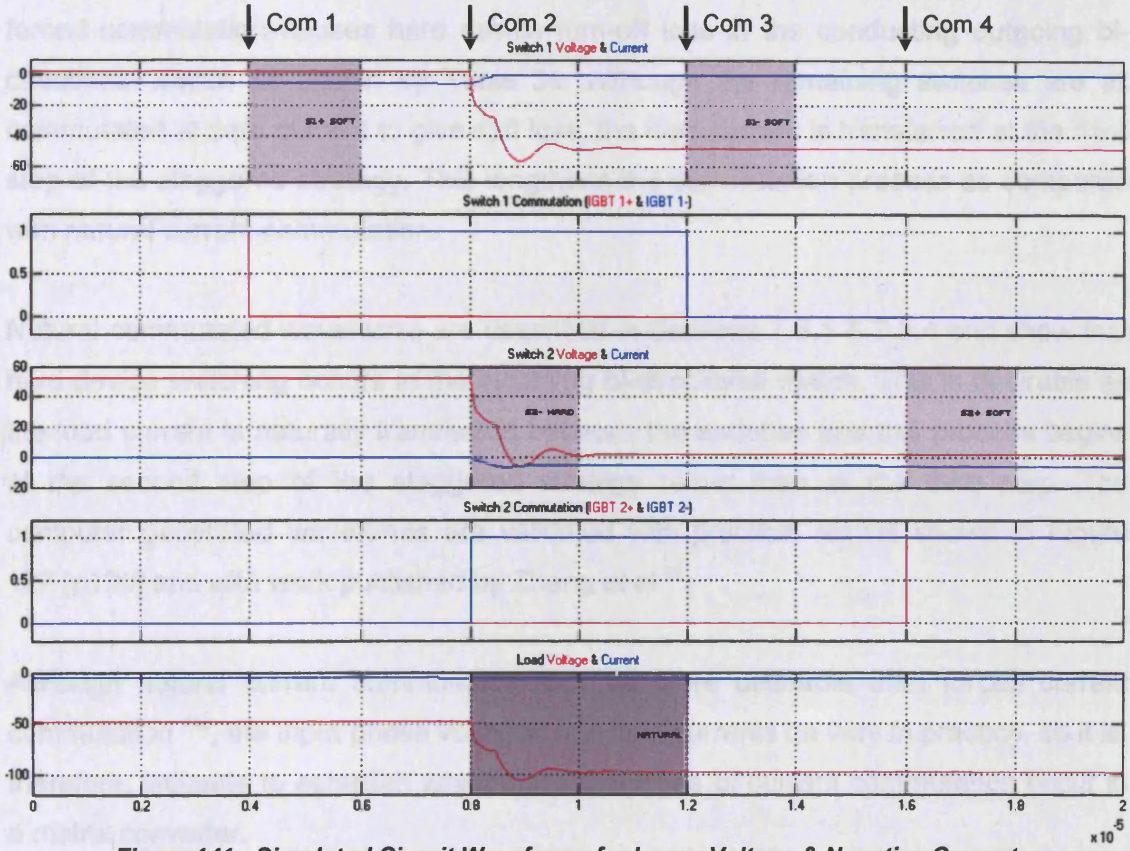

Figure 141 - Simulated Circuit Waveforms for Lower Voltage & Negative Current

The lower incoming switch voltage induces a circulating current that reduces the current flowing through the outgoing switch to zero for natural current commutation between the bi-directional switches. These results show that this process is natural.

7.3.5 Summary of Matrix Converter Commutations

The computer model showed that two distinct types of current commutation occur when a matrix converter employs a four-step staggered switching strategy. Table 34 summarises the results obtained and lists the type of commutation experienced by both semiconductor switches within each bi-directional switch [112].

Section	Incoming Voltage	Load Current	Current Commutation	Commutation Start Point	Outgoing Switch		Incoming Switch	
					S1+	S1-	S2+	S2-
7.3.1	Higher	Positive	Natural	2nd Step	Soft	Soft	Hard	Soft
7.3.2	Lower	Positive	Forced	3rd Step	Hard	Soft	Soft	Soft
7.3.3	Higher	Negative	Forced	3rd Step	Soft	Hard	Soft	Soft
7.3.4	Lower	Negative	Natural	2nd Step	Soft	Soft	Soft	Hard

Table 34 - Bi-directional Switch Current Commutations & Loss Distribution

The simulated circuit waveforms in Sections 7.3.2 & 7.3.3 show forced current commutation between input phases. Considering the individual switching devices, then forced commutation causes hard device turn-off loss in the conducting outgoing bi-directional switch as shown by Table 34. Although the remaining switches are all commutated at zero current to give soft loss, the load current is transferred at the third step of the staggered strategy. This lengthens the commutation process as compared with natural current commutation.

Natural commutated waveforms are described in Sections 7.3.1 & 7.3.4 and show that hard device switching occurs in the incoming bi-directional switch. This is desirable as the load current is naturally transferred between the switches and this process begins at the second step of the staggered strategy rather than at the third step. The computer generated waveforms are validated with practical results shown in Figure 127 [p136] and with work published by Zhang et al [83].

Although natural current commutation may be more desirable than forced current commutation [113], the input phase voltages and load currents do vary in practice, so it is, therefore, valuable to establish when these two types of current commutation occur in a matrix converter.

7.4 Commutation Event Analysis

The three-phase supply voltage waveform can in effect be divided into six individual regions where the signs of the voltage differences between the three input phases do not change. This is shown in Figure 142.

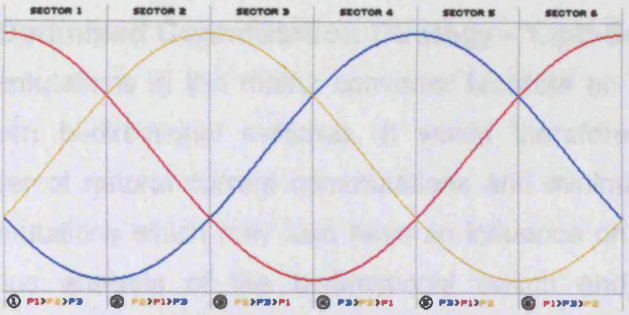

Figure 142 - Six Sectors of the Supply Waveform

Venturini control strategies for the matrix converter often employ a sequential (1-2-3) commutation order with each switching cycle containing three commutations, see Figure 28 [p52]. As each output phase of a matrix converter is generating either a positive or negative load current, depending on the fundamental output waveform, there are therefore twelve possible states for the input voltage and output current operating conditions. Thus for each voltage sector (Figure 142) and for both positive and negative load current conditions, the total number of natural commutations can be determined for any commutation sequence over a supply waveform cycle.

Table 35 shows the result of employing the standard sequential commutation sequence. The distinction between 'natural' and 'forced' commutation has been determined by the load current polarity and the relative magnitude of the incoming and outgoing switch voltages, as defined by Table 34 [p158].

Sector	Voltages	Load Current	Commutation 1	Commutation 2	Commutation 3
1	V1>V2>V3	Positive	Forced (P1-P2)	Forced (P2-P3)	Natural (P3-P1)
		Negative	Natural (P1-P2)	Natural (P2-P3)	Forced (P3-P1)
2	V2>V1>V3	Positive	Natural (P1-P2)	Forced (P2-P3)	Natural (P3-P1)
		Negative	Forced (P1-P2)	Natural (P2-P3)	Forced (P3-P1)
3	V2>V3>V1	Positive	Natural (P1-P2)	Forced (P2-P3)	Forced (P3-P1)
		Negative	Forced (P1-P2)	Natural (P2-P3)	Natural (P3-P1)
4	V3>V2>V1	Positive	Natural (P1-P2)	Natural (P2-P3)	Forced (P3-P1)
		Negative	Forced (P1-P2)	Forced (P2-P3)	Natural (P3-P1)
5	V3>V1>V2	Positive	Forced (P1-P2)	Natural (P2-P3)	Forced (P3-P1)
		Negative	Natural (P1-P2)	Forced (P2-P3)	Natural (P3-P1)
6	V1>V3>V2	Positive	Forced (P1-P2)	Natural (P2-P3)	Natural (P3-P1)
		Negative	Natural (P1-P2)	Forced (P2-P3)	Forced (P3-P1)

Total Forced	(18) 50%
Total Natural	(18) 50%

Table 35 - Standard Sequential (1-2-3) Switching Analysis

Table 35 shows that 50% of converter commutations are 'natural' with the standard commutation order and staggered switching strategy, as confirmed by Beasant et al [110]. The results also show that half of the switching cycles contain two natural current commutations while the remainder contain only one. This suggests that a matrix converter employing the standard switching sequence is not optimised with respect to maximising natural current commutations.

7.5 A Proposed Optimised Commutation Strategy - 'Opti-Soft'

Natural current commutations in the matrix converter facilitate an earlier transfer of load current between bi-directional switches. It would therefore be desirable to maximise the number of natural current commutations and minimise the number of forced current commutations which may also have an influence on switching loss. In view of the previous analysis of the bi-directional switch and, specifically, the conditions required for natural current commutation, it was concluded that matrix converter switching strategy may be further optimised and the number of natural commutations increased by reordering the switching sequence. An approach to maximising natural commutations in the matrix converter has therefore been developed. The newly proposed sequence selects the order of commutation in relation to the instantaneous voltage of the supply and the load current direction to satisfy the conditions required for natural current commutation.

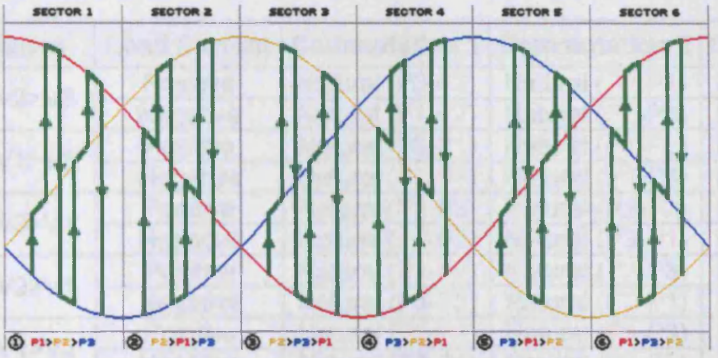

Figure 143 - 'Positive Voltage Stepping' with Positive Load Current

With positive load current, commutation would begin with the input phase at the lowest voltage, continue to the next lowest until the highest voltage phase is reached. Figure 143 demonstrates two 'positive voltage stepping' switching cycles in each of the six supply sectors. Each of these steps produces a natural current commutation with the exception of the final forced commutation; from highest to lowest supply voltage.

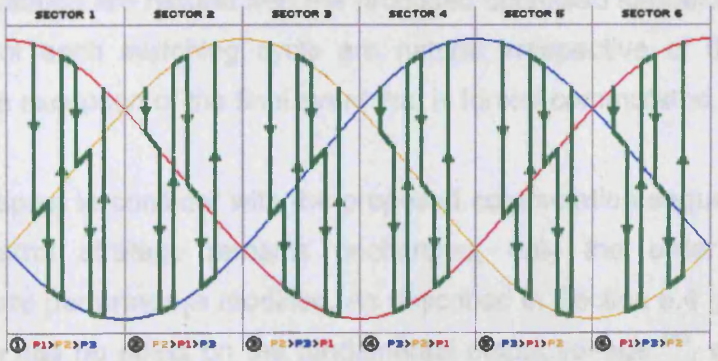

Figure 144 - 'Negative Voltage Stepping' with Negative Load Current

However, the opposite will occur with a negative load current. Switching will start with the highest voltage and continues downwards to the lowest voltage. Figure 144

demonstrates two 'negative voltage stepping' switching cycles in each of the six supply sectors. As before, each of these current commutations is 'natural', apart from the final 'forced' step that completes the switching cycle. A three-phase fed converter implementing this switching strategy could therefore operate with 66.67% natural current commutations, a significant increase over existing strategies.

Load Current	Commutation 1	Commutation 2	Commutation 3
Positive	MIN(V1,V2,V3)	MEDIAN (V1,V2,V3)	MAX(V1,V2,V3)
Negative	MAX(V1,V2,V3)	MEDIAN (V1,V2,V3)	MIN(V1,V2,V3)

Table 36 - Proposed Commutation Sequence Rule

Referring to Figure 142 [p159], when operating in supply sector 1 with a positive load current, the correct commutation sequence is P3-P2-P1. If operating within sector 5 with negative load current, the commutation sequence becomes P3-P1-P2.

Sector	Voltages	Load Current	Commutation 1	Commutation 2	Commutation 3
1	V1>V2>V3	Positive	Natural (P3-P2)	Natural (P2-P1)	Forced (P1-P3)
		Negative	Natural (P1-P2)	Natural (P2-P3)	Forced (P3-P1)
2	V2>V1>V3	Positive	Natural (P3-P1)	Natural (P1-P2)	Forced (P2-P3)
		Negative	Natural (P2-P1)	Natural (P1-P3)	Forced (P3-P2)
3	V2>V3>V1	Positive	Natural (P1-P3)	Natural (P3-P2)	Forced (P2-P1)
		Negative	Natural (P2-P3)	Natural (P3-P1)	Forced (P1-P2)
4	V3>V2>V1	Positive	Natural (P1-P2)	Natural (P2-P3)	Forced (P3-P1)
		Negative	Natural (P3-P2)	Natural (P2-P1)	Forced (P1-P3)
5	V3>V1>V2	Positive	Natural (P2-P1)	Natural (P1-P3)	Forced (P3-P2)
		Negative	Natural (P3-P1)	Natural (P1-P2)	Forced (P2-P3)
6	V1>V3>V2	Positive	Natural (P2-P3)	Natural (P3-P1)	Forced (P1-P2)
		Negative	Natural (P1-P3)	Natural (P3-P2)	Forced (P2-P1)

Total Forced	(12) 33.33%
Total Natural	(24) 66.67%

Table 37 - Proposed Commutation Sequence Analysis

An analysis of all possible operating conditions in Table 37 shows that 66.67% of all current commutations are natural with the proposed optimised sequence. The first two commutations of each switching cycle are natural irrespective of the load current polarity, with the exception of the final event that is forced commutated.

An important aspect to consider with the proposed commutation sequencer is that the modulation control strategy remains unchanged, only the order in which the commutations are performed is modified. As described in Section 6.4 [p141], the order of commutation has no effect on the fundamental output voltage [109], so the proposed strategy can be expected not to disturb the operation of the matrix converter and more importantly the output waveform. Implementation of this strategy requires continuous tracking of the supply voltages to accurately determine the correct commutation

sequence. Output current measurement is also necessary to correctly select between positive or negative voltage stepping.

As the bi-directional switch topology employed in the laboratory converter made practical implementation of 'Opti-Soft' difficult without an extensive rebuild, the previously developed and validated computer model, as used in Chapter Two and Chapter Five, was adapted to investigate the proposed concept. Based upon the standard Venturini control strategy, the revised single-phase output model, see Appendix A27 [p310], was developed around three independent bi-directional switch modules that employ four-step staggered commutation and follow the sequencing strategy defined in Section 2.4.3 [p46]. The optimised commutation strategy measures the supply voltages as well as the load current to select between positive or negative voltage stepping. The completed model allows operation with either the standard, semi-symmetrical PWM or the proposed 'Opti-Soft' switch sequencers for comparison.

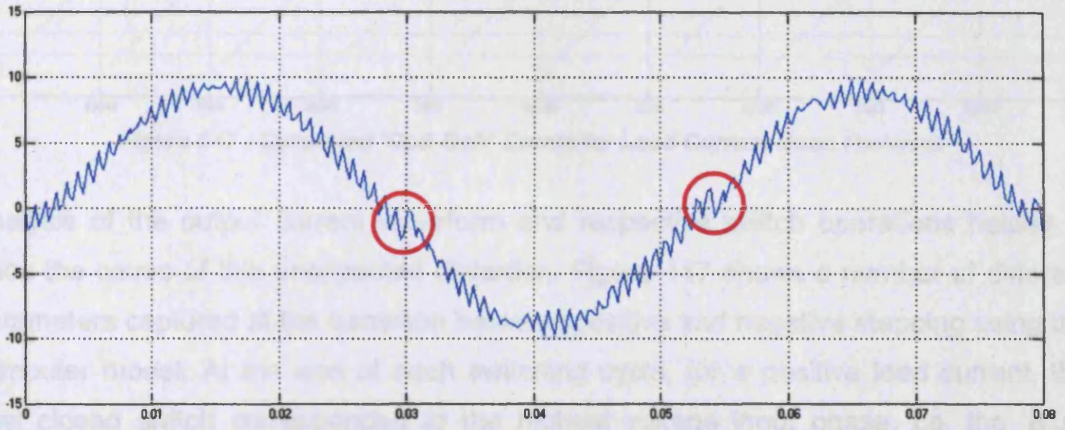

Figure 145 - Proposed Sequencer Simulated Output Current 1.2kHz : F_{out} = 20Hz

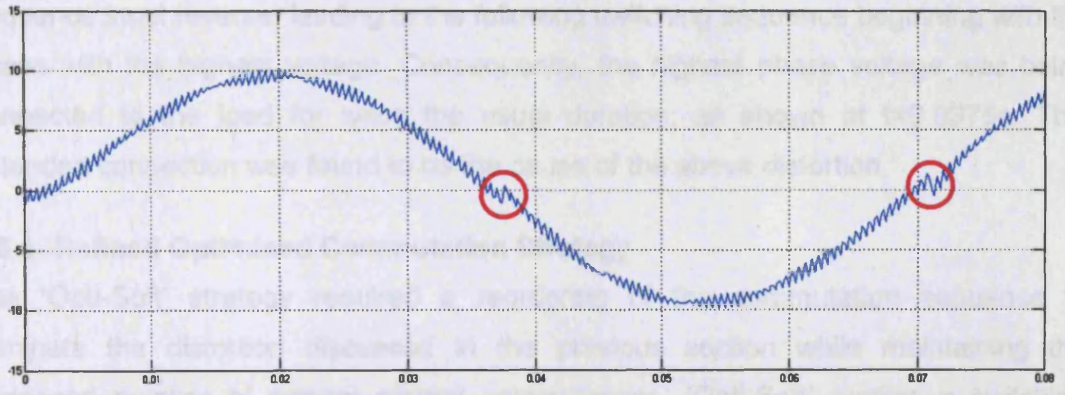

Figure 146 - Proposed Sequencer Simulated Output Current 2kHz : F_{out} = 15Hz

Figure 145 and Figure 146 show the simulated output current waveform for the proposed commutation strategy with converter switching frequencies of 1.2kHz and 2kHz. A distortion in the output current waveform is evident every time at the zero current crossing, corresponding to the point at which the positive stepping sequence

changes to the negative stepping sequence. Such distortion would be unacceptable in practice so a modification of the original 'Opti-Soft' strategy became necessary.

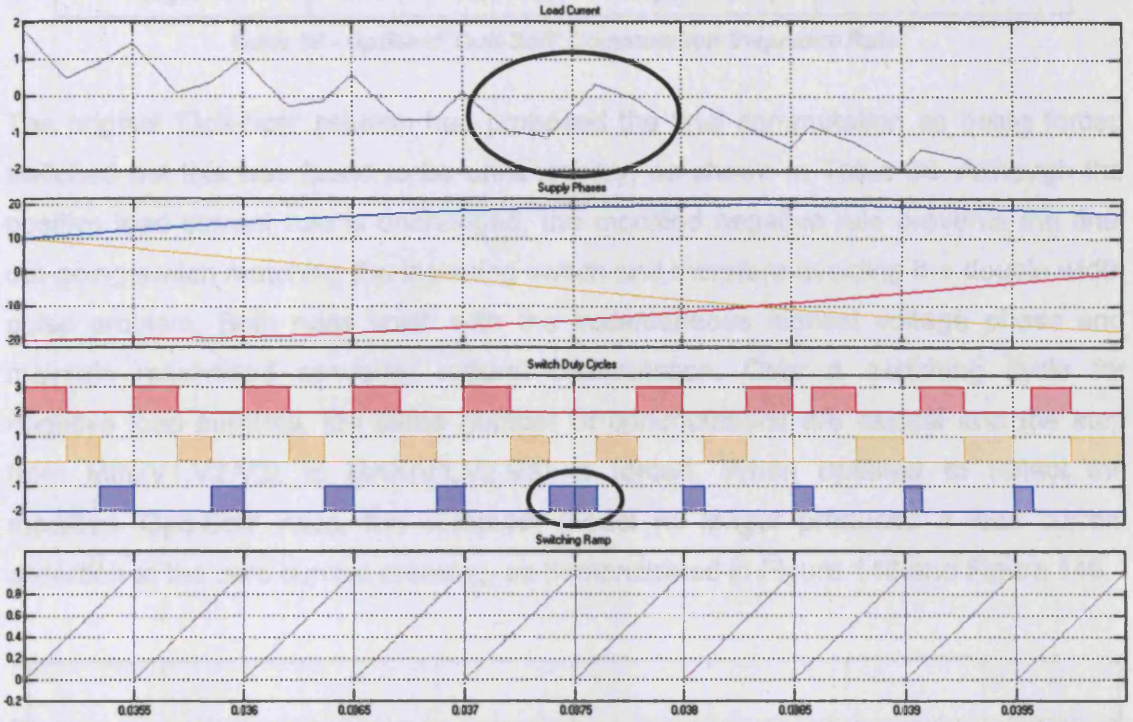

Figure 147 - Simulated 'Opti-Soft' Converter Load Current Upon Reversal

Analysis of the output current waveform and respective switch operations helped to trace the cause of this unexpected distortion. Figure 147 shows a number of different parameters captured at the transition between positive and negative stepping using the computer model. At the end of each switching cycle, for a positive load current, the final closed switch corresponded to the highest voltage input phase, i.e. the 'Blue' phase in Figure 147. When the load current polarity changes, the commutation sequence must reverse, leading to the following switching sequence beginning with the phase with the highest voltage. Consequently, the highest phase voltage was being connected to the load for twice the usual duration, as shown at t=0.0375s. This extended connection was found to be the cause of the above distortion.

7.5.1 Refined Optimised Commutation Strategy

The 'Opti-Soft' strategy required a reordering of the commutation sequence to eliminate the distortion discussed in the previous section while maintaining the increased number of natural current commutations. 'Opti-Soft' applies a switching sequence derived from the supply voltage magnitudes and load current polarity. The increase in natural current commutations is achieved by stepping through the supply voltages with a single unavoidable 'forced' current commutation each cycle.

Load Current	Commutation 1	Commutation 2	Commutation 3
Positive	MIN(V1,V2,V3)	MEDIAN (V1,V2,V3)	MAX(V1,V2,V3)
Negative	MEDIAN (V1,V2,V3)	MIN(V1,V2,V3)	MAX(V1,V2,V3)

Table 38 - Updated 'Opti-Soft' Commutation Sequence Rule

The original 'Opti-Soft' solution had proposed the final commutation as being forced switched but this was found to be unnecessary, as shown in Table 38. Although the positive load current rule is unchanged, the modified negative rule prevents the final out-going switch matching the incoming switch and therefore avoiding the double width pulse problem. Both rules finish with the instantaneous highest voltage phase and maintain maximised converter natural commutation. Over a switching cycle for negative load currents, the same number of commutations are natural and the step from MIN(V1,V2,V3) to MAX(V1,V2,V3) is forced. When updated to reflect the modified 'Opti-Soft' rules, the computer model no longer produced a load current distortion at the zero current crossing, as demonstrated in Figure 148 and Figure 149.

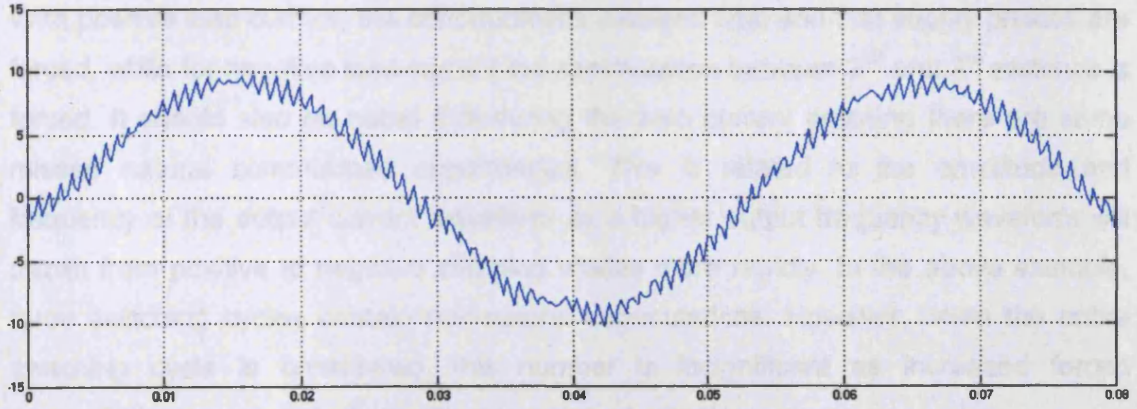

Figure 148 - Revised 'Opti-Soft' Computer Model Results 1.2kHz : F_{out} = 20Hz

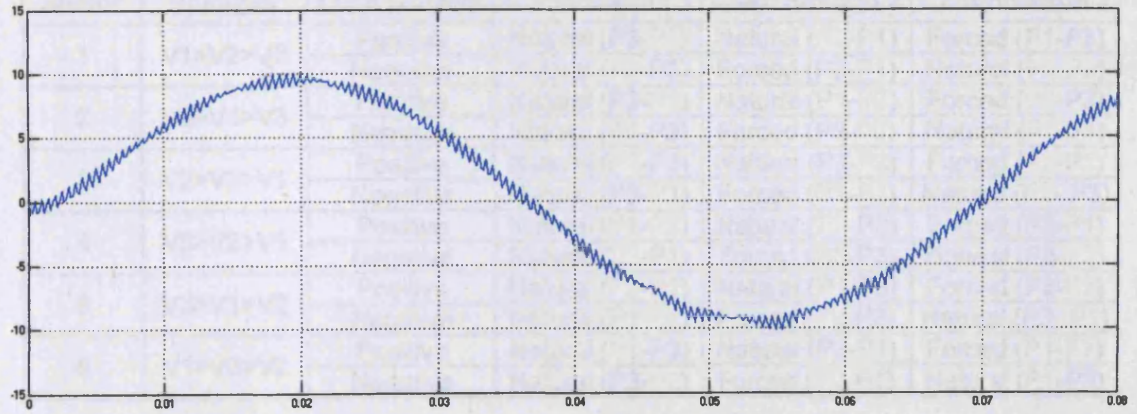

Figure 149 - Revised 'Opti-Soft' Computer Model Results 2kHz : F_{out} = 15Hz

More detailed analysis of the circuit voltages close to the load current reversal confirms this in Figure 150 where the natural current commutations are highlighted.

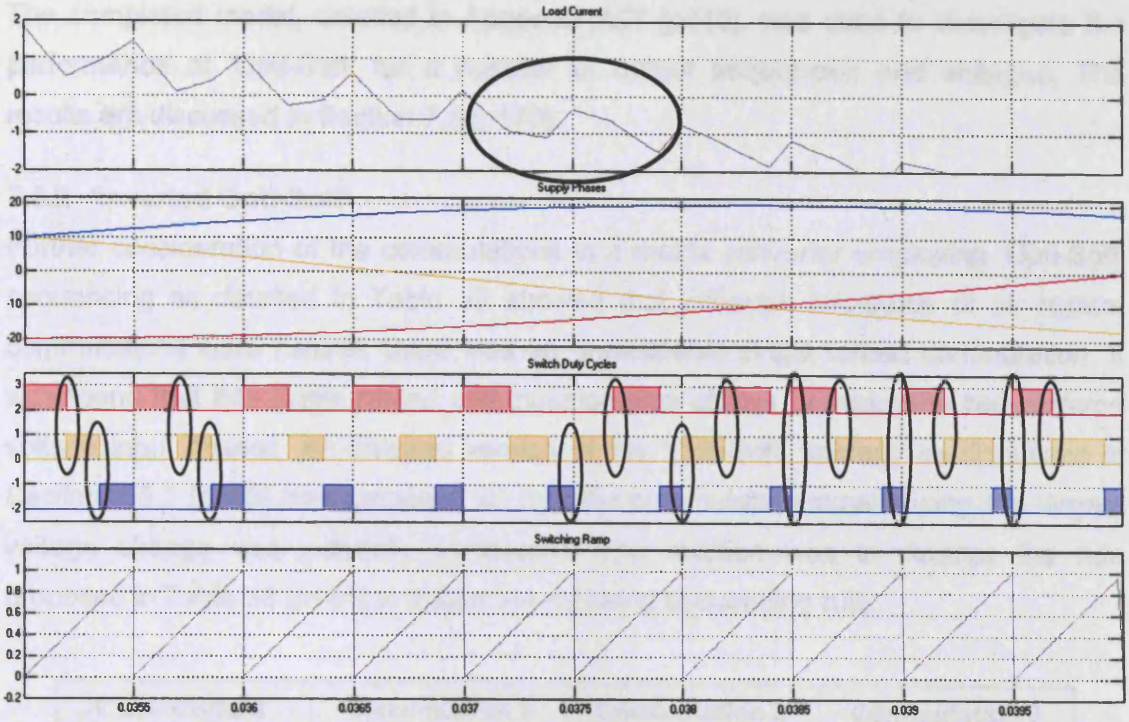

Figure 150 - Corrected 'Opti-Soft' Load Current Data upon Reversal

With positive load current, the commutations between final and first supply phases are forced, while for negative load current the commutation between 2nd and 3rd switches is forced. It should also be noted that during the zero current crossing there are some missed natural commutated opportunities. This is related to the amplitude and frequency of the output current waveform as a higher output frequency waveform will transit from positive to negative stepping modes more rapidly. In the above example, three switching cycles contain non-natural commutations. However, when the entire switching cycle is considered, this number is insignificant as increased forced commutations occur only during the zero current crossing.

Sector	Voltages	Load Current	Commutation 1	Commutation 2	Commutation 3
1	V1>V2>V3	Positive	Natural (P3-P2)	Natural (P2-P1)	Forced (P1-P3)
		Negative	Natural (P2-P3)	Forced (P3-P1)	Natural (P1-P2)
2	V2>V1>V3	Positive	Natural (P3-P1)	Natural (P1-P2)	Forced (P2-P3)
		Negative	Natural (P1-P3)	Forced (P3-P2)	Natural (P2-P1)
3	V2>V3>V1	Positive	Natural (P1-P3)	Natural (P3-P2)	Forced (P2-P1)
		Negative	Natural (P3-P1)	Forced (P1-P2)	Natural (P2- P3)
4	V3>V2>V1	Positive	Natural (P1-P2)	Natural (P2-P3)	Forced (P3-P1)
		Negative	Natural (P2-P1)	Forced (P1-P3)	Natural (P3-P2)
5	V3>V1>V2	Positive	Natural (P2-P1)	Natural (P1-P3)	Forced (P3-P2)
		Negative	Natural (P1-P2)	Forced (P2-P3)	Natural (P3- P1)
6	V1>V3>V2	Positive	Natural (P2-P3)	Natural (P3-P1)	Forced (P1-P2)
		Negative	Natural (P3-P2)	Forced (P2-P1)	Natural (P1-P3)

Total Forced	(12) 33.33%
Total Natural	(24) 66.67%

Table 39 - Matrix Converter Employing Updated 'Opti-Soft' Switching Analysis

The completed model, detailed in Appendix A27 [p310], was used to investigate the performance of 'Opti-Soft' for a number of output frequencies and voltages. The results are discussed in Section 7.8 [p170].

7.5.2 'Inverted Opti-Soft'

Further consideration of the commutations in a matrix converter employing 'Opti-Soft' sequencing as detailed in Table 39 showed that although two-thirds of all current commutations were natural, there was an unavoidable single forced commutation. It was found that this single forced commutation was always between the two extreme voltage input phases. An inverted version of the 'Opti-Soft' strategy as discussed in Section 7.5.1 [p163] was proposed so that the commutation experiencing the largest voltage change was naturally commuted. The solution was to reverse the rule proposed in Table 38 [p164] to obtain the following sequencing rule:

Load Current	Commutation 1	Commutation 2	Commutation 3
Positive	MEDIAN (V1,V2,V3)	MIN(V1,V2,V3)	MAX(V1,V2,V3)
Negative	MIN(V1,V2,V3)	MEDIAN (V1,V2,V3)	MAX(V1,V2,V3)

Table 40 - 'Inverted Opti-Soft' Commutation Sequence Rule

Although the above sequencing rule achieves the aim of naturally commutating between the extreme voltage input phases, the remaining commutations are forced.

Sector	Voltages	Load Current	Commutation 1	Commutation 2	Commutation 3
1	V1>V2>V3	Positive	Forced (P2-P3)	Natural (P3-P1)	Forced (P1-P2)
		Negative	Forced (P2-P2)	Forced (P2-P1)	Natural (P1-P3)
2	V2>V1>V3	Positive	Forced (P1-P3)	Natural (P3-P2)	Forced (P2-P1)
		Negative	Forced (P3-P1)	Forced (P1-P2)	Natural (P2-P3)
3	V2>V3>V1	Positive	Forced (P3-P1)	Natural (P1-P2)	Forced (P2- P3)
		Negative	Forced (P1-P3)	Forced (P3-P2)	Natural (P2-P1)
4	V3>V2>V1	Positive	Forced (P2-P1)	Natural (P1-P3)	Forced (P3-P2)
		Negative	Forced (P1-P2)	Forced (P2-P3)	Natural (P3-P1)
5	V3>V1>V2	Positive	Forced (P1-P2)	Natural (P2-P3)	Forced (P3- P1)
		Negative	Forced (P2-P1)	Forced (P1-P3)	Natural (P3-P2)
6	V1>V3>V2	Positive	Forced (P3-P2)	Natural (P2-P1)	Forced (P1-P3)
		Negative	Forced (P2-P3)	Forced (P3-P1)	Natural (P1-P2)

Total Forced	(24) 66.67%
Total Natural	(12) 33.33%

Table 41 - Matrix Converter Employing 'Inverted Opti-Soft' Switching Analysis

Although 'Inverted Opti-Soft' may operate with a reduced number of natural commutations, as shown by Table 41, the effect on converter loss was investigated using a computer model described in Section 7.9 [p172].

7.6 Practical Implementation of 'Opti-Soft'

Some hardware additions to the matrix converter may be required when implementing the proposed 'Opti-Soft' sequencer in a practical matrix converter. These include instrumentation to monitor the supply voltages and the output current polarity and to enable accurate implementation of the commutation sequence to maximise converter efficiency. A typical practical matrix converter would already contain the instrumentation necessary to implement the 'Opti-Soft' sequencer as input voltages and output currents are normally measured.

7.6.1 Voltage Measurement

The majority of Venturini converters implement closed-loop algorithms that track the supply voltage in order to be more tolerant of supply distortion. The instantaneous voltage is sampled at the beginning of each switching cycle using an analogue-to-digital converter. The associated buffer circuitry is already present and it could be employed by the 'Opti-Soft' sequencer. Although a minor increase in processor utilisation would be incurred in ranking the supply voltages in order of magnitude, this could be minimised through efficient software design.

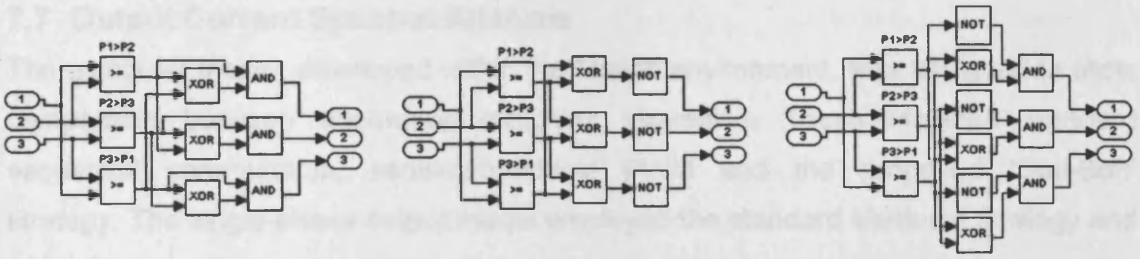

Figure 151 - (a) Highest, (b) Median & (c) Lowest Voltage Comparator Logic Networks

An alternative solution would be to implement an external comparison system composed of discrete logic devices to increase resolution and reduce control system software overhead, as shown in Figure 151. A network of voltage comparators is connected between buffered input phases, using a set of high-speed logic gates used to select the instantaneous highest, median and lowest voltages. In Figure 151(a), the outputs indicate which of the three input phases is the highest in magnitude by setting the corresponding output to a logic level '1'. The same approach could be repeated for the median and lowest voltage comparators. The outputs could connect directly to the control system processor for minimal processing overhead.

7.6.2 Current Measurement

The load current polarity for each output phase determines the switching sequence implemented by the novel optimised control strategy. Only the direction not magnitude of the load current is required so a simplified transducer is sufficient for this application. However, the anti-parallel bi-directional switches used to implement the

optimised control strategy already possess current polarity transducers. These are used to determine the correct staggered commutation order and can be used for the 'Opti-Soft' sequencer. A simple comparator circuit can then derive a signal for connection to the MCU, as shown in Section 3.7 [p77].

Section 7.6.1 and Section 7.6.2 have shown that little additional hardware is required to implement the new commutation strategy. Low cost logic gates can be used to perform the majority of the computations to limit processor utilisation. The control system software will require minor modifications to allow reordering of the switching sequence in response to I/O information. Voltage levels can be monitored at each commutation to maximise natural switching potential, for example when the relative supply voltages change during a switching cycle. However, an improved solution may be to operate the converter at a multiple of the supply frequency. This would avoid a change in the voltage ranking across a switching cycle and simplify the commutation logic. The controller will also check the load current at the beginning of each switching cycle to select the correct stepping direction.

7.7 Output Current Spectral Analysis

The computer model, developed within the Matlab environment, was designed to allow comparison between alternative switching strategies. These included standard sequential commutation, semi-symmetrical PWM and the proposed 'Opti-Soft' strategy. The single-phase output model employed the standard Venturini strategy and a spectral analysis comparison of the three switching sequences is shown in the following figures.

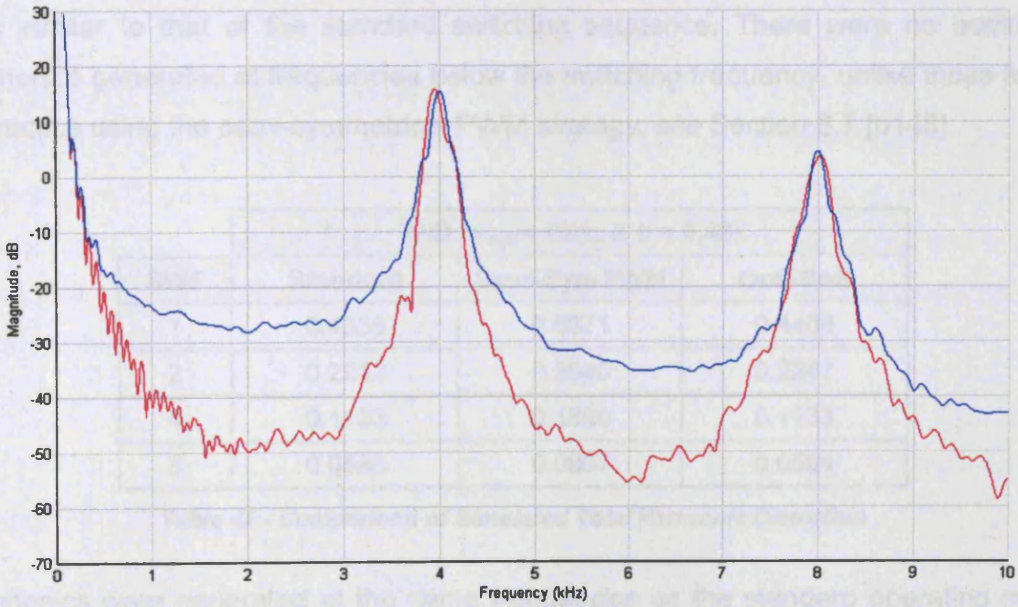

Figure 152 - Standard & 'Opti-Soft' Output Current Spectrum SWF=4kHz F_{out}=10Hz

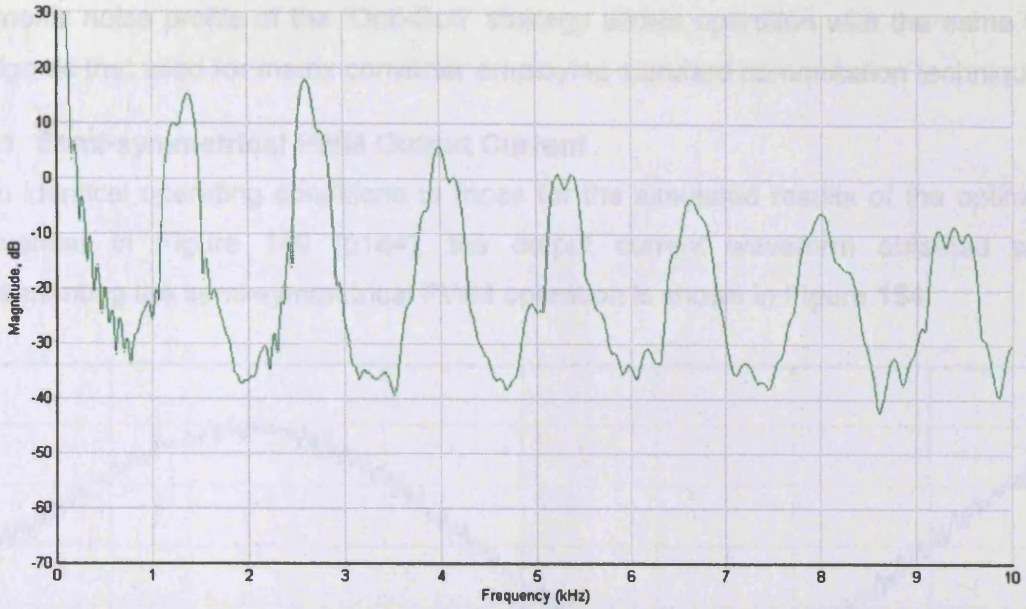

Figure 153 - Semi-symmetrical PWM Output Current Spectrum SWF=4kHz F_{out}=10Hz

The semi-symmetrical PWM strategy discussed in Section 6.7 [p145] and its harmonic current spectrum shown in Figure 153 produces considerably increased harmonic noise in the output current, compared to the standard and 'Opti-Soft' strategies shown in Figure 152. Moreover, the dominant harmonic was no longer located at the switching frequency but at one-thirds and two-third of this value, supporting the practical observations in Chapter Six. The output waveform contained harmonics at more discrete frequencies, with practical implications such as increased harmonic noise. If harmonics were to occur close to the fundamental frequency of the supply filter, the filter could experience excitation and lead to quality-of-supply issues.

The proposed 'Opti-Soft' sequencer produced an output spectrum, shown in Figure 152, similar to that of the standard switching sequence. There were no additional harmonics generated at frequencies below the switching frequency, unlike those found in practice using the semi-symmetrical PWM strategy, see Section 6.7 [p145].

	THD (F_{out} = 10Hz & q = 0.45)		
SWF	**Standard**	**Semi-Sym PWM**	**Opti-Soft**
1	0.4338	0.6671	0.4408
2	0.2212	0.3640	0.2247
4	0.1133	0.1890	0.1135
8	0.0586	0.0967	0.0584

Table 42 - Comparison of Simulated Total Harmonic Distortion

Harmonics were generated at the same frequencies as the standard operating mode with similar magnitude and THD. Unlike the semi-symmetrical PWM strategy, the

harmonic noise profile of the 'Opti-Soft' strategy allows operation with the same filter design as that used for matrix converter employing standard commutation techniques.

7.7.1 Semi-symmetrical PWM Output Current

With identical operating conditions to those for the simulated results of the optimised sequencer in Figure 149 [p164], the output current waveform obtained when implementing the semi-symmetrical PWM operation is shown in Figure 154.

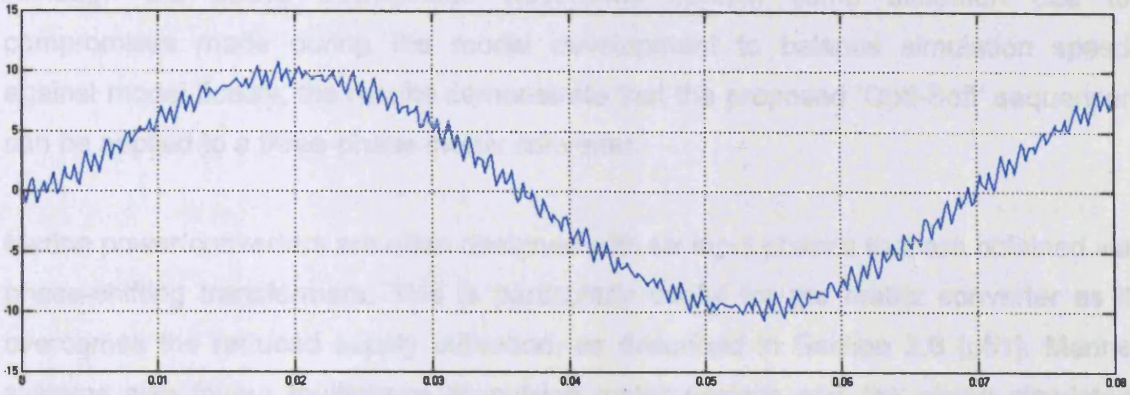

Figure 154 - Semi-symmetrical PWM Output Current Model Results 2kHz : F_{out} = 15Hz

The output current waveform observed with the computer model of the semi-symmetrical PWM strategy shows a significant increase in waveform ripple. Although the ripple can be reduced by increasing the converter switching frequency, as described earlier, a marine drive is unlikely to operate with a switching frequency above 4-5kHz to limit converter loss. Practical results from the laboratory also highlighted the increase in switching harmonics generated in the input and output lines of the converter when implementing semi-symmetrical PWM switching, see Section 6.7.1 [p146]. The implication is that the supply filter would require significant upgrading to cope with the increased low frequency harmonic noise.

7.8 Multi-phase Matrix Converter Application

The single output phase computer model was expanded to demonstrate the proposed 'Opti-Soft' commutation sequence in a multi-phase system by modelling a three-phase output matrix converter, described in Appendix A28 [p311]. The following results show the output currents of two load configurations, star-connected load in Figure 155 and delta-connected load in Figure 156.

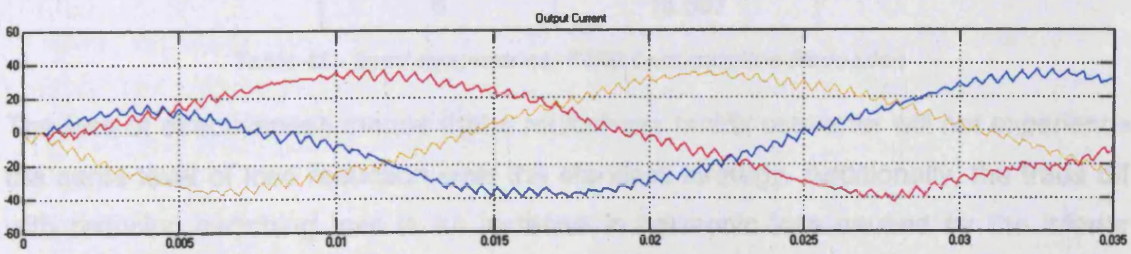

Figure 155 - 'Opti-Soft' Matrix Converter Simulation - Star Connected Load Current

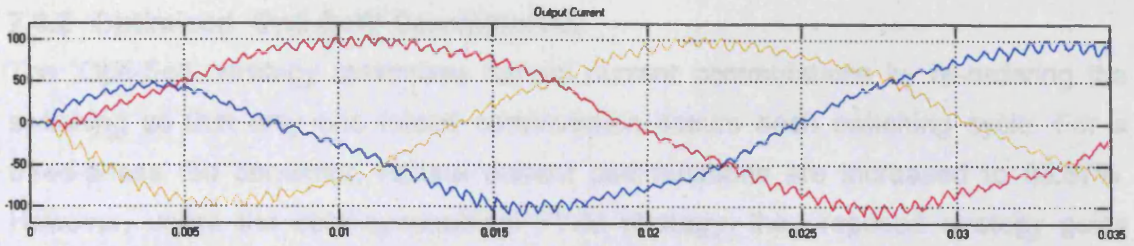

Figure 156 - 'Opti-Soft' Matrix Converter Simulation - Delta Connected Load Current

Although the above three-phase waveforms contain some distortion due to compromises made during the model development to balance simulation speed against model fidelity, the results demonstrate that the proposed 'Opti-Soft' sequencer can be applied to a three-phase matrix converter.

Marine power converters are often designed with six input phases that are obtained via phase-shifting transformers. This is particularly useful for the matrix converter as it overcomes the reduced supply utilisation, as described in Section 2.6 [p51]. Marine systems also favour multiphase propulsion motor designs and the above simulated results demonstrate that the 'Opti-Soft' switching strategy is compatible with these requirements. As 'Opti-Soft' is independently applied to each converter output phase, it can be easily stacked to give larger converter configurations.

7.8.1 Semi-symmetrical PWM

The semi-symmetrical PWM method reduces the total number of converter commutations required each switching cycle by retaining the final switch of each switching cycle as the first switch of the following cycle. This is significant as the total number of switch commutations is reduced by one third for a three-phase fed matrix converter. However, as the number of input phases is increased, the effectiveness of this technique is reduced as only one switch can be retained into the following switching cycle, as demonstrated in Table 43.

Number Of Input phases	(%) Reduction in Commutations
3	33.333
4	25
5	20
6	16.667

Table 43 - Semi-symmetrical PWM Commutation Reduction

The loss of effectiveness means that a multiphase matrix converter will not experience the same level of loss reduction over the standard strategy. Additionally, the trade off with reducing switching loss is an increase in harmonic loss caused by the inferior output waveform quality.

7.8.2 Optimised 'Opti-Soft' Commutation

The 'Opti-Soft' strategy maximises natural current commutations by re-ordering the switching so that only one forced commutation occurs each switching cycle. For a three-phase fed converter, natural current commutations are increased to 66.67%. However, unlike the semi-symmetrical PWM strategy, the proposed strategy gains effectiveness as the number of converter input phases increases.

Number of Input Phases	(%) Natural Commutations	
	'Opti-Soft'	Inv. 'Opti-Soft
3	66.667	33.33
4	75	25
5	80	20
6	83.333	16.67

Table 44 - Percentage 'Opti-Soft' Natural Commutations for Multiphase Converter

The inverted 'Opti-Soft' sequencer, discussed in Section 7.5.2 [p166], produces a natural current commutation between the extreme voltage input phases and it therefore suffers reduced total natural current commutation. This is further compounded as the number of input phases is increased.

7.9 Computer Loss Model

A numerical loss model was created to analyse the converter loss associated with the proposed 'Opti-Soft' commutation strategy. This simulates the loss in a three-phase input, single-phase output matrix converter configuration employing anti parallel IGBT bi-directional switches. The simulated converter employs the Advanced Venturini control algorithm that tracks the supply voltage and maintains a unity input displacement angle. The model calculates the precise supply voltages and load current at each commutation event so that low switching frequencies do not reduce model accuracy as the voltage may change significantly during a single commutation cycle. The load current is calculated with knowledge of the converter output frequency and load. This is then used to determine the current flowing through each switch during commutation to calculate the individual device switching loss.

7.9.1 Loss Model Assumptions

From the detailed analysis of current commutation between anti-parallel bi-directional switches in Section 7.3 [p153], two types of commutation emerged, dependent on the load current polarity and the relative switch voltages. These are summarised in Table 34 [p158] and the following assumptions are made:

- Soft IGBT commutations to be lossless as the energy loss is an order of magnitude less than hard commutations [111].

- Diode turn-on losses are ignored "...because they are very small" [114].

In view of the above assumptions and the results from the computer modelling in Section 7.3 [p153], Table 45 summarises the switching losses in an anti-parallel IGBT matrix converter employing four-step switch commutation, with the values ignored by the computer model shown in grey.

Incoming Voltage	Load Current	Current Commutation	Outgoing Switch		Incoming Switch	
			IGBT	Diode	IGBT	Diode
Higher	Positive	Natural		Rev-Rec	Hard	
Higher	Negative	Forced	Hard			
Lower	Positive	Forced	Hard			
Lower	Negative	Natural		Rev-Rec	Hard	

Table 45 - Switching Loss in Anti-parallel IGBT Matrix Converter

7.9.2 Switching Loss

The IGBT switching loss was modelled using a similar approach to that published by Apap et al [112]. The turn-on and turn-off energy loss is assumed to vary linearly with both the device voltage change during the commutation event and the conducted collector current [111]. The device switching loss is therefore calculated as:

$$\text{IGBT Turn-on Loss, } E_{on} = e_{on}\,\Delta V_{ce}\,\Delta I_c$$

$$\&$$

$$\text{IGBT Turn-off Loss, } E_{off} = e_{off}\,\Delta V_{ce}\,\Delta I_c$$

Equation 25

e_{on} & e_{off} = Respective energy loss per unit voltage and current

ΔV_{ce} = Change in collector-emitter voltage during commutation

ΔI_c = Change in collector-emitter current during commutation

The diode recovery loss can also be derived similarly:

$$\text{Diode recovery energy loss, } E_{rec} = e_{rec}\,\Delta V_d\,\Delta I_d$$

Equation 26

e_{rec} = Diode recovery energy loss per unit voltage and current

ΔV_d = Change in voltage across diode during commutation

ΔI_d = Change in diode conducted current during commutation

The loss experienced by the diode depends on the nature of the associated switching event, and the results in Section 7.3 [p153] show that incoming switch diodes experience no switching loss. Table 46 summaries the switching loss calculations for a staggered switching strategy:

Incoming Voltage	Load Current	Current Commutation	Outgoing Switch		Incoming Switch	
			IGBT	Diode	IGBT	Diode
Higher	Positive	Natural	0	$e_{rec}\,\Delta V_d\,\Delta I_d$	$e_{on}\,\Delta V_{ce}\,\Delta I_c$	0
Higher	Negative	Forced	$e_{off}\,\Delta V_{ce}\,\Delta I_c$	0	0	0
Lower	Positive	Forced	$e_{off}\,\Delta V_{ce}\,\Delta I_c$	0	0	0
Lower	Negative	Natural	0	$e_{rec}\,\Delta V_d\,\Delta I_d$	$e_{on}\,\Delta V_{ce}\,\Delta I_c$	0

Table 46 - Anti-parallel IGBT Switching Loss Equations (Staggered Commutation)

7.9.3 Conduction Loss

Although complex forward voltage drop models could have been derived for the converter devices, these would have been limited by the available data and would not have significantly improved model accuracy. The $V_{ce(sat)}$-I_c characteristics were therefore linearised in the form:

$$V_{ce(sat)} = V_{ce0} + r_{ce}\, I_c$$

Equation 27

V_{ce0} = IGBT collector-emitter voltage at zero current

r_{ce} = IGBT on-state resistance for the linearised characteristic

The instantaneous conduction loss in an IGBT can be approximated by:

$$P_{cond,IGBT}(t) = V_{ce0}\, I_c\,(t) + r_{ce}\, I_c^2\,(t)$$

Equation 28

Similarly, the instantaneous diode conduction loss is:

$$P_{cond,Diode}(t) = V_{f0}\, I_c\,(t) + r_d\, I_c^2\,(t)$$

Equation 29

V_{f0} = Diode forward voltage drop at zero current

r_{ce} = Diode on-state resistance for the linearised characteristic

As the sinusoidal load current is always conducted by a series combination of a diode and IGBT (with anti-parallel IGBT bi-directional switches), assuming an output current of RMS magnitude I_o, the mean conduction loss per output phase is [114]:

$$P_{cond,phase} = (V_{ce0} + V_{f0})I_o\,[(2\sqrt{2})/\pi] + (r_{ce} + r_d)I_o^2\,(t)$$

Equation 30

These equations were implemented in a Matlab program to allow comparison between three commutation sequences: Standard, Semi-symmetrical PWM and 'Opti-Soft'. This computer loss model is described in Appendix A14 [p277] along with the numerical results used to produce the graphs in the following sections.

7.9.4 Loss in Anti-Parallel IGBT Matrix Converter

The primary result obtained from the numerical matrix converter loss model showed that the 'Opti-Soft' strategy does not reduce total converter loss. Figure 157 compares 'Opti-Soft' switching with the standard sequential and semi-symmetrical PWM strategies as the output waveform frequency is increased.

Venturini	SWF	F_{out}	q	Load R (Ω)	Load L (H)
Advanced	2.4 kHz	1 - 20 Hz	0.866	2	0.02

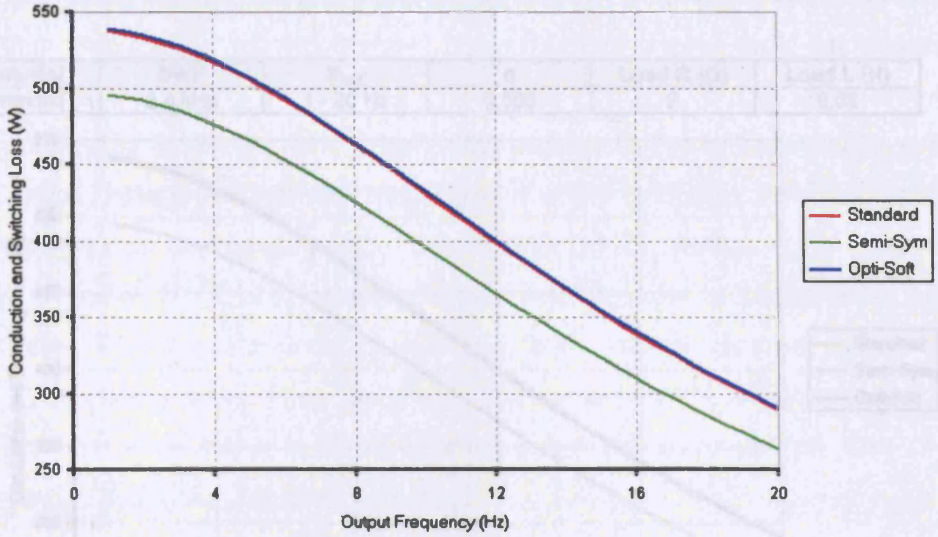

Figure 157 - Converter Loss Vs Output Frequency (e_{on} > e_{off})

Figure 158 compares the converter loss for the three sequencers across the converter voltage transfer ratio (q) range.

Venturini	SWF	F_{out}	q	Load R (Ω)	Load L (H)
Advanced	2.4 kHz	10 Hz	0 - 0.866	2	0.02

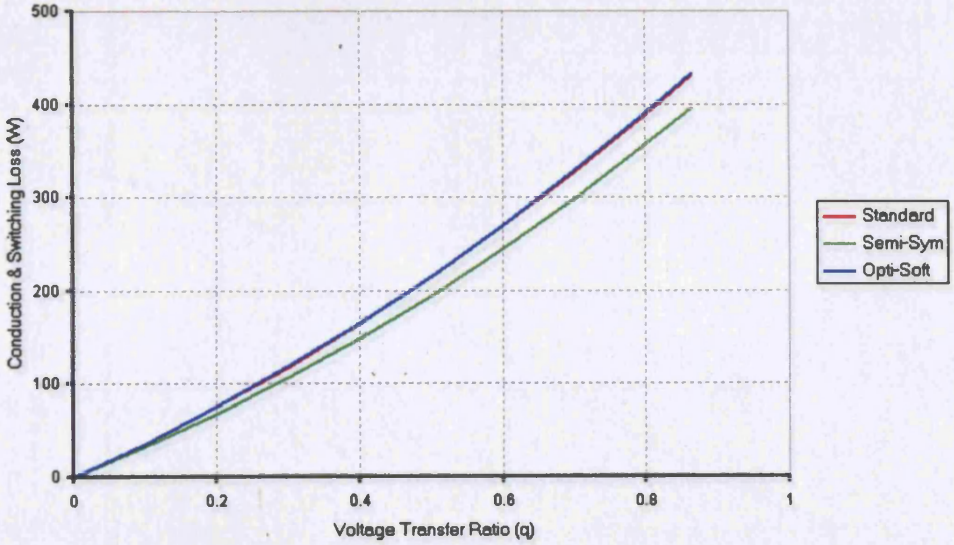

Figure 158 - Converter Loss Vs Voltage Transfer Ratio (e_{on} > e_{off})

Figure 157 & Figure 158 show that 'Opti-Soft' produces almost identical total loss to the standard Venturini strategy, as demonstrated for changing output frequency and

amplitude conditions. Although semi-symmetrical PWM is found to minimise loss, the loss model does not consider harmonic loss in the electrical system and therefore greater total loss would be expected in practice.

The IGBT parameters employed in the matrix converter loss model were such that the e_{on} loss was greater than the e_{off} loss. However some devices can possess the opposite characteristic. To ensure that 'Opti-Soft' did not increase loss in this situation, the loss model parameters for e_{on} and e_{off} were reversed and the above simulations repeated.

Venturini	SWF	F_{out}	q	Load R (Ω)	Load L (H)
Advanced	2.4 kHz	1 - 20 Hz	0.866	2	0.02

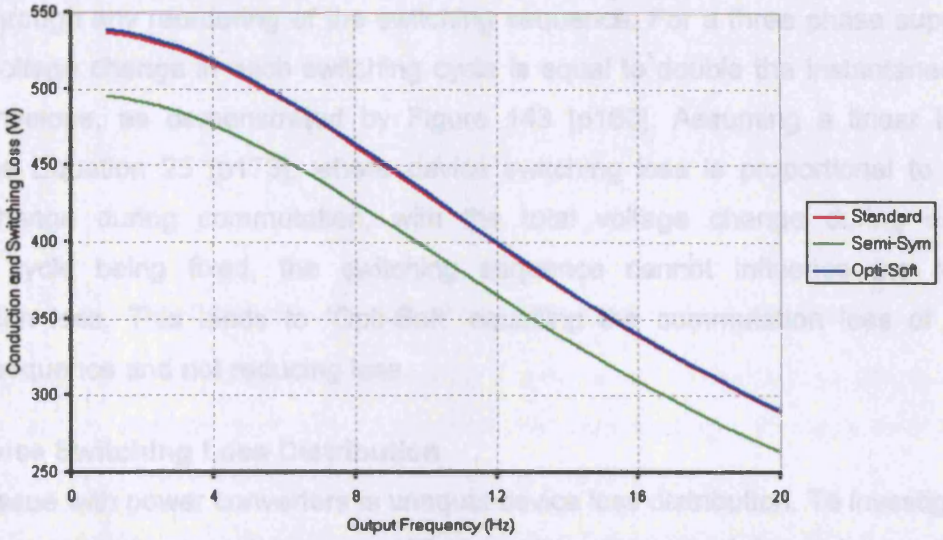

Figure 159 - Converter Loss Vs Output Frequency ($e_{off} > e_{on}$)

Venturini	SWF	F_{out}	q	Load R (Ω)	Load L (H)
Advanced	2.4 kHz	10 Hz	0 - 0.866	2	0.02

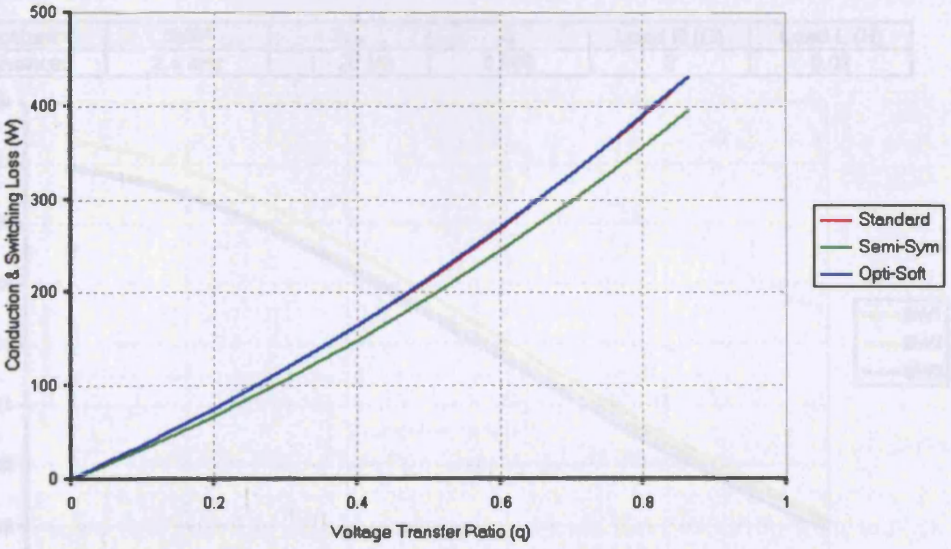

Figure 160 - Converter Loss Vs Voltage Transfer Ratio ($e_{off} > e_{on}$)

The comparative converter loss results obtained with $e_{off} > e_{on}$ are identical to those for when $e_{on} > e_{off}$ indicating that 'Opti-Soft' can be implemented without an efficiency penalty. Although the semi-symmetrical PWM strategy provides lower loss, this is at the cost of significant low frequency harmonics that make implementation of this strategy undesirable.

While Opti-Soft had been originally proposed as a possible approach to reduce switching loss, computer loss models have shown this not to be true. Assuming equally spaced supply phases and the requirement that all supply phases must be connected to each output phase during a switching cycle, it can be shown that loss cannot be reduced through any reordering of the switching sequence. For a three phase supply, the total voltage change in each switching cycle is equal to double the instantaneous voltage envelope, as demonstrated by Figure 143 [p160]. Assuming a linear loss model, see Equation 25 [p173], where device switching loss is proportional to the voltage change during commutation, with the total voltage change during each switching cycle being fixed, the switching sequence cannot influence the total commutation loss. This leads to 'Opti-Soft' equalling the commutation loss of the standard sequence and not reducing loss.

7.9.5 Device Switching Loss Distribution

A further issue with power converters is unequal device loss distribution. To investigate this, the numerical loss model was modified to allow capture of the switching loss occurring in each converter switch. A comparison between the standard, semi-symmetrical and 'Opti-Soft' strategies is shown in the following three figures.

Venturini	SWF	F_{out}	q	Load R (Ω)	Load L (H)
Advanced	2.4 kHz	1 - 20 Hz	0.866	2	0.02

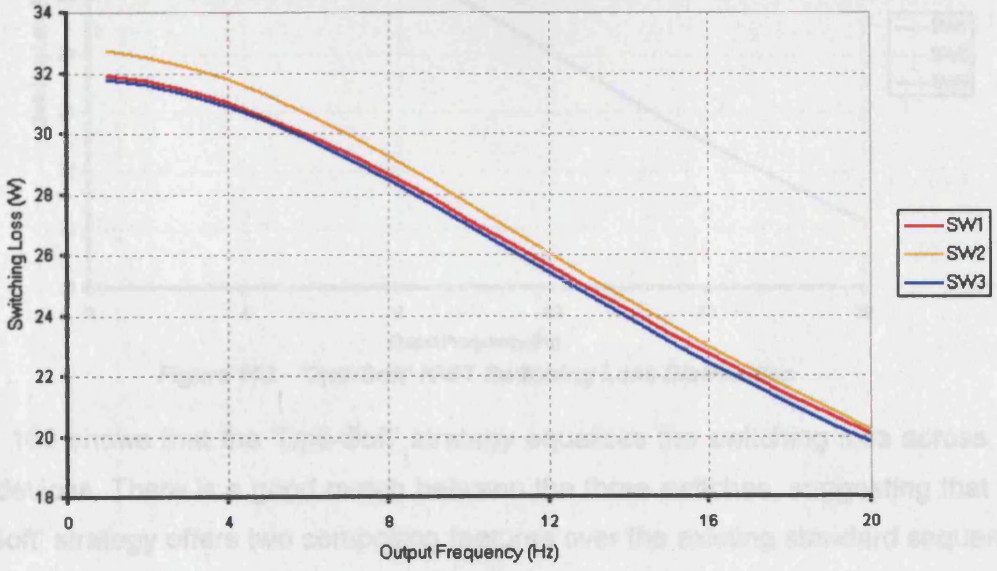

Figure 161 - Standard Strategy IGBT Switching Loss Distribution

Figure 161 shows that the standard sequential strategy produces increased loss in the middle converter switch, across the output frequency range. This is unwanted as it can have a detrimental effect on the device lifespan.

Venturini	SWF	F_{out}	q	Load R (Ω)	Load L (H)
Advanced	2.4 kHz	1 - 20 Hz	0.866	2	0.02

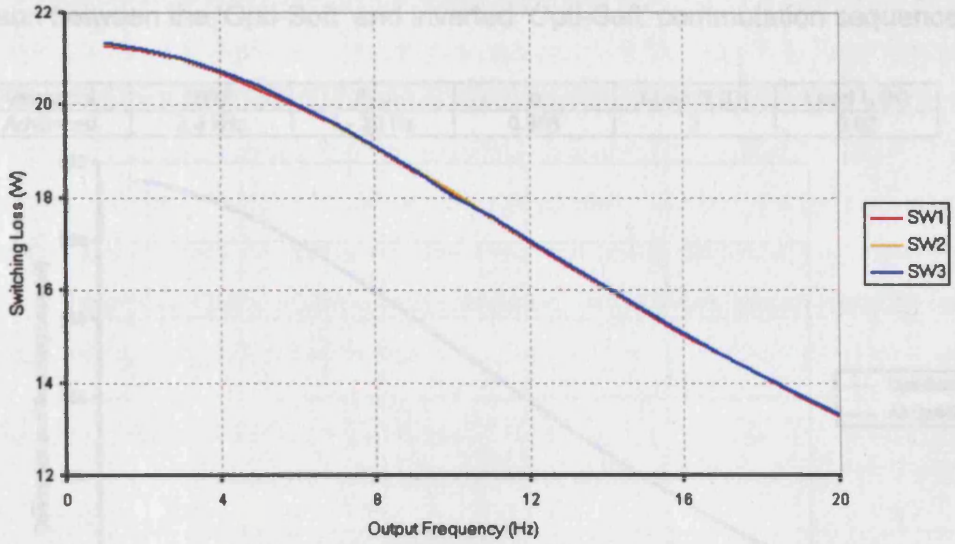

Figure 162 - Semi-symmetrical PWM Strategy IGBT Switching Loss Distribution

The semi-symmetrical PWM strategy produces a very balanced switch loss distribution across the output frequency range. Unlike the standard strategy, there is very little variation between the three switches and is therefore more desirable.

Venturini	SWF	F_{out}	q	Load R (Ω)	Load L (H)
Advanced	2.4 kHz	1 - 20 Hz	0.866	2	0.02

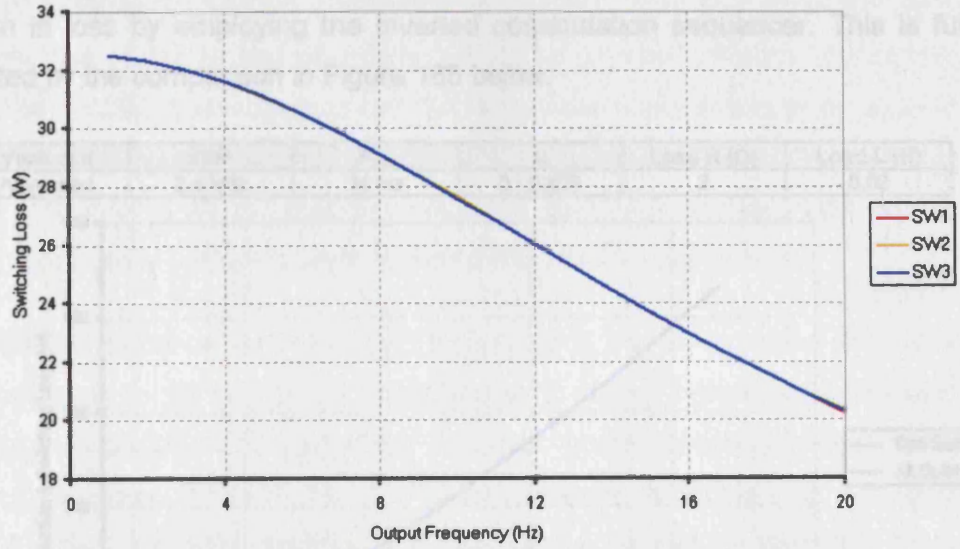

Figure 163 - 'Opti-Soft' IGBT Switching Loss Distribution

Figure 163 shows that the 'Opti-Soft' strategy equalises the switching loss across the IGBT devices. There is a good match between the three switches, suggesting that the 'Opti-Soft' strategy offers two compelling features over the existing standard sequential strategy: maximised natural commutation and balanced switching loss.

7.9.6 Inverted 'Opti-Soft' Converter Loss

The inverted version of the 'Opti-Soft' sequencer was also investigated using the developed computer loss model. Since the sequencing rule in Table 40 [p166] is simply the reverse of the standard Opti-Soft rule, the computer model required a trivial modification to the model described in Appendix 14 [p277]. This was used to conduct a comparison between the 'Opti-Soft' and inverted 'Opti-Soft' commutation sequencers.

Venturini	SWF	F_{out}	q	Load R (Ω)	Load L (H)
Advanced	2.4 kHz	1 - 20 Hz	0.866	2	0.02

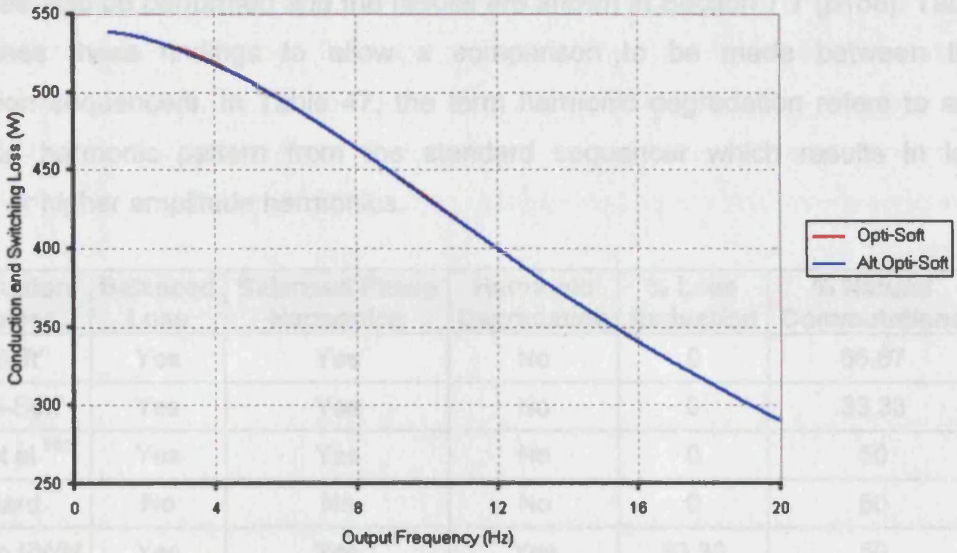

Figure 164 - Inverted 'Opti-Soft' Converter Loss Vs Output Frequency Comparison

The comparison between 'Opti-Soft' and the inverted 'Opti-Soft' converter loss across the output frequency range between 0-20 Hz, Figure 164, shows that there is little reduction in loss by employing the inverted commutation sequencer. This is further highlighted by the comparison in Figure 165 below.

Venturini	SWF	F_{out}	q	Load R (Ω)	Load L (H)
Advanced	2.4 kHz	10 Hz	0 - 0.866	2	0.02

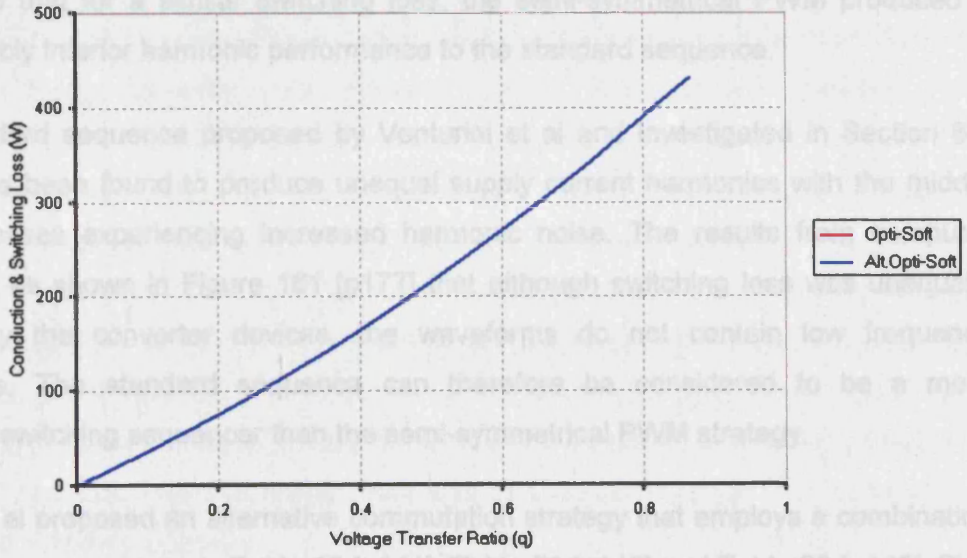

Figure 165 - Inverted 'Opti-Soft' Converter Loss Vs Voltage Transfer Ratio Comparison

Although the inverted 'Opti-Soft' sequencer produces a natural commutation between the extreme supply voltage phases, this has no discernable difference in converter loss, as highlighted by the results in Appendix 14 [p277] used to create the above graphical comparisons.

7.10 Comparison of Commutation Sequencers

The results produced by the loss model, as described in Section 7.9, have compared the performance of a number of different commutation switch sequencers. Harmonic analysis has also be performed and the results are shown in Section 7.7 [p168]. Table 47 combines these findings to allow a comparison to be made between the commutation sequencers. In Table 47, the term harmonic degradation refers to any changes in harmonic pattern from the standard sequencer which results in low frequency or higher amplitude harmonics.

Commutation Sequencer	Balanced Loss	Balanced Phase Harmonics	Harmonic Degradation	% Loss Reduction	% Natural Commutations
'Opti-Soft'	Yes	Yes	No	0	66.67
Inv 'Opti-Soft'	Yes	Yes	No	0	33.33
Bernet et al [109]	Yes	Yes	No	0	50
Standard	No	No	No	0	50
Semi-Sym PWM	Yes	Yes	Yes	33.33	50

Table 47 - Comparison of Commutation Sequencers

The semi-symmetrical PWM strategy has been investigated in Section 6.7 [p145] and shown to produce significant harmonics at $^1/_3$ and $^2/_3$ of the converter switching frequency that degrades the waveform quality as shown in Figure 153 [p169] and Figure 154 [p170]. Semi-symmetrical PWM reduces commutations by a third and balances switching loss across the converter devices. However it was shown in Chapter 6 that for a similar switching loss, the semi-symmetrical PWM produced a considerably inferior harmonic performance to the standard sequence.

The standard sequence proposed by Venturini et al and investigated in Section 6.4 [p141] has been found to produce unequal supply current harmonics with the middle supply phases experiencing increased harmonic noise. The results from computer modelling as shown in Figure 161 [p177] that although switching loss was unequally shared by the converter devices, the waveforms do not contain low frequency harmonics. The standard sequence can therefore be considered to be a more attractive switching sequencer than the semi-symmetrical PWM strategy.

Bernet et al proposed an alternative commutation strategy that employs a combination of the sequences shown in Table 18 [p141], Table 21 [p143] and Table 22 [p143]. This

strategy involves alternating between these sequences at an arbitrary period of 50ms [109]. A periodic change of the switching sequence has the effect of balancing the switching loss across the converter devices and balancing the harmonics in each phase. It does not increase the number of natural current commutations.

'Opti-Soft' and inverted 'Opti-Soft' switching strategies offer a more sophisticated approach. This involves periodically changing the commutation sequence in relation to the supply voltages and the load currents. These techniques have been shown to equalise switching loss across the devices as shown in Figure 163 [p178] and also balancing harmonic noise across the supply phases. The inverted 'Opti-Soft' version was developed to obtain natural current commutation when switching between the extreme supply voltages however it minimises the number of natural current commutations. The conventional 'Opti-Soft' maximises natural current commutations in the matrix converter so it may therefore be considered to be the more desirable switching strategy.

7.11 Conclusions

Analysis of the four-step staggered strategy, using a computer model, has shown that four types of current commutation between bi-directional switches exist. If the incoming switch is at a higher voltage with a negative load current or the incoming switch is at a lower voltage with a positive load current, a hard current commutation between switches will occur. Conversely, if the incoming voltage is at a higher voltage with a positive load current or the incoming voltage is at a lower voltage with a negative load current, then natural current commutation results, see Table 34 [p158]. Additionally, current begins to commutate between switches at the second step of the staggered strategy with natural commutation as opposed to the third step with forced commutation, making the switch commutation period shorter.

The distribution of converter commutation loss was subsequently examined using the developed matrix converter loss computer models. The standard operating mode switches between each input phase in fixed sequential order and this was shown to produce an equal number of natural and forced current commutations between bi-directional switches, see Table 35 [p159]. The semi-symmetrical PWM regime [67] reduces the total commutations in the matrix converter by one-third with a three-phase fed matrix converter but the effectiveness of this technique diminishes with increasing input phases, see Table 43 [p171]. Computer simulations in Appendix A14 [p277] also showed significantly increased harmonic noise in the converter waveforms, resulting in increased harmonic loss that would most likely necessitate a larger filter compared to that for the standard operation.

A novel strategy, 'Opti-Soft', has been proposed by the author as a possible solution to reducing switching loss and to maximise natural current commutation in the matrix converter. Developed in response to existing strategy limitations, the switching sequence has been reordered according to the instantaneous supply voltages and load current and only one forced current commutation between bi-directional switches occurs in each switching cycle irrespective of the number of input phases. The simulated converter harmonics are similar to those produced by the standard sequential strategy and eliminate the lower order harmonic noise that compromises the performance of the semi-symmetrical PWM technique, allowing the use of smaller standard filter designs. A numerical loss model has been developed and showed that the 'Opti-Soft' overcomes the loss imbalance evident with the standard sequential strategy but does not achieve a reduction in switching loss. With the standard sequence, the middle switch experienced greater commutation loss than the remaining switch, while the 'Opti-Soft' strategy produced equal commutation loss across the converter switches.

An alternative commutation sequencer, 'Inverted Opti-Soft', has also been proposed, producing a natural commutation between the extreme supply voltage phases. This was achieved with the penalty of minimising natural current commutations but with no increase in converter loss. Its benefits are therefore limited to balancing device switching loss.

The data presented in Table 47 [p180] compares the operating characters of the commutation strategies and shows that a balanced loss is achieved only when the switching sequence is not fixed. Practical results presented in Chapter 6 confirmed that a fixed switching sequence leads to the middle supply phase experiencing increased harmonic noise and computer loss models in this chapter showed that the middle supply phase experienced increased switching loss. These observations are further confirmed by Bernet et al [109]. Therefore, approaches that alternate the commutation sequence and equally distribute the middle commutation step across the supply phases will produce balanced switching loss and supply harmonics.

The proposed 'Opti-Soft' strategy requires measurement of both the supply voltage levels and the load current polarity in order to determine the correct switching strategy. Since the benefits of this strategy can only be exploited with a converter that employs anti-parallel bi-directional switches, little or no additional hardware is required, as these switches already possess the necessary voltage and current transducers and therefore can be implemented at no extra cost. The only additional hardware that may be required would rank the supply line voltages in order of magnitude to reduce the

control system burden with a network of low cost logic components. The outputs from these comparators govern the order in which the control system orders the converter switching sequence. However, an advanced matrix converter would be expected to implement a control strategy that tracks the supply voltage to compensate for distortion and would therefore be equipped with supply analogue-to-digital converters, as discussed in Section 2.9 [p63]. With this such accurate data, ordering the supply voltage magnitudes would be a trivial operation for a practical control system. The load current polarity is the second required variable and easily obtained from the anti-parallel bi-directional switches that track this value to control the staggered commutation strategy, see Section 2.4.3 [p46].

Commutation in a matrix converter with more than three supply phases provides a greater degree of freedom in the possible switching orders that may be employed and this requires further analysis. Should the 'Opti-Soft' switching strategy be applied in six-phase applications, the positive and negative stepping will result in an output current with increased ripple at the converter switching frequency. This may be undesirable in terms of waveform harmonic noise and converter performance, as shown in Figure 166(a). A possible approach may be to sequence the commutations in such a way as to maximise the ripple frequency in the output current waveform. This could be implemented by developing an algorithm that continually alternates between higher and lower supply voltages at each commutation, see Figure 166(b).

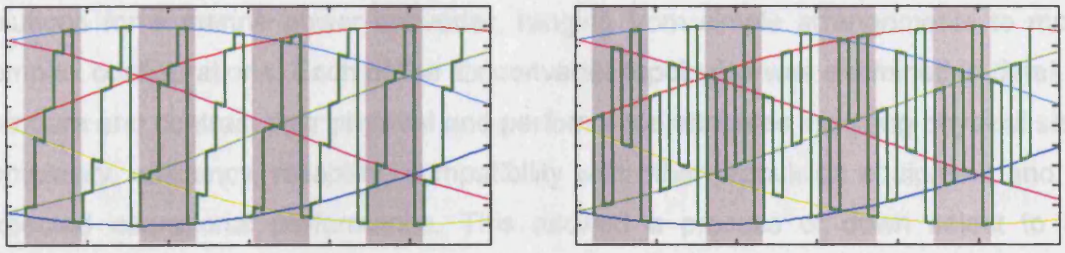

Figure 166 - Six Phase Supply Commutations for (a) Opti-Soft and (b) Maximum Ripple Approach

Although 'Opti-Soft' was not found to reduce commutation loss in a three-phase system, it does appear to have the potential to reduce commutation loss for systems with greater than three-phases, as suggested by comparing the voltage steps in Figure 166. This is an area for potential further work.

Section 7.10 [p180] compares the available commutation sequencers and concludes that by maximising natural current commutations and employing existing modern matrix hardware, the novel 'Opti-Soft' strategy ensures that switching loss is evenly distributed across the devices and that supply waveform harmonics are balanced and no additional harmonics are introduced.

8. Chapter Eight - Conceptual Design of a Marine Matrix Converter

8.1 Introduction

The present generation of electric drives used in marine electrical propulsion applications was discussed in Chapter One where it was concluded that each type of drive possessed merits and limitations but none possessed all the characteristics required of an 'ideal' power converter, see Table 2 [p33]. The merits of the matrix converter topology were discussed in Chapters One and Two and this type of converter appeared to have a greater proportion of the attributes required of the 'ideal' marine converter. However, the matrix converter needs to demonstrate clear performance advantages over the present generation of electrical drives and more recent developments such as the AFE-PWM converter in order to compete successfully in the electrical propulsion market.

In this chapter, the feasibility of a practical marine matrix converter for use in marine electrical propulsion systems is investigated. The work presented here includes the conceptual design of a 20MW practical marine converter and the analysis of its operational performance. An important consideration was the selection of the appropriate matrix converter topology for a conceptual marine drive and one was selected against a set of predetermined design objectives and operational requirements.

Six conceptual matrix converter topologies were initially identified as being potential solutions for a marine power converter, ranging from simple arrangements to more complex configurations. Each of the six converter topologies was examined in detail to compare and contrast their physical and performance attributes including physical size, complexity, efficiency, reliability, compatibility with other propulsion equipment and its expected operational performance. This allowed a process of down select to be undertaken until the most suitable marine matrix converter topology was identified.

The hardware of the selected drive is discussed in detail, including the circuit topology, the design of the bi-directional switch and the choice of power electronic device. Auxiliary circuits and protection circuits are also considered and design solutions proposed. A state of the art control system for the conceptual marine matrix converter is detailed, including the adoption and implementation of the 'Opti-Soft' commutation strategy, as described in Chapter Seven. The operational performance of the conceptual drive is investigated using a computer model against operational and performance requirements. The results obtained for the matrix converter are compared and contrasted against the alternative drive solutions. Finally, conclusions are made on the feasibility of a matrix converter as a practical marine drive solution.

8.2 Marine Converter General Requirements

Electric propulsion systems of large ships such as frigates and cruise ships generally employ large diameter propellers to reduce the pressure loading (pressure/unit area) on the propeller and to increase cavitation inception speeds. Propeller rotational speed needs to be reduced as the propeller diameter increases to avoid cavitation at the blade tips which can lead to unwanted noise and vibration. In direct drive electrical propulsion, the speed of the propulsion motor must match the propeller speed so avoiding the need for a gearbox. Electric propulsion motors used in this way have typical maximum rotational speeds of between 120-180rpm and usually have a minimum of six phase windings for reasons of redundancy.

The generators providing electrical power for propulsion are always three-phase types operating (under steady state) at constant voltage and constant frequency. Usually, generator capacity needs to match the needs of the ship's powering profile which includes propulsion and service loads. The size of individual generator sets is selected to match the operating profile (e.g. cruising at sea/in port) to maintain high efficiency.

The marine matrix converter needs to be compatible with existing marine motor and generator designs. The key design features for a marine converter can be summarised as:

- Operate from standard marine supply voltages, e.g. 3.3kV, 4.16kV, 6.6kV etc.
- Operate from a three-phase source either directly or via (phase shifting) transformers
- High power density to minimise space and weight
- Efficient operation to minimise cooling requirements
- Operate from full ahead to full astern
- Physically robust and tolerant of electrical power fluctuations
- Minimise harmonic content in supply and output waveforms
- Allow safe power regeneration during vessel deceleration

These design requirements impose considerable constraints on the design of a marine electric propulsion system and trade-offs must therefore be carefully assessed. High switching speeds of modern semiconductor switches has the potential to reduce harmonic noise generation in the input and output waveforms of converters but at the cost of increased commutation loss. A power dense converter saves space but it becomes more difficult to cool and may be more difficult to maintain.

8.3 Hullform Resistance

A ship moving through water experiences three main types of resistive force; frictional (or viscous), form, and wave resistance. Air resistance can generally be ignored in ships operating up to 30 knots (e.g. frigates and cruise liners). The sum of the main resisting forces, R, is approximately proportional to the square of the ship speed, V_s:

$$R = C_1 V_s^2$$

Equation 31

C_1 is not a fixed constant but will vary according to the ship speed, ship displacement, sea state, hull fouling and water depth.

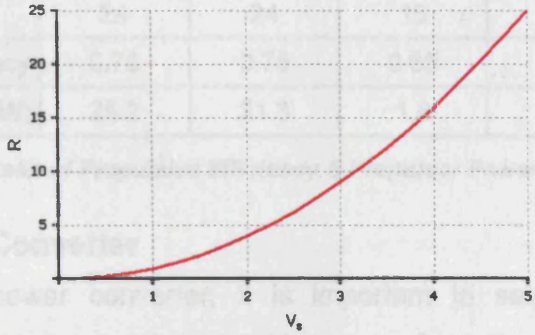

Figure 167 - Typical Ship Resistance-Speed Curve

Figure 167 shows a hypothetical ship resistance-speed curve. It should be noted that the relationship changes with the hullform design and a more efficient and clean hullform experiences less resistive force at the same speed than a poorly designed dirty hullform. The effective power, P_e, required to tow a vessel, with resistance R, at a speed V_s can be determined from:

$$P_e = R V_s$$

Equation 32

Combining Equation 31 with Equation 32 shows that the required propulsive power is proportional to the cube of the ship speed.

$$P_e = C_1 V_s^3$$

Equation 33

The effective power is the propulsive thrust required to maintain a steady ship speed. Shaft power, P_s, can be calculated from the effective power by considering the inefficiency of the propulsor (usually 70% at full speed) [2].

$$P_s = P_e / \eta_{prop}$$

Equation 34

Shaft power allows the required motor brake power, P_b, to be calculated by considering the transmission inefficiencies, η_{trm}.

$$P_b = P_s / \eta_{trm}$$

Equation 35

The total power must also include consideration for accelerating of the ship. Table 48 compares the propulsive efficiency and propulsor power for three container ships and a frigate travelling at 20 and 30 knots [2]. The propulsive efficiencies for all the vessels are broadly similar, but the required propulsive power is dependent upon the vessel's displacement and its speed. Most significant are the results for the frigate: a change in speed from 20 to 30 knots requires an almost four-fold increase in propulsive power.

Vessel	Container Ship 1	Container Ship 2	Container Ship 3	Frigate (20 Knots)	Frigate (30 Knots)
DWT (tons)	70000	45500	3750	3500	3500
Speed (knots)	24	24	15	20	30
Propulsive Efficiency	0.75	0.75	0.65	0.70	0.70
Propulsor Power (MW)	25.2	21.3	1.8	5.3	19.7

Table 48 - Comparison of Propulsive Efficiency & Propulsor Power for Various Ships [2]

8.4 Marine Matrix Converter

When designing a power converter, it is important to select the most suitable configuration to extract the maximum performance from the converter technology. Many designs were postulated but six matrix converter designs were identified as being appropriate. A detailed analysis then compared the attributes of these designs against the previously listed general requirements in Section 8.2 [p185] before selecting the most viable marine matrix converter topology.

8.4.1 Supply Utilisation

Supply utilisation is often cited as a drawback of the matrix converter. When an existing power converter is to be replaced by a matrix converter it is likely there would be a reduction in the output motor voltage. While it is possible to redesign existing propulsion motor designs to allow operation with reduced voltage, a marine matrix converter would be more attractive if it was compatible with existing motor and generator designs since risk and cost will be considerably reduced. This is true where harmonic tolerant designs are needed. Appropriate topology selection could therefore improve both the compatibility of the matrix converter in marine electrical propulsion systems and its prospects of practical implementation. Venturini et al derived a relationship describing the absolute maximum voltage transfer ratio of a matrix converter with an odd numbers of supply (n) and load (m) phases [52]:

$$\frac{V_o}{V_i} \leq \frac{\left(\cos\frac{\pi}{2n}\right)^2}{\cos\frac{\pi}{2m}}$$

Equation 36

Venturini's equation holds true for an odd number of input and odd number of output phases since induced harmonics cannot be added to even numbers of equally spaced supply and output phases to increase output voltage levels [52]. Odd phase systems have non-simultaneous points of waveform constraint allowing the addition of harmonics to increase the voltage transfer ratio, as described in Section 2.8.3 [p56]. However, in an even equally spaced system simultaneous points of waveform crossing occur, preventing the use of harmonic techniques, as demonstrated by Figure 168.

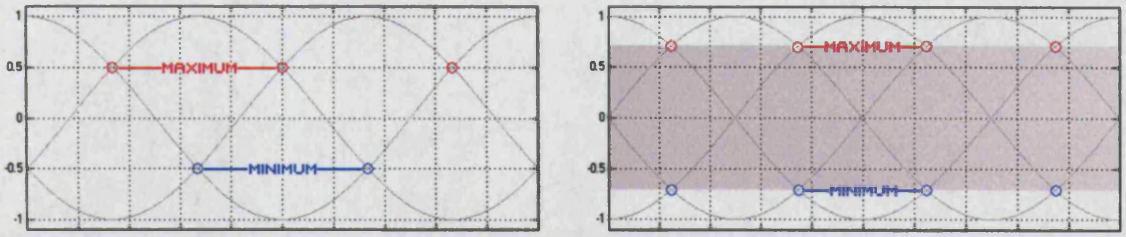

Figure 168 - Odd (3) and Even (4) Phase Constraints

The maximum supply utilisations for a range of matrix converter configurations are shown for comparison in Table 49. See also Appendix A2 [p249].

		Output Phases						
		3	4	5	6	7	8	9
Input Phases	3	86.60	75.00	78.86	75.00	76.93	75.00	76.16
	4	81.65	70.71	74.35	70.71	72.53	70.71	71.80
	5	***104.44***	90.45	95.11	90.45	92.78	90.45	91.85
	6	100	86.60	91.06	86.60	88.83	86.60	87.94
	7	***109.75***	95.05	99.94	95.05	97.49	95.05	96.51
	8	***106.68***	92.39	97.14	92.39	94.76	92.39	93.81
	9	***111.99***	96.98	***101.98***	96.98	99.48	96.98	98.48

Table 49 - Matrix Converter % Supply Utilisation for various Input & Output Configurations

Previous reports into matrix conversion have described increasing the number of input phases (using phase shifting transformers) to the matrix converter in order to improve supply utilisation [84,99], however, the opposite effect results when the number of output phases is increased. Table 49 highlights the trend for supply utilisation to tend towards that of the maximum available supply voltage envelope [99]. This suggests, therefore, that to optimise output voltage the matrix converter configuration should maximise the number of input phases and minimise the number of output phases. It should be noted that it is possible to achieve 100% or greater supply utilisation, which can be exploited to allow the use of existing motor designs, however this must be balanced against the increase in converter and system complexity.

8.4.2 Redundancy

Redundancy is a significant factor in the design of propulsion systems as it can increase both safety and the availability of the vessel. This is particularly important for the navy where combat damage should not impede operational readiness. Propulsion systems are therefore designed with several levels of redundancy so that operation is maintained despite one or more individual component failures. Usually 'n+1' switching devices are employed in each leg of the converter, where 'n' is the required number that depends upon voltage and current ratings. In case of a failure of a device, which will ultimately fail to open circuit, then the remaining devices will continue to operate within their ratings. In addition to failure of a device, consideration is also needed in case of a winding failure in the propulsion motor. Electrical propulsion motors usually have a minimum of six independent phase windings. Failure of up to three phase windings can occur before the motor becomes inoperable.

A full propulsion converter backup represents 100% redundancy, allowing full performance operation to be preserved should the in-service unit fail. However, such a 'cold spare' approach is entirely impractical on economic and volumetric grounds and a degradation of performance must therefore be accepted in the event of individual component failures.

8.4.3 Cooling

Cooling plays a significant role in the safe operation of a marine electric propulsion system. Although forced air-cooling is sometimes used, water-cooling is preferred in high power applications where converter power density is important. Direct seawater cooling is the most economical solution although this may not always be feasible due to corrosion issues so alternatively fresh or de-ionised water and a heat exchanger may be employed. The cooling requirement and hence cost can be managed by maximising converter efficiency by ensuring that the topology shares the power loss across a greater number of devices but without resulting in an excessively large converter. Existing cooling systems would be suited to matrix conversion.

8.4.4 Maintenance

The design of the marine matrix converter should preferably mean reduced and at a minimum no increased maintenance and repair issues. This suggests that device counts should be kept to manageable levels to ease the maintenance regimes and reduce time required to track down faults in the event of a malfunction. A desirable requirement is that in the event of a fault, the converter topology allows propulsion to be maintained by a section of the converter, albeit at a reduced level, whilst allowing repairs to be performed on the isolated section safely. This suggests that a modular approach of identical converters is a valid approach.

8.5 Topology Evaluation

8.5.1 Variant One

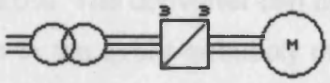

- 1 Converter
- 9 Bi-directional Switches
- 3 Input Phases
- 3 Output Phases
- 1 Transformer (optional)
- No Redundancy
  - (0) *1X: $3\Phi_{in}$ - $3\Phi_{out}$:86.6%*

Figure 169 - Marine Matrix Converter Variant One

A single converter is fed from a three-phase supply via an optional input transformer to drive a three-phase motor. The electrical power is shared between only nine switches with each requiring a very high power rating to satisfy the converter power requirements, complicating device selection. Although the electrical circuit is simple, a single semiconductor switch stack failure could immobilise the propulsion system.

8.5.2 Variant Two

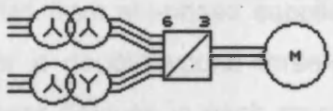

- 1 Converter
- 18 Bi-directional Switches
- 6 Input Phases
- 3 Output Phases
- 2 Transformers
- 1 Redundancy Level
  - (1) *1X: $6\Phi_{in}$ - $3\Phi_{out}$:100%*
  - (0) *1X: $3\Phi_{in}$ - $3\Phi_{out}$:86.6%*

Figure 170 - Marine Matrix Converter Variant Two

A single matrix converter, fed from a six-phase supply using a pair of transformers, drives a three-phase motor. The phase shifting transformers also allow the voltage utilisation of the converter to be increased to 100%. The electrical power, however, is shared between relatively few switches that require a high power rating to satisfy the converter electrical specification, making device selection difficult, although less so than Variant One. The increased switch count requires a more complex control system but in the event of a device failure or loss of supply to a single transformer, the converter can revert to a three-phase input, three-phase output mode, albeit with a reduced supply utilisation of 86.6%.

8.5.3 Variant Three

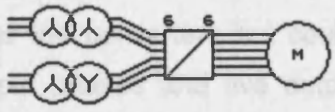

- 1 Converter
- 36 Bi-directional Switches
- 6 Input Phases
- 6 Output Phases
- 2 Transformers
- 2 Redundancy Levels
  - (2) *1X: $6\Phi_{in}$ - $6\Phi_{out}$:86.6%*
  - (1) *1X: $3\Phi_{in}$ - $6\Phi_{out}$:75%*
  - (0) *1X: $3\Phi_{in}$ - $3\Phi_{out}$:86.6%*

Figure 171 - Marine Matrix Converter Variant Three

A single symmetrical six-phase input converter, fed via a pair of transformers, drives a six-phase motor, allowing direct generator-motor connection (discussed later). However, the even number of equally spaced input and output phases results in a voltage transfer ratio of only 86.6%. The converter can operate with either a three input phases or three output phases in the event of supply or motor winding failures, albeit with reduced supply utilisation. Device selection is eased as the electrical power is shared across more bi-directional switches for a lower average conducted power.

8.5.4 Variant Four

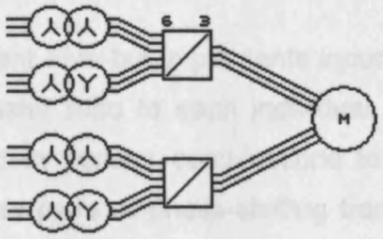

- 2 Converters
- 36 Bi-directional Switches
- 6 Input Phases
- 6 Output Phases
- 4 Transformers
- 2 Redundancy Levels
  - (2) *2X: $6\Phi_{in}$ - $3\Phi_{out}$:100%*
  - (1) *2X: $3\Phi_{in}$ - $3\Phi_{out}$:86.6%*
  - (0) *1X: $3\Phi_{in}$ - $3\Phi_{out}$:86.6%*

Figure 172 - Marine Matrix Converter Variant Four

Two identical converters are fed from six-phase supplies using independent pairs of phase-shifting transformers (or a double-wound three-phase generator) to increase supply utilisation to 100%. Fewer devices in each converter reduce the overall drive and control system complexity although each requires a moderate power rating. The two converters can be operated individually, in addition to operating with only three input phases, for reduced propulsion power in the event of a failed device or partial loss of supply.

8.5.5 Variant Five

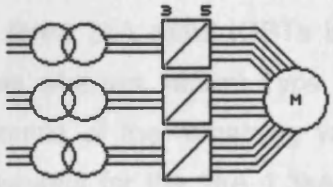

- 3 Converters
- 45 Bi-directional Switches
- 3 Input Phases
- 15 Output Phases
- 3 Transformers (optional)
- 2 Redundancy Levels
  - (2) *3X: $3\Phi_{in}$ - $5\Phi_{out}$:78.9%*
  - (1) *2X: $3\Phi_{in}$ - $5\Phi_{out}$:78.9%*
  - (0) *1X: $3\Phi_{in}$ - $5\Phi_{out}$:78.9%*

Figure 173 - Marine Matrix Converter Variant Six

Three independent converters are fed from three-phase supplies to drive a 15 phase motor, emulating the arrangement of the Royal Navy Type 45 Destroyer. Three transformers electrically isolate the converters but could be omitted to reduce drive size. Operating with three input phases and five output phases, limits the voltage transfer ratio to 78.9%. The high device count, although requiring a complex control system, reduces the power rating of each to allow the use of smaller switches to ease selection. This converter variant is used as the reference induction motor drive.

8.5.6 Variant Six

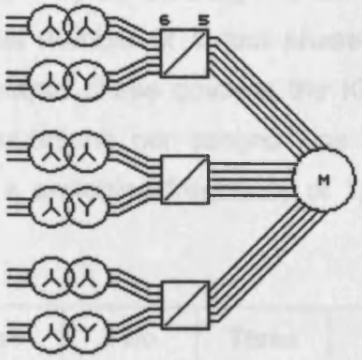

- 3 Converters
- 90 Bi-directional Switches
- 6 Input Phases
- 15 Output Phases
- 6 Transformers
- 3 Redundancy Levels
  - (3) *3X: $6\Phi_{in}$ - $5\Phi_{out}$:91.1%*
  - (2) *2X: $6\Phi_{in}$ - $5\Phi_{out}$:91.1%*
  - (1) *1X: $6\Phi_{in}$ - $5\Phi_{out}$:91.1%*
  - (0) *1X: $3\Phi_{in}$ - $5\Phi_{out}$:78.9%*

Figure 174 - Marine Matrix Converter Variant Six

Variant Six is similar to Variant Five but implements input phase shifting transformers to increase the voltage transfer ratio to each individual power converter. The three converters can be operated in various combinations to attain the highest level of redundancy while the multiple pairs of phase-shifting transformers allow operation to continue in the event of device failure. The high device count and numerous transformers results in a very large drive requiring a complex control system with increased associated costs such as cooling and assembly.

8.5.7 Evaluation and Topology Selection

Evaluation of the proposed converter topologies was performed with the intended role for a 20MW, 4.16kV propulsion system. This involved comparison of the relative merits of each drive topology enabling the selection of the most suitable configuration for detailed analysis. The device selection and comparison between the conduction loss was performed using a spreadsheet, detailed in Appendix A29 [p312], which included the specifications of the ABB range of Press Pack-IGBT (PP-IGBT) devices, although several other devices also met these requirements [115]. Converter variants Types One and Two were modelled with three 2kA rated IGBTs in parallel to satisfy their high conducted current requirements whereas variant Type Three required two paralleled devices. The higher device counts of the remaining variants allowed non-paralleled devices to be used. The datasheets for the 1kA 1.3kA and 2kA PP-IGBTs provided information on the device volume, weight and forward voltage drop against conducted current. For parity, each converter assumes five series connected devices to satisfy the supply voltage, however device redundancy was not considered as this affects each type equally. It is important for the reader of this thesis to appreciate that the following calculations are provided by way of example and they ignore the impact upon motor design such as number of motor phases and do not include any derating factors that industry might apply in a practical system.

Conduction loss was calculated by considering the conduction path of each phase, supply utilisation and the total number of output phases, assuming a 20MW motor load. The current for each output phase governs the IGBT voltage drop and hence conduction loss. Total commutations per second was calculated from the number converter phases assuming a switching frequency of 1kHz to simplify the following comparison.

Converter Variant	One	Two	Three	Four	Five	Six
Individual Converters (Input X Output)	1 X (3X3)	1 X (6X3)	1 X (6X6)	2 X (6X3)	3 X (3X5)	3 X (6X5)
Total Transformers	1	2	2	4	3	6
Converter Input Phases	3	6	6	6	3	6
Motor Output Phases	3	3	6	6	15	15
Devices in Parallel	3	3	2	1	1	1
Voltage Transfer Ratio (%)	86.6	100	86.6	100	78.9	91.1
Number of Switches & Gate Drive Circuits	9	18	36	36	45	90
Relative Drive Device Count Comparison	1.00	2.00	2.67	1.33	1.67	3.33
Relative Drive IGBT Weight Comparison	1.18	2.37	2.00	1.00	1.25	2.50
Generator-Motor Direct Connection?	Yes	No	Yes	Yes	No	No
Relative Conduction Loss Comparison	1.22	1.00	1.26	1.18	1.31	1.22
Relative Commutation Loss Comparison	1.00	2.00	2.67	1.33	1.67	3.33
Control System Complexity	Low	Low	Medium	Medium	High	High
Levels of Redundancy	0	1	2	2	2	3
Semiconductor Utilisation	1/6	1/12	1/12	1/12	1/6	1/12
(%) Natural Current Commutations	66.7	83.3	83.3	83.3	66.7	83.3

Table 50 - Comparison of Converter Topology

A comparison of the six potential converter configurations for a 20MW marine propulsion drive is shown in Table 50. When selecting the optimum drive configuration a balance between drive complexity, loss and redundancy and other important factors as given by Section 8.2, must be reached. The following is a summary of the findings:

- Variant One is a compact topology that uses the fewest semiconductor switches and is low in weight. Although a low number of devices reduces commutation loss, this is offset by the need to use devices with much higher voltage and current ratings which incur greater conduction loss. Failing this, devices in triple parallel are necessary to

satisfy the high current rating, as was the case in the above comparison, therefore increasing the device count. However, the main reason to eliminate this topology for a marine drive is that it has poor supply utilisation compared to the other variants and is a single module that reduces redundancy and precludes maintenance during operation.

- Variant Two is also a compact topology that uses 18 semiconductor switches with the potential for low weight. Unlike Variant one, there are sufficient devices to allow operation from six input phases for 100% supply utilisation but like variant one it requires triple paralleled devices to satisfy voltage and current ratings leading to a large and heavy converter. Although achieving the lowest conduction loss, the high commutation loss and the inadequate level of redundancy were the main reasons for variant two being rejected for further development as a marine drive.

- Variant Three is a more complex and therefore less compact topology that requires 36 semiconductor switches. Although this increases the device count over the previous converter topologies, it allows six output phase connections to the motor and this helps to reduce the current ratings of the devices that operate in double parallel. However, the resulting high device count leads to high commutation loss and high weight. The single converter module reduces converter redundancy and precludes operation during maintenance making this topology unsuitable as a practical marine drive.

- Variant Four overcomes the limitations of the previous converter topologies by implementing two identical converter modules for improved redundancy and allows maintenance on a failed module without impeding vessel propulsion. This is also achieved without exceeding the device count (36) of the previous topology and without paralleled devices that leads to the lowest projected weight. Operation from six input phases increases supply utilisation to 100% and contributes towards a low converter commutation and conduction loss. The resultant converter balances redundancy against complexity and has been selected for further study as a marine propulsion converter.

- Variant Five reflects the topology selected for the Type 45 propulsion system with three identical converters fed from 3 input phase to drive a fifteen phase motor [8]. While this reduces current requirements and allows the use of non-parallel devices, this topology achieves the lowest supply utilisation (78.9%). As a consequence conduction loss is the worst of the variants considered with average commutation loss. Ultimately, the added complexity fails to improve converter redundancy and makes Variant Five unsuitable as a practical marine drive.

- Variant Six improves on the supply utilisation and redundancy of Variant five by doubling the number of converter input phases. This results in a very large and complex converter with the highest commutation loss and average conduction loss. Overall, Variant Six is unnecessarily complex and has no compelling reason to be considered for further study.

Of the six topologies considered, Variant Four was considered to meet the requirements of Section 8.2 most closely and has therefore been selected for further analysis in the role of a marine matrix converter. It offers compatibility with existing propulsion motor designs and low semiconductor utilisation that has the potential for device de-rating and a smaller drive. It offers two levels of redundancy with potential for spatial redundancy, competitive levels of commutation and conduction loss and can be operated without paralleled devices.

8.6 Matrix Converter Hardware Design

A marine matrix converter must be designed with the objective of minimising conduction and commutation loss and maximising the operational envelope to ensure competitiveness with existing marine variable speed drives. Additional factors that require careful consideration include the cooling and protection of the semiconductor devices and how to most effectively distribute electrical power through the converter.

8.6.1 Bi-directional Switch Type & Topology

The marine matrix converter requires a bi-directional switch having a rating of at least 2kA with an acceptable switching frequency to produce high quality waveforms. Bi-directional switches are not commercially available at these powers or switching rates, however, the IGBT meets these requirements and can be developed into a suitable bi-directional switch using blocking diodes for protection, see Section 2.3.2 [p42]. The IGBT remains the only current realistic solution for a marine matrix converter [27], although some alternatives may appear in the future, see Section 2.3.4 [p44].

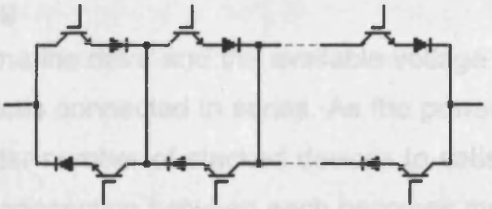

Figure 175 - Proposed Bi-directional Switch Topology

To control conduction between input and output phases, matrix converters generally employ configurations of unidirectional devices to realise bi-directional operation, as described in Section 2.3.2 [p42]. Bi-directional current conduction takes place through separate switches for each direction and allows staggered commutation that promotes

safe current transfer [55]. The proposed switch topology is shown in Figure 175, and retains the common link that aid commutation [55]. The sharing of voltage across series connected devices is discussed in Section 8.6.6 [p199].

8.6.2 Switch De-rating

Another issue when selecting an appropriate device is that in a three-phase fed matrix converter, each bi-directional switch conducts for, on average, one-third of the time. Semiconductor utilisation, mentioned in Section 2.7 [p51], falls as the number of converter input phases is increased and this is further compounded by the need for a unidirectional device for each conducted current direction, as shown in Table 51. Consequently each device conducts for one-sixth of the time in a three-phase fed matrix converter leading to a significant semiconductor under-utilisation and allowing lower power and, therefore, possibly cheaper semiconductor switches to replace larger more expensive devices.

Number of Input Phases	Mean Device Duty Cycle (%)
3	16.67
4	12.50
5	10.00
6	8.33

Table 51 - Mean Device Duty Cycle vs. Converter Input Phases

While cost savings may be possible, it must be ensured that the device safe operating area (SOA) is not exceeded. Savings in component volume may be possible, although manufacturers tend to retain the same packaging for each device in a family of switches [115] so this may not occur in practice. The reduced mean duty cycle also means that there is less power loss per switching device allowing proportionally smaller heat-sinks to be installed, helping to reduce cooling requirements and converter volume and weight.

8.6.3 Device Packaging

The requirements of a marine drive and the available voltage range of IGBT switches necessitate several devices connected in series. As the power output of the converter grows, there are a greater number of stacked devices to satisfy voltage requirements and the reliability of the connection between each becomes more important. A solution to this problem is to use PP-IGBT technology, similar to that used for high power thyristor modules and found in the Alstom ALSPA MV7000 marine power converter [39]. This has recently been installed in the Ifremer deep sea research vessel, Pourquoi Pas [116]. PP-IGBT technology is a double-sided compression housing that eliminates the wire bonds used in conventional flat pack IGBTs and results in a more reliable drive

system [39]. Of particular interest is the improved cooling of these devices, the significantly increased thermal cycling life and the ease with which devices can be stacked to achieve the desired operating voltage [39]. A further aspect is that the devices can be very securely clamped together to form each converter leg, improving the stack electrical and mechanical reliability in the event of shock loads. One drawback is that any water channels or jackets stacked between the PP-IGBT devices become electrically live (See Figure 180 [p200]) and so a de-ionised water-cooling system and associated heat exchanger must be employed. Overall, a marine matrix converter, or indeed any large drive, would benefit from this packaging technology [39].

8.6.4 Converter Interconnections

As the size of the converter increases, design and layout become more of an issue due to the numerous electrical connections. Connections and cables produce stray inductance that has been shown to cause over-voltage transients during commutation [117]. As the converter gets larger, this problem is exacerbated so precautions must be taken to minimise circuit inductance. A solution is to use laminated power planes with the supply and output connections made using layered metallic strips with an insulator between each conducting surface [63]. Connection to either plane is made by removing sufficient sections of the obstructing layers until the desired level is reached, see Figure 176.

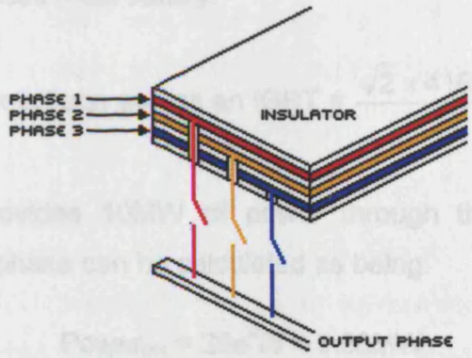

Figure 176 - Laminated Power Planes

It would be sensible to use this approach in the construction of a marine matrix converter as it has been found to reduce inductance and shown to allow snubberless operation [117]. Although it could also be possible to implement the same structure with the output phases, this may lead to assembly and maintenance problems.

8.6.5 IGBT Selection

Following the converter topology evaluation and selection of Section 8.4 and the above criteria for the semiconductor switch, the switch can now be chosen. The proposed converter design operates from a 21MW 4.16kV six-phase supply derived from a three-phase supply to drive a 20MW six-phase advanced induction motor through a

pair of modular six-phase input, three-phase output converters. The transformers, although undesirable in a Naval application due to their weight and volume [8], provide additional line inductance to limit currents during commutations. Using these criteria, the IGBT requirements have been calculated.

The worst case voltage across an IGBT in a matrix converter occurs when it is connected to an evenly distributed even number of supply phases as is the case with the proposed six-phase fed marine matrix converter drive. In this case the maximum peak voltage of one supply phase will occur simultaneously with the minimum voltage of another supply phase. Results from the computer simulations presented in Section 7.3 [p153] show that at the end of each commutation cycle, the (open) outgoing bi-directional switch is connected across two supply phases. The example in Section 7.3.3 [p156] demonstrates the four-step commutation strategy when switching the load from -50V to 50V. At the end of the commutation period, the voltage across the outgoing switch is 100V. In the circumstance where the load is commutated between the maximum peak voltage phase and the minimum voltage phase, the IGBT semiconductor devices in a matrix converter will experience a worst case collector-emitter voltage of twice the maximum peak supply voltage and this has therefore been used as the worst case rating in subsequent calculations. Therefore the voltage rating of the stacked IGBT devices must satisfy:

$$\text{Peak to peak voltage across an IGBT} = \frac{\sqrt{2} \times 4160 \times 2}{\sqrt{3}} \approx 6.8\text{kV}$$

Each converter half provides 10MW of power through three output phases and therefore the power per phase can be calculated as being:

$$\text{Power}_{PH} = 20e^6/6 = 3.33\text{MW}$$

Assuming an induction motor power factor of 0.85 and a line voltage of 4160V, the peak current per output phase can be calculated as:

$$V_{PH} = V_{LINE} / \sqrt{3}$$

$$\therefore$$

$$I_{PK} \text{ (per phase)} = \sqrt{2} \times \frac{\text{Power}_{PH}}{V_{PH} \times VTR \times PF} = \sqrt{2} \times \frac{3.33e^6}{\left(\frac{4160}{\sqrt{3}}\right) \times 1.0 \times 0.85} \approx 2.3\text{kA}$$

Device selection focused on obtaining PP-IGBT switches to maximise converter reliability and aid cooling. It became evident that few devices satisfy the requirements for a marine matrix converter. However in view of the device de-rating possible with the

matrix converter, discussed above in Section 8.6.2, the ABB StakPak family of devices provided the PP-IGBT devices (5SNR 20H2500) rated at 2.5kV and 2kA with a low conduction loss, short circuit failure mode that facilitates 'n+1' redundancy [39] and the requisite packaging technology. The IGBT switch also requires no snubber protection. Stacking becomes necessary to meet the requirements of the marine converter so four devices are connected in series to allow for 'n+1' operational redundancy. Should an individual IGBT fail, the remaining switches are capable of maintaining full converter performance. However, provision to replace the failed unit at the earliest opportunity should be made to return the converter to peak redundancy.

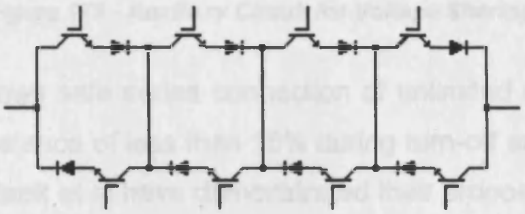

Figure 177 - Bi-directional Switch Construction

Each bi-directional switch contains two sets of four series connected PP-IGBT devices and therefore the two six-by-three phase matrix converters have a total of 288 devices. For comparison, the Type 45 PWM converter contains three identical converters. Each six-pulse rectifier has four thyristors in each leg, for a total of 72 thyristors [118]. Each 'H' bridge inverter contains 20 IGBT for a total of 300 IGBT [118]. This demonstrates despite the lack of a true high power bi-directional switch the matrix converter remains competitive with existing converter technology.

8.6.6 IGBT Stacking

The bi-directional switch configuration shown in Figure 177 requires four series connected IGBT devices to satisfy the converter voltage requirements but this is not easy to achieve in practice due to unequal switching rates, leakage currents, stray inductance and gate drive characteristics. Typical circuits used to overcome these problems are shown in Figure 178 but these are unsuited to high power applications and incur increased loss [119].

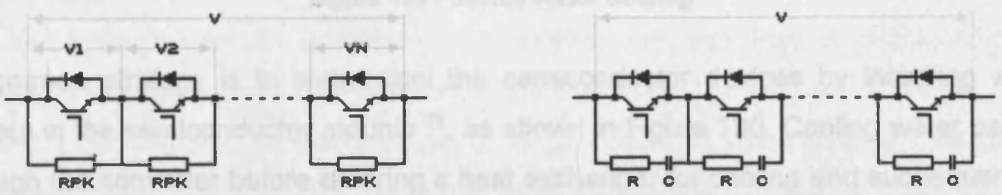

Figure 178 - Conventional Voltage Sharing Configurations (a) Steady State & (b) Transients

Various active gate control approaches have been proposed but these tend to require additional sensing components that increase system complexity. A recently proposed

solution to this problem is an auxiliary circuit composed of two small capacitors, three small resistors and a small diode [119]. This combination connected across each IGBT provides a similar effect to active gate control but with lower loss and cost.

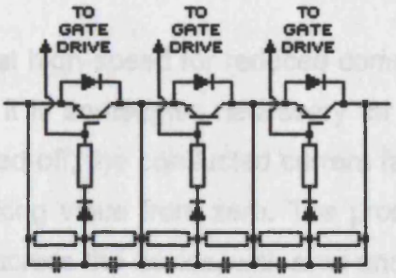

Figure 179 - Auxiliary Circuit for Voltage Sharing

The auxiliary circuit allows safe series connection of unlimited unmatched IGBTs and achieves a voltage imbalance of less than 15% during turn-off and less than 5% during turn-on transients [119]. Baek et al have demonstrated their proposed auxiliary circuit with sixteen series connected IGBTs and suggest that it is suitable for high-voltage, high-power applications [119].

8.6.7 IGBT Thermal Protection

Adequate cooling of the semiconductor devices is essential to ensure safe and reliable operation and in this application with stacked devices in series, each device must be maintained at the same temperature for matched performance. The selected IGBT device has a maximum operating temperature of 125°C but due to the positive temperature coefficient associated with the IGBT, an operating temperature of 80°C was selected as a balance between efficiency, cooling plant capacity and thermal reserve.

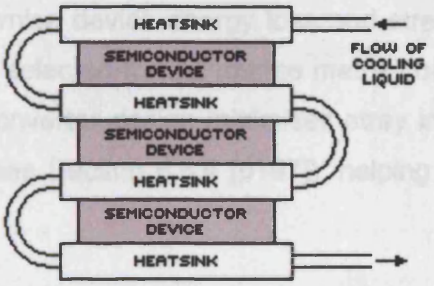

Figure 180 - Device Water Cooling

A common strategy is to water cool the semiconductor devices by installing water jackets in the semiconductor mounts [72], as shown in Figure 180. Cooling water passes through the converter before entering a heat exchanger for cooling and subsequent re-circulation. It is sometimes possible to eliminate the large heat exchanger and use seawater to directly cool the converter, as proposed for the advanced PWM converter designed for the future Royal Navy Type 45 Destroyer [8]. However, the live heat-sinks

of stacked PP-IGBTs precludes this approach as seawater is conductive so de-ionised water cooling is selected by necessity in conjunction with a suitably rate seawater heat exchanger.

8.6.8 IGBT Protection

The IGBT switch operates at high-speed for reduced commutation loss but in order to ensure low loss operation, it is sometimes necessary for additional devices to aid in this. When a device is turned off, the conducted current falls to almost zero whilst the voltage returns to the blocking value from zero. The product of these two quantities determines the power loss across the device, with area under the power curve showing the commutation energy loss.

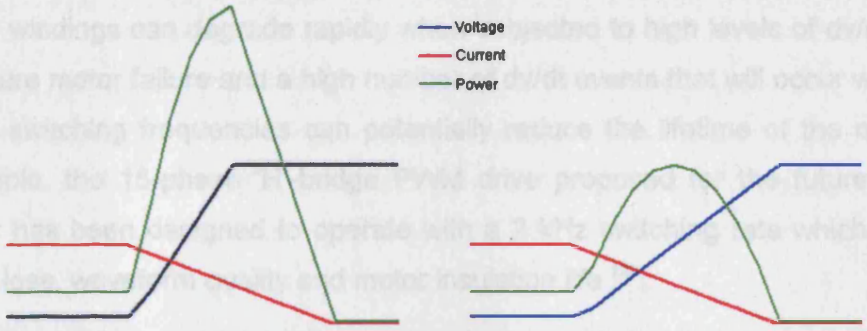

Figure 181 - Generic Switch Turn-off Commutation (a) Without & (b) With Snubber

Figure 181(a) shows the voltage and current measured across a hypothetical unsnubbered device when the current decays more slowly than the voltage recovers. The commutation is complete once both properties have reached steady-state conditions, so if the voltage recovers before the current, increased energy loss occurs. An RC snubber can protect against damagingly high rates of change of voltage (dv/dt) and can also help to minimise device energy loss and stress during commutation [73]. The ABB PP-IGBT device selected for the marine matrix converter allows snubberless operation assuming the converter design minimises stray inductance (with the use of laminated power planes, see Section 8.6.4 [p197]), helping the converter to be made smaller and lighter.

8.6.9 Supply Filter

The matrix converter is attractive from a harmonic perspective, eliminating the expensive low frequency filters required in the traditional LCI propulsion system drive. However, harmonics have been shown to be generated at side bands at multiples of the switching frequency [60] and, since the switching frequency may be changed (filter design permitting), power loss may be optimised against harmonic distortion and associated permitted noise and vibration of the motor. The requirements of the supply filter are:

- Low voltage drop
- Approaching unity displacement angle
- Stable displacement angle across power range
- High impedance to high frequency components
- Low impedance to low frequency components
- Satisfy all EMC regulations

The matrix converter switching frequency governs the filter size with higher switching frequencies giving improved waveform quality that requires smaller and potentially cheaper filters. On the other hand, higher switching frequencies will increase matrix converter loss because of the increased switching losses. Also important is the issue of dv/dt which must also be considered carefully with the motor design. Insulation of the motor windings can degrade rapidly when subjected to high levels of dv/dt leading to premature motor failure and a high number of dv/dt events that will occur with higher converter switching frequencies can potentially reduce the lifetime of the motor [35,36]. For example, the 15-phase 'H'-bridge PWM drive proposed for the future Type 45 Destroyer has been designed to operate with a 2 kHz switching rate which balances switching loss, waveform quality and motor insulation life [120].

During the practical supply filter design, it was evident that compromises are necessary to satisfy the above requirements. The laboratory converter employed a single-stage second-order harmonic filter containing three inductors and three capacitors, see Section 3.5 [p74]. Detailed calculations described in Section 3.5 [p74] showed that the inductor solely contributes towards the voltage drop across the filter and so steps to minimise inductor size were taken. However, the size of capacitance affects the filter input displacement angle so voltage drop and displacement angle must be balanced to achieve the required filter attenuation [99].

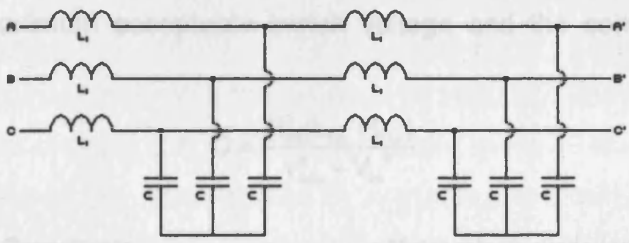

Figure 182 - Two-Stage LC Filter for Marine Matrix Converter

Figure 182 shows the proposed second-order two-stage supply filter configuration for the marine matrix converter. As the pass band of the low pass filtering is reduced to compensate for the increased switching harmonics resulting from the lower operating frequency, the component tolerance becomes more critical and this will make the filter an expensive item. The relative costs of the single-stage and two-stage designs are shown in Table 52 [121].

Filter Type	Cost Comparison
Single-Stage	1
Two-Stage	1.35

Table 52 - Relative Comparison of Filter Cost

Wheeler et al concluded that although the single-stage second-order filter is economical for higher frequency applications, the larger and more expensive two-stage filter may be necessary for the comparatively slower switched marine matrix to satisfy future EMC requirements [122].

8.6.10 Voltage Clamp

The matrix converter presents a number of unique protection issues compared with existing conventional rectifier/inverter drives [123]. In the event of an electrical fault, the matrix drive cannot be immediately turned-off as the energy stored in the motor inductance lead to potentially dangerous overvoltages that damage the semiconductor switches [55,76]. The solution is a diode-bridge, or voltage clamp, connected across the converter input and output lines with a capacitor to safely de-energise the load and prevent overvoltages [123].

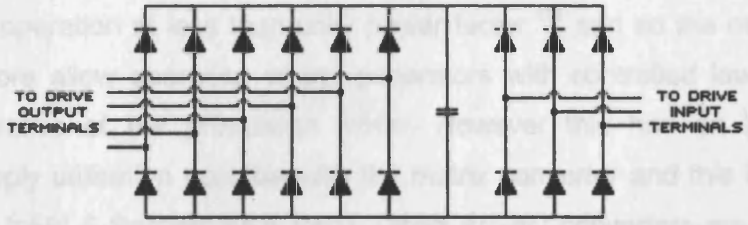

Figure 183 - Marine Matrix Converter Voltage Clamp

The clamp capacitor is subject to a very small RMS current and is sized according to the total energy stored in the motor inductances with knowledge of the motor leakage inductance, the maximum acceptable switch voltage and the converter current limit [74,76].

$$C = \frac{\frac{3}{2} I_{lim}^2 (L_{\delta,s} + L_{\delta,r})}{V_{max}^2 - V_{co}^2}$$

Equation 37

C = Clamp Circuit Capacitance
I_{lim} = Maximum converter current
$L_{\delta,s}$ = Motor stator leakage inductance
$L_{\delta,r}$ = Motor rotor leakage inductance
V_{max} = Maximum clamp voltage
V_{co} = Initial/charged clamp voltage

Prior to the converter fault, the capacitor is charged to the peak line input voltage (V_{co}). During a converter fault with all the devices turned off, the clamp diodes conduct and connect the clamp capacitor across the input terminals of the motor with a voltage polarity that de-energises the motor [124]. The clamp diodes conduct until the stator

current reaches zero and all the magnetic energy has been transferred from the motor to the capacitor [124]. Once de-energised, the inertia of the motor and load determines the time taken to come to a halt [76]. In comparing a matrix converter with an AFE-PWM drive, Bernet et al required a dc-link capacitor six times larger than the clamp capacitor [74]. While the clamp capacitor is subject to a very small RMS current, the value of the VSI dc-link capacitor is set mainly current stress and life-time considerations [74].

Section 2.5.4 [p50] discussed methods for rationalising the voltage clamp circuit to reduce size [76], however, these are unfeasible for the conceptual marine matrix converter because of the stacked devices in each bi-directional switch. The voltage clamp circuit, shown in Figure 183, requires 18 diodes and these must be rated to suit the operating voltage. Using the value calculated in Section 8.6.5 [p197], the ABB press packed diode 5SDF 10H6004 [125], 6kV 1.1kA may be used three in series for 'n+1' redundancy.

8.7 Converter Control System

Continuous development has resulted in two robust control strategies for the matrix converter, the Venturini and Space-Vector modulators. These provide high performance with the ability to control the displacement angle and reduce the need for expensive harmonic tolerant generators. However, some marine generators are often optimised for operation at less than unity power factor [126] and so the matrix converter should therefore allow operation of the generators with controlled levels of reactive power irrespective of the propulsion motor. However this has an impact on the maximum supply utilisation possible with the matrix converter and this is discussed in Section 2.8.4 [p59] & Section 2.8.6 [p61]. Direct AC-AC converters are susceptible to the output waveforms being contaminated with any supply distortion necessitating a control strategy that can compensate for such imperfection, something both of the two main control strategies allow.

8.7.1 Motor Control

There are many types of control strategies used for motor control including the scalar control method, field-oriented control and direct torque control. Potentially, any of these motor-control strategies can be employed by a matrix converter motor drive system. Propulsion motor drives use different types of control strategies for different purposes with different manufacturers often favouring their own drive control system e.g. ABB and Direct Torque Control [127].

8.7.2 Commutation Control

Earlier current commutation problems between switching in the matrix converter have now been largely overcome [60]. Staggered commutation strategies have been shown to maintain a continuous current path to the load and reliably prevent load open circuits

[110]. These have been demonstrated successfully in many motor drives [96,128] and are described in Section 2.4.3 [p46]. A four or three step staggered commutation strategy represents the best solution for the marine matrix converter.

8.7.3 Control System Hardware

The advance in high-speed and inexpensive processors means that the most complex control algorithm can now be executed using a low-cost processor, as demonstrated by the control system developed for the laboratory matrix converter. This should not change in a marine converter, as only a switching frequency in the range of 1-3kHz is considered viable. The experience gained during the design of the control software showed that to achieve the necessary resolution, the majority of calculations were longer than the 8-bit instruction set supported by the MCU. To overcome this, it is recommended that the practical control system employ:

- A 16-bit processor to provide high resolution and maximise performance
- An external high-speed DSP to manage commutation and reordering

Any commercial off-the-shelf controller, that satisfies the above requirements, will suffice to fully implement a matrix converter control strategy. The proposed configuration for the control system is shown below, with the additional transducers to employ 'Opti-Soft' commutation.

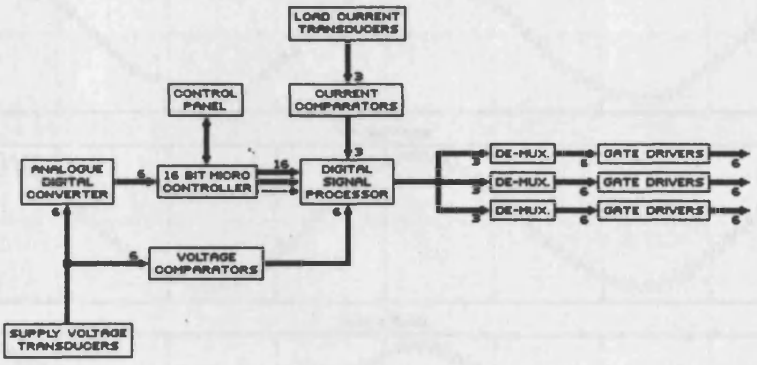

Figure 184 - Proposed Matrix Converter Control System

Measurement of the instantaneous supply voltages and load current allows the commutation sequence to be reordered to maximise soft switching. Similar to the laboratory control system, output de-multiplexers would provide reliable protection against potential supply short-circuits due to switching errors.

8.7.4 Switching Frequency vs. Drive Losses

As described in Section 6.2 [p135], loss in the matrix converter can be divided into predominantly conduction or commutation loss. Commutation loss occurs when a semiconductor switch is turned-on or turned-off. Although proposed as a solution to the safe current commutation problem, semi-soft staggered commutation was also found to

halve commutation loss by facilitating soft-switching [68]. The semi-symmetrical PWM switching strategy is another approach to reducing commutation loss, see Section 6.7 [p145]. While succeeding in reducing commutation loss, it generates significant sub-harmonics of the switching frequency in the supply filter making this technique practically and economically unfeasible for marine matrix converter propulsion.

An additional factor is that a six phase input matrix converter switches between six supply voltages and this has some effect on the quality of the output waveforms. The greater number of commutations serve to improve the output waveform resolution. As the voltage change during each commutation is proportionally smaller and commutation loss is not significantly increased. A computer model of the output current waveforms produced by three, four, five and six phase input matrix converters generating an output current at 25Hz with a converter switching frequency of 1kHz is shown in Figure 185.

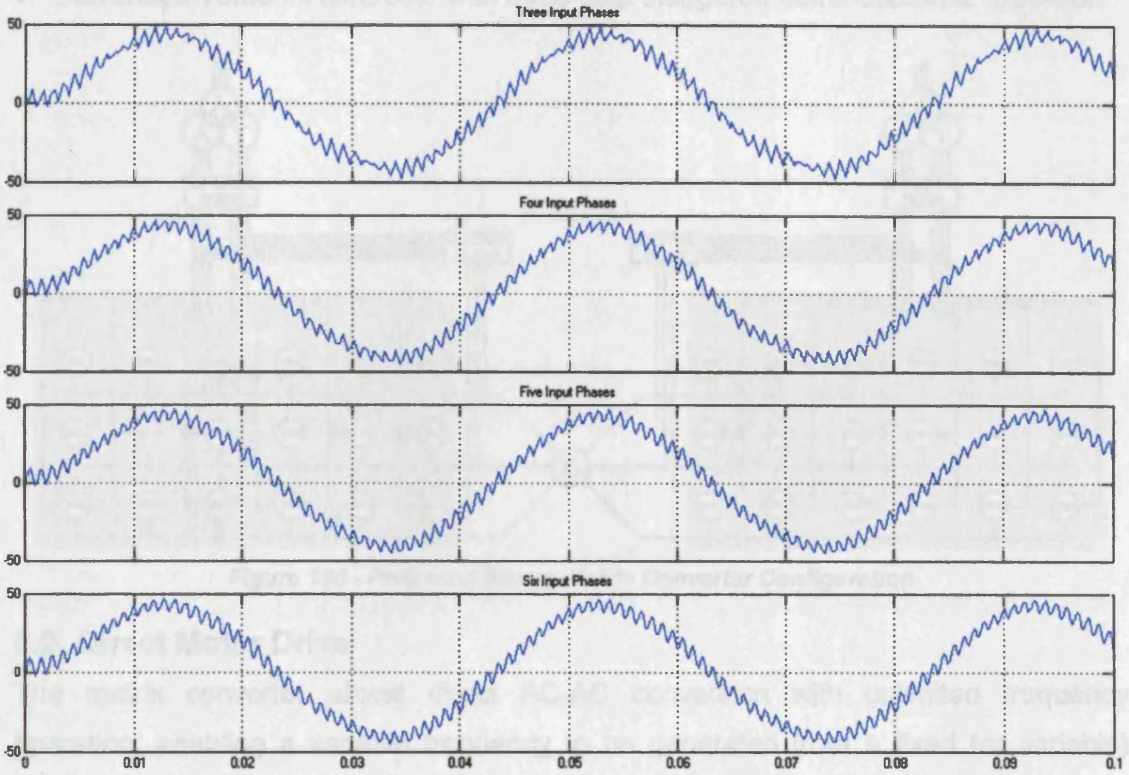

Figure 185 - Output Current Waveforms (25Hz) with Increasing Supply Phases

Increasing the number of input phases to the matrix converter helps to moderately reduce the level of ripple evident on the output waveform. This is most evident at the peaks and troughs; the most rippled area of the three-phase fed converter waveform. Increasing the number of supply phases improves the resolution of the six phase fed converter, exerting greater control over the output current and reducing the variation in ripple throughout the waveform.

8.8 Summary of Conceptual Matrix Converter Design

The specification of the proposed marine matrix converter is summarised as:

- Twin Yy0:(Yy0 + Yy6) phase shifting supply transformers
- Two converter modules with six input phases and three output phases each
- Laminated power planes reduce stray circuit inductances
- ABB press-pack 2.5kV 2kA IGBT stacked in groups of four for 'n+1' redundancy
- Water jackets stacked between IGBTs with de-ionised water and heat exchanger
- Auxiliary circuit used to safely share voltage across unmatched IGBT devices
- Two stage second order harmonic AC input filter
- 100% supply utilisation
- Voltage clamp - ABB press-pack 6kV 1.1kA diodes stacked in threes
- Six phase inductor motor
- 16-bit processor for high resolution with external DSP to manage commutation
- Advanced Venturini controller with three step staggered commutation & 'Opti-Soft'

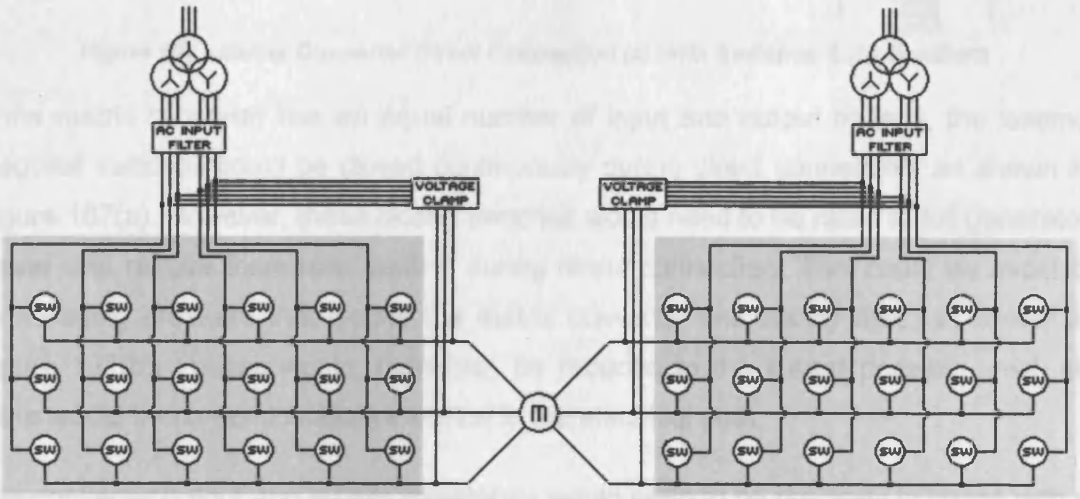

Figure 186 - Proposed Marine Matrix Converter Configuration

8.9 Direct Motor Drive

The matrix converter allows direct AC-AC conversion with unlimited frequency operation, enabling a variable frequency to be generated from a fixed (or variable) power supply. These characteristics are very different to those of existing converters and therefore an alternative operating mode for a marine converter was explored. Power converters conventionally operate at all vessel speeds and therefore incur maximum loss when the vessel is moving at full speed. If converter switching could be eliminated at maximum vessel speed, loss would be considerably reduced.

Consider a vessel with a propulsion motor designed so that the maximum vessel speed matches the generated supply frequency. This could be achieved by either

reducing the generator frequency to 15-20Hz, an unlikely proposition as ship service systems are designed for 50-60Hz operation, or increasing the motor pair poles so that maximum shaft speed occurs with a 50-60Hz waveform. At low to medium speeds, the converter operates in the conventional manner generating a variable frequency waveform to meet the desired vessel speed. When top speed is demanded, the vessel increases in speed until the converter output frequency matches that of the supply frequency. The motor can then be connected directly to the generator, bypassing the matrix converter and eliminating commutation loss.

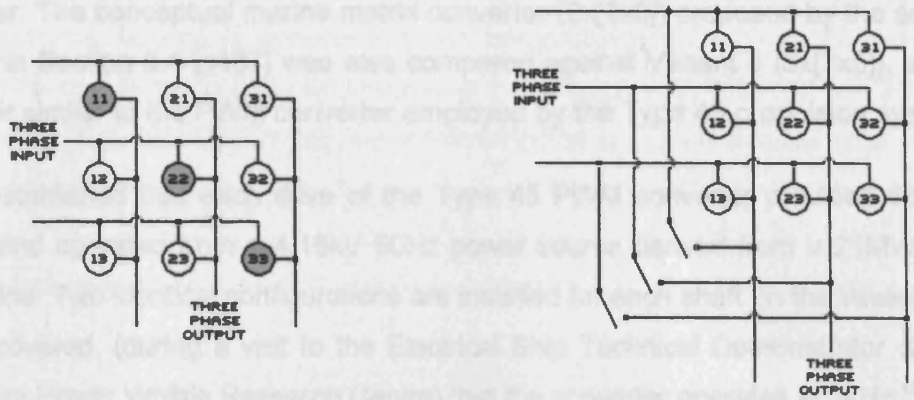

Figure 187 - Matrix Converter Direct Connection (a) With Switches & (b) Breakers

If the matrix converter has an equal number of input and output phases, the leading diagonal switches could be closed continuously during direct connection, as shown in Figure 187(a). However, these closed switches would need to be rated to full generator power and require increased cooling during direct connection. This could be avoided by installing breakers that isolate the matrix converter and supply filter, as shown in Figure 187(b). Losses would, therefore, be reduced to the lowest possible level, as there would be no semiconductor device in the electrical path.

The converter output and supply waveforms would need to be precisely in phase with a compatible (unity or similar) voltage transfer ratio to avoid a speed discontinuity upon initiating direct-connection. The converter input displacement angle may also need to be equalised with the propulsion motor power factor prior to direct-connection, to avoid an instantaneous change in generator loading conditions. However, while the matrix converter can achieve 100% supply utilisation, this constrains operation to a unity input displacement angle and so power factor matching is only possible by reducing the supply utilisation.. Nevertheless, this effect may be minimised if the generator set and propulsion motor are designed with similar displacement angles. The propulsion system must also be carefully matched to the vessel; in particular the speed resistance to ensure that the direct connected shaft speed is compatible with the ship maximum speed. Although the proposed mode of operation is unconventional, it is broadly similar to the system employed by the QE2 cruise liner, which has a LCI and a controllable

pitch propeller. As the QE2 operates a transatlantic route that entails full speed for considerable periods of its life, the potential through-life savings offsets the initial expense. However, where full speed is not used significantly, the additional cost of direct connection is not viable.

8.10 Marine Matrix Converter Performance Evaluation

A design study to investigate the viability of the matrix converter for marine propulsion was conducted to design a converter to examine the feasibility of replacing the 15-phase PWM drive proposed for installation in the future Royal Navy Type 45 Destroyer. The conceptual marine matrix converter (2x[6x3]) proposed by the selection process in Section 8.4 [p187] was also compared against Variant 5 (3x[3x5]), a matrix converter similar to the PWM converter employed by the Type 45 propulsion system.

It was established that each drive of the Type 45 PWM converter provided 15 output phases and operated from a 4.16kV 60Hz power source derived from a 21MW WR21 gas turbine. Two identical configurations are installed for each shaft on the vessel. It was also discovered, (during a visit to the Electrical Ship Technical Demonstrator centre at the Alstom Power Whittle Research Centre) that the converter operates at 2kHz [120].

8.10.1 Conduction Loss Model

Converter conduction loss was modelled using the same methodology described in Section 7.9.3 [p174]. The voltage drop across a semiconductor device varies with the conducted current so linearised approximations for both IGBT and diode were derived using the PP-IGBT 5SNR 20H2500 datasheet, as shown by Figure 188. These figures show that a linear relationship provides a sufficiently accurate representation of the device forward voltage characteristic and that a more complex approach would not have significantly improved the accuracy of the converter model.

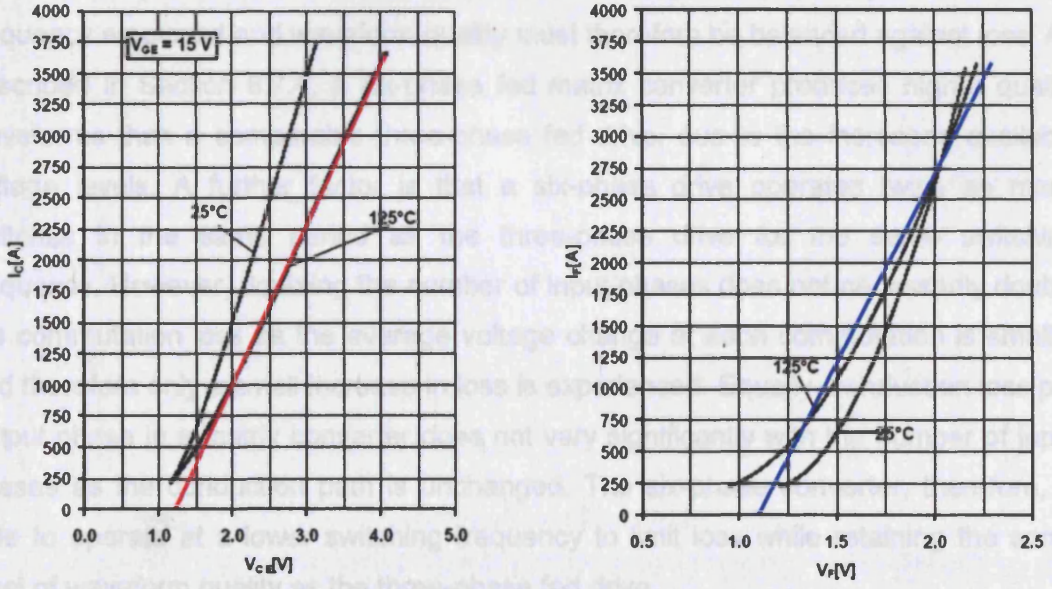

Figure 188 - 2.5kV 2kA PP-IGBT Forward Voltage Linearised Characteristics

Approximate values for both the V_{ce} & V_{d0} at zero conducted current and the gradient (r_{ce} & r_d) were measured for the matrix converter loss model, see Appendix A30 [p315].

IGBT		Diode	
V_{ce0}	r_{ce}	V_{f0}	r_d
1.25 V	0.000778 Ω	1.12 V	0.00033 Ω

Table 53 - 2.5kV 2kA PP-IGBT Conduction Loss Model Parameters at 125°C

8.10.2 Commutation Loss Model

As in Section 7.9.2 [p173], the IGBT switching loss is assumed to vary linearly with both the device voltage change during the commutation event and the conducted current. The commutation loss parameters for the selected PP-IGBT (5SNR 20H2500) were derived from the related datasheet following the approach employed by Apap et al [112]. This was performed for both turn-on and turn-off switching events assuming a worst case operating temperature of 125°C. Practical operation at a more normal temperature of 80°C would show lower loss than those predicted by the computer model.

IGBT		Diode
e_{on}	e_{off}	e_{rec}
1.44 µJ/V/A	1.86 µJ/V/A	0.27 µJ/V/A

Table 54 - 2.5kV 2kA PP-IGBT Commutation Loss Model Parameters at 125°C

Total converter commutation loss was then calculated assuming the use of anti-parallel bi-directional switches with four-step staggered commutation and 'Opti-Soft' to reduce switching stress. The numerical loss model is described in Appendix A30 [p315].

8.10.3 Model Results

The switching loss in a matrix converter is directly influenced by the switching frequency employed and waveform quality must therefore be balanced against loss. As described in Section 8.7.4, a six-phase fed matrix converter produces higher quality waveforms than a comparable three-phase fed drive, due to the increased available voltage levels. A further factor is that a six-phase drive operates twice as many switches in the same period as the three-phase drive for the same switching frequency. However, doubling the number of input phases does not necessarily double the commutation loss as the average voltage change at each commutation is smaller and therefore only a small increase in loss is experienced. Equally, conduction loss per output phase in a matrix converter does not vary significantly with the number of input phases as the conduction path is unchanged. The six-phase converter, therefore, is able to operate at a lower switching frequency to limit loss while retaining the same level of waveform quality as the three-phase fed drive.

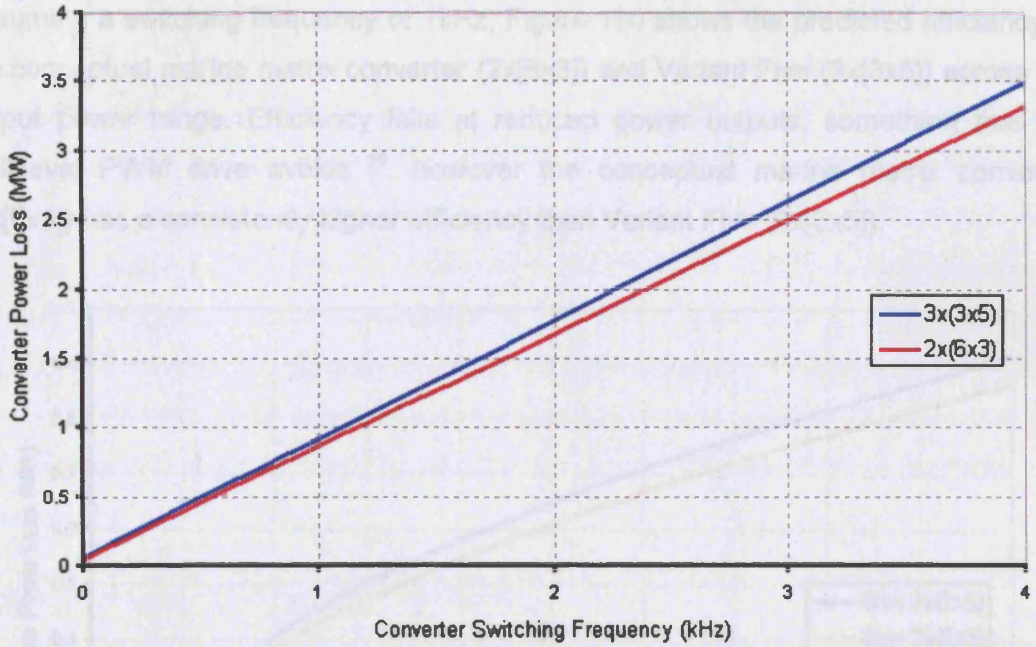

Figure 189 - Power Loss in Conceptual 20MW Marine Drive vs. Switching Frequency

Figure 189 shows that converter loss varies linearly with the switching frequency when generating 20MW at 18Hz. It is evident that converter loss increases quickly with the switching frequency, demonstrating the attraction of the multilevel PWM converter. The inferior supply utilisation of Variant 5 (3x[3x5], see Section 8.5.5 [p191]) is evident in the higher power loss when compared with the conceptual marine matrix converter (2x[6x3], see Section 8.5.4 [p191]). As power loss must be balanced against efficiency and the requirement for adequate cooling of the power converter, a converter switching frequency of 1kHz was selected for further evaluation.

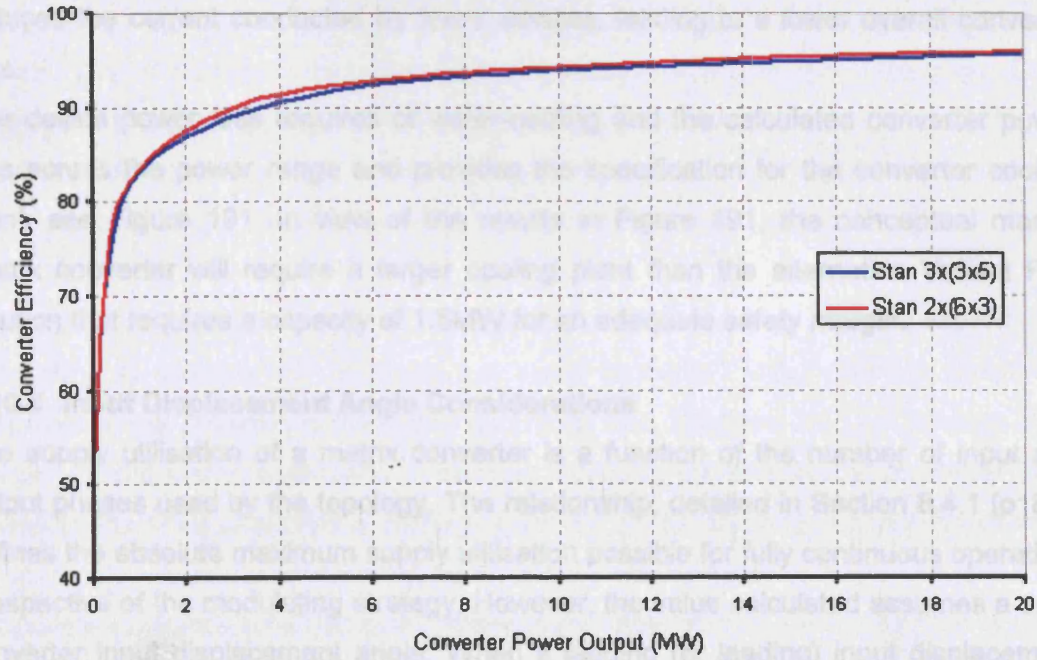

Figure 190 - Conceptual Marine Drive Efficiency vs. Output Power at 1kHz Operation

Assuming a switching frequency of 1kHz, Figure 190 shows the predicted efficiency of the conceptual marine matrix converter (2x[6x3]) and Variant Five (3x[3x5]) across the output power range. Efficiency falls at reduced power outputs, something that the multilevel PWM drive avoids [36], however the conceptual marine matrix converter (2x[6x3]) has a consistently higher efficiency than Variant Five (3x[3x5]).

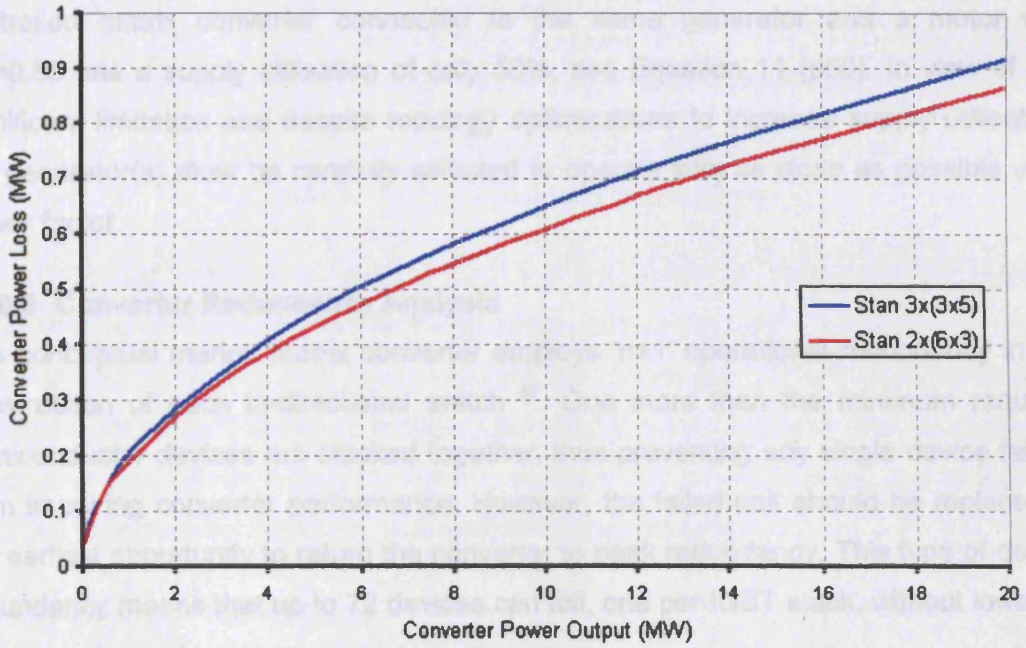

Figure 191 - Conceptual Marine Drive Cooling Requirements

Variant Five (3x[3x5]) experiences greater loss due to the reduced supply utilisation (78.8%) that therefore requires a higher current to the motor. By contrast, the conceptual marine matrix converter (2x[6x3]) operates with 100% supply utilisation that reduces the current conducted by fewer devices, leading to a lower overall converter loss.

The device power loss requires of water-cooling and the calculated converter power loss across the power range and provides the specification for the converter cooling plant, see Figure 191. In view of the results in Figure 191, the conceptual marine matrix converter will require a larger cooling plant than the alternative Variant Five solution that requires a capacity of 1.5MW for an adequate safety margin.

8.10.4 Input Displacement Angle Considerations

The supply utilisation of a matrix converter is a function of the number of input and output phases used by the topology. The relationship, detailed in Section 8.4.1 [p187], defines the absolute maximum supply utilisation possible for fully continuous operation, irrespective of the modulating strategy. However, the value calculated assumes a unity converter input displacement angle. When a lagging (or leading) input displacement angle is required (for compatibility with a particular generator), the maximum possible

supply utilisation must be reduced for correct operation, see Section 2.8.4 [p59] & Section 2.8.6 [p61]. This is a drawback in marine propulsion where electrical generators often operate at less than a unity power factor angle [126]. For example, a SVM operated three-phase input, three-phase output matrix converter supplied from a GE LM2500 gas turbine generator that operates best with PF=0.85 would have maximum supply utilisation of 73.6%, see Equation 13 [p63]. A similar Venturini controlled matrix converter connected to the same generator and a motor with PF=0.85 has a supply utilisation of only 50%, see Equation 11 [p59]. In view of this significant limitation and despite topology optimisations to increase supply utilisation, the generator(s) must be carefully selected to operate with as close as possible unity power factor.

8.10.5 Converter Redundancy Analysis

The conceptual marine matrix converter employs 'n+1' operational redundancy in the construction of each bi-directional switch [39]. One more than the minimum required semiconductor devices are stacked together, thus preventing any single device failure from impairing converter performance. However, the failed unit should be replaced at the earliest opportunity to return the converter to peak redundancy. This type of device redundancy means that up to 72 devices can fail, one per IGBT stack, without lowering the converter performance.

The two modules of the conceptual marine matrix converter operate from six input phases to produce power for three motor windings. In the event of a loss of an input phase(s), due to a transformer or generator failure, converter operation is maintained by reconfiguring the converter for three-phase input, three-phase output operation to bypass the inoperative input phase(s). This reduces the supply utilisation of the damaged converter module from 100% to 86.6% and lowers performance. It is then necessary to impose a similar restriction on the remaining fully operational module to ensure equally share electrical power across the generators and transformers.

The conceptual paired converter design also offers another form of redundancy: propulsion is possible with a single functional converter. This, however, halves the electrical power provided to the propulsion motor and degrades the performance of the system. In the extreme situation where one converter module has failed and an input phase to the other converter is damaged, limited operation using a three-phase input, three-phase output configuration is also possible. Performance is further degraded but propulsion is maintained. This is summarised by Table 55.

Converter Performance	Converter Configuration	Cause of Failure
100 %	2 x [6 x 3]	• None
100 %	2 x [6 x 3]	• Up to 1 IGBT in each stack
86.6 %	2 x [3 x 3]	• Two or more failed IGBTs in one stack, or • Partial supply failure
50 %	1 x [6 x 3]	• Converter module failure, or • Partial supply failure, or • Partial motor failure
43.3 %	1 x [3 x 3]	• Converter module failure + partial supply failure, or • Converter module failure + partial motor failure, or • Partial supply failure + partial motor failure

Table 55 - Proposed Converter Failure Modes

The above approaches to redundancy are examples of functional redundancy. However, the proposed converter configuration also lends itself to spatial redundancy where multiple units are installed in separate compartments [2]. In the event of flooding or fire, two redundant modules in separated compartments are less likely to suffer the same damage, thereby increasing system availability. It is therefore prudent to assume a similar approach for the conceptual marine matrix converter.

8.11 Converter Comparison

The PWM drive is the most modern of the existing drives and operates at a high frequency to produce good quality output waveforms but is reliant on a central capacitor, suffers high commutation loss and draws a poor quality input current waveform. Discussed in Chapter One, none of the existing drives can be considered the 'ideal' marine converter and the matrix converter represents a viable alternative. Table 56 compares the PWM drive, the AFE-PWM Drive and the matrix converter. The AFE-PWM overcomes many of the limitations associated with the PWM converter and represents a logical comparison.

Converter	PWM Drive	AFE PWM Drive	Matrix Converter
Circuit	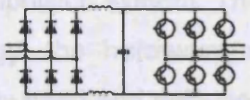	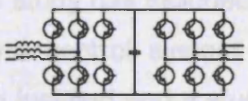	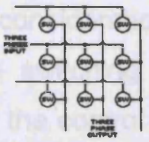
Device No.	Diode (6) GTO/IGBT/IGCT (6)	GTO/IGBT/IGCT (12)	IGBT/IGCT (18) + Diode (12) (Vclamp)
Conversion Process	AC - DC - AC	AC - DC - AC	AC - AC
DC-Link Required	Yes	Yes	No
Voltage/Current Source	Voltage	Voltage	Voltage
Slow Speed Controllability	Good	Good	Good
Maximum Output Voltage	$\sqrt{2}\,V_{line}$	$\sqrt{2}\,V_{line}$	$0.866V_{in}$
Output Frequency	Wide Range	Wide Range	Wide Range
Commutation	Rectifier - Natural Inverter - Forced	Rectifier - Forced Inverter - Forced	Standard = 50% Natural 'Opti-Soft' = 67% Natural
Regeneration	No	Yes	Yes
Dynamic Performance	Very Good	Very Good	Very Good
Converter Complexity	Low	Medium	Medium
Converter Losses	Medium	High	High
Converter Dimensions	Medium	Large	Large
Displacement Angle Control?	No	Yes	Yes
Input Current Waveform Quality	Poor	Very Good	Very Good
Output Wave-form Quality	Good	Good	Very Good
Simulated Output Voltage Waveforms	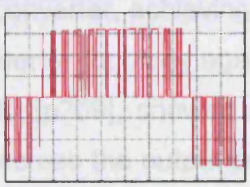	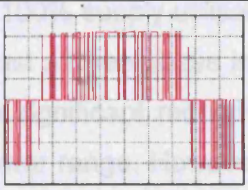	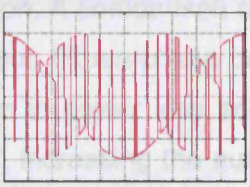

Table 56 - Comparison of Matrix Converter with Competing Marine Drives

8.12 Conclusions

This chapter describes the issues in designing a conceptual marine matrix converter for use in a marine propulsion system. The study has included the consideration of the design of the topology, the hardware and control system. The switching method selected has been discussed and selection justified and a study of the control aspects is presented. This has been a conceptual study and whilst the practical matrix converter remains unproven for high power applications, this study has shown the possible scenarios that may be suited to electrical propulsion.

An inferior supply utilisation has long been a drawback of the matrix converter and Section 8.4.1 [p187] explored the relationship between the number of input and output phases and the maximum possible output voltage. This study found that a six-phase input, three-phase output converter topology achieved 100% supply utilisation independently of the control strategy employed. However the supply utilisation of the matrix converter falls when drawing a non-unity input displacement angle, see Section 2.8.4 [p59] and Section 2.8.6 [p61]. As marine electrical generators may operate with a lagging power factor, e.g. 0.85 for the GE LM2500, gains made in supply utilisation by optimising the converter topology are negated. This is a problem that can be minimised by selecting a generator which can operate with a displacement angle as close to unity as possible.

The switching mechanism and motor control systems have been considered and proposed to enable safe current commutation between the IGBT switches. Staggered commutation is a well proven solution that maintains a continuous current path to the load with the benefit of halving the switching loss. This approach can also be used in conjunction with the 'Opti-Soft' switch sequencer and represents a viable solution for a marine matrix converter.

The operation of a conceptual drive design for the future Royal Navy Type 45 Destroyer has been demonstrated using appropriately developed and verified models. Results from these models have also confirmed that the most viable approach for a marine matrix converter is to maximise input phases and minimises output phases. A pair of six-phase input, three-phase converters was therefore selected as the topology for the marine matrix converter, achieving 100% supply utilisation. A comparison of the conceptual matrix converter topology against a three-phase input, fifteen-phase output converter, Section 8.10 [p209], showed a significant reduction in power loss and an increase in efficiency across the output power range. However, increasing the number of converter input phases has a weight and volume penalty and the disadvantage of reduced semiconductor utilisation. This final issue cannot be entirely overcome by

device de-rating as operation within the SOA must be ensured under all conditions irrespective of low switching duty cycles.

The array of semiconductor switches in the matrix converter is a disadvantage as each input phase must be connectable to any output phase. If it is preferable to have a greater number of input phases in order to maximise supply utilisation, it is equally desirable to minimise the total output phases and limit converter loss. The present state-of-the-art power converters are the fifteen-phase 'H'-bridge converter proposed for the Royal Navy Type 45 Destroyer and the US Navy's 17 level Multilevel converter. Unfortunately the high device count of a similarly multi output phase matrix converter makes it unlikely that the efficiency could match these proposed converters.

Although the conceptual matrix converter design would provide enhanced capability and flexibility, the limitation of current device technology curbs any potential savings in size and weight, in particular the requirement for a diode bridge to protect the converter. Should future bi-directional device designs scale suitably and integrated reverse blocking switches enter the market, the matrix converter may then become more competitive in terms of size and weight.

An alternative operational philosophy that takes advantage of the unlimited output waveform conversion possible with the matrix converter is proposed. If operated as a gearbox, a direct connected matrix converter would reach the maximum possible efficiency of any drive when operating at high power. Although an higher rated set of semiconductor switches could be used, an alternative solution of mechanical switches engaged only at top speed could directly connect the power supply to the motor and entirely bypass the matrix converter. This approach is only possible if the vessel speed-resistance characteristic and motor speed are accurately matched to avoid a speed discontinuity. Notwithstanding this, a direct connected drive could allow increased efficiency and potentially facilitate an increase in overall ship speed. However, the use of direct-drive is appears best suited to vessels that operate at maximum speed for long periods.

The benefits of a matrix converter are outweighed by the various problems encountered in the design of a practical marine converter. This study has shown that a marine matrix converter will be large due to the lack of a suitable bi-directional switch and the requirement for a voltage clamp for protection. Furthermore, although supply utilisation can be maximised through careful topology selection, this may be negated due to the drop in converter output voltage when a non unity input displacement angle is necessary. It is therefore considered that the matrix converter does not appear to satisfy the requirements of an 'ideal' drive and is less suited to marine propulsion.

9. Chapter Nine - Conclusions and Recommendations

9.1 Introduction

This thesis considers the design and feasibility of a matrix converter in a marine electric propulsion system. It describes the assembly of a 10kVA matrix converter and related ancillaries to establish the expected performance and operational limitations. The converter was constructed using high-speed IGBT devices that used a standalone control system employing a number of optimised Venturini algorithms. Studies included the effect of switching sequence on loss and harmonic generation. In addition, computer models were developed and verified by the laboratory converter.

The thesis reports on five key areas of investigation. The first presents an overview of existing marine electric propulsion technology including a review of potential future variable speed drives and explains why the matrix converter was selected for further investigation. The second contains a detailed literature survey of state-of-the-art matrix converter publications and a study on all aspects of this topology. The third describes the design and construction of the laboratory converter and a practical review of operating characteristics. The fourth involved a detailed examination of switch sequencing and the effect on loss and harmonic noise, culminating in the proposed novel 'Opti-Soft' strategy. This was undertaken using computer software in addition to the laboratory converter. The design of a conceptual marine matrix converter was investigated in the final area and its likely performance compared with competing drive technology.

9.2 Conclusions

A number of aims for this investigation were established in the introduction to this thesis, see Section 1.1 [p21]. These are now discussed and the success with which each aim was met is considered.

9.2.1 Technology Review

Chapter One presented a review of existing converter technology and established the requirements of future drives for the marine industry. Electric propulsion was found to possess advantages over conventional mechanical propulsion systems, including low noise, flexibility and reduced maintenance requirements for some types of ships. For these and the other reasons, electric propulsion has become popular in cruise liner and ice-breaking vessels as well as in applications where dynamic positioning is important. Looking into the future, electric propulsion appears set to become the standard solution for naval propulsion with several proposed designs eschewing traditional mechanical propulsion. Today, three main types of electric drives are found

in marine electric propulsion systems: the cycloconverter, the LCI and the PWM drive. Although these drive types possess individual strengths, a comparison showed that each has its limitations and falls short of representing the 'ideal' drive. The emergence of a new drive that overcomes these limitations would, therefore, be of particular interest to the marine propulsion market. A subsequent survey of novel and experimental variable speed drives highlighted a number of potential topologies, including the multilevel PWM, AFE-PWM drive and Matrix converter as well as resonant converters.

A detailed literature survey reinforced the belief that the matrix converter appeared to be a promising alternative to existing marine electric drives but also highlighted that no published work existed on this application. The matrix converter is a direct AC-AC converter with a symmetrical electrical path that allows bi-directional power flow and lacks significant capacitive or inductive components. A high switching speed allows production of high-quality sinusoidal input and output waveforms with more easily filtered high frequency harmonics. The matrix converter can also vary the input displacement angle irrespective of the demanded load power-factor, allowing the prime-mover generator sets to operate at maximum power levels. Overall, the matrix converter possesses a greater number of the necessary attributes and approximates the 'ideal' marine drive more closely.

9.2.2 Matrix Conversion

A comprehensive literature review was conducted in Chapter Two, to obtain an up-to-date perspective on the state of matrix converter development. This found that the matrix converter had undergone sustained development, solving many of the problems that had prevented its widespread adoption. Earlier concerns over safe current commutation have been overcome by the development of a family of strategies that staggered the switching of the two independent devices that form each bi-directional switch. Safe operation of these semiconductor devices was possible using robust and mature control algorithms that produced sinusoidal input and output waveforms with easily filterable harmonics. While reduced supply utilisation remained a problem for the matrix converter, this can be minimised by increasing the number of supply phases, as is common in marine propulsion systems using phase shifting transformers. However, it was found that peak supply utilisation can only be achieved with a unity input displacement angle.

The matrix converter topology was initially examined using computer models developed in the Matlab Simulink PSB environment. Accurate models of the various control algorithms were developed for evaluation and comparisons were made with conventional variable speed drives. More complex computer models were later

developed to investigate the effect of switch sequencing on waveform quality and the results were compared with the practical matrix converter to gain a level of validation for these models. The computer environment also served as a development aid for the control algorithm used by the embedded control system.

9.2.3 Converter Assembly

The design and assembly of the laboratory 10kVA matrix converter was documented in Chapters Three and Four. A fully standalone control system based around an inexpensive micro-controller was developed progressively with a simplified initial configuration, later expanded to match the developing hardware. Control software was written entirely in assembler language for maximum performance and reliability. The final developed version of the original Venturini strategy allowed full control of the input displacement angle and a wide range of switching frequencies to compare performance. The advanced Venturini strategy was subsequently implemented to maximise the performance of the laboratory converter. The completed laboratory matrix converter was used to drive an induction motor with a load so as to approximate the performance of a full size marine motor drive. This experimental configuration successfully allowed safe and comprehensive testing of the matrix converter with a highly flexible control system.

9.2.4 Converter Performance

The operation of the practical laboratory matrix converter was examined in Chapter Five. This confirmed that both output frequency and output voltage could be varied independently. The matrix converter draws and produces high-quality waveforms that are dependent on the switching frequency. The input displacement angle was easily controlled and, when set to unity, was shown to be unaffected by variations in the load characteristics. Spectral analysis of the generated waveforms indicated that harmonics were produced at multiples of the switching frequency. The laboratory matrix converter was compared with a computer model and good correlation was found between both output voltage and current waveforms.

9.2.5 Converter Harmonics

Chapter Six presented a detailed harmonic analysis of the practical converter input and output waveforms which revealed an imbalance across the three input phases. The middle input phase contained increased harmonic noise at the switching frequency, irrespective of the switching frequency employed. In order to eliminate a hardware cause, this effect was verified by implementing a number of alternative reordered commutation sequences, confirming the observations of Bernet et al. The experiments undertaken suggest that this phenomenon is a result of the first and final connected input phases having a fixed start and end point in each switching cycle. The middle

phase in the switching cycle has no fixed start or end point and so it experiences increased harmonic distortion. An attempt at solving this problem was explored using a staggered switching sequence, but while this managed to equalise the harmonic performance, practical results showed that the staggered switching sequence increased harmonic distortion in all phases.

The semi-symmetrical PWM strategy, applied to the advanced Venturini control algorithm, was also investigated in Chapter Six. This strategy reduces the total number of commutations by one-third by maintaining the final switch of each switching cycle into the following cycle, however practical testing found significantly increased converter noise. Spectral analysis showed that the semi-symmetrical PWM strategy altered the harmonic characteristic of the matrix converter and that the dominant harmonics were no longer produced only at sidebands of multiples of the switching frequency but also at one-third and two-thirds of this value. This resulted in the tuned filter being excited much closer to the resonant frequency, leading to noisy operation. Since switching frequency is a compromise between loss incurred and harmonic generation, it is unlikely that semi-symmetrical PWM with its associated sub-harmonics can be considered for marine applications.

9.2.6 Commutation Optimisation

In Chapter Seven, the staggered switching sequences, that facilitate safe current commutation between bi-directional switches, allow half of all resulting switching events to be naturally commutated and were investigated. A computer model of the requirements for natural current commutation showed that these could be increased above existing levels. The outcome of a rigorous study was a novel commutation strategy, 'Opti-Soft', that maximised natural current commutation between bi-directional switches in the matrix converter by reordering the sequence according to the instantaneous supply voltage and output current conditions. Natural commutations could be increased to 66.67% (from 50%) for a three input phase matrix converter, or up to 83.3% for six input phases. An accurate loss model showed 'Opti-Soft' also balanced the commutation loss across the converter switches, overcoming a limitation of the existing standard sequence. Modelling additionally showed that the loss produced by 'Opti-Soft' was independent of the IGBT turn-on and turn-off loss distribution and remained very similar to the conventional strategy. Harmonic analysis showed that 'Opti-Soft' closely matched the characteristics of the standard sequence and avoided the lower order harmonics observed with the semi-symmetrical PWM strategy. Very little, if any, additional hardware is required to implement the 'Opti-Soft' strategy as a typical matrix converter already contains the necessary monitoring equipment. The 'Opti-Soft' strategy is particularly suited to multiphase fed matrix

converters where a high number of input phases increase natural commutations without generating low order harmonics that require expensive supply filtering. With the increase in natural commutation possible using the optimised strategy, the matrix converter has the potential to be operated at the higher power levels required in marine applications. Increased natural current commutation could also reduce shock on the electrical system and reduce insulation degradation.

An 'inverted' version of the 'Opti-Soft' was also proposed in Chapter Seven as an alternative to the standard version. This reorders the switching sequence so that the commutation between the extreme supply voltages becomes natural, with the remaining smaller voltage steps being forced commutated. While this proposed strategy has the effect of minimising natural commutations in the matrix converter, simulated results suggest that commutation loss would not be increased.

9.2.7 Marine Matrix Conversion

With the experience acquired through theoretical and practical investigation, the feasibility of a practical 20MW marine matrix converter was examined in Chapter Eight. Supply utilisation was judged a significant issue for the matrix converter as custom motor designs would add substantial costs to a propulsion system, so an evaluation of potential converter designs and their supply utilisation was performed. A direct matrix converter replacement of the PWM converter proposed for the T45 frigate (three input phases with 15 motor phases) was considered and found to limit the performance of the matrix converter as supply utilisation was only 78.8%. The study concluded that supply utilisation can be maximised by increasing the number of input phases and minimising the number of output phases. A six-phase input, three-phase output configuration was shown to offer 100% supply utilisation and, therefore, a marine converter based upon two modules of this type was selected for further analysis.

While IGBT technology remains the best solution for satisfying the high power and low loss requirements, the demands for bi-directional conduction in the matrix converter leads to a high device count. Protection against overvoltage in the form of the diode bridge further increases the size of the matrix converter. Furthermore, the requirement for compatibility with existing marine hardware also extends to the marine electrical generator. Whereas an operating unity input displacement is ideal for low power applications, a marine generator may operate more efficiently with a lagging power factor, e.g. 0.85. As supply utilisation drops as the input power factor is reduced, this would impair compatibility with existing motor designs. This offsets gains made by optimising the matrix converter topology and reduces efficiency.

An alternative mode of operation for the matrix converter was also considered. In this case, the drive is operated as an electrical gearbox at all speeds up to full speed when the generator is connected directly to the propulsion motor. This could be achieved using appropriate circuit breakers. Assuming that generator and motor windings permit, the resultant marine drive would achieve maximum efficiency at full speed. However, this approach is only really viable for vessels that travel at high speeds for significant periods of time (e.g. LNG tanker) where gains in efficiency may outweigh the initial cost of installation.

9.2.8 Summary

The matrix converter has a wider range of attributes when compared with existing marine drives that tend to be used in specific applications, e.g. cycloconverter for high torque at low speed, LCI for compact size and PWM for higher frequency (low harmonic noise) operation. When the full specification is considered, the matrix converter appears to satisfy more of the requirements of a marine drive. The advantages include direct AC-AC power conversion, intrinsic power regeneration and input displacement angle control. However, the benefits of matrix conversion must be balanced against the complications of designing a practical marine converter. The higher commutation loss associated with the matrix converter make it less competitive than multilevel converters that operate at the fundamental waveform frequency. Chapter Eight has shown that a marine matrix converter will be large due to the requirement for over-voltage protection. Furthermore, while supply utilisation can be maximised through careful topology selection, this may be negated due to the drop in converter output voltage when a non-unity input displacement angle is necessary. While the matrix converter does not at present demonstrate a clear performance advantage over the present generation of marine converters, future advances in device technology may improve the viability of a marine matrix converter.

9.3 Recommendations for Further Work

The experimental investigations documented in this thesis have raised questions on the merits of using matrix converters in future marine electric propulsion schemes. The laboratory matrix converter developed during this investigation offered a robust platform for experimentation and produced useful data. The control system designed and assembled proved to be both reliable and flexible, particularly in the control of switch sequencing. However, the decision to employ a diode bridge switch prevented practical investigation of the proposed 'Opti-Soft' switching strategy and could only be tested using a computer model. In view of this, the author recommends that design improvements and further investigations be explored as follows:

- The bi-directional switch employed in the laboratory converter precluded practical testing of the proposed 'Opti-Soft' and 'Inverted Opti-Soft' sequencers, so an upgrade with anti-parallel bi-directional switches is necessary to enable staggered commutation. This would also allow the implementation of a closed loop Venturini strategy to improve immunity to supply distortion. Additionally, the control system hardware could be redesigned, moving commutation control to a dedicated DSP to reduce processor utilisation and improve switching resolution.

- Chapter Seven considered the performance of matrix converters with more than three supply phases, concluding that the greater degree of freedom could be exploited to either reduce load current ripple or reduce commutation loss. Alternative switching sequences, including the Opti-Soft', should be investigated using modified versions of the loss models developed and described in this thesis.

- The performance of the proposed 'Opti-Soft' and 'Inverted Opti-Soft' commutation sequencers should be investigated using the revised laboratory matrix converter. This will target the input and output harmonic performance, converter efficiency and measure the switch commutation loss distribution. Additional experiments should examine whether these novel sequencer equalises the input current waveform spectrum in practice, as predicted by computer modelling.

- Concerns remain over operation of the matrix converter at the higher power levels required by a marine drive. Although safe commutation in the matrix converter has been demonstrated and proven at low power [63], the effect of high-voltage and current allied to high-speed switching remains largely unknown. It is envisaged a future marine application could be investigated using a simplified configuration. Instead of designing and assembling an entire marine matrix converter and associated ancillaries, a single-phase output could be tested. This would take the form of the simplest configuration possible, a three-phase fed converter with a single-phase output. Marine drives, by virtue of the rating of present semiconductor switches, require stacked devices to achieve high power output and the same situation occurs with the matrix converter. It would be possible to investigate all aspects of performance using this simplified configuration with the benefit of reduced control complexities.

- The requirement for a diode bridge to protect the converter against over-voltages was found to add significantly to the size of a marine matrix converter. As a consequence, developing a more compact solution for protection during fault conditions may have significant benefits in optimising converter dimensions.

References

[1] B. Sharman, Electric Propulsion: A Review, Lloyd's Register of Shipping Technical Association, Paper No.2, 1987

[2] H. Woud & D. Stapersma, Design of Propulsion and Electric Power Generation Systems, IMarEST Publications, Marine Engineering, 2002

[3] C. Hodge & D. Mattick, The Electric Warship, Trans. IMarE, Vol. 108, Part 2, p109-125, 1995

[4] R. Bucknall & K. Ciaramella, Electrical Drives for Ships in the 21st Century, Ship Propulsion Systems International Conference, Lloyds List Event, Manchester, 4-5th Decemeber 2000

[5] A. Fitzgerald, C. Kingsley & S. Umans, Electric Machinery, 5th Edition, McGraw Hill, 1992

[6] M. Venturini, A New Sine Wave In, Sine Wave Out Conversion Technique Eliminates Reactive Elements, Proceedings Powercon 7, E3-1, 1980

[7] R. Bucknall, An Investigation into the Performance of a Marine Cycloconverter Propulsion System, PhD Thesis, Royal Naval Engineering College, Plymouth, 1995

[8] W. Uhbi & P. Norton, Advanced Induction Motor operation, results and acceptance, AES2003, p405-416, 2003

[9] D. Finney, Variable Frequency AC Motor Drive Systems, IEE Power engineering Series 8, Peter Peregrinus Ltd, London, 1988

[10] K. Oh, Fairchild Semiconductor Application Note 9016: IGBT Basics 1, February http://www.fairchildsemi.com/an/AN/AN-9016.pdf, 2001

[11] North Cheshire Marine, http://www.north-cheshire-marine.org.uk/smSep.htm

[12] The Canadian Coast Guard Website, 2004: http://www.ccg-gcc.gc.ca/vessels-navires/details_e.asp?id=B-2

[13] An Independent website with information on the QE2 engine and propulsion system, http://www.qe2.org.uk/engine.html

[14] Naval Technology, Website for Defence Industries-Navy: http://www.naval-technology.com/projects/t23/

[15] Kvaerner Masa-Yards Inc, Website, 1998: http://www.masa-yards.fi/news.asp?id=22&m=1

[16] Ship Technology, Website for the cruise and ship Industry:

http://www.ship-technology.com/projects/cable/

[17] United States Coast Guard website, 2004: http://www.uscg.mil/pacarea/healy/

[18] Ship Technology, Website for the cruise and ship Industry: http://www.ship-technology.com/projects/princess/

[19] Ship Technology, Website for the cruise and ship Industry: http://www.ship-technology.com/projects/elation/

[20] Sam Electronics Website, Aurora Propulsion System Description: http://www.sam-electronics.de/neue_dateien/pad/broschueren/1.059.pdf

[21] Ship Technology, Website for the cruise and ship Industry: http://www.ship-technology.com/projects/munin/

[22] J. Pike, Global Security, 2002: http://www.globalsecurity.org/military/world/europe/albion.htm

[23] Ship Technology, Website for the cruise and ship Industry: http://www.ship-technology.com/projects/queen_mary/

[24] The Type 45 Website, source of information on the Royal Navy Type 45 Destroyer, http://www.type45.com

[25] J. Boreman, The Electric Propulsion System of the QE2: Some Aspects of the Design and Development, IMAS 88: The Design and Development of Passenger Ships, Paper 19, p181-190, Vol. 100, IMarE, 1988

[26] G. Little, S. Young, J. Newell, The Electric Warship VIII - The Reality, IMarEST Proceedings

[27] C. Hodge & D. Mattick, The Electric Warship II, MOD, p127-144, 1996

[28] C. Lloyd, R. Simpson & G. Reid, The Type 45 Destroyer - Powering to Success, AES, Edinburgh, Proceedings, p198-210, 2003

[29] M. Hamer, Ships Lose Their Rudders, New Scientist Magazine, Vol. 181, No.2440, p24, 27 March 2004

[30] C. Howard & S. Large, Fast Trimaran Frigate, MSC ship design project, University College London - Naval Architecture and Marine Engineering Internal report, 1999

[31] R. Boulby, M. Gendle & W. Uhbi, Pentamaran AAW Frigate, University College London, MSc Ship Design Exercise Report, 2000

[32] C. Hodge & D. Mattick, The Electric Warship III, Trans. IMarE, Vol. 110, Part 2, p119-134, 1997

[33] D. Hall, Practical Marine Electrical Knowledge, 2nd Edition, Witherby, 1999

[34] M. Lehti, P. Hyvärinen & T. Tissari, The New Generation of Propulsion Drive Systems, AES, Edinburgh, Proceedings, p211-225, 2003

[35] D. Doull, Pulse Width Modulation - Single and Multi Level Techniques to Control Electrical Motors, University College London, MSc Marine Engineering Report, 1999

[36] L. Tolbert, F. Peng & T. Habetler, Multilevel Converters for Large Electric Drives, Industry Applications, IEEE Transactions, Volume: 35 Issue: 1, p36-44, 1999

[37] K. Corzine, Performance Characteristics of Cascaded Multilevel Converters: http://www.ece.purdue.edu/~esac/esac/cconverters.pdf

[38] K. Corzine, Operation and Design of Multilevel Inverters, Electric Ship Research and Development Consortium, 2003: http://nerc.aticorp.org/papers/inverters.pdf

[39] B. Gollentz, N. Gruau, A. Mirzaian & W. Lewis, A New Medium Voltage IGBT Press-Pack Converter: A Significant Step in Electrical Propulsion Drives, AES, Edinburgh, Proceedings, p226-238, 2003

[40] D. Holmes & T. Lipo, Pulse Width Modulation for Power Converters, IEE Power Engineering Series, Wiley, 2003

[41] J. Dixon, F. Ríos & A. Bretón, Multi-Stage Converters: A New Technology for Traction Drive Systems, 20th Electric Vehicle Symposium, November 15-19, 2003

[42] D. Holmes & T. Lipo, Implementation of a Controlled Rectifier using AC-AC Matrix Converter Theory, Power Electronics, IEEE Transactions, Vol.7, p240-250, 1992

[43] A. Green, J. Boys & G. Gates, Three-Phase Voltage Sourced Reversible Rectifier, IEE Proceedings, Electric Power Applications, Vol. 135 No. 6, p362-370, 1988

[44] A. Green & J. Boys, Hysteresis Current-forced Three-Phase Voltage-Sourced Reversible Rectifier, Electric Power Applications, IEE Proceedings, Vol. 136, No. 3, p113-120, 1989

[45] J. Boys & A. Green, Current-Forced Single-Phase Reversible Rectifier, Electric Power Applications, IEE Proceedings, Vol. 136, No. 5, p205-211, 1989

[46] T. Green, M. Taha, N. Rahim & B. Williams, Three-Phase Step-Down Reversible AC-DC Power Converter, IEEE Transactions, Power Electronics, Vol.12, No.2, 1997

[47] W. Koellner, J. Rodríguez & A. Weinstein, AC Drive System With Active Front End (AFE) for Mining Excavators, www.bucyrus.com/pdf/articles/ACTech_CIM2001.pdf, Siemens & Bucyrus Technical Paper, 2001

[48] G. Brown, B. Ebacher & W. Koellner, Increased Productivity with AC Drives for Mining Excavators and Haul Trucks, Industry Applications, Vol. 1, p28-37, 2000

[49] R. Limpaecher, Novel Converters for Electric Ship Propulsion System and Shipboard Power Distribution, IEEE, Power Modulation Symposium, p89-95, 2000

[50] J. Voyce, An Investigation into the Sequential Capacitive Discharge Converter, University College London MSc Project Thesis, 1999

[51] R. Dougal & M. Blackwelder, Detailed Modelling of the Limpaecher-design Resonant Power Converter, IEEE, Power Modulator Symposium, p48-51, 1998

[52] A. Alesina & M. Venturini, Analysis and Design of Optimum-Amplitude Nine-Switch Direct AC-AC Converters, IEEE Transactions on Power Electronics, Vol. 4 No. 1, p101-112, 1989

[53] J. Oyama, T. Higuchi, E. Yamada, T. Koga & T. Lipo, New Control Strategy for Matrix Converter, Proc. of PESC'89, p360-367, Vol. 1, 1989

[54] L. Huber & D. Borojevic, Space Vector Modulator for Forced Commutated Cycloconverters, IEEE Conf. Rec. of Industry Applications, p871-876, 1989

[55] P. Wheeler, J. Rodriguez, J. Clare, L. Empringham & A. Weinstein. Matrix Converters: A Technology Review, IEEE Transactions on Industrial Electronics, Vol.49 Issue 2, p276-288, 2002

[56] A, Lindemann, Characteristics and Applications of a Reverse Blocking IGBT, PCIM Europe Magazine, p12-16, Jan/Feb 2002

[57] F. Heinke & R. Sittig, The Monolithic Bi-directional Switch (MBS), ISPSD, France, p237-240, 2000

[58] M. Hornkamp, M. Loddenkötter, M. Münzer, O. Simon & M. Bruckmann, EconoMAC the First All-in-one IGBT Module for Matrix Converters, Eupec

[59] L. Gyugi & B. Pelly, Static Frequency Changers, Wiley, New York, 1976

[60] P, Wheeler, J, Clare, L, Empringham, M, Apap & M, Bland, Matrix Converters, Power engineering journal, p273-282, Dec 2002

[61] C. Klumpner, P. Nielsen, I. Boldea & F. Blaabjerg, New Steps towards a low-cost Power Electronic Building Block for Matrix Converters, IEEE IAS 2000, Vol. 3, p1964-1971, 2000

[62] P. Wheeler, J. Clare & L. Empringham, A MCT Based Matrix Converter with Minimized Commutation Times and Enhanced Waveform Quality, Power Electronics, Machines & Drives, IEE, 2002

[63] T. Podlesak, D. Katsis, P. Wheeler, J. Clare, L. Empringham, M. Bland, A 150-kVA Vector-Controlled Matrix Converter Induction Motor Drive, Industry Applications, IEEE, Vol. 41, Issue 3, p841-847, 2005

[64] F. Heinke & R. Sittig. The Monolithic Bi-directional Switch (MBS) in a Matrix Converter Application, Power Semiconductor Devices & ICs, ISPSD, p367-371, 2001

[65] T, Niel, Trends in Electronic Power Devices, Electronic Engineering, p50-52, 1994

[66] C. Jin, T. Sun, W. Anhua & D. Braun. Compact AC-AC Converter using 3-in-1 IBPMs and Adaptive Commutation, Power Electronic & Drive Systems, Vol. 1, p438-443, 1999

[67] P. W. Wheeler & D. A Grant, A Low Loss Matrix Converter for AC Variable-Speed Drives, EPE Brighton conference, 1993

[68] N, Burany, Safe Control of Four-Quadrant Switches, IEEE IAS, p1190-1194, 1989

[69] L. Empringham, P. Wheeler & J. Clare, Intelligent Commutation of Matrix Converter Bi-directional Switch Cells using Novel Gate Drive Techniques, PESC, Vol. 1, p707-713, 1998

[70] M, Ziegler & W, Hofmann, Implementation of a Two Steps Commutated Matrix Converter, Power Electronics Specialists Conference, Vol. 1, p175-180, 1999

[71] M, Bland, L, Empringham, J, Clare & P, Wheeler, A New Resonant Soft-Switched Topology for Direct AC-AC Converters, IEEE, p72-77, 2002

[72] F. Mazda, Power Electronic Handbooks, Components, Circuits and Applications, Butterworths, 1993

[73] C. Lander, Power Electronics, 3rd Edition, McGraw-Hill, ISBN 0-07-707714-8, 1993

[74] S. Bernet, S. Ponnaluri & R. Teichmann, Design and Loss Comparison of Matrix Converters and Voltage-Source Converters for Modern AC Drives, IEEE Transactions on Industrial Electronics, Vol. 49 Issue 2, p304-314, 2002

[75] D. Chamund, W. Findlay, K. Birkett, (Dynex Semiconductor), Bi-directional Switch Packaging for Higher Power Matrix Converters, IEE Matrix Converter Seminar, Birmingham, 2003

[76] P. Nielsen, F. Blaabjerg & J. Pedersen, Novel Solutions for Protection of Matrix Converter to Three-Phase Induction Machine, Industry Applications Conference, IAS '97, Vol. 2, p1447-1454, 1997

[77] P. Wheeler & D. Grant, Reducing the Semiconductor Losses in a Matrix Converter, IEEE colloquium on Variable Speed Drives and Motion Control, p14/1-14/5, 1992

[78] A. Alesina & M. Venturini, Solid-State Power Conversion: A Fourier Analysis Approach to Generalised transformer Synthesis, IEEE Transactions on Circuits and Systems, 1981

[79] K. Doherty, A Simulation Analysis Investigation into the Operation and Performance of a Matrix Converter, University College London, MSc Thesis, 1996

[80] P. Ziogas, S. Khan & M. Rashid, Some Improved Forced Commutated Cycloconverter Structures, IEEE Trans. On Industrial Applications, Vol. IA-21, No. 5, p1242-1253, 1985

[81] P. Ziogas, S. Khan & M. Rashid, Analysis and Design of Forced Commutated Cycloconverter Structures with Improved Transfer Characteristics, IEEE Trans. On Industrial Electronics, Vol. IE-33, No. 3, p271-280, 1986

[82] P. Wheeler, J. Clare & L. Empringham & M. Bland, Matrix Converters: The Technology and Potential for Exploitation, The Drives and Controls Power Electronics Conference, Section 5, 2001

[83] L. Zhang, C. Watthanasarn & W. Shepherd, Analysis and Comparison of Control Techniques for AC-AC Matrix Converters, IEE Proc. -Electr. Power Appl. Vol. 145, No.4, p284-294, 1998

[84] A, Helps, Design and Construction of a Matrix Converter, University College London MSc Project Thesis, 1998

[85] P. Nielsen, F. Blaabjerg & J. Pedersen, Space Vector Modulated Matrix Converter with Minimised Number of Switchings and a Feedforward Compensation of Input Voltage Unbalance, Proc. of PEDES '96, Vol. 2, p833-839, 1996

[86] L. Helle & S. Munk-Nielsen, A Novel Loss Reduced Modulation Strategy for Matrix Converters, Proceedings of PESC'01, Vol. 2, p1102-1107, 2001

[87] D. Casadei, G. Serra, A. Tani & P. Nielsen, Performance of SVM Controlled Matrix Converter with Input and Output Unbalanced Conditions, EPE, Vol. II, p628-633, 1995

[88] F. Blaabjerg, D. Casadei, M. Matteini & C. Klumpner, Comparison of Two Current Modulation Strategies for Matrix Converters under Unbalanced Input Voltage Conditions, Proceedings of ISIE'00, Vol. 2, p465-470, 2000

[89] P. Wheeler, J. Clare, L. Empringham, M. Apap, M. Bland, Matrix Converters, IEE Matrix Converter Seminar, Birmingham, 2003

[90] International Rectifier IRG4PC40UD IGBT Datasheet:
http://www.irf.com/product-info/datasheets/data/irg4pc40ud.pdf

[91] International Rectifier Fast Recovery Diode Datasheet: http://www.irf.com/product-info/datasheets/data/40hfl.pdf

[92] International Rectifier IRG4PC40ud IGBT datasheet: http://www.irf.com/product-info/datasheets/data/irg4pc40ud.pdf

[93] P. Wheeler & D. Grant, Optimised Input Filter Design and Low-loss Switching Techniques for a Practical Matrix Converter, IEE Proceeding Electric Power Applications. Vol. 144, No. 1, p53-60, 1997

[94] Agilent Technolgies HCPL-3120 2.0 Amp IGBT Gate Drive Optocoupler Datasheet: http://literature.agilent.com/litweb/pdf/5988-8710EN.pdf

[95] L. Huber, D. Borojevic, X. Zhuang & F. Lee, Design and Implementation of a Three-Phase to Three Phase Matrix Converter with Input Power Factor Correction, IEEE Proc. Of Applied Power Electronics Conference, p860-865, 1993

[96] S. Sűnter & J. Clare, Development of a Matrix Converter Induction Motor Drive, MELECON'94, p833-836, 1994

[97] C. Klumpner, I. Boldea, F. Blaabjerg & P. Nielsen, A New Modulator for Matrix Converters with Input Current Ripple Reduction, Proc. of OPTIM, p487-492, 2000

[98] C. Neft & C. Schauder, Theory and Design of a 30-hp Matrix Converter, IEEE Trans. on Industry Applications, Vol. 28, No. 3. p546-551, 1988

[99] G, Nicolandis, Investigation into the Operation and Performance of the Matrix Converter, University College London MSc Project Thesis, 2000

[100] D. Casadei, G. Serra & A. Tani, Theoretical and Experimental Analysis of SVM-controlled Matrix Converters under Unbalanced Supply Conditions, Electromotion Journal, Vol. 4, No. 1-2, p28-37, 1997

[101] Cygnal Integrated Products, http://www.cygnal.com/datasheets/c8051f02x.pdf

[102] Fairchild Semiconductor, 74AC139 Datasheet: http://www.fairchildsemi.com/ds/74/74AC139.pdf

[103] Samsung, 8MB Smartmedia datasheet: http://www.samsung.com/Products/Semiconductor/Flash/FlashCard/SmartMedia/8MByte/K9S6408V0C/K9S56_28_64.PDF

[104] Samsung, Smartmedia White Paper: http://www.samsung.com/Products/Semiconductor/Flash/SmartmediaWhitepaper/white_paper.

[105] 8052.COM-ONLINE RESOURCE: http://www.8052.com

[106] S. Yerlan & A. Ahluwalia, Programming and Interfacing the 8051 Microcontroller, Addison Wesley, ISBN 0 - 201 - 63365 - 5, 1995

[107] D. Calcutt, F. Cowan & G. Parchizadeh, 8051 Microcontrollers: Harware Software and Applications, Arnold, ISBN 0 - 340 - 67707 - 4, 1998

[108] Website detailing different Sine Wave generation techniques: http://www.interstice.com/~sdattalo/technical/theory/sinewave.html

[109] S. Bernet, T. Matsuo & T. Lipo, A Matrix Converter Using Reverse Blocking NPT-IGBT's and Optimised Pulse Patterns, IEEE Proc. of PESC'96, p107-113, 1996

[110] R. Beasant, W. Beattie & A, Refsum, Current Commutation Problems in the Venturini Converter, Proc. of UPEC'89, p43-46, 1989

[111] M. Bland, P. Wheeler, J. Clare & L. Empringham, Comparison of Calculated and Measured Losses in Direct AC-AC Converters, PESC, Vol.2, p1096-1101, 2001

[112] M. Apap, J. Clare, P. Wheeler, M. Bland, K. Bradley, Comparison of Losses in Matrix Converters and Voltage Source Inverters, IEE Matrix Converter Seminar, Birmingham, 2003

[113] R. Beasant, W. Beattie & A. Refsum, An Approach to the Realisation of a High-Power Venturini Converter, IEEE Proc. of PESC'90, p291-297, 1990

[114] J. Kang, H. Hara, E. Yamamoto & E. Watanabe, Analysis and Evaluation of Bi-Directional Power Switch Losses for Matrix Converter Drive, IEEE, p438-443, 2002

[115] The ABB group website link to data about their range of PP-IGBT devices: http://www.abb.com/global/abbzh/abbzh251.nsf!OpenDatabase&db=/global/seitp/seitp325.nsf&v=9AAC910029&e=us&c=E19CC2BEF4F2868DC1256E9000488BF5

[116] The Motor Ship, the magazine article on the Ifremer deep sea research vessel Pourquoi Pas: http://ms.myhyve.com/currentnews/article.asp?ARTICLEID=1475

[117] K. Kerris, P. Wheeler, J. Clare & L. Empringham, Implementation of a Matrix Converter using P-Channel Mos-Controlled Thyristors, Power Electronics & Variable Speed Drives, No. 475, p35-39, 2000

[118] C. Ferreira, Modelling and Real-Time Simulation of an Advanced Marine Full-Electrical Propulsion System, M.Phil Thesis, University College London, 2003.

[119] J. Baek, W. Yoo, & H. Kim, High-voltage Switch Using Series-Connected IGBTs with Simple Auxiliary Circuit, IEEE transactions on Industry Applications, p1832-1839, 2001

[120] C. Lewis, The Advanced Induction Motor, Power Engineering Society Summer Meeting, IEEE, Vol.1, p250-253, 2002

[121] P. Wheeler, H. Zhang & D. Clare, A Theoretical and Practical Consideration of Optimised Input Filter Design for a low loss Matrix Converter, IEE, Electromagnetic Compatibility, September, p138-142, 1994

[122] P. Wheeler, H. Zhang & D. Grant, A Theoretical and Practical Investigation of Switching Frequency Harmonics in a Matrix Converter, UPEC'93, p502-505, 1993

[123] S. Large, A. Green, S. Mason, S. Bhatia, J. Clare, P, Zanchetta, L, Empringham & P. Wheeler, Matrix Converter Solution for Aircraft Starting, AES, Edinburgh, p143-158, 2003

[124] P. Nielsen, F. Blaabjerg & J. Pedersen, New Protection Issues of a Matrix Converter: Design Considerations for Adjustable-Speed Drives, IEEE Trans. on Industry Applications, Vol. 35, no. 5, p1150-1161, 1999

[125] The ABB group website link to data on their range of PP-diode devices: http://www.abb.com/global/abbzh/abbzh251.nsf!OpenDatabase&db=/global/seitp/seitp325.nsf&v=9AAC910029&e=us&c=655E136B296ED885C1256E90002B48C0

[126] The GE website link to data on their 20MW LM2500 gas turbine generator: http://www.gepower.com/prod_serv/products/aero_turbines/en/downloads/lm2500.pdf

[127] ABB Technical Guide No.1 - Direct Torque Control: http://www.abb.se/product/ap/seitp322/c1256c84007b2e7e412567c30057e931.aspx

[128] C. Klumpner, P. Nielsen, I. Boldea & F. Blaabjerg, A New Matrix Converter-Motor (MCM) for Industry Applications, IEEE IAS 2000, Vol. 3, p1394-1402, 2000

Appendices

A1 Matrix Converter Literature Review & Significant Publications

1976

- Gyugi and Pelly et al propose an idealised converter characterised by an array of switches allowing any input phase to be connected to any output phase. Bi-directional power flow is possible with direct AC-AC conversion eliminating any requirement for intermediate energy storage devices. A scalar control strategy is also proposed but generates input current and output voltage harmonics that are difficult to filter [1].

1980

- Venturini proposes a generalised mathematical approach to control the bi-directional switches. It is characterised by sinusoidal waveforms at both input and output. The strategy allows full control over input displacement angle, output amplitude, frequency and phase. The output voltage amplitude is limited to 50% of the supply voltage [2].

1981

- Venturini & Alesina develop a generalised theorem based on Fourier analysis. A method for straightforward converter design from the desired specifications is proposed, providing certain conditions are met. The three-phase matrix converter is examined in detail [3].

1985

- Ziogas et al present a comparison of four different PWM control schemes for the matrix converter. These techniques demonstrates improvements in voltage utilisation and reduced harmonic distortion [4].

1986

- A practical investigation is carried out by Ziogas et al to verify the performance of the new PWM control schemes [5].

- Ma investigates alternative and novel control schemes. Although achieving increased voltage utilisation, hardware and performance shortcomings mean that these strategies are not yet mature [6].

1988

- Neft et al describe the theory and design of a 30hp matrix converter using a variation of the DC-link type control and diode-bridge transistor switch arrangement [7].

- Alesina & Venturini prove mathematically that the voltage transfer ratio of 0.866 is an intrinsic limit independent of the control strategy implemented. A novel control algorithm is presented that incorporates third harmonic modulation to achieve the maximum voltage transfer ratio. The strategy also permits unconstrained control of the input phase displacement within a limited range of voltage gain with respect to the output phase displacement. A feedback implementation of the controller is also discussed [8].

1989

- Oyama et al also propose a control strategy that achieves the maximum voltage transfer ratio of 0.866. They also demonstrate a static induction thyristor (SIT) based matrix converter [9].

- Beasant et al investigate the matrix converter's current commutation problem. A new method for switch control for the common collector bi-directional switch is proposed to make use of both natural and forced commutation. This is known as Semi-natural commutation. By reducing circulating currents, the new circuit topology no longer requires a snubber circuit to protect switches against overvoltage [10].

- The Space Vector Modulator (SVM) used for PWM drive control is applied to the matrix converter by Huber & Borojevic. Achieves a voltage utilisation of 0.866. Describes a possible implementation of the SVM algorithm with reduced real-time computation by using lookup tables [11].

1990

- Beasant et al investigate the current commutation problem and find that with the use of semi-natural commutation, commutation loss could be reduced to a level possible with the standard PWM drive [12].

1991

- Cho et al present a soft-switched matrix converter employing zero voltage switching. Existing bi-directional switch combinations are used with reactive components added only to the output of the converter. Low switching loss is achieved with high dynamic and spectral performance without the need of a snubber network. Unfortunately, performance is found to be inferior to the conventional converter by exhibiting increased conduction loss and a practical voltage transfer ratio of only approximately 0.8 [13].

- A new Scalar Control Algorithm is proposed by Roy et al. The method uses the instantaneous voltage ratio of specific input phase voltages to generate the active and

zero states of the various switches. Voltage utilisation is 0.866. Timing synchronisation error affects both input power displacement and the voltage transfer ratio [14].

1992

- A general model of N-input K-output matrix converters is proposed by Tenti et al to derive optimum control criteria [15].

1993

- Ching et al present a low loss bi-directional switch that is able to turn on at zero current and turn off at zero voltage to achieve almost zero loss and soft switching. Switch configuration requires considerably increased number of components and efficiency is less that 85% [16].

- A new control strategy using state functions is proposed by Sobczyk for N-phase input M-phase output matrix converters [17].

- Wheeler et al present results from a low-loss matrix converter. Semisoft commutation is used along with semi-symmetrical PWM to significantly reduce switching loss. Shows that total loss in a matrix converter can be comparable to those of a conventional inverter drive [18].

- Switching frequency harmonics drawn from the supply by the matrix converter are examined by Wheeler et al. They examine the regulations and recommendations in the EMC region between 10kHz and 150kHz where a matrix converter is like to cause new noise problems. It is shown that to comply with possible future regulations, the matrix converter will need to operate at high switching frequencies to minimise the size (and cost) of supply filter components. The simple LC filter is shown to be the most economical [19].

1994

- Vlatko et al present the preliminary results from a SVM matrix converter that implements zero voltage switching for reduced loss. The SVM algorithm is applied using a digital signal processor based controller to allow very high processing and switching speed.[20]

- An optimised modulation function is proposed by Jun for microprocessor implementation. It indicates that a voltage transfer ratio in excess of the 0.866 limit can be reached at the cost of increased harmonic distortion [21].

- Sűnter et al present an IGBT based matrix converter that implements a novel gate drive circuit that eliminates the need for isolated power supplies for reduced cost. Isolation is achieved with the use of pulse transformers. Practical results closely match the computer-simulated results [22].

1995

- Hey et al propose a Commutation Auxiliary Circuit (CAC) to obtain zero voltage switching in a matrix converter. Self commutation of all switches is independent of the load value but increases reactive energy in the converter. Only a low power drive is described [23].

- Casadei et al present an analysis of the behaviour of the three-phase matrix converter under input and output unbalanced condition. A general approach makes it possible to derive new input current modulation strategies to reduce input current harmonic content. A new space vector control strategy for unbalanced conditions is also presented [24].

- A logic circuit for controlling the commutation procedure of a matrix converter is presented by Zhang et al. Using simple logic gates, the circuit provides full protection and safe commutation of matrix converter under any input conditions [25].

1996

- Watthanasarn et al perform analysis of both Venturini and SVM control strategies using a DSP system. Both strategies are shown to reach the intrinsic voltage transfer ratio of 0.866 with full control of output voltage waveform and input current displacement. The SVM method has 20% fewer switch commutations and a less complex computational procedure than the Venturini method [26].

- Zuckerberger et al simulate an Induction motor driven by a matrix converter using the Matlab SimuLink environment [27].

- The Auxiliary Resonant Commutated Pole matrix converter (ARCPMC) is proposed by Bernet et al. An accurate semiconductor loss model shows that the ARCPMC realises substantially lower switching and total loss than a hard switched matrix converter at medium and high switching frequencies [28].

- Nielsen et al present a modified SVM control strategy by modelling the converter as having independent rectifying and inverting stages. This results in approximately 10% fewer switching operations [29].

- Oyama et al analyse their previous control strategy and investigate the effect of PWM pulse number on the matrix converter characteristics. They conclude that odd triangular pulse number in 60 degree of the supply voltage is preferable to reduce distortion and commutation loss [30].

- Technical issues applying the matrix converter to field orientated Induction motors are investigated by Matsuo et al. It is demonstrated that small size capacitors work efficiently as supply filters [31].

- Bernet et al analyse the effect of switch sequencing on the Venturini strategy. Input current characteristics are found to be influenced by the switching sequence with no effect on the output current. An optimised switching sequence is proposed that maintains a balanced three-phase supply while reducing input current harmonics by 31%. Bernet et al. also present work on reverse blocking NPT-IGBT switches. Using this type of the switch, the size of a matrix converter can be halved to only 18 unidirectional conducting switches, less than a conventional PWM drive and with reduced conduction loss [32].

1997

- Wheeler considers the main areas that have delayed the use of the matrix converter for industrial applications. Some possible solutions are proposed for these problems [33].

- Zuckerberger et al propose a single-phase output matrix converter. Using four bi-directional switches, it operates as a frequency step up and voltage step down converter. A limited practical implementation is described. Suggested uses are traction applications [34].

1998

- Zhang et al perform comparison analysis of the Venturini and SVM control strategies. The SVM is shown to have simpler control of the power factor and reduced switching loss but is less tolerant to supply unbalance and distortion. The Venturini method is able to compensate for input current imbalance and offers better overall performance in terms of harmonic generation [35].

- Empringham et al describe a new commutation technique for anti-parallel unidirectional switch modules that improves reliability in current direction sensing. The voltage across each unidirectional device is measured to accurately deduce direction of current flow. Associated logic circuitry then gates the appropriate device individually to achieve a quasi two-step commutation strategy. The new commutation control

allows accurate current direction to be detected down to 100μA, something not possible with existing systems [36].

- Zhang et al propose wind generation as a possible application for the matrix converter. This system allows maximum energy to be extracted from the wind [37].

1999

- Two new snubber/clamp circuits requiring considerably fewer (half as many) components are presented by Nielsen et al for matrix converters driving induction motors. Test results verify circuit design [38].

- Chang et al present a medium power matrix converter based on Integrated Bi-directional Power Modules. These integrate the gate drive and the power electronic devices required for each output phase into a single module. The result is a reduction in critical parasitic inductance with minimised connection terminals and simplified wiring. Initial calculations indicate that it possible to achieve a 4-to-1 size reduction in comparison with conventional, industrial regenerative AC drives. A novel adaptive commutation control is presented that adjusts the switch transition time according to the load current [39].

2000

- Blaabjerg et al perform comparison of two Current modulation strategies for the SVM to reduce low order output voltage harmonics under unbalanced supply conditions. Modulation of the input current vector dynamically around the direction of the line-to-neutral voltage vector was found to reduce output harmonics [40].

- Kerris et al assemble a single-phase output matrix converter based upon two different MOS-controlled thyristor (MCT) modules. The MCT has the potential for reduced conduction loss. Semisoft commutation is demonstrated to require at least a 6.5μs interval for fault free commutation when using the MCT modules. Impressive waveforms are shown, obtained without snubber circuitry [41].

- Klumpner et al investigate methods of reducing the cost and the number of components in a matrix converter, by integrating key ancillary elements into a single unit. The optimum bi-directional switch configuration is proposed for both low and high power applications to minimise the number of isolated power supplied. The modules integrate gate drive and commutation control to reduce the number of external connections. A new supply filter design that reduces both the cost and size is described. Only two choke cores are used, one with a single winding and the other with two windings. Testing proves validity of design [42].

- Watanabe et al analyse the performance of the matrix converter as a motor drive. Practical experiments show that matrix converter offers significantly better speed step-response and impact-load response. Unity displacement angle was achieved at all operating conditions with significantly lower harmonic distortion than the conventional PWM drive [43].

- Klumpner et al present a prototype 4kW integrated Matrix-Converter-Motor (MCM) for industrial applications. Paper describes how the various disadvantages delaying industrial implementation are overcome, resulting in a very compact drive [44].

2001

- Wheeler et al suggest that although the common collector IGBT-diode arrangement requires only 6 isolated gate drives, in practice there are problems with inductance between commutator cells. Resonant switching techniques "...significantly increase the component count in the matrix converter, (and) increase conduction losses...". The maximum voltage transfer ratio of 86% is viewed as a disadvantage of the matrix converter but this is only a factor when replacing an existing conventional converter. New installations can be optimised for the matrix converter. Wheeler et al suggest that effort should now focus on protection, as this is the "last remaining obstacle to commercial exploitation" [45].

- Heinke et al demonstrate a new Monolithic Bi-directional Switch in a simplified commutation circuit for both forced and natural commutation. The MBS blocks both positive and negative voltages and can control currents in either direction with gate drive requirements similar to that of an IGBT device. Although switching commutation speed is considerably lower than an IGBT, the MBS is suitable for matrix converter application [46].

- Helle et al present a modified SVM strategy that reduces switching loss by 15-35% when the target output voltage is less than half the supply voltage. Simulations indicate that the technique works, reducing output voltage harmonic content but deteriorating the input current harmonic spectra [47].

2002

- Casadei et al propose a novel matrix converter switch state representation to allow direct performance comparisons between different modulation strategies to be made. The geometric representation comparison considers maximum voltage transfer ratio, switching frequency and input/output ripple. Using this approach, the space vector modulator emerges as the optimum solution to matrix converter control [48].

- Teichmann et al compare three topologies for the auxiliary resonant commutated pole (ARCP) matrix converter that use soft switching to reduce loss. Although the number of active devices and gate drives can be reduced to 33% less than the conventional matrix converter, the necessity for a considerably more complex control strategy prevents foreseeable widespread application. Further unsolved problems exist and the ARCP matrix converter will only be suitable for niche applications [49].

- Klumpner et al propose a new topology that reduces the number of isolated power supplies required for a three-phase output matrix converter to three for low power (<4kW) applications. A pair of common-collector switches are combined with a single common-emitter switch and a bootstrap circuit to provide gate drive power for half of each c-c switch. This topology requires a specific start-up sequence to correctly charge-up the bootstrap circuit and the condition that the c-e switch may not conduct for more than a critical period to retain adequate bootstrap energy [50].

- Wheeler et al review the state of matrix converter development and conclude that strong competition from the three-phase AFE-VSI offering similar characteristics may reduce market share. Improvements are required to reduce cost and size and increase reliability [51].

- Mahlien et al present an alternative solution to matrix converter protection when driving an Induction motor. Varistors are connected across the output lines with suppressor diodes protecting each IGBT switch. When IGBT voltage exceeds the diode rating, the diode conducts and very quickly (<100ns) forces the IGBT into the off state. The IGBT protection is also suitable for integrating into switch modules [52].

- Bernet et al perform a loss comparison between the AFE-VSI and the matrix converter. They conclude that the matrix converter has lower loss in high power applications with a size advantage, notwithstanding a 50% higher semiconductor switch and gate drive count. The AFE-VSI is able to operate from a single-phase supply and has a superior voltage transfer ratio [53].

- Wheeler et al present a simple reliable method for current direction detection in a bi-directional switch. Using a resistor and diode, accurate direction can be measured, even at troublesome low powers. The implementation, using intelligent gate drive circuits, is demonstrated in an 18kW matrix converter without snubber circuitry [54].

2003

- Chamund et al (Dynex Semiconductor) describe the ratings and characteristics of an integrated common-emitter based bi-directional switch. This is realised using

existing manufacturing techniques and uses a standard plastic package. Also announced is a fully integrated matrix converter voltage clamp, again within standard packaging [55].

- Apap et al perform comparison of the predicted loss in a matrix converter, PWM drive and AFE PWM drive. The PWM drive has the lowest loss followed by the matrix converter with the AFE PWM drive being the least efficient due to the increased number of controlled devices. A comparison of matrix converter modulators shows that the Venturini control results in reduced loss compared with various SVM implementations [56].

- Large et al postulate that the matrix converter may be the ideal solution for aircraft starting. The design of 40kVA drive is described and compared with an existing PWM drive. In some areas the matrix converter exceeds the design criteria but savings in weight and volume have not yet been realised, due to the stringent harmonic performance requiring a complex supply filter. The matrix converter is the ideal topology to exploit future technologies such as high temperature silicon carbide devices [57].

2004

- Wheeler et al demonstrate that the commutation time for a matrix converter can be minimized to zero, thereby enhancing the output waveform quality substantially. The resulting switch timings lead to a three-step current commutation strategy instead of the traditional four-step commutation technique. The use of a single-step commutation strategy is also shown to maximise the available output voltage [58].

- Bland et al assess the performance of bi-directional switch components for matrix converter applications. They show that the Silicon Carbide diode performs significantly better than equivalent hyper-fast Silicon diode under most conditions. The Reverse Blocking IGBT converter showed a decrease in conduction loss of about 50% compared with the converter using Silicon diodes. However, the switching loss is about 5 times higher in the RB-IGBT converter [59].

2005

- Podlesak et al describe the design, construction and testing of a 150-kVA closed-loop vector-controlled matrix converter induction motor drive. This employs 1400V 600A IGBT devices with a three step staggered commutation strategy with minimised commutations to 'eliminate output waveform distortion'. The efficiency of the converter is also compared with a developed computer loss model with very good correlation [60].

Significant Publications Identified by Matrix Converter Literature Survey

---

[1] L. Gyugi & B. Pelly, Static Frequency Changers, Wiley, New York, 1976

[2] M. Venturini, A new Sine Wave in, Sine Wave out Conversion Technique Eliminates Reactive Elements, Proceedings Powercon 7, E3-1, 1980

[3] A. Alesina & M. Venturini, Solid-State Power Conversion: A Fourier Analysis Approach to Generalised transformer Synthesis, IEEE Transactions on Circuits and Systems, 1981

[4] P. Ziogas, S. Khan & M. Rashid, Some Improved Forced Commutated Cycloconverter Structures, IEEE Trans. On Industrial Applications, Vol. IA-21, No. 5, p1242-1253, 1985

[5] P. Ziogas, S. Khan & M. Rashid, Analysis and Design of Forced Commutated Cycloconverter Structures with Improved Transfer Characteristics, IEEE Trans. On Industrial Electronics, Vol. IE-33, No. 3, p271-280, 1986

[6] X. Ma, High Performance PWM Frequency Changers, IEEE Trans. On Industrial Applications, Vol. IA-22, No. 2, p267-279, 1986

[7] C. Neft & C. Schauder, Theory and Design of a 30-hp Matrix Converter, iEEE Trans. on Industry Applications, Vol. 28, No. 3. p546-551, 1988

[8] A. Alesina & M. Venturini, Analysis and Design of Optimum-Amplitude Nine-Switch Direct AC-AC Converters, IEEE Transactions on Power Electronics, Vol. 4 No. 1, p101-112, 1989

[9] J. Oyama, T. Higuchi, E. Yamada, T. Koga & T. Lipo, New Control Strategy for Matrix Converter, Proc. of PESC'89, p360-367, Vol. 1, 1989

[10] R. Beasant, W. Beattie & A, Refsum, Current Commutation Problems in the Venturini Converter, Proc. of UPEC'89, p43-46, 1989

[11] L. Huber & D. Borojevic, Space Vector Modulator for Forced Commutated Cycloconverters, IEEE Conf. Rec. of Industry Applications, p871-876, 1989

[12] R. Beasant, W. Beattie & A. Refsum, An Approach to the Realisation of a High-Power Venturini Converter, IEEE Proc. of PESC'90, p291-297, 1990

[13] J. Cho & G. Cho, Soft Switched Matrix Converter for High Frequency Direct AC-to-AC Power Conversion, EPE'91, Vol. 4, p196-201, 1991

[14] G. Roy & G. April, Direct Frequency Changer Operation Under a New Scaler Control Algorithm, IEEE Trans. On Power Electronics, Vol. 6, No. 1, p100-107, 1991

[15] P. Tenti, L. Malesani & L. Rossetto, Optimum Control of N-Input K-Output Matrix Converters, IEEE Trans. on Power Electronics, Vol. 7, N° 4, Oct, p707-713, 1992

[16] T. Ching, C. Tsung & J. Jenn, A Zero Switching Loss Matrix Converter, IEEE Power Electronics Specialists Conference, 1993

[17] T. Sobczyk, Control Strategy of Matrix Converters, EPE Brighton conference, 1993

[18] P. Wheeler & D. Grant, A Low Loss Matrix Converter for AC Variable-Speed Drives, EPE Brighton conference, 1993

[19] P. Wheeler, H. Zhang & D. Grant, A Theoretical and Practical Investigation of Switching Frequency Harmonics in a Matrix Converter, UPEC'93, p502-505, 1993

[20] V. Vlatko & D. Borojevic, Digital-Signal-Processor-Based Control of Three Phase Space Vector Modulated Converters, IEEE Trans. on Industrial Electronics, 1994

[21] L. Jun, Analysis and Research of Generalized Matrix Converter, IPEMC'94, p889-894, 1994

[22] S. Sűnter & J. Clare, Development of a Matrix Converter Induction Motor Drive, MELECON'94, p833-836, 1994

[23] H. Hey, H. Pinheiro & J. Pinheiro, A New Soft-Switched AC-AC Matrix Converter with a single Activated Commutation Auxiliary Circuit, IEEE PESC, 1995

[24] D. Casadei, G. Serra, A. Tani & P. Nielsen, Performance of SVM Controlled Matrix Converter with Input and Output Unbalanced Conditions, EPE, Vol. II, p628-633, 1995

[25] L. Zhang, C. Wathanasarn & W. Shepherd, Switch Sequencer circuit for safe commutation of a Matrix Converter, Electronic Letters, Vol. 31, No. 18, p1530-1532, 1995

[26] C. Watthanasarn, L. Zhang & D. Liang, Analysis and DSP-Based Implementation of Modulation Algorithms for AC-AC Matrix Converters, IEEE PESC96, p1053-1058, 1996

[27] A. Zuckerberger, D. Weinstock & A. Alexandrovitz, Simulation of Three-Phase loaded Matrix Converter, IEE Proc.-Electr. Power Applications, 1996

[28] S. Bernet, K. Bernet & T. Lipo, The Auxiliary Resonant Commutated Pole Matrix Converter - A New Topology for High Power Applications, IPCC, p1242-1249, 1996

[29] P. Nielsen, F. Blaabjerg & J. Pedersen, Space Vector Modulated Matrix Converter with minimised number of switchings and a Feedforward Compensation of Input Voltage Unbalance, Proc. of PEDES '96, Vol. 2, p833-839, 1996

[30] J. Oyama, X. Xia, T. Higuchi & E. Yamada, Effect of PWM Pulse Number on Matrix Converter Characteristics, IEEE, p1306-1311, 1996

[31] T. Matsuo, S. Bernet, R. Colby & T. Lipo, Application of the Matrix Converter to Induction Motor Drives, IEEE Proc. of IAS, p60-67, 1996

[32] S. Bernet, T. Matsuo & T. Lipo, A Matrix Converter Using Reverse Blocking NPT-IGBT's and Optimised Pulse Patterns, IEEE Proc. of PESC'96, p107-113, 1996

[33] P. Wheeler, The Matrix Converter - Future Possibilities, IEE Colloquium on New Power Electronic Techniques, 1997

[34] Zuckerberger, D. Weinstock & A. Alexandrovitz, Single Phase Matrix Converter, IEE Proc.-Electr. Power Applications, 1997

[35] L. Zhang, C. Watthanasarn & W. Shepherd, Analysis and comparison of control techniques for AC-AC matrix converters, IEE Proc. Electr. Power Appl. Vol. 145, No.4, p284-294, 1998

[36] L. Empringham, P. Wheeler & J. Clare, Intelligent Commutation of Matrix Converter Bi-directional Switch Cells using Novel Gate Drive Techniques, PESC, Vol. 1, p707 - 713, 1998

[37] L. Zhang & C. Watthanasarn, A Matrix Converter excited Doubly-Fed Induction Machine as a Wind Power Generator, IEE Power Electronics & Variable Speed Drives, No. 456, p532-537, 1998

[38] P. Nielsen, F. Blaabjerg & J. Pedersen, New Protection Issues of a Matrix Converter: Design Considerations for Adjustable-Speed Drives, IEEE Trans. on Industry Applications, Vol. 35, No. 5. p1150-1161, 1999

[39] J. Chang, T. Sun, A. Wang & D. Braun, Medium Power AC-AC Converter Based on Integrated Bi-directional Power Modules, Adaptive Commutation and DSP Control, IEEE 34th IAS, p1864-1870, 1999

[40] F. Blaabjerg, D. Casadei, M. Matteini & C. Klumpner, Comparison of two current Modulation Strategies for Matrix Converters under Unbalanced Input Voltage Conditions, Proceedings of ISIE'00, Vol. 2, p465-470, 2000

[41] K. Kerris, P. Wheeler, J. Clare & L. Empringham, Implementation of a Matrix Converter using P-Channel Mos-Controlled Thyristors, Power Electronics & Variable Speed Drives, No. 475, p35-39, 2000

[42] C. Klumpner, P. Nielsen, I. Boldea & F. Blaabjerg, New Steps towards a low-cost Power Electronic Building Block for Matrix Converters, IEEE IAS 2000, Vol. 3, p1964-1971, 2000

[43] E. Watanabe, S. Ishii, E. Yamamoto, H. Hara & J. Kang, High Performance Motor Drive Using Matrix Converter, IEE, Induction Motor Control, p7/1-7/6, 2000

[44] C. Klumpner, P. Nielsen, I. Boldea & F. Blaabjerg, A New Matrix Converter-Motor (MCM) for Industry Applications, IEEE IAS 2000, Vol. 3, p1394-1402, 2000

[45] P. Wheeler, J. Clare & L. Empringham & M. Bland, Matrix Converters: The Technology and Potential for Exploitation, The Drives and Controls Power Electronics Conference, London, Section 5, 2001

[46] F. Heinke & R. Sittig, The Monolithic Bi-directional Switch (MBS) in a Matrix Converter Application, Power Semiconductor Devices & ICs, ISPSD, p367-371, 2001

[47] L. Helle & S. Munk-Nielsen, A Novel Loss Reduced Modulation Strategy for Matrix Converters, Proceedings of PESC'01, Vol. 2, p1102-1107, 2001

[48] D. Casadei, G. Serra, A. Tani & L. Zarri. Matrix Converter Modulation Strategies: A New General Approach based on Space-Vector Representation of the Switch State, IEEE Transactions on Industrial Electronics, Vol. 49 Issue 2, p370-381, 2002

[49] R. Teichmann & J. Oyama, ARCP Soft-Switching Technique in Matrix Converters, IEEE Transactions on Industrial Electronics, Vol. 49 Issue 2, p353-361, 2002

[50] C. Klumpner, P. Nielsen, I. Boldea & F. Blaabjerg. New Solutions for a Low-Cost Power Electronic Building Block for Matrix Converters, IEEE Transactions on Industrial Electronics, Vol. 49 Issue 2, p336-344, 2002

[51] P. Wheeler, J. Rodriguez, J. Clare, L. Empringham & A. Weinstein. Matrix Converters: A Technology Review, IEEE Transactions on Industrial Electronics, Vol.49 Issue 2, p276-288, 2002

[52] J. Mahlein, M. Bruckmann & M. Braun. Passive Protection Strategy for a Drive System with a Matrix Converter and an Induction Machine, IEEE Transactions on Industrial Electronics, Vol. 49 Issue 2, p297-303, 2002

[53] S. Bernet, S. Ponnaluri & R. Teichmann. Design and Loss Comparison of Matrix Converters and Voltage-Source Converters for Modern AC Drives, IEEE Transactions on Industrial Electronics, Vol. 49 Issue 2, p304-314, 2002

[54] P. Wheeler, J. Clare, L. Empringharn, M. Bland & M. Apap, Gate Drive Level Intelligence and Current Sensing for Matrix Converter Current Commutation, IEEE Transactions on Industrial Electronics, Vol. 49 Issue 2, p382-389, 2002

[55] D. Chamund, W. Findlay & K. Birkett, (Dynex Semiconductor), Bi-directional Switch Packaging for Higher Power Matrix Converters, IEE Matrix Converter Seminar, Birmingham, 2003

[56] M. Apap, J. Clare, P. Wheeler, M. Bland & K. Bradley, Comparison of Losses in Matrix Converters and Voltage Source Inverters, IEE Matrix Converter Seminar, Birmingham, 2003

[57] S. Large, A. Green, S. Mason, S. Bhatia, J. Clare, P, Zanchetta, L, Empringham & P. Wheeler, Matrix Converter Solution for Aircraft Starting, AES, Edinburgh, p143-158, 2003

[58] P. Wheeler, J. Clare & L. Empringham, Enhancement of Matrix Converter Output Waveform Quality using Minimized Commutation Times, Industrial Electronics, IEEE, Vol. 51, Issue 1, p240-244, 2004

[59] M. Bland, P. Wheeler, J. Clare & L. Empringham, Comparison of Bi-directional Switch Components for Direct AC-AC Converters, Power Electronics Specialists Conference,. IEEE, Vol. 4, p2905-2909, 2004

[60] T. Podlesak, D. Katsis, P. Wheeler, J. Clare, L. Empringham & M. Bland, A 150-kVA Vector-Controlled Matrix Converter Induction Motor Drive, Industry Applications, IEEE, Vol. 41, Issue 3, p841-847, 2005

A2 Harmonic Injection to Maximise Supply Utilisation

NOTE: The matrix converter topology and its control strategies assume operation from equally distributed supply voltage waveforms. This convention in some cases may differ to those waveforms commonly generated by standard rotating machines. The required supply waveforms for multi-phase matrix converters are shown diagrammatically below and the type of electrical machine required to generate them is also stated.

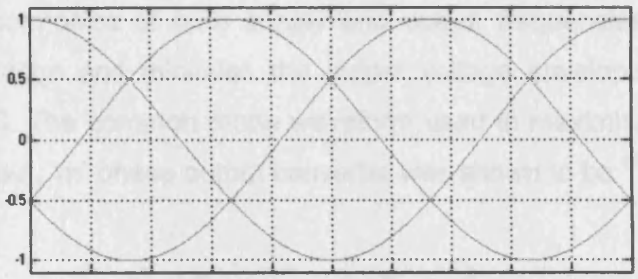

Figure 192 - Three Equally Distributed Supply Phases

The three-phase matrix converter supply waveform can be provided by a conventional three-phase generator.

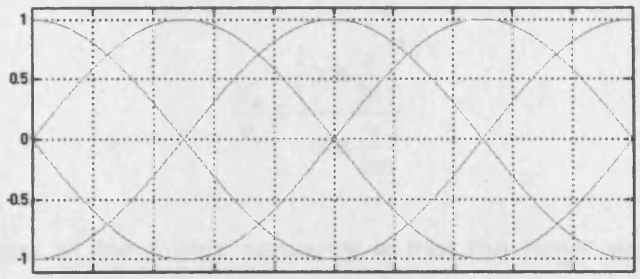

Figure 193 - Four Equally Distributed Supply Phases

The four-phase matrix converter supply waveform can be provided by a double-wound two-phase generator.

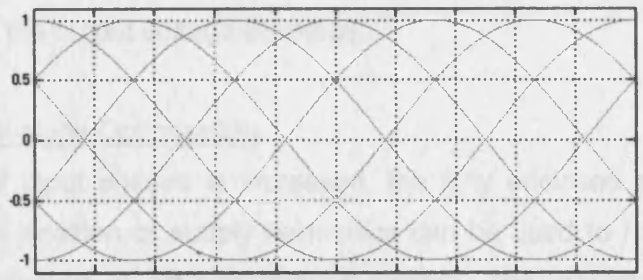

Figure 194 - Six Equally Distributed Supply Phases

The six-phase matrix converter supply waveform can be provided by a double-wound three-phase generator.

Although the reduced supply utilisation has often been cited as a major drawback of the matrix converter, this is generally referring to the three-phase input, three-phase output configuration found in small to medium sized motor drives. However, in a marine electric motor drive, there are a greater number of supply and motor phases and these can be harnessed to improve the supply utilisation of the matrix converter.

Alesina and Venturini derived the intrinsic maximum amplitude for a three-phase input, three-phase output converter to be 86.6% of the supply voltage [52]. This required the addition of third harmonics of both supply and output frequencies to maximise the available supply range and minimise the output voltage envelope, as described in Section 2.8.3 [p56]. The common mode waveform used to maximise supply utilisation for an 'n'-phase input, 'm'-phase output converter was shown to be [52]:

$$f_x(t) = v_g\left(\sin\frac{\pi}{2n}\right)^2\cos(n\omega_{in}t) - \frac{v_o}{m}\sin\frac{\pi}{2m}\cos(m\omega_o t)$$

Also derived was the formula describing the intrinsic maximum amplitude possible for an 'n'-phase input, 'm'-phase (n & m are odd) output converter [52]:

$$\frac{V_o}{V_i} \le \frac{\left(\cos\frac{\pi}{2n}\right)^2}{\cos\frac{\pi}{2m}}$$

The key requirement of the matrix converter is that the target waveform fit entirely within the supply waveforms. It is this factor that limited the original Venturini strategy to only 50% of the supply voltage [6]. Optimising the allowable output voltage required two approaches:

- Maximising the available supply voltage envelope
- Minimising the output voltage envelope

Supply Voltage Envelope Optimisation

As the number of input phases is increased, the fully enclosed supply region also increases. But the addition of supply harmonics can be used to further increase the supply voltage envelope in an odd phased system. The magnitude of the supply harmonic is calculated using [52]:

$$\text{Supply Harmonic Amplitude} = \left(\sin\frac{\pi}{2n}\right)^2$$

Input Phases	Supply Voltage Envelope	Enhanced Supply Voltage Envelope
3	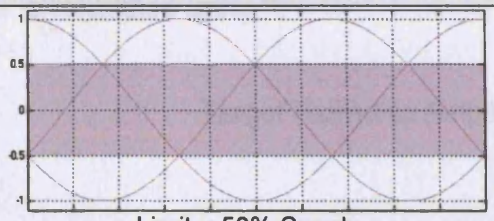 Limit = 50% Supply	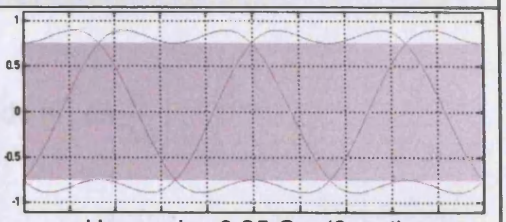 Harmonic : 0.25 Cos(3 ω_{in} t) Enhanced Range = 75%
4	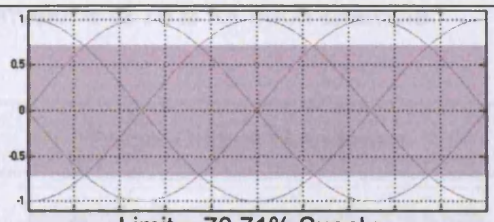 Limit = 70.71% Supply	No enhancement possible
5	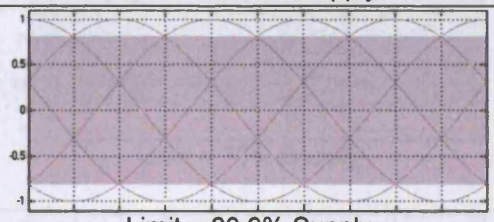 Limit = 80.9% Supply	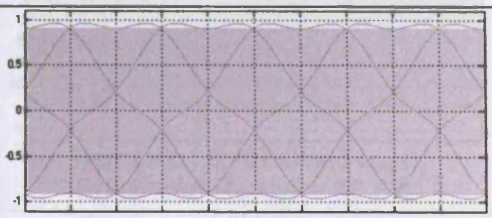 Harmonic : 0.0955 Cos(5 ω_{in} t) Enhanced Range = 90.45%
6	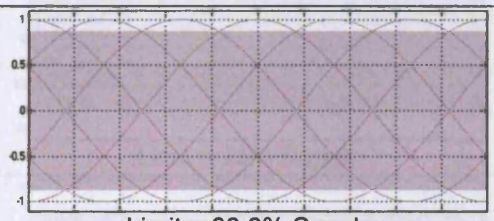 Limit = 86.6% Supply	No enhancement possible
7	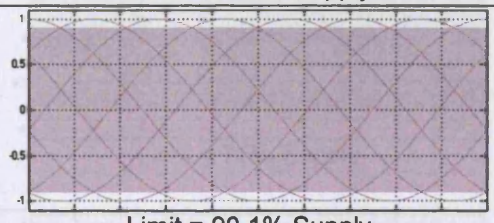 Limit = 90.1% Supply	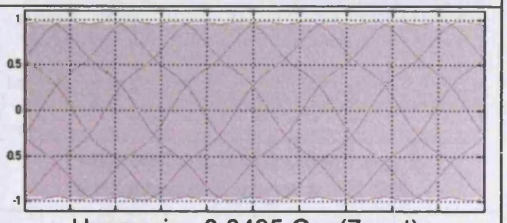 Harmonic : 0.0495 Cos(7 ω_{in} t) Enhanced Range = 95.05%

Table 57 - Supply Waveform Optimisation

There are diminishing returns however, as increasing the number of input phases past a certain level adds cost and complexity without significant improvement in supply utilisation.

Target Voltage Envelope Optimisation

The second step to optimising the matrix converter supply voltage utilisation is to inject harmonics of the target waveform frequency to reduce the target output voltage envelope. For fully continuous operation (allowing operation at all output frequencies), the target waveform must not exceed that of the available supply envelope, so the

harmonic is subtracted from the target waveform. The magnitude of the target voltage harmonic is calculated using [52]:

$$\text{Target Harmonic Amplitude} = \left(\sin\frac{\pi}{2m}\right)$$

This is demonstrated in the following table that assumes an optimised three-phase supply envelope of 75% for each example.

Output Phases	Target Output Waveforms	Enhanced Target Output Waveforms
3	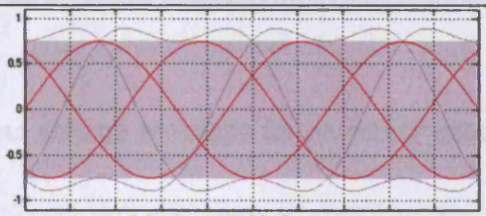 Limit = 75% Supply	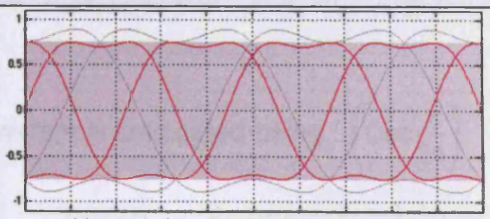 Harmonic : 0.167 Cos(3 ω_{out} t) Enhanced Range = 86.6%
4	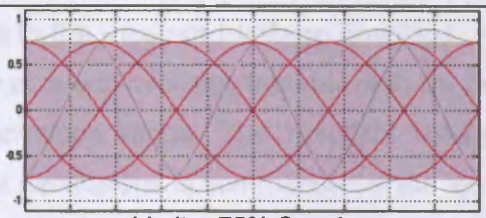 Limit = 75% Supply	No enhancement possible
5	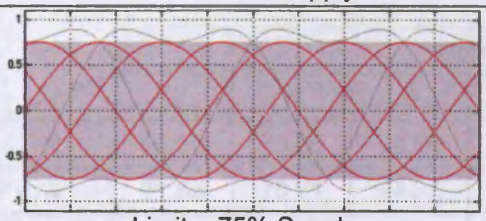 Limit = 75% Supply	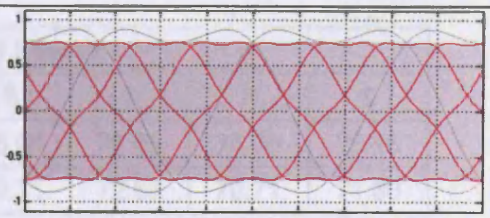 Harmonic : 0.0618 Cos(5 ω_{out} t) Enhanced Range = 78.9%
6	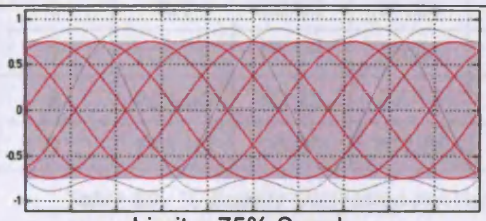 Limit = 75% Supply	No enhancement possible
7	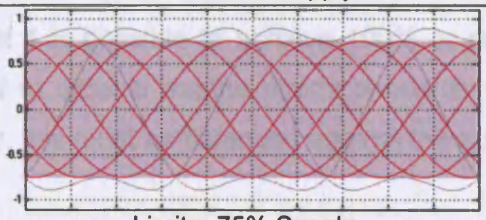 Limit = 75% Supply	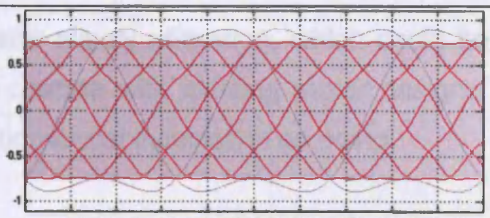 Harmonic : 0.0318 Cos(7 ω_{out} t) Enhanced Range = 76.9%

Table 58 - Target Waveform Optimisation

The previous tabulated results demonstrate that the voltage transfer ratio of a three-phase fed matrix converter tends towards 75% as the number of output phases is increased. This is equal to the available supply voltage envelope and suggests that optimisation of matrix converter supply utilisation requires that the number of output phases be kept as low as practicably possible. The voltage transfer ratio for converters with even numbers of equally spaced output phases cannot be increased with the addition of harmonics and must therefore equal that of the optimised supply voltage envelope.

The input voltage envelope for an odd phased system is calculated using : $\left(\text{Cos}\frac{\pi}{2n}\right)^2$

The output voltage envelope for an odd phased system is calculated using : $\left(\text{Cos}\frac{\pi}{2n}\right)$

For even numbers of equally spaced input or output phases, the voltage transfer ratio is limited to the unaltered voltage envelope. In this way it is possible to calculate the resultant converter voltage transfer ratio by dividing the supply envelope range by the output envelope range. The resultant voltage transfer ratio for a range of matrix converter dimensions is summarised in the following table:

		Output Phases						
		3	**4**	**5**	**6**	**7**	**8**	**9**
Input Phases	**3**	86.60	75.00	78.86	75.00	76.93	75.00	76.16
	4	81.65	70.71	74.35	70.71	72.53	70.71	71.80
	5	***104.44***	90.45	95.11	90.45	92.78	90.45	91.85
	6	100	86.60	91.06	86.60	88.83	86.60	87.94
	7	***109.75***	95.05	99.94	95.05	97.49	95.05	96.51
	8	***106.68***	92.39	97.14	92.39	94.76	92.39	93.81
	9	***111.99***	96.98	***101.98***	96.98	99.48	96.98	98.48

Table 59 - % Supply Utilisation for Varying Converter Configurations

Note that it is possible to achieve 100% or greater supply utilisation, which could be exploited to allow a marine matrix converter to operate with existing motor designs. However, this must be balanced against the additional cost incurred in so doing.

A3 Converter Instrumentation

For accurate and reliable current measurement, six isolated half-effect current transducers (LEM LA 25-NP) were permanently installed on each input and output line of the matrix converter, allowing analysis of any current imbalance between each phase. The transducer outputs were monitored using a digital storage oscilloscope with the ability to capture screenshots for subsequent analysis. Circuit voltage waveforms were measured directly using a power-oscilloscope with a connection to the storage-oscilloscope allowing capture of voltage waveforms. The current traducers were also monitored using a PC based oscilloscope allowing harmonic analysis of the current waveforms. Additionally, three analogue AC ammeters were permanently connected to each supply line to check the level of power being drawn by the converter during operation.

A small DOS based computer program, custom written using Quick-Basic, communicated with the storage oscilloscope via a serial cable to enable direct digital capture of stored waveforms. The 'scope' software allowed the captured data to be saved as a standard image file with a date-stamp to facilitate storage and documentation. A screen shot is shown in Figure 195.

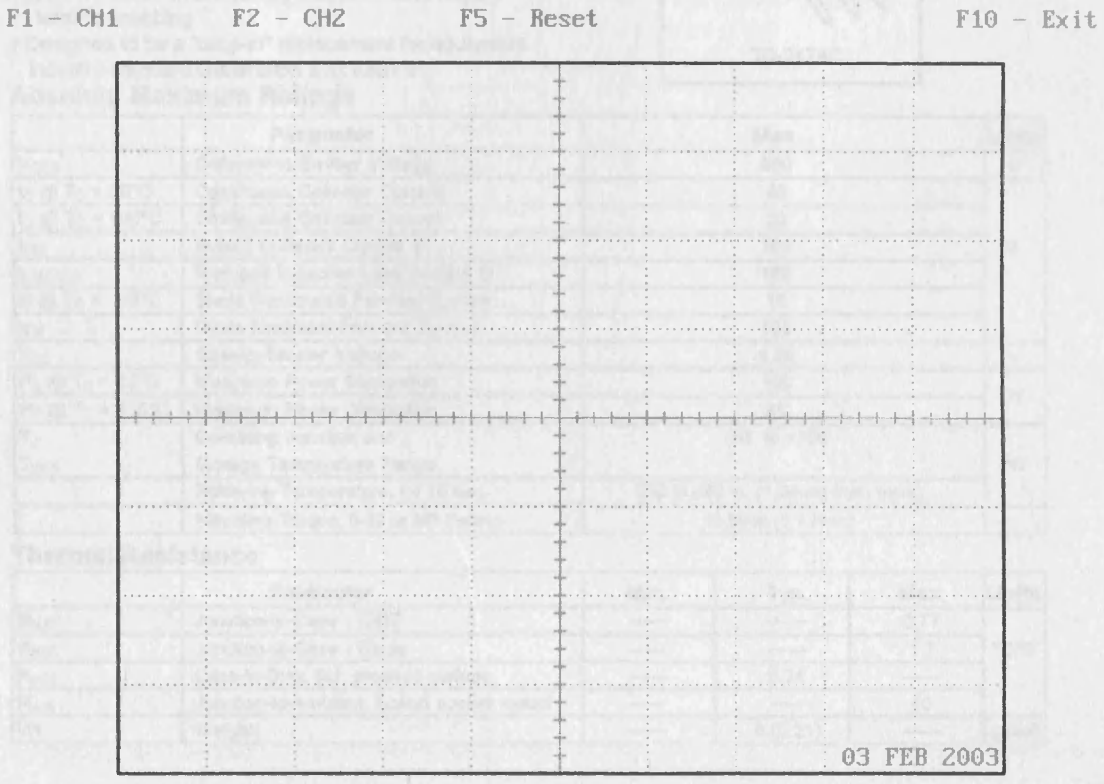

Figure 195 - Custom Oscilloscope Capture Software Screenshot

A4 International Rectifier IRG4PC40UD IGBT Datasheet

This is an extract from the original datasheet available from the International Rectifier website.

http://www.irf.com/product-info/datasheets/data/irg4pc40ud.pdf

International
IOR Rectifier

PD 9.1467D

IRG4PC40UD

INSULATED GATE BIPOLAR TRANSISTOR WITH ULTRAFAST SOFT RECOVERY DIODE

UltraFast CoPack IGBT

Features

- UltraFast: Optimized for high operating frequencies 8-40 kHz in hard switching, >200 kHz in resonant mode
- Generation 4 IGBT design provides tighter parameter distribution and higher efficiency than Generation 3
- IGBT co-packaged with HEXFRED™ ultrafast, ultra-soft-recovery anti-parallel diodes for use in bridge configurations
- Industry standard TO-247AC package

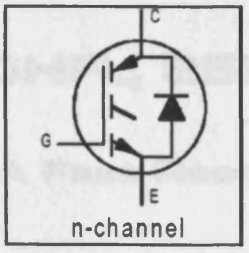

n-channel

V_{CES} = 600V

$V_{CE(on)\ typ.}$ = 1.72V

@V_{GE} = 15V, I_C = 20A

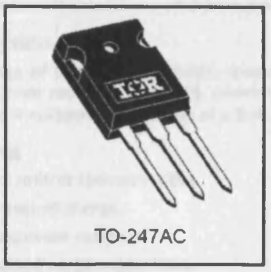

TO-247AC

Benefits

- Generation -4 IGBT's offer highest efficiencies available
- IGBT's optimized for specific application conditions
- HEXFRED diodes optimized for performance with IGBT's . Minimized recovery characteristics require less/no snubbing
- Designed to be a "drop-in" replacement for equivalent industry-standard Generation 3 IR IGBT's

Absolute Maximum Ratings

	Parameter	Max.	Units
V_{CES}	Collector-to-Emitter Voltage	600	V
I_C @ T_C = 25°C	Continuous Collector Current	40	A
I_C @ T_C = 100°C	Continuous Collector Current	20	
I_{CM}	Pulsed Collector Current ①	160	
I_{LM}	Clamped Inductive Load Current ②	160	
I_F @ T_C = 100°C	Diode Continuous Forward Current	15	
I_{FM}	Diode Maximum Forward Current	160	
V_{GE}	Gate-to-Emitter Voltage	± 20	V
P_D @ T_C = 25°C	Maximum Power Dissipation	160	W
P_D @ T_C = 100°C	Maximum Power Dissipation	65	
T_J T_{STG}	Operating Junction and Storage Temperature Range	-55 to +150	°C
	Soldering Temperature, for 10 sec.	300 (0.063 in. (1.6mm) from case)	
	Mounting Torque, 6-32 or M3 Screw.	10 lbf•in (1.1 N•m)	

Thermal Resistance

	Parameter	Min.	Typ.	Max.	Units
$R_{\theta JC}$	Junction-to-Case - IGBT	------	------	0.77	°C/W
$R_{\theta JC}$	Junction-to-Case - Diode	------	------	1.7	
$R_{\theta CS}$	Case-to-Sink, flat, greased surface	------	0.24	----	
$R_{\theta JA}$	Junction-to-Ambient, typical socket mount	----	-----	40	
Wt	Weight	------	6 (0.21)	------	g (oz)

4/17/97

A5 International Rectifier 40HFL Diode Datasheet

This extract is from the original datasheet available on the International Rectifier website.

http://www.irf.com/product-info/datasheets/data/40hfl.pdf

Data Sheet No. PD-2.093

INTERNATIONAL RECTIFIER IOR

40HFL, 70HFL, 85HFL SERIES

40A, 70A, 85A Fast Recovery Rectifiers

Major Ratings and Characteristics

		40HFL...	70HFL...	85HFL...	Units
$I_{F(AV)}$		40	70	85	A
@ Max T_C		75	75	75	°C
I_{FSM}	50Hz	400	700	1100	A
	60Hz	420	730	1151	A
I^2t	50Hz	800	2450	6050	A^2s
	60Hz	730	2240	5523	A^2s
$I^2\sqrt{t}$		11 300	34 650	85 560	$A^2\sqrt{s}$
t_{rr} range		see table			
V_{RRM} range		100 to 1000			V
T_J range		–40 to 125			°C

Description

This range of fast recovery diodes is designed for applications in DC power supplies, inverters, converters, choppers, ultrasonic systems and for use as a free wheeling diode.

Features

- Short reverse recovery time.
- Low stored charge.
- Wide current range.
- Excellent surge capabilities.
- Stud cathode and stud anode versions.
- Types up to 1000V V_{RRM}

CASE STYLE AND DIMENSIONS

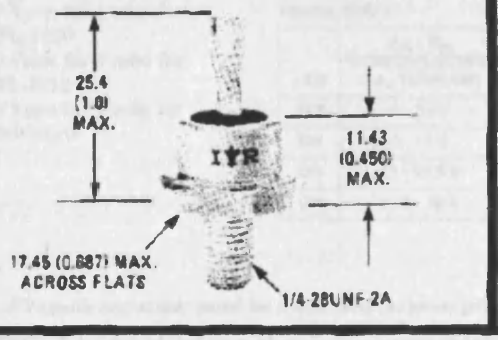

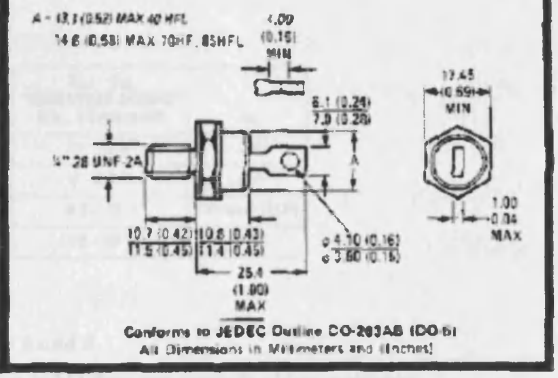

Conforms to JEDEC Outline DO-203AB (DO-5)
All Dimensions in Millimeters and (Inches)

A6 Agilent Technologies HCPL-3120 Gate Driver Datasheet

This extract is from the original datasheet available from the Agilent Technologies website.

http://literature.agilent.com/litweb/pdf/5988-8710EN.pdf

Agilent Technologies

2.0 Amp Output Current IGBT Gate Drive Optocoupler

Technical Data

HCPL-3120
HCPL-J312
HCNW3120

Features

- **2.0 A Minimum Peak Output Current**
- **15 kV/μs Minimum Common Mode Rejection (CMR) at V_{CM} = 1500 V**
- **0.5 V Maximum Low Level Output Voltage (V_{OL})** Eliminates Need for Negative Gate Drive
- **I_{CC} = 5 mA Maximum Supply Current**
- **Under Voltage Lock-Out Protection (UVLO) with Hysteresis**
- **Wide Operating V_{CC} Range: 15 to 30 Volts**
- **500 ns Maximum Switching Speeds**
- **Industrial Temperature Range:** -40°C to 100°C
- **Safety Approval**
  UL Recognized
  2500 Vrms for 1 min. for HCPL-3120
  3750 Vrms for 1 min. for HCPL-J312
  5000 Vrms for 1 min. for HCNW3120

CSA Approval
VDE 0884 Approved
V_{IORM} = 630 Vpeak for HCPL-3120 (Option 060)
V_{IORM} = 891 Vpeak for HCPL-J312
V_{IORM} = 1414 Vpeak for HCNW3120
BSI Certified (HCNW3120 only) (Pending)

Applications

- **IGBT/MOSFET Gate Drive**
- **AC/Brushless DC Motor Drives**
- **Industrial Inverters**
- **Switch Mode Power Supplies**

Functional Diagram

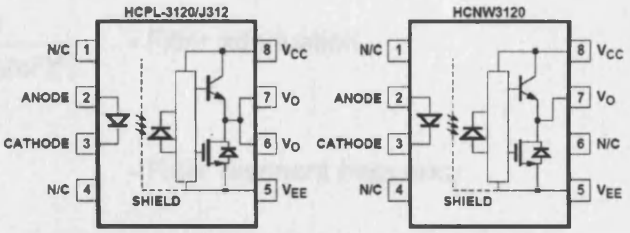

TRUTH TABLE

LED	V_{CC} - V_{EE} "POSITIVE GOING" (i.e., TURN-ON)	V_{CC} - V_{EE} "NEGATIVE GOING" (i.e., TURN-OFF)	V_O
OFF	0 - 30 V	0 - 30 V	LOW
ON	0 - 11 V	0 - 9.5 V	LOW
ON	11 - 13.5 V	9.5 - 12 V	TRANSITION
ON	13.5 - 30 V	12 - 30 V	HIGH

A 0.1 μF bypass capacitor must be connected between pins 5 and 8.

CAUTION: It is advised that normal static precautions be taken in handling and assembly of this component to prevent damage and/or degradation which may be induced by ESD.

A7 Supply Filter Design

A single-stage second-order low-pass filter was selected for the laboratory matrix converter as it represents a proven design and is less sensitive to component tolerance. It represents an economical solution and the lack of a tuned diversion path allowed a range of converter switching frequencies to be employed.

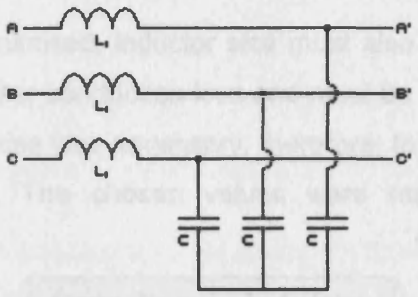

Figure 196 - Single-Stage Second-Order Low-Pass Filter

The low pass supply filter was designed with the requirement to block noise above a frequency of 2kHz and enable converter operation at 4kHz and above. Two governing equations describe the characteristics of a single-stage second-order filter and can be used to calculate the attenuation and the resonant frequency of a capacitor-inductor combination. The resonant frequency must be sufficiently spaced from the intended operating frequency to avoid unstable filter behaviour. Careful design should also minimise the voltage drop across the inductor and ensure that the filter power factor does not vary significantly across the expected operating range.

$$\frac{V_o}{V_i} = \frac{1}{1-(LC(2\pi F)^2)} \quad \text{- Filter attenuation}$$

$$F_O = \frac{1}{2\pi\sqrt{LC}} \quad \text{- Filter resonant frequency}$$

With the requirement for a converter switching frequency of 4kHz and above, a computer model of the proposed supply filter was designed to allow graphical representation of the response and allow comparison between different component combinations. Analysis of filter attenuation showed that a filter resonant frequency of approximately 1.5kHz would be required to meet the design specification. Therefore, a relationship between the desired L and C values was derived as:

$$LC = \frac{1}{88826440}$$

The next step was to examine the power-factor of the proposed filter. Unity power factor is desirable at all operating conditions to minimise converter disturbance. It can

be shown, consequently, that the capacitor is more detrimental to filter PF than the inductor. It is necessary, therefore, to minimise the capacitor size while maintaining the desired filter resonant frequency.

$$X_L = 2\pi fL \qquad \& \qquad X_c = \frac{1}{2\pi fC}$$

If capacitance must be minimised, inductor size must also be carefully considered. A larger inductor increases filter conduction loss and must be balanced to avoid reducing filter efficiency. A compromise was necessary, therefore, to achieve a flat power factor without a large inductor. The chosen values were matched with off the shelf components and are:

Capacitor	Inductor
6μF	1.8mH

Table 60 - Supply Filter Component Values

A metalised polypropylene non-polar capacitor motor start capacitor was selected for its rating of 600v and 10A. The inductor carries the supply directly and so also had to be sized correctly for the current demand, calculated to be a maximum of 10A during maximum power.

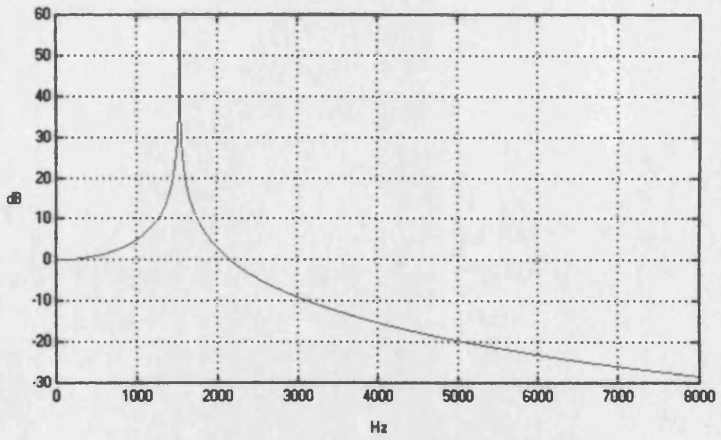

Figure 197 - Filter Attenuation (dB) vs. Frequency

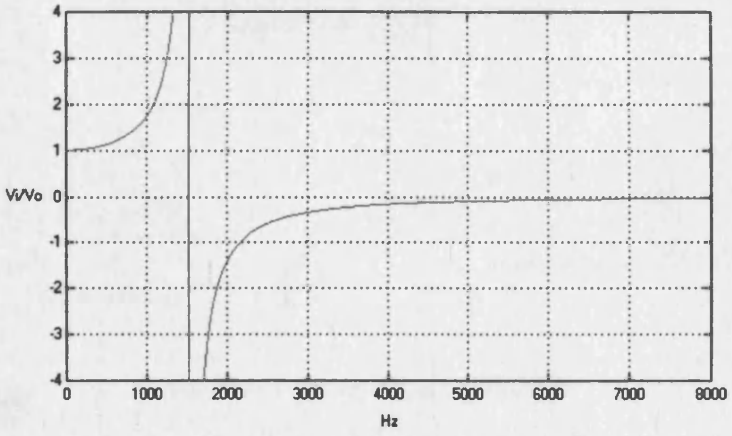

Figure 198 - Filter Voltage Transfer Ratio vs. Frequency

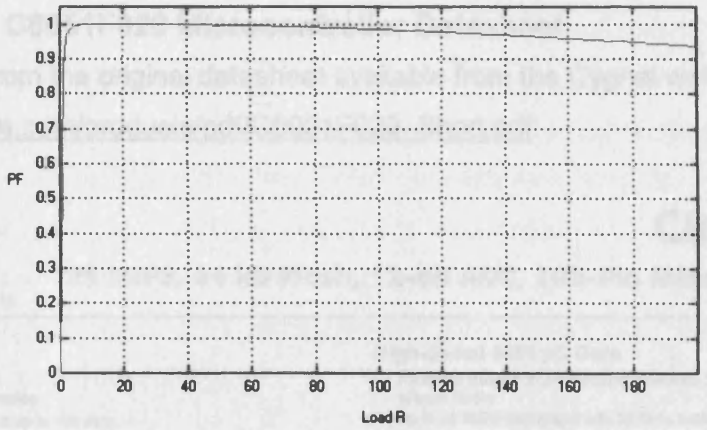

Figure 199 - Filter Power Factor vs. Load

As testing progressed from passive loads to a larger induction motor, the supply filter was found to emit a loud high-pitched whining noise, particularly when employing the semi-symmetrical PWM strategy. This was traced to the inductors that were found to be saturating with the increased conducted current and impairing supply filter operation. Larger inductors with increased current rating were obtained and overcame this problem.

A8 Cygnal C8051F020 Microcontroller Datasheet

This extract is from the original datasheet available from the Cygnal website.

http://www.silabs.com/products/pdf/C8051F020_Short.pdf

C8051F020

25 MIPS, 64 kB Flash, 12-Bit ADC, 100-Pin Mixed-Signal MCU

Analog Peripherals

12-Bit ADC

- ±1 LSB INL; no missing codes
- Programmable throughput up to 100 ksps
- 8 external inputs; programmable as single-ended or differential
- Programmable amplifier gain: 16, 8, 4, 2, 1, 0.5
- Data-dependent windowed interrupt generator
- Built-in temperature sensor (±3 °C)

8-Bit ADC

- ±1 LSB INL; no missing codes
- Programmable throughput up to 500 ksps
- 8 external inputs
- Programmable amplifier gain: 4, 2, 1, 0.5

Two 12-Bit DACs

- Can synchronize outputs to timers for jitter-free waveform generation

Two Comparators

Internal Voltage Reference

V_{DD} Monitor/Brown-out Detector

On-Chip JTAG Debug & Boundary Scan

- On-chip debug circuitry facilitates full speed, non-intrusive in-system debug (no emulator required)
- Provides breakpoints, single stepping, watchpoints, stack monitor
- Inspect/modify memory and registers
- Superior performance to emulation systems using ICE-chips, target pods, and sockets
- IEEE1149.1 compliant boundary scan

High-Speed 8051 µC Core

- Pipelined instruction architecture; executes 70% of instructions in 1 or 2 system clocks
- Up to 25 MIPS throughput with 25 MHz system clock
- 22 vectored interrupt sources

Memory

- 4352 bytes data RAM
- 64 kB Flash; in-system programmable in 512-byte sectors (512 bytes are reserved)
- External parallel data memory interface

Digital Peripherals

- 64 port I/O; all are 5 V tolerant
- Hardware SMBus™ (I2C™ compatible), SPI™, and two UART serial ports available concurrently
- Programmable 16-bit counter/timer array with 5 capture/compare modules
- 5 general-purpose 16-bit counter/timers
- Dedicated watchdog timer; bidirectional reset
- Real-time clock mode using Timer 3 or PCA

Clock Sources

- Internal programmable oscillator: 2–16 MHz
- External oscillator: Crystal, RC, C, or Clock
- Can switch between clock sources on-the-fly

Supply Voltage: 2.7 to 3.6 V

- Typical operating current: 10 mA at 25 MHz
- Multiple power saving sleep and shutdown modes

100-Pin TQFP

Temperature Range: –40 to +85 °C

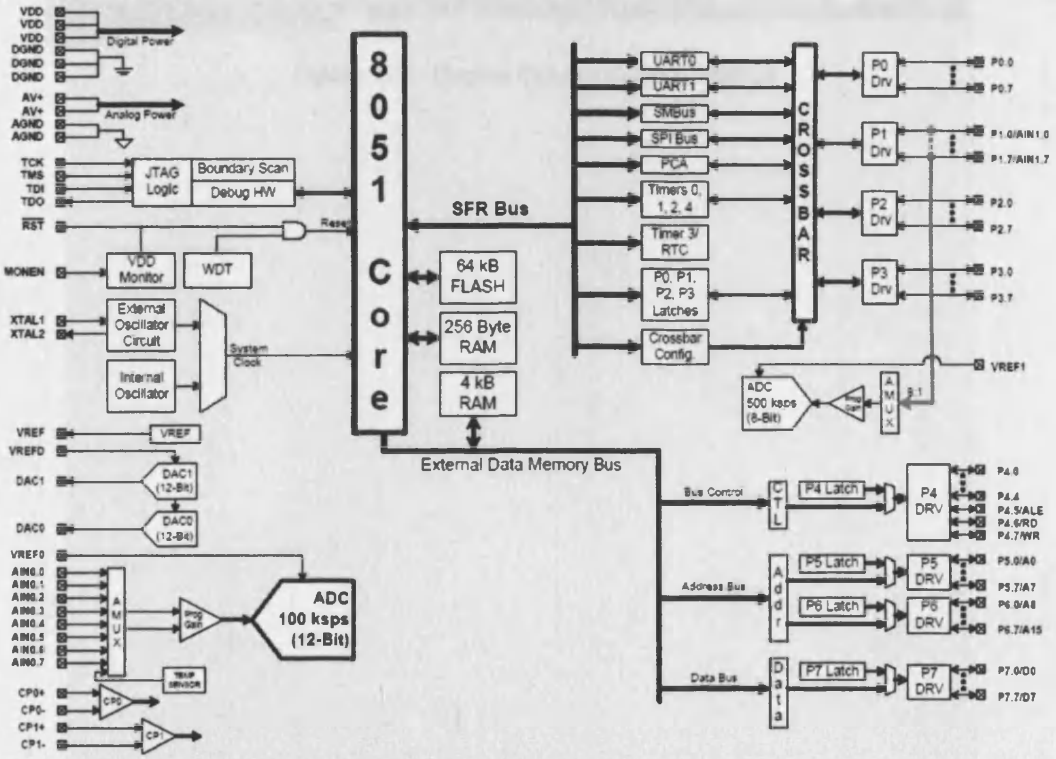

The laboratory matrix converter control system clock the microcontroller at 24MHz to simplify operating frequency selection. A processor instruction executed in 41.667ns allowed for very fine control of switch commutation and conducting duration. The standard 8051 processor generally has 32 I/O pins whereas the C8051F020 derivative has 64 I/O pins, making hardware interfacing less challenging when implementing several resource hungry components. Additional useful features of the MCU include multiple analogue-to-digital and digital-to-analogue converters, should these be required by future control strategies.

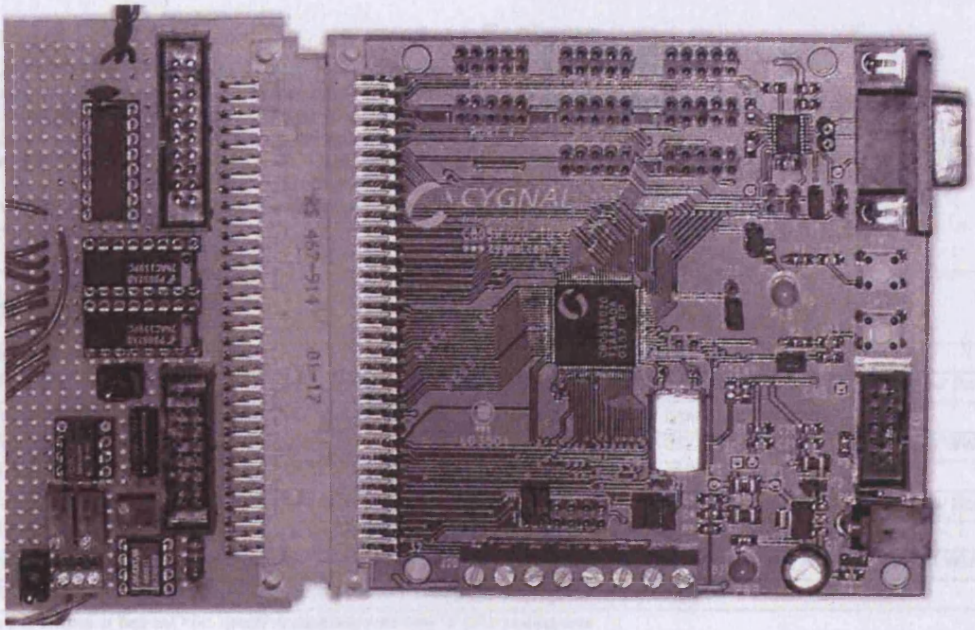

Figure 200 - Cygnal Control System Boards

A9 Fairchild Semiconductor 74AC139 Binary Decoder Datasheet

This extract is from the datasheet available on the Fairchild Semiconductor website:

http://www.fairchildsemi.com/ds/74/74AC139.pdf

FAIRCHILD SEMICONDUCTOR™

November 1988
Revised November 1999

74AC139 • 74ACT139
Dual 1-of-4 Decoder/Demultiplexer

General Description

The AC/ACT139 is a high-speed, dual 1-of-4 decoder/demultiplexer. The device has two independent decoders, each accepting two inputs and providing four mutually-exclusive active-LOW outputs. Each decoder has an active-LOW Enable input which can be used as a data input for a 4-output demultiplexer. Each half of the AC/ACT139 can be used as a function generator providing all four minterms of two variables.

Features

- I_{CC} reduced by 50%
- Multifunction capability
- Two completely independent 1-of-4 decoders
- Active LOW mutually exclusive outputs
- Outputs source/sink 24 mA
- ACT139 has TTL-compatible inputs

Ordering Code:

Order Number	Package Number	Package Description
74AC139SC	M16A	16-Lead Small Outline Integrated Circuit (SOIC), JEDEC MS-012, 0.150" Narrow Body
74AC139SJ	M16D	16-Lead Small Outline Package (SOIC), EIAJ Type II, 5.3mm Wide
74AC139MTC	MTC16	16-Lead Thin Shrink Small Outline Package (TSSOP), JEDEC MO-153, 4.4mm Wide
74AC139PC	N16E	16-Lead Plastic Dual-In-Line Package (PDIP), JEDEC MS-001, 0.300" Wide
74ACT139SC	M16A	16-Lead Small Outline Integrated Circuit (SOIC), JEDEC MS-012, 0.150" Narrow Body
74ACT139SJ	M16D	16-Lead Small Outline Package (SOIC), EIAJ Type II, 5.3mm Wide
74ACT139MTC	MTC16	16-Lead Thin Shrink Small Outline Package (TSSOP), JEDEC MO-153, 4.4mm Wide
74ACT139PC	N16E	16-Lead Plastic Dual-In-Line Package (PDIP), JEDEC MS-001, 0.300" Wide

Device also available in Tape and Reel. Specify by appending suffix letter "X" to the ordering code.

Connection Diagram

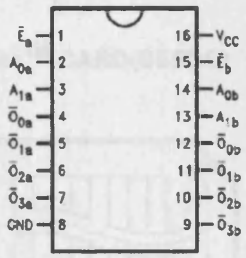

Pin Descriptions

Pin Names	Description
A_0, A_1	Address Inputs
$\overline{E}$	Enable Inputs
$\overline{O}_0$–$\overline{O}_3$	Outputs

FACT™ is a trademark of Fairchild Semiconductor Corporation.

A10 Samsung Smartmedia Memory Card Datasheet

This extract is from the original datasheet available from the Samsung website.

http://www.samsung.com/Products/Semiconductor/Flash/FlashCard/SmartMedia/8MByte/K9S6408V0C/K9S56_28_64.PDF

SmartMedia™ Card

FEATURES

- Single 2.7V~3.6V Supply
- Organization
  - Memory Cell Array :
    8MB(K9S6408V0X) : (8M + 256K)bit x 8bit
    16MB(K9S2808V0X) : (16M + 512K)bit x 8bit
    32MB(K9S5608V0X) : (32M + 1,024K)bit x 8bit
  - Data Register : (512 + 16)bit x8bit
- Automatic Program and Erase
  - Page Program : (512 + 16)Byte
  - Block Erase
    32MB, 16MB(K9S56/2808V0X) : (16K + 512)Byte
    8MB (K9S6408V0X) : (8K + 256)Byte
- 528-Byte Page Read Operation
  - Random Access : 10μs(Max.)
    " K9S6408V0B/A : 7μs(Max.)
    " K9S6408V0C : 10μs(Max.)
  - Serial Page Access : 50ns(Min.)
- Fast Write Cycle Time
  - Program Time : 200μs(Typ.)
  - Block Erase Time : 2ms(Typ.)
- Command/Address/Data Multiplexed I/O Port
- Hardware Data Protection
  - Program/Erase Lockout During Power Transitions
- Reliable CMOS Floating-Gate Technology
  - Endurance : 100K Program/Erase Cycles
    " K9S6408V0X : 1Million Program/Erase Cycles
  - Data Retention : 10 years
- Command Register Operation
- 22pad SmartMedia™(SSFDC)
- Unique ID for Copyright Protection

GENERAL DESCRIPTION

Using Nand flash memory, SmartMedia provides the most cost-effective solution for the solid state mass storage market. A program operation is implemented by the single page of 528 bytes in typical 200μs and an erase operation is done by the single block of 16K bytes (K9S6408V0X: 8K bytes) in typical 2ms. Data in a page can be read out at 50ns cycle time per byte. The I/O pins serve as ports for address and data inputs/outputs as well as command inputs. The on-chip writing controller automates all program and erase functions including pulse repetition, where required, and internal verification and margining of data. Even the write-intensive systems can take advantage of the SmartMelda's extended reliability of 100K program/erase cycles by providing ECC(Error Correcting Code) with real time mapping-out algorithm. (*Endurance varies according to its density, please refer to Features). SmartMedia is an optimum solution for data storage applications such as solid state file storage, digital voice recorder, digital still camera and other portable applications requiring non-volatility.

PIN DESCRIPTION

Device	Unique ID Support
K9S2808V0X K9S5608V0X K9S6408V0C	O
K9S6408V0A/M	X

SmartMedia™ CARD(SSFDC)

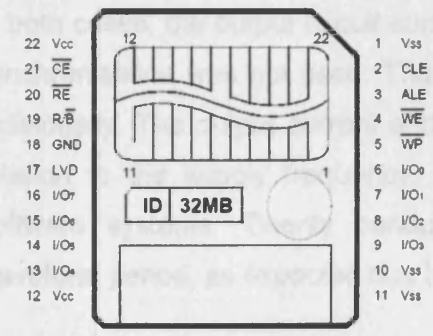

22 PAD SmartMedia™

PIN DESCRIPTION

Pin Name	Pin Function
I/O0 ~ I/O7	Data Input/Outputs
CLE	Command Latch Enable
ALE	Address Latch Enable
$\overline{CE}$	Chip Enable
$\overline{RE}$	Read Enable
$\overline{WE}$	Write Enable
$\overline{WP}$	Write Protect
LVD	Low Voltage Detect
GND	Ground
R/$\overline{B}$	Ready/Busy output
Vcc	Power
Vss	Ground
N.C	No Connection

NOTE : Connect all Vcc and Vss pins of each device to common power supply outputs and do not leave Vcc or Vss disconnected.
The pin 17(LVD) is used to detect 5V or 3.3V product electrically. Please, refer to the SmartMedia Application note for detail.

A11 Initial Converter Testing

DC Testing

The majority of the electrical components used in the laboratory matrix converter were inherited from a previous investigation. Each set of bi-directional switch modules were checked, both physically and then electrically using a low voltage DC supply to verify the ability to both block and conduct electric current in the forwards direction. A resistive 25Ω load was connected between the output of each switch and ground to form a simple circuit, as shown below:

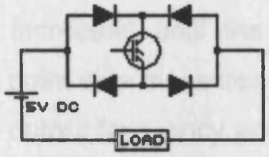

Figure 201 - DC Test Circuit

The power supply connections were then reversed in order to verify bi-directional conduction. A subsequent experiment saw each bi-directional module rapidly switched on and off using a single output from the control board to confirm operation at the intended switching frequency for the completed system.

AC Testing

Each individual bi-directional switch was then tested using a AC power source. This was derived from the mains electrical supply with an autotransformer to reduce this to a safer 20V with the same 25Ω load resistance. The switches were individually tested at a frequency of 1kHz with a fixed duty-cycle. Three switch modules were subsequently connected to the supply to confirm simultaneous operation. As expected in both cases, the output circuit currents were found to drift in relation to the supply as synchronisation was not used. This was then enabled, with each switch again tested individually. The output current and voltage pulses were observed to be stationary in relation to the supply frequency, thus verifying the synchronisation hardware and software systems. Twenty conduction pulses were evident during each supply waveform period, as expected due to the 1kHz switching frequency and 50Hz supply.

AC Experimentation

The first 'full' matrix converter test was conducted using a three-phase input single-phase output configuration, comprised of three bi-directional switch modules as shown in Figure 202. The load resistance used initially was augmented with a variable inductor to remove the high frequency harmonics and release the fundamental output current waveform.

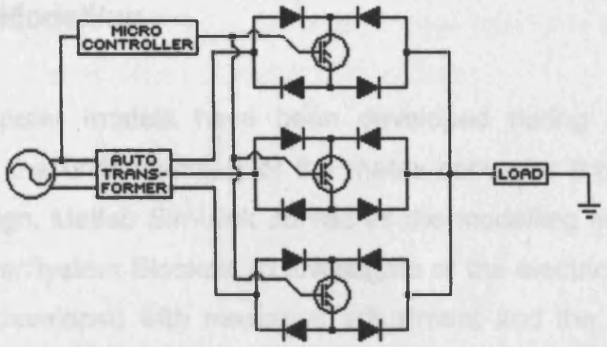

Figure 202 - Single-Phase Output Test Configuration

With the matrix converter controller set to generate an output frequency of 50Hz, the load inductance was gradually increased until the fundamental current waveform emerged. The inductance at this point was measured to be approximately 1.8mH. The MCU was then used to vary the output frequency and amplitude to test the converter and control system.

A12 Computer Modelling

A number of computer models have been developed during the course of this investigation to aid the understanding of the matrix converter topology and facilitate control system design. Matlab Simulink served as the modelling environment with the addition of the PowerSystem Blockset to investigate of the electrical circuit behaviour. The models were developed with maximum adjustment and the ability to modify all operating parameters, including the switching frequency, during model execution.

Simulink is a graphical programming environment for users of Matlab, allowing modelling and analysis of dynamic systems. Blocks representing individual mathematical processes can be joined graphically to create system models with optimised Matlab code generated upon execution of Simulink. This is a powerful program as it allows complex systems to described and modelled mathematically with little programming knowledge required. The PowerSystem Blockset is an additional module that contains accurate models of individual electrical devices such as diodes, MOSFETs and thyristors and more complex components like synchronous and induction machines. It is also possible to use the standard mathematical blocks that are included within Simulink for constructing control systems for the power electronic devices. All models developed typically used a variable ODE solver as recommended by Matlab when implementing models containing elements from the PowerSystem Blockset. The variable step solver, as opposed to a fixed step solver, reduced model execution times while maintaining detail at key points of the simulation.

Original Model

Initial efforts focused on implementation of the Original Venturini algorithm. The equations for the calculation of the switch conduction duration are:

$$[M_{(t)}] = \left(\frac{\alpha_1}{3}\right)\begin{Bmatrix} 1+2qCS(0) & 1+2qCS(-\frac{2}{3}\pi) & 1+2qCS(-\frac{4}{3}\pi) \\ 1+2qCS(-\frac{4}{3}\pi) & 1+2qCS(0) & 1+2qCS(-\frac{2}{3}\pi) \\ 1+2qCS(-\frac{2}{3}\pi) & 1+2qCS(-\frac{4}{3}\pi) & 1+2qCS(0) \end{Bmatrix} +$$

$$\left(\frac{\alpha_2}{3}\right)\begin{Bmatrix} 1+2qCA(0) & 1+2qCA(-\frac{2}{3}\pi) & 1+2qCA(-\frac{4}{3}\pi) \\ 1+2qCA(-\frac{2}{3}\pi) & 1+2qCA(-\frac{4}{3}\pi) & 1+2qCA(0) \\ 1+2qCA(-\frac{4}{3}\pi) & 1+2qCA(0) & 1+2qCA(-\frac{2}{3}\pi) \end{Bmatrix}$$

Where:

$CS(x) = Cos(\omega_m t + x)$ $\quad$ $CA(x) = Cos[-(\omega_m + \omega_i)t + x]$ $\quad$ $\omega_m = \omega_o - \omega_i$

$\alpha_1 = \frac{1}{2}(1 + Tan\ \phi_i\ Cot\ \phi_o)$ $\quad$ $\alpha_2 = 1 - \alpha_1$ $\quad$ $\alpha_1, \alpha_2 \geq 0$

$q = V_o / V_i$ $\quad$ $0 \leq q \leq \frac{1}{2}$ = output amplitude

The first model was designed with the assumption that input and output displacement angles were equal, to simplify the calculation. Therefore:

$$\text{If:} \quad \phi_i = \phi_o \quad \therefore \quad \alpha_1 = \tfrac{1}{2}(1 + \text{Tan}\,\phi_i \,\text{Cot}\,\phi_o) = 1 \quad \& \quad \alpha_2 = 0$$

$$\therefore$$

$$[M_{(t)}] = \left(\frac{1}{3}\right)\begin{Bmatrix} 1+2q\text{Cos}(\omega_m t) & 1+2q\text{Cos}(\omega_m t - \frac{2}{3}\pi) & 1+2q\text{Cos}(\omega_m t - \frac{4}{3}\pi) \\ 1+2q\text{Cos}(\omega_m t - \frac{4}{3}\pi) & 1+2q\text{Cos}(\omega_m t) & 1+2q\text{Cos}(\omega_m t - \frac{2}{3}\pi) \\ 1+2q\text{Cos}(\omega_m t - \frac{2}{3}\pi) & 1+2q\text{Cos}(\omega_m t - \frac{4}{3}\pi) & 1+2q\text{Cos}(\omega_m t) \end{Bmatrix}$$

As only a single-phase output matrix converter was being modelled here, only the first column of equations was required. The following equations could then be used to calculate the conduction duration.

$$T_1 = \frac{T_{seq}}{3}\,[1 + 2\,q\,\text{Cos}\,(K\,T_{seq}\,\omega_m)]$$

$$T_2 = \frac{T_{seq}}{3}\,[1 + 2\,q\,\text{Cos}\,(K\,T_{seq}\,\omega_m - \tfrac{4}{3}\pi)]$$

$$T_3 = \frac{T_{seq}}{3}\,[1 + 2\,q\,\text{Cos}\,(K\,T_{seq}\,\omega_m - \tfrac{2}{3}\pi)]$$

$$0 \le q \le \tfrac{1}{2}$$

$$\omega_m = \omega_i - \omega_o$$

$$K = 1, 2, 3\ldots$$

T_{seq} = Length of Switching period

The resultant Simulink model subroutine for the calculation of T_2 is shown in Figure 203. The subroutine received data from four input blocks, shown as the lozenge shapes labelled K, T_{seq}, q and ω_m, to provide the result at Out2.

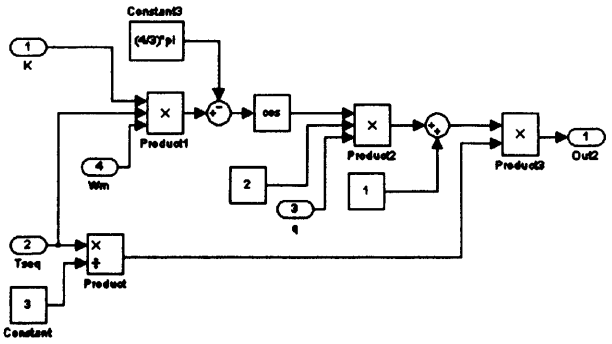

Figure 203 - Venturini Calculation Subroutine

The first step in the calculation multiplies K, T_{seq} and ω_m together. A phase lag (if required) is then inserted with the subtraction of $\frac{4}{3}\pi$. The cosine of this result is then

calculated before being doubled and multiplied by q. The final result is then obtained by multiplying the previous result by ⅓ T_{seq}.

There are two similar versions of the above subroutine for the calculation of T_1 & T_3. These are grouped together and receive identical input parameters, as in Figure 204.

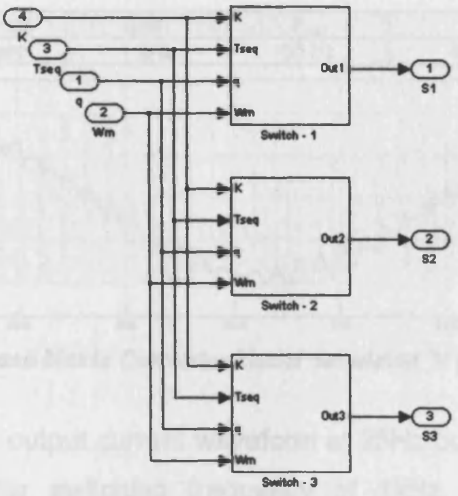

Figure 204 - 'Switches' Subroutine

The topmost view of the model shows the complete configuration (Figure 205). The output amplitude (q) and frequency (ω_o) and switching frequency are entered into the blocks on the far top left. The parameter ω_o is used to calculate ω_m assuming a supply frequency of 50Hz. This value is then converted from a frequency to radians by the triangular gain block. The third, larger block is used to specify the switching frequency and subsequently generates the values T_{seq} and K.

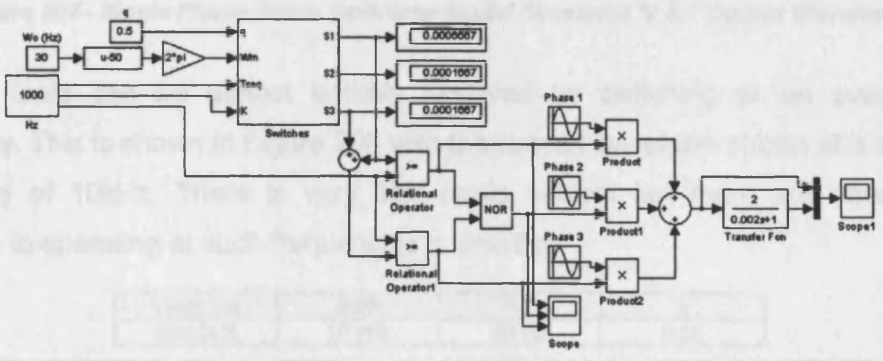

Figure 205 - Single Output Phase Matrix Converter Model Top View

Each 'switches' subblock (Figure 204) receives the specified data and provides three outputs, the values T_1, T_2 & T_3. The numerical value of each is shown in the three model display blocks. Twin relational operators are used to determine the phase conducting sequencing on the basis of T_1, T_2 & T_3 and the switching frequency.

For simplicity, this first model did not employ any PSB elements, but used standard Simulink models. The sine function generators represent the power supply with multiply blocks that allow 'conduction' to occur. The resulting summed output is short samples of the three-phase supplies, as shown in Figure 206. The 'current' waveform is derived by passing the output 'voltage' through a transfer function that models a resistive/inductive load.

Venturini	SWF	F_{out}	Q
Standard	1 kHz	30 Hz	0.50

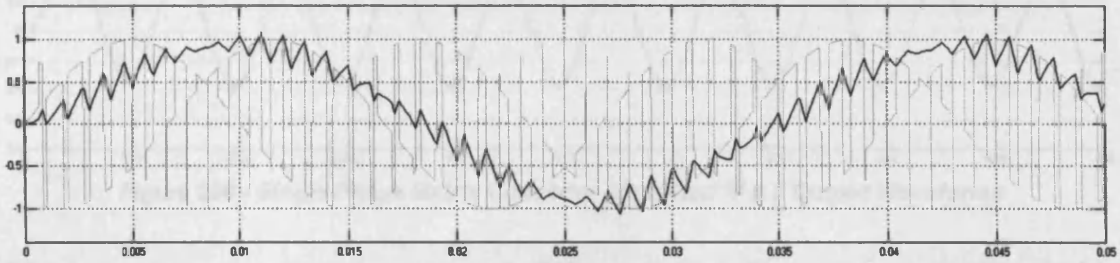

Figure 206 - Single Phase Matrix Converter Model Simulated 'V & I' Output Waveforms

It shows the fundamental output current waveform at 25Hz but exhibits rippling. This is due to the low converter switching frequency of 1kHz. Doubling the switching frequency has the effect of reducing current ripple considerably (Figure 207).

Venturini	SWF	F_{out}	q
Standard	2 kHz	30 Hz	0.50

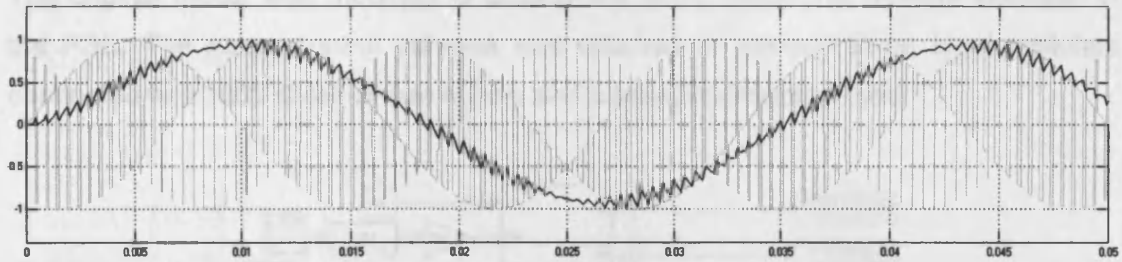

Figure 207 - Single Phase Matrix Converter Model Simulated 'V & I' Output Waveforms

Current ripple can be almost entirely removed by switching at an even higher frequency. This is shown in Figure 208 with the current waveform shown at a switching frequency of 10kHz. There is very little ripple evident but there are considerable penalties to operating at such frequencies in practice.

Venturini	SWF	F_{out}	q
Standard	10 kHz	30 Hz	0.50

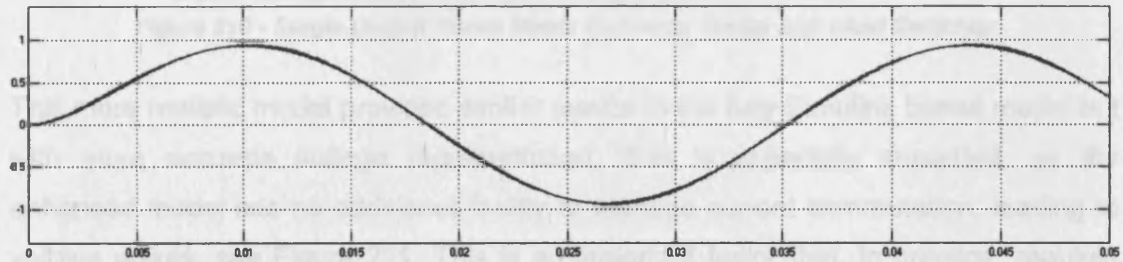

Figure 208 - Single Phase Matrix Converter Simulated 'V & I' Output Waveforms

An increase in converter switching frequency increases the number of times the power electronic devices must turn on and off. Each time a device is turned on and then off, switching loss occur. A balance must, therefore, be found between reducing output waveform ripple and converter switching loss.

Venturini	SWF	F_{out}	q
Standard	10 kHz	200 Hz	0.50

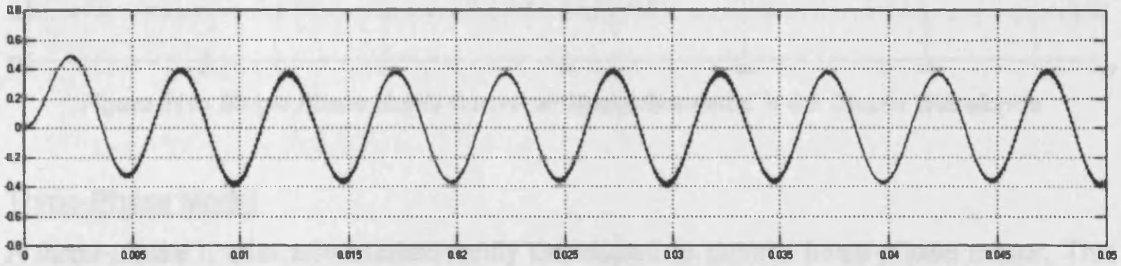

Figure 209 - Single Phase Matrix Converter Simulated 'V & I' Output Waveforms

There is also no output frequency limitation, making the matrix converter highly flexible. This is demonstrated in Figure 209 that shows an output waveform frequency of 200Hz, something not possible with the only other direct AC-AC converter, the Cycloconverter.

Original Model with PSB Switches

The original model was modified to employ the power electronic models available in the PSB. The same control scheme was retained to operate three ideal switches connected to a 100V three-phase supply and a resistive-inductive load.

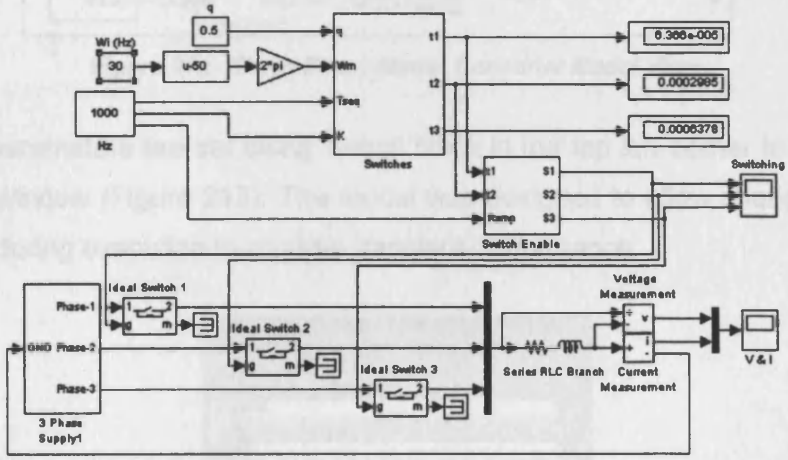

Figure 210 - Single Output Phase Matrix Converter Model with Ideal Switches

This more realistic model provided similar results to the fully Simulink based model but with more accurate voltage representation. This is especially important, as the enhanced model has no additional facility to manage current commutation, leading to voltage spikes, see Figure 211. This is an important factor that, in practice, requires voltage clamping or more advanced switch commutation strategy.

Venturini	SWF	F_{out}	q	Load R	Load L
Standard	1 kHz	30 Hz	0.50	0.5 Ω	8 mH

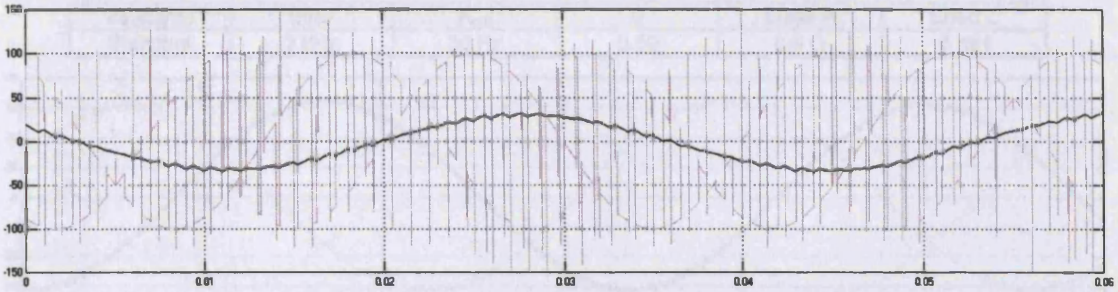

Figure 211 - Single Phase Matrix Converter Model Simulated 'V & I' Output Waveforms

Three-Phase Model

A three-phase model was subsequently developed to drive a three-phase motor. This model employed the full Venturini control scheme without assuming equal input & output displacement angles. The model is shown in Figure 212 and is based on nine bi-directional switches contained within the 'Switch Matrix' block. A three-phase resistive-inductive load is star connected to ground.

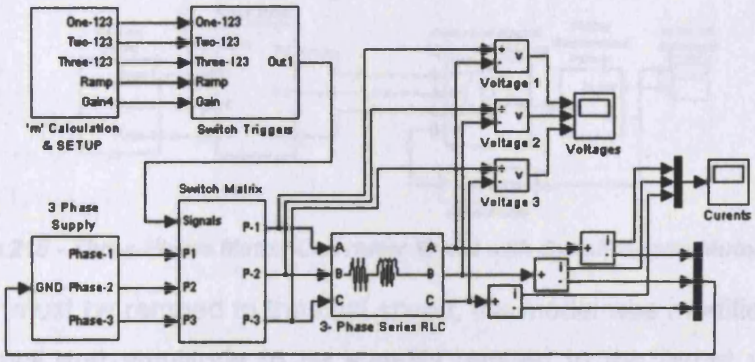

Figure 212 - Three-Phase Matrix Converter Model View

The model parameters are set using 'setup' block in the top left corner to bring up the parameters window (Figure 213). The model was designed to allow changes to model parameters during execution to analyse transient performance.

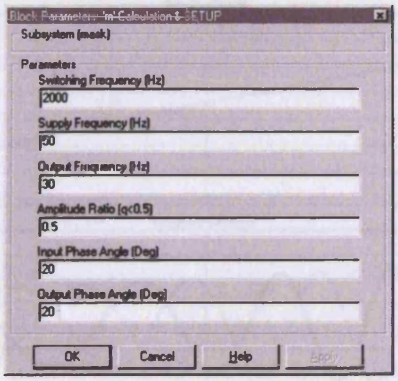

Figure 213 - Three-Phase Matrix Converter Model 'Parameters' Window

A sample output waveform is shown in Figure 214 with the above parameters.

Venturini	SWF	F_{out}	q	Load R	Load L
Standard	2 kHz	30 Hz	0.50	0.5 Ω	8 mH

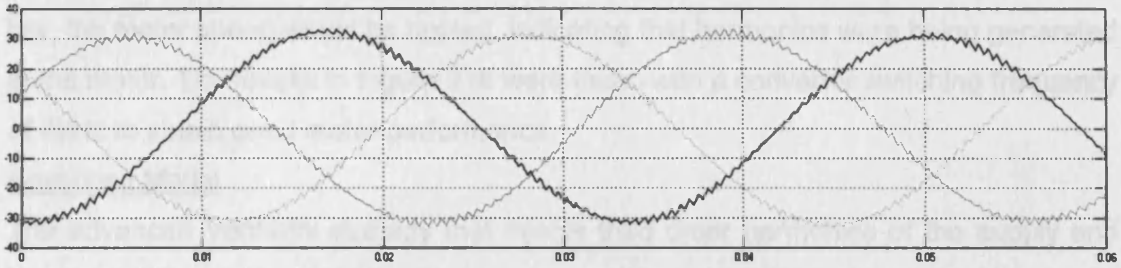

Figure 214 - Three-Phase Matrix Converter Model Simulated Output Current Waveforms

The passive resistive-inductive load was then replaced with a permanent magnet synchronous motor. A propeller load is simulated with a motor torque load related to the square of the rotor speed.

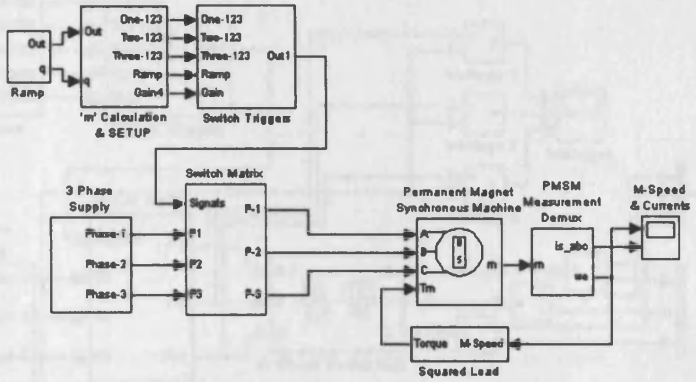

Figure 215 - Three-Phase Matrix Converter Model with Synchronous Motor Load

Since a motor must be ramped to the final speed, the model was modified to allow the output frequency and amplitude to be steadily ramped to the target values. These parameters are set in the 'ramp' block. The matrix converter is started at zero output amplitude and frequency, before being ramped to the final values of 20Hz and q=0.5. The motor speed is also measured and the results shown in Figure 216.

Venturini	SWF	F_{out}	q
Standard	4 kHz	0 - 20 Hz	0 - 0.50

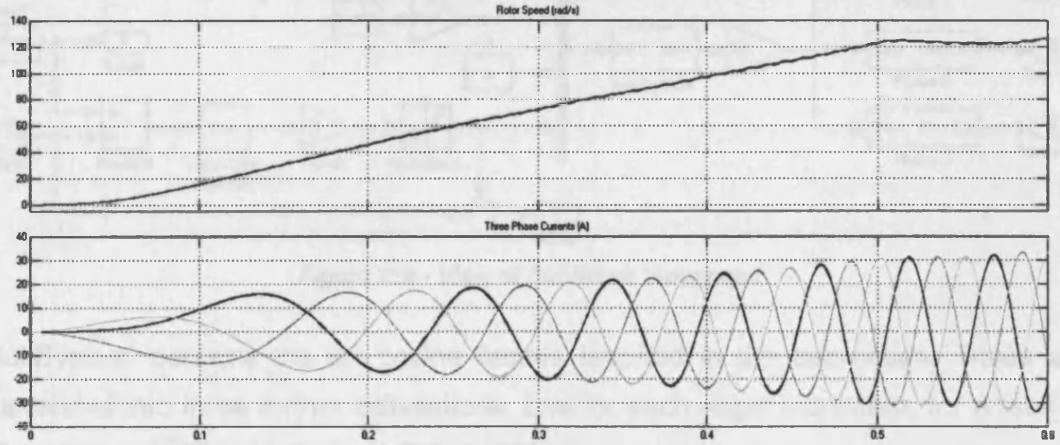

Figure 216 - Three-Phase Matrix Converter Model Simulated 'Motor & I' Waveforms

The motor speed ramps up gently to the target value under the control of the matrix converter before reaching a steady state value. It was found that the switching frequency had a considerable impact on the motor speed. If the frequency was too low, the motor speed would be rippled, indicating that harmonics were being generated in the motor. The results in Figure 216 were taken with a converter switching frequency of 4kHz to obtain good motor performance.

Advanced Model

The advanced Venturini strategy that injects third order harmonics of the supply and target waveforms to maximise the converter voltage transfer ratio was subsequently developed. Using the same approach as that used in the laboratory converter, the advanced Venturini was based around the six cosine operations necessary, contained in a single subsystem to simplify model configuration.

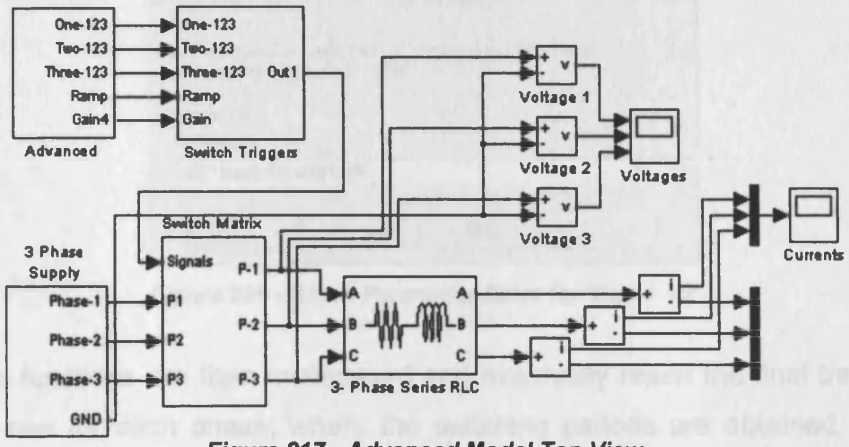

Figure 217 - Advanced Model Top View

The advanced Venturini strategy, contained in the 'Advanced' block, calculates the switching periods for the nine switches. The four parameters for the calculation, shown on the left of the block in Figure 218, are multiplexed to together into a single line for entry into the block called 'SubSystem'.

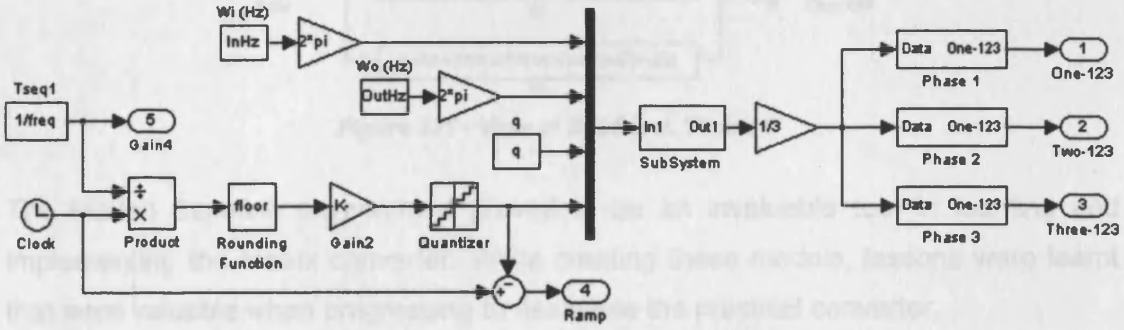

Figure 218 - View of SubBlock 'Advanced'

'SubSystem' contains the six cosine factors required in the calculation. These are subdivided into three further calculations, one for each angle increment, for a total of 18 equations boxes, as shown in Figure 219.

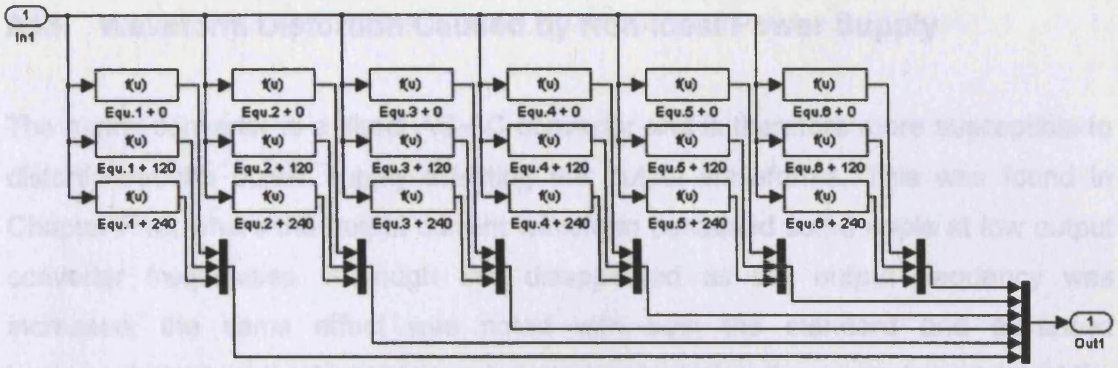

Figure 219 - View of SubBlock 'SubSystem'

Each cosine function block has an entry similar to that shown in Figure 220, for the block called 'Equ.1 + 0'. The parameters u[*x*] refer to the multiplexed inputs in numerical order.

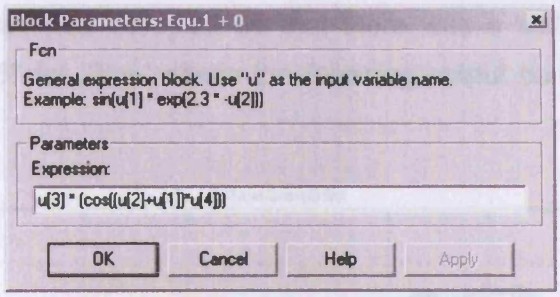

Figure 220 - Block Parameter Entry for 'Equ.1 +0'

The cosine functions are then multiplexed and eventually reach the final three 'Phase *X*' blocks, one for each phase, where the switching periods are obtained. Using the correct summation, Figure 221, shows the functions required to determine the switching periods for the switches of output Phase 1.

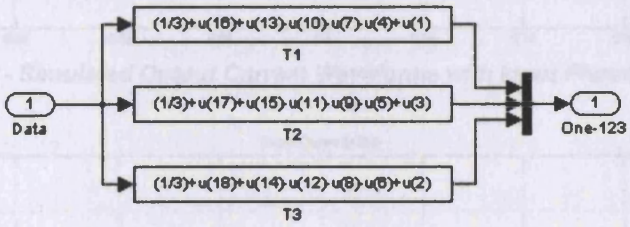

Figure 221 - View of SubBlock 'Phase 1'

The Matlab Simulink environment proved to be an invaluable tool in learning and implementing the matrix converter. While creating these models, lessons were learnt that were valuable when progressing to assemble the practical converter.

A13 Waveform Distortion Caused by Non-ideal Power Supply

The matrix converter is a direct AC-AC converter and is therefore more susceptible to distortion in the power supply affecting the output waveforms. This was found in Chapter Five, where the output current waveform contained some ripple at low output converter frequencies. Although this disappeared as the output frequency was increased, the same effect was noted with both the standard and advanced implementations of the Venturini control strategies. Using the computer model of the matrix converter described earlier in Appendix A12 [p267], supply distortion, similar to that shown in Figure 49 [p73], was added to the simulation. Although common mode distortion was cancelled out in the converter load, phase angle imbalance was found to cause the effect found with the laboratory converter. When the phase angle between the three input phases was modified so that there was a distortion of +4° for the 'Yellow' phase and -5° for 'Blue' phase the following output current waveforms were found at 5Hz.

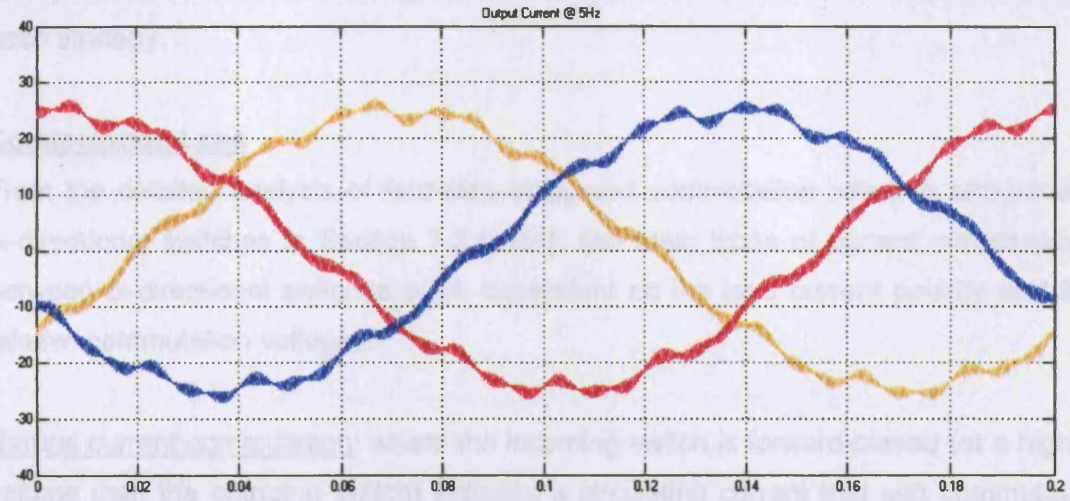

Figure 222 - Simulated Output Current Waveforms with Input Phase Distortion

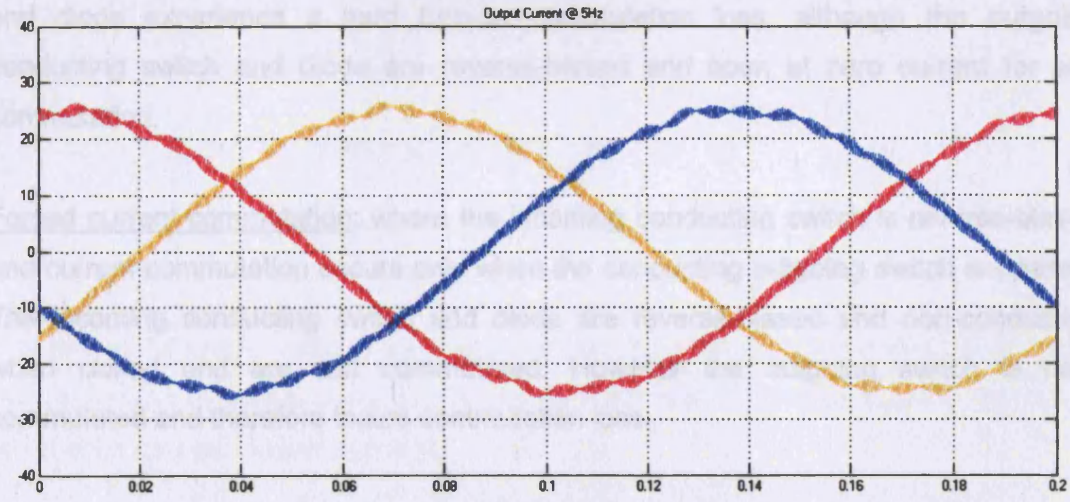

Figure 223 - Simulated Output Current Waveforms Without Input Phase Distortion

A14 Anti-Parallel IGBT Matrix Converter Numerical Loss Model

A numerical loss model was also developed within Matlab Simulink to simulate a three-phase anti-parallel IGBT based matrix converter employing four-step staggered commutation. The model assumes snubberless operation to reduce complexity and mirrors the approach used by Apap et al [112], therefore allowing verification of this model with published data. The model calculates the load current with knowledge of the converter output frequency, load resistance and inductance to determine conduction loss. IGBT and diode switching loss is assumed to vary linearly with the device voltage change during the commutation event. The turn-on and turn-off energy loss is also assumed to vary linearly with the conducted collector current. The model calculates the precise supply voltages and load current at each commutation event so that low converter switching frequencies do not reduce model accuracy due to significant changes in supply voltage during a commutation cycle. Comparison between the standard, semi-symmetrical PWM and 'Opti-Soft' switching sequences is also possible in addition to being able to compare the device loss in each IGBT for each strategy.

Commutation Loss

From the detailed analysis of four-step staggered commutation between anti-parallel bi-directional switches in Section 7.3 [p153], two main types of current commutation between bi-directional switches exist, dependent on the load current polarity and the relative commutation voltages.

Natural current commutation: where the incoming switch is forward-biased (at a higher voltage than the outgoing switch) inducing a circulating current that soft commutates the outgoing conducting devices. When closed, both the incoming conducting switch and diode experience a hard turn-on commutation loss, although the outgoing conducting switch and diode are reverse-biased and open at zero current for soft commutation.

Forced current commutation: where the incoming conducting switch is reverse-biased and current commutation occurs only when the conducting outgoing switch is opened. The incoming conducting switch and diode are reverse-biased and non-conducting when closed and are soft commutated. However the outgoing switch is hard commutated and therefore incurs commutation loss.

The numerical model also makes the following assumptions:

"Soft IGBT Commutations are assumed lossless as the energy loss is an order of magnitude less than hard commutations" Comparison of Calculated and measured losses in Direct AC-AC converters, M. Bland, P. Wheeler, J. Clare, L. Empringham 2001

Diode turn-on losses *"...can be neglected in diode switching losses because they are very small."* Analysis and Evaluation of Bi-Directional Power Switch Losses for Matrix Converter Drive, J. Kang, H, Hara, E, Yamamoto, E, Watanabe. 2002

Therefore Table 61 describes the numerical relationship between conducted voltage and current with commutation loss, as implemented in the loss model.

Incoming Voltage	Load Current	Current Commutation	Outgoing Switch		Incoming Switch	
			IGBT	Diode	IGBT	Diode
Higher	Positive	Natural	0	$e_{rec}\,\Delta V_d\,\Delta I_d$	$e_{on}\,\Delta V_{ce}\,\Delta I_c$	0
Higher	Negative	Forced	$e_{off}\,\Delta V_{ce}\,\Delta I_c$	0	0	0
Lower	Positive	Forced	$e_{off}\,\Delta V_{ce}\,\Delta I_c$	0	0	0
Lower	Negative	Natural	0	$e_{rec}\,\Delta V_d\,\Delta I_d$	$e_{on}\,\Delta V_{ce}\,\Delta I_c$	0

Table 61 - Anti-parallel IGBT (Four-Step) Commutation Loss Summary

Conduction Loss

The $V_{ce(sat)}$-I_c characteristic of the IGBT are linearised in the form:

$$V_{ce(sat)} = V_{ce0} + r_{ce}\, I_c$$

V_{ce0} = IGBT collector-emitter drop voltage at zero current

r_{ce} = IGBT on-state resistance for the linearised characteristic

The instantaneous conduction loss in an IGBT is therefore:

$$P_{cond,IGBT}(t) = V_{ce0}\, I_c\,(t) + r_{ce}\, I_c^{\,2}\,(t)$$

Similarly, the instantaneous diode conduction loss is:

$$P_{cond,Diode}(t) = V_{f0}\, I_c\,(t) + r_d\, I_c^{\,2}\,(t)$$

V_{f0} = Diode forward voltage drop at zero current

r_{ce} = Diode on-state resistance for the linearised characteristic

The sinusoidal load current is always conducted by a series combination of an IGBT and diode and therefore assuming an output RMS current of magnitude I_o, the mean conduction loss per output phase is:

$$P_{cond,Phase} = (V_{ce0} + V_{f0})I_o\,[(2\sqrt{2})/\pi] + (r_{ce} + r_d)I_o^{\,2}\,(t)$$

Operation

The model starts by defining the operating conditions of the converter and the IGBT and diode device characteristics, before initialising the required matrices to store model parameters. A loop then calculates the three-phase supply voltages (supply(i,1-3) before implementing the advanced Venturini control algorithm to determine the switching periods (AMods(i,1-3)). This is used to determine the output voltage (AVout(i,1)) and current (AIout(i,1)). The three commutation sequences, Standard(i,1-3), Semisym(i,1-3) and Optisoft(i,1-3) are then calculated for later implementation and comparison followed by the (per-output-phase) conduction loss (CondLoss), as described above.

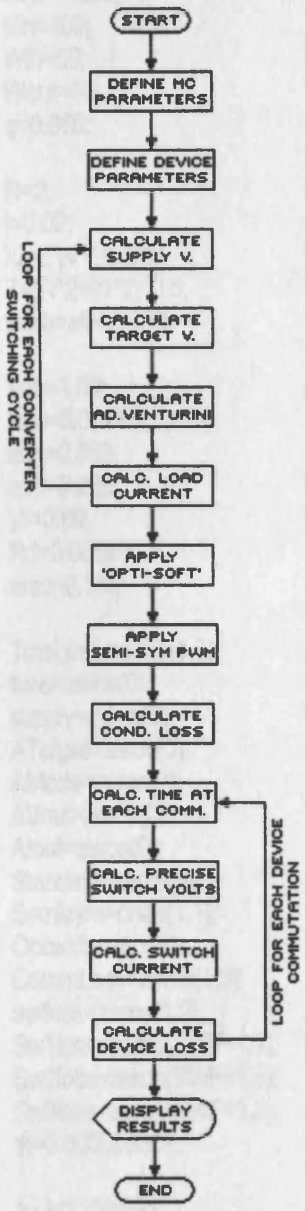

The second loop then iterates through each device commutation of each switching cycle at the instant defined by 'Tcom' that is obtained from the individual switching periods. 'SwOut' and 'SwIn' store the outgoing and incoming switches respectively and therefore 'SwVoltOut' and 'SwVoltIn' hold the respective instantaneous outgoing and incoming switch voltages. These two voltages then provide the voltage change (Vdif) at each commutation. To complete the commutation loss calculation, the instantaneous load current (IoutINST) at time 'Tcom' is found. The outgoing (Eoff) and incoming (Eon) IGBT commutation loss, as defined by Table 61 is subsequently calculated with the total diode loss (Erec). At the end of every commutation loop, the switching loss is summed and stored in 'CommLoss(1,1-3)', one for each of the three commutation orders. The individual commutation loss experienced by each IGBT is also stored in 'swtloss' for subsequent comparison

The model iterates through each device commutation for a number equal to the converter switching frequency, calculating loss for one second of operation. As commutation loss is in Joules, one second of simulated operation provides a wattage loss. Once all the device commutations and switching sequences have been considered, the total converter loss is stored in 'TotaLoss(1,1-3)', and the results displayed.

Model Software

The complete Matlab software listing follows overleaf:

```
% Anti-parallel IGBT Matrix Converter Loss Model
% Models a three phase input, single phase output converter
% Employs the Advanced Venturini Control algorithm and compares Standard, SemiSym and Opti-Soft

SWF=1000;                                   % Converter Switching Frequency (Hz)
Vin=400;                                    % Supply Voltage (P-P)
Win=50;                                     % Supply Frequency (Hz)
Wout=10;                                    % Output Frequency (Hz)
q=0.866;                                    % Converter Voltage Transfer Ratio

R=2;                                        % Load Resistance (Ohm)
l=0.02;                                     % Load Inductance (Henry)
Xl=2*pi*Wout*l;                             % Inductor Impendence
Z=(R^2+Xl^2)^0.5;                           % Resultant Resistance
theta=atan(Xl/R);                           % Phase angle between load voltage and current

Vce=1.09;                                   % IGBT Collector-Emitter Voltage at Zero Current
Rce=0.00715;                                % IGBT Linearised On-state Resistance
eon=0.333;                                  % IGBT Turn-on Switching Energy Loss (microJ/VA)
eoff=0.225;                                 % IGBT Turn-off Switching Energy Loss (microJ/VA)
Vf=0.89;                                    % Diode Forward Voltage Drop at Zero Current
Rd=0.00589;                                 % Diode Linearised On-state Resistance
erec=0.166;                                 % Diode Recovery Energy Loss (microJ/VA)

TotaLoss=zeros(1,3);
time=zeros(0);
supply=zeros(0);
ATarget=zeros(0);
AMods=zeros(0);
AVout=zeros(0);
Alout=zeros(0);
Standard=zeros(0);
Semisym=ones(1,1);                          % Define 1st Switch In Semi-Symmetrical Sequence
Optisoft=zeros(0);
CommLoss=zeros(1,3);
swtloss=zeros(1,9);
Sw1loss=zeros(SWF+1,3);
Sw2loss=zeros(SWF+1,3);
Sw3loss=zeros(SWF+1,3);
tk=0.000000001;

for i=1:SWF+1;
 time(i,1)=((i-1)/SWF)+tk;

 supply(i,1)=Vin*cos(2*Win*pi*time(i,1));
 supply(i,2)=Vin*cos(2*Win*pi*time(i,1)-(2*pi/3));
 supply(i,3)=Vin*cos(2*Win*pi*time(i,1)-(4*pi/3));

 x=((1/(2*sqrt(3)))*cos(6*pi*Win*time(i,1)))-((1/6)*cos(6*pi*Wout*time(i,1)));
 ATarget(i,1)=q*Vin*(cos(2*pi*Wout*time(i,1))+x);

 AMods(i,1)=(1/3)*[1+(2*supply(i,1)*ATarget(i,1))/(Vin^2)];
 AMods(i,1)=AMods(i,1)+[((4*q)/(9*sqrt(3)))*sin(2*pi*Win*time(i,1)-0)*sin(3*2*pi*Win*time(i,1))];
 AMods(i,2)=(1/3)*[1+(2*supply(i,2)*ATarget(i,1))/(Vin^2)];
 AMods(i,2)=AMods(i,2)+[((4*q)/(9*sqrt(3)))*sin(2*pi*Win*time(i,1)-(2*pi/3))*sin(3*2*pi*Win*time(i,1))];
 AMods(i,3)=(1/3)*[1+(2*supply(i,3)*ATarget(i,1))/(Vin^2)];
 AMods(i,3)=AMods(i,3)+[((4*q)/(9*sqrt(3)))*sin(2*pi*Win*time(i,1)-(4*pi/3))*sin(3*2*pi*Win*time(i,1))];
```

```
 AVout(i,1)=[supply(i,1)*AMods(i,1)]+[supply(i,2)*AMods(i,2)]+[supply(i,3)*AMods(i,3)];
 Alout(i,1)=(Vin*q/Z)*cos((2*pi*time(i,1)*Wout)-theta);

% DETERMINES STANDARD SWITCHING ORDER
 Standard(i,1)=1;
 Standard(i,2)=2;
 Standard(i,3)=3;

% DETERMINES SEMI-SYMMETRICAL PWM SWITCHING ORDER
 Semisym(i,2)=mod(Semisym(i,1),3)+1;
 Semisym(i,3)=mod(Semisym(i,2),3)+1;
 Semisym(i+1,1)=Semisym(i,3);

% DETERMINES OPTI-SOFT SWITCHING ORDER
 if Alout(i,1)>0;
  if supply(i,1)==min(supply(i,1:3)); Optisoft(i,1)=1;
   elseif supply(i,2)==min(supply(i,1:3)); Optisoft(i,1)=2;
   else Optisoft(i,1)=3; end

   if supply(i,1)==median(supply(i,1:3)); Optisoft(i,2)=1;
   elseif supply(i,2)==median(supply(i,1:3)); Optisoft(i,2)=2;
   else Optisoft(i,2)=3; end

   if supply(i,1)==max(supply(i,1:3)); Optisoft(i,3)=1;
   elseif supply(i,2)==max(supply(i,1:3)); Optisoft(i,3)=2;
   else Optisoft(i,3)=3; end
  else
   if supply(i,1)==median(supply(i,1:3)); Optisoft(i,1)=1;
   elseif supply(i,2)==median(supply(i,1:3)); Optisoft(i,1)=2;
   else Optisoft(i,1)=3; end

   if supply(i,1)==min(supply(i,1:3)); Optisoft(i,2)=1;
   elseif supply(i,2)==min(supply(i,1:3)); Optisoft(i,2)=2;
   else Optisoft(i,2)=3; end

   if supply(i,1)==max(supply(i,1:3)); Optisoft(i,3)=1;
   elseif supply(i,2)==max(supply(i,1:3)); Optisoft(i,3)=2;
   else Optisoft(i,3)=3; end
  end
 end

% CALCULATES CONVERTER CONDUCTION LOSS
 Ioutrms=[(Vin*q)/Z]/sqrt(2);                                  % per output phase
 CondLoss=[(Vce+Vf)*Ioutrms*(2*sqrt(2)/pi)]+[(Rce+Rd)*Ioutrms^2]; % anti-parallel IGBT Conduction loss

% CALCULATES COMMUTATION LOSS FOR THREE SEQUENCES WITH STAGGERED COMMUTATION
for k=1:3;                                                     % Implements all three commutation sequences

 for i=1:SWF;                                                  % Loop through each converter switching cycle
  Tcom=time(i,1);
  for j=1:3;                                                   % Loops through each commutation of each cycle

   if k==1; SwOut=Standard(i,j);                               % Defines Outgoing Switch at Commutation
    SwIn=Standard(i+floor(j/3),mod(j,3)+1);                    % Defines Incoming Switch at Commutation
   elseif k==2; SwOut=Semisym(i,j);                            % Defines Outgoing Switch at Commutation
    SwIn=Semisym(i+floor(j/3),mod(j,3)+1);                     % Defines Incoming Switch at Commutation
   else SwOut=Optisoft(i,j);                                   % Defines Outgoing Switch at Commutation
    SwIn=Optisoft(i+floor(j/3),mod(j,3)+1);                    % Defines Incoming Switch at Commutation
```

```
    end

    Tcom=Tcom+AMods(i,SwOut)/SWF;                % Time of Commutation
    SwVoltOut=Vin*cos(2*Win*pi*Tcom-(2*(SwOut-1)*pi/3)); % Outgoing Switch Voltage at Commutation
    SwVoltIn=Vin*cos(2*Win*pi*Tcom-(2*(SwIn-1)*pi/3)); % Incoming Switch Voltage at Commutation
    Vdif=SwVoltIn-SwVoltOut;                     % Accurate Voltage Change during Commutation
    IoutINST=(Vin*q/Z)*cos((Wout*2*pi*Tcom)-theta);  % Precise load Current at commutation

    if (IoutINST>0);
     if (Vdif>0);
       Eoff=0;                                   % If I>0 & Vdif>0, Outgoing switch is soft-switched
       Eon=abs(IoutINST*Vdif*eon);               % If I>0 & Vdif>0, Incoming switch is Hard-switched
       Erec=abs(IoutINST*Vdif*erec);             % Outgoing Diode Reverse Recovery Loss
     else
       Eoff=abs(IoutINST*Vdif*eoff);             % If I>0 & Vdif<0, Outgoing switch is hard-switched
       Eon=0;                                    % If I>0 & Vdif<0, Incoming switch is soft-switched
       Erec=0;                                   % Incoming Diode Reverse Recovery Loss
     end
    else
     if (Vdif>0);
       Eoff=abs(IoutINST*Vdif*eoff);             % If I<0 & Vdif>0, Outgoing switch is hard-switched
       Eon=0;                                    % If I<0 & Vdif>0, Incoming switch is soft-switched
       Erec=0;                                   % Incoming Diode Reverse Recovery Loss
     else
       Eoff=0;                                   % If I<0 & Vdif<0, Outgoing switch is soft-switched
       Eon=abs(IoutINST*Vdif*eon);               % If I<0 & Vdif<0, Incoming switch is hard-switched
       Erec=abs(IoutINST*Vdif*erec);             % Outgoing Diode Reverse Recovery Loss
     end
    end

    swtloss(1,SwOut+3*(k-1))=swtloss(1,SwOut+3*(k-1))+(Eoff/1e6);% Records outgoing switching loss
    swtloss(1,SwIn+3*(k-1))=swtloss(1,SwIn+3*(k-1))+(Eon/1e6);  % Records incoming switching loss
    CommLoss(1,k)=CommLoss(1,k)+(Eoff+Eon+Erec)/1e6;

   end
  end
end

TotaLoss=CommLoss+CondLoss;
disp('-------------------------');
disp('Commutation Loss (W)');
disp('  Standard  Semi-Sym  OptiSoft');
disp(CommLoss);
disp('Anti-parallel IGBT Conduction Loss (W)');
disp(CondLoss);
disp('Total Loss (W)');
disp('  Standard  Semi-Sym  OptiSoft');
disp(TotaLoss);
disp('-------------------------');
disp('Switch Converter Loss Distribution')
disp('  |____Standard Sequence_____|_____Semi-Sym PWM_____|_____Opti-Soft_____|')
disp('  |SW 1(W)   SW 2(W)   SW 3(W) | SW 1(W)   SW 2(W)   SW 3(W) | SW 1(W)   SW 2(W)   SW 3(W)|');
disp(swtloss);
disp('-------------------------');

beep
```

Model Results

Assuming the following converter parameters:

				Load	
SWF (Hz)	Supply V	F_{in} (Hz)	q	R (Ω)	L (H)
2400	400	50	0.866	2	0.02

IGBT and Diode device data from paper published by Apap et al [112]:

IGBT Characteristics				Diode Characteristics		
V_{ce0}	R_{ce}	e_{on}	e_{off}	V_{f0}	R_d	e_{rec}
1.09	0.00715	$0.333e^{-6}$	$0.255e^{-6}$	0.89	0.00589	$0.166e^{-6}$

The sensitivity of the three commutation sequences to the device loss distribution was examined in Section 7.9.4 [p175] by considering two situations where turn-on loss is greater than turn-off (E_{on}>E_{off}) loss and the opposite case (E_{off}>E_{on}) for various output amplitude and frequency conditions, for the same above parameters:

q=0.866	Converter Loss (W): E_{on} > E_{off}		
F_{out}	Standard	SemiSym	Opti-Soft
1	537.88	495.78	539.39
2	533.60	491.74	535.10
3	526.66	485.20	528.14
4	517.32	476.40	518.77
5	505.92	465.67	507.35
6	492.84	453.36	494.24
7	478.47	439.85	479.83
8	463.18	425.48	464.50
9	447.31	410.59	448.59
10	431.04	395.45	432.40
11	415.00	380.30	416.19
12	399.02	365.33	400.16
13	383.37	350.70	384.48
14	368.18	336.51	369.25
15	353.53	322.83	354.53
16	339.49	309.73	340.47
17	326.07	297.23	327.01
18	313.28	285.34	314.19
19	301.14	274.05	302.02
20	289.62	263.35	290.46

See Figure 157 [p175]

q=0.866	Converter Loss (W): E_{off} > E_{on}		
F_{out}	Standard	SemiSym	Opti-Soft
1	537.82	495.71	539.32
2	533.54	491.68	535.03
3	526.60	485.14	528.08
4	517.27	476.36	518.72
5	505.89	465.64	507.31
6	492.82	453.34	494.21
7	478.47	439.84	479.82
8	463.19	425.49	464.50
9	447.34	410.61	448.61
10	431.08	395.49	432.43
11	415.06	380.35	416.24
12	399.09	365.40	400.23
13	383.46	350.78	384.56
14	368.29	336.61	369.34
15	353.64	322.94	354.64
16	339.62	309.86	340.60
17	326.20	297.37	327.14
18	313.43	285.48	314.34
19	301.30	274.21	302.17
20	289.78	263.52	290.63

See Figure 159 [p176]

F_{out}=10	Converter Loss (W): $E_{on} > E_{off}$		
q	Standard	SemiSym	Opti-Soft
0	0.00	0.00	0.00
0.1	35.59	31.47	35.61
0.2	74.89	66.64	74.96
0.3	117.89	105.53	118.05
0.4	164.59	148.12	164.88
0.5	214.99	194.41	215.45
0.6	269.10	244.41	269.75
0.7	326.91	298.12	327.80
0.8	388.42	355.53	389.58
0.866	431.04	395.45	432.40

See Figure 158 [p175]

F_{out}=10	Converter Loss (W): $E_{off} > E_{on}$		
q	Standard	SemiSym	Opti-Soft
0	0.00	0.00	0.00
0.1	35.59	31.47	35.61
0.2	74.89	66.65	74.96
0.3	117.89	105.53	118.05
0.4	164.60	148.13	164.88
0.5	215.01	194.43	215.46
0.6	269.12	244.44	269.77
0.7	326.94	298.15	327.82
0.8	388.45	355.57	389.61
0.866	431.08	395.49	432.43

See Figure 160 [p176]

As described in Section 7.9.5 [p177], a comparison of the IGBT loss distribution for the Standard sequence, Semi-symmetrical PWM and the proposed 'Opti-Soft' switching strategies, produces the following results:

q=0.866	Switch Loss (W)								
	Standard Sequence			Semi-Sym. PWM			'Opti-Soft'		
F_{out}	SW_1	SW_2	SW_3	SW_1	SW_2	SW_3	SW_1	SW_2	SW_3
1	31.91	32.73	31.80	21.31	21.33	21.35	32.53	32.53	32.53
2	31.74	32.53	31.61	21.19	21.20	21.22	32.34	32.34	32.34
3	31.44	32.22	31.31	20.98	21.00	21.02	32.03	32.03	32.03
4	31.03	31.78	30.89	20.71	20.72	20.74	31.61	31.61	31.61
5	30.51	31.25	30.41	20.35	20.39	20.42	31.07	31.09	31.11
6	29.96	30.64	29.80	19.98	19.99	20.01	30.49	30.49	30.49
7	29.32	29.96	29.15	19.54	19.55	19.57	29.82	29.82	29.82
8	28.63	29.22	28.45	19.07	19.09	19.10	29.11	29.11	29.11
9	27.91	28.45	27.72	18.58	18.59	18.61	28.35	28.35	28.35
10	27.19	27.66	26.83	18.10	18.11	18.04	27.56	27.64	27.53
11	26.41	26.86	26.18	17.55	17.57	17.58	26.79	26.79	26.79
12	25.64	26.05	25.41	17.03	17.05	17.06	26.00	26.00	26.00
13	24.89	25.25	24.64	16.52	16.53	16.54	25.21	25.21	25.21
14	24.14	24.47	23.88	16.01	16.03	16.04	24.44	24.43	24.44
15	23.41	23.69	23.14	15.52	15.53	15.54	23.67	23.67	23.67
16	22.70	22.95	22.42	15.04	15.05	15.06	22.94	22.94	22.94
17	22.01	22.23	21.72	14.57	14.58	14.59	22.23	22.23	22.23
18	21.34	21.53	21.05	14.12	14.13	14.14	21.54	21.54	21.54
19	20.70	20.86	20.40	13.68	13.69	13.70	20.88	20.88	20.88
20	20.07	20.22	19.78	13.26	13.28	13.29	20.20	20.28	20.24

See Figure 161 [p177] See Figure 162 [p178] See Figure 163 [p178]

An investigation of the inverted 'Opti-Soft' commutation sequencer, Section 7.9.6 [p179], compared the converter loss against those of the standard 'Opti-Soft' strategy. The model parameters were as described above and produced the follow results:

q=0.866	Converter Loss (W)		
F_{out}	Standard	Opti-Soft	Inv.Opti-Soft
1	537.88	539.39	539.02
2	533.60	535.10	534.73
3	526.66	528.14	527.78
4	517.32	518.77	518.43
5	505.92	507.35	507.02
6	492.84	494.24	493.93
7	478.47	479.83	479.54
8	463.18	464.50	464.23
9	447.31	448.59	448.34
10	431.04	432.40	432.18
11	415.00	416.19	415.99
12	399.02	400.16	399.99
13	383.37	384.48	384.32
14	368.18	369.25	369.11
15	353.53	354.53	354.41
16	339.49	340.47	340.38
17	326.07	327.01	326.93
18	313.28	314.19	314.13
19	301.14	302.02	301.96
20	289.62	290.46	290.42

See Figure 164 [p179]

F_{out}=10	Converter Loss (W)		
q	Standard	Opti-Soft	Inv.Opti-Soft
0	0.00	0.00	0.00
0.1	35.59	35.61	35.60
0.2	74.89	74.96	74.94
0.3	117.89	118.05	118.02
0.4	164.59	164.88	164.83
0.5	214.99	215.45	215.37
0.6	269.10	269.75	269.65
0.7	326.91	327.80	327.65
0.8	388.42	389.58	389.39
0.866	431.04	432.40	432.18

See Figure 165 [p179]

A15 Diode-Bridge Matrix Converter Numerical Loss Model

A numerical loss model was developed within Matlab Simulink to simulate a snubberless three-phase diode-bridge based matrix converter. This calculates the load current with knowledge of the converter output frequency, load resistance and inductance to determine conduction loss. IGBT switching loss is assumed to vary linearly with the device voltage change during the commutation event. The turn-on and turn-off energy loss is also assumed to vary linearly with the conducted collector current. The model calculates the precise supply voltages and load current at each commutation event so that low converter switching frequencies do not reduce model accuracy due to significant changes in supply voltage during a commutation cycle.

Commutation Loss

With a diode-bridge matrix converter employing break-before-make commutation, there are four diodes in each switch, two conducting at any time instance. Since all commutations are hard switched for a diode bridge converter [93], Table 62 describes the numerical relationship between conducted voltage and current with commutation loss, as implemented in the loss model.

Incoming Voltage	Load Current	Outgoing Switch		Incoming Switch	
		IGBT	Diode	IGBT	Diode
Higher	Positive	$e_{off}\,\Delta V_{ce}\,\Delta I_c$	$2\,e_{rec}\,\Delta V_d\,\Delta I_d$	$e_{on}\,\Delta V_{ce}\,\Delta I_c$	$2\,e_{rec}\,\Delta V_d\,\Delta I_d$
Higher	Negative	$e_{off}\,\Delta V_{ce}\,\Delta I_c$	$2\,e_{rec}\,\Delta V_d\,\Delta I_d$	$e_{on}\,\Delta V_{ce}\,\Delta I_c$	$2\,e_{rec}\,\Delta V_d\,\Delta I_d$
Lower	Positive	$e_{off}\,\Delta V_{ce}\,\Delta I_c$	$2\,e_{rec}\,\Delta V_d\,\Delta I_d$	$e_{on}\,\Delta V_{ce}\,\Delta I_c$	$2\,e_{rec}\,\Delta V_d\,\Delta I_d$
Lower	Negative	$e_{off}\,\Delta V_{ce}\,\Delta I_c$	$2\,e_{rec}\,\Delta V_d\,\Delta I_d$	$e_{on}\,\Delta V_{ce}\,\Delta I_c$	$2\,e_{rec}\,\Delta V_d\,\Delta I_d$

Table 62 - Diode Bridge Commutation Loss Summary

Conduction Loss

The $V_{ce(sat)}$-I_c characteristic of the IGBT were linearised in the form:

$$V_{ce(sat)} = V_{ce0} + r_{ce}\,I_c$$

V_{ce0} = IGBT collector-emitter drop voltage at zero current

r_{ce} = IGBT on-state resistance for the linearised characteristic

The instantaneous conduction loss in an IGBT is therefore:

$$P_{cond,IGBT}(t) = V_{ce0}\,I_c\,(t) + r_{ce}\,I_c^2\,(t)$$

Similarly, the instantaneous diode conduction loss is:

$$P_{cond,Diode}(t) = V_{f0}\,I_c\,(t) + r_d\,I_c^2\,(t)$$

V_{f0} = Diode forward voltage drop at zero current

r_{ce} = Diode on-state resistance for the linearised characteristic

As the sinusoidal load current is always conducted by a series combination of two diodes and an IGBT (diode-bridge bi-directional switch), assuming an output RMS current of magnitude I_o, the mean conduction loss per output phase is:

$$P_{cond,Phase} = (V_{ce0} + 2\,V_{f0})I_o\,[(2\sqrt{2})/\pi] + (r_{ce} + 2\,r_d)I_o^2\,(t)$$

Operation

The model starts by defining the operating conditions of the converter and the IGBT and diode device characteristics, before initialising the required matrices to store model parameters. A loop then calculates the three-phase supply voltages (supply(i,1), supply(i,2) & supply(i,3)) before implementing the advanced Venturini control algorithm to determine the switching periods (AMods(i,1), AMods(i,2) & AMods(i,3)). This is used to determine the output voltage (AVout(i,1)) and current (AIout(i,1)) assuming the standard sequential switching order. The (per-output-phase) conduction loss (Loss(1,1)) is then calculated, as described above.

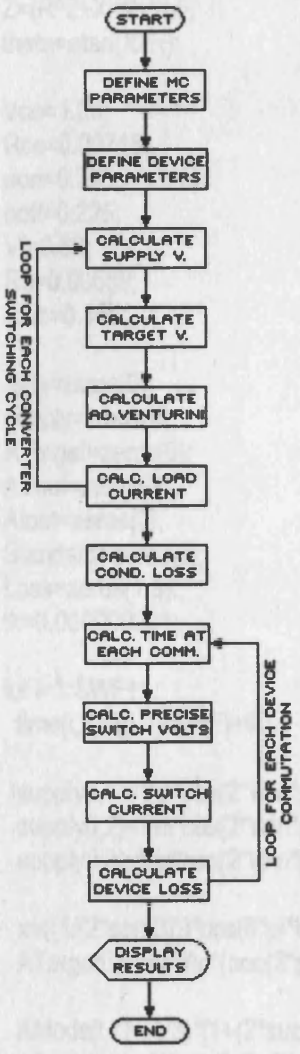

A second loop then iterates through each device commutation of each switching cycle at the instant defined by 'Tcom' that is obtained from the individual switching periods. 'SwOut' and 'SwIn' store the outgoing and incoming switches respectively and therefore 'SwVoltOut' and 'SwVoltIn' hold the respective instantaneous outgoing and incoming switch voltages. These two voltages then provide the voltage change (Vdif) at each commutation. To complete the commutation loss calculation, the instantaneous load current (IoutINST) at time 'Tcom' is found. The outgoing (Eoff) and incoming (Eon) IGBT commutation loss is subsequently calculated with the total diode loss (Erec). At the end of every commutation loop, the switching loss is summed and stored in 'Loss(1,2)'. Once all the commutations have been considered, the total converter loss is stored in 'Loss(1,3)', and the results displayed.

Model Software

The complete Matlab software listing follows overleaf:

```
% Diode Bridge Matrix Converter Loss Model
% Models a three phase input, single phase output converter
% Employs the Advanced Venturini Control algorithm

SWF=1000;                    % Converter Switching Frequency (Hz)
Vin=250;                     % Supply Voltage (P-P)
Win=50;                      % Supply Frequency (Hz)
Wout=10;                     % Output Frequency (Hz)
q=0.866;                     % Converter Voltage Transfer Ratio

R=2;                         % Load Resistance (Ohm)
l=0.02;                      % Load Inductance (Henry)
Xl=2*pi*Wout*l;              % Inductor Impendence
Z=(R^2+Xl^2)^0.5;            % Resultant Resistance
theta=atan(Xl/R);            % Phase angle between load voltage and current

Vce=1.09;                    % IGBT Collector-Emitter Voltage at Zero Current
Rce=0.00715;                 % IGBT Linearised On-state Resistance
eon=0.333;                   % IGBT Turn-on Switching Energy Loss (microJ/VA)
eoff=0.225;                  % IGBT Turn-off Switching Energy Loss (microJ/VA)
Vf=0.89;                     % Diode Forward Voltage Drop at Zero Current
Rd=0.00589;                  % Diode Linearised On-state Resistance
erec=0.166;                  % Diode Recovery Energy Loss (microJ/VA)

time=zeros(0);               % Defines Matrix Array storing switch cycle times
supply=zeros(0);             % Defines Matrix Array storing supply voltages
ATarget=zeros(0);
AVout=zeros(0);
Alout=zeros(0);
Standard=zeros(0);
Loss=zeros(1,3);
tk=0.000000001;

for i=1:SWF+1;
 time(i,1)=((i-1)/SWF)+tk;

 supply(i,1)=Vin*cos(2*Win*pi*time(i,1));
 supply(i,2)=Vin*cos(2*Win*pi*time(i,1)-(2*pi/3));
 supply(i,3)=Vin*cos(2*Win*pi*time(i,1)-(4*pi/3));

 x=((1/(2*sqrt(3)))*cos(6*pi*Win*time(i,1)))-((1/6)*cos(6*pi*Wout*time(i,1)));
 ATarget(i,1)=q*Vin*(cos(2*pi*Wout*time(i,1))+x);

 AMods(i,1)=(1/3)*[1+(2*supply(i,1)*ATarget(i,1))/(Vin^2)];
 AMods(i,1)=AMods(i,1)+[((4*q)/(9*sqrt(3)))*sin(2*pi*Win*time(i,1)-0)*sin(3*2*pi*Win*time(i,1))];
 AMods(i,2)=(1/3)*[1+(2*supply(i,2)*ATarget(i,1))/(Vin^2)];
 AMods(i,2)=AMods(i,2)+[((4*q)/(9*sqrt(3)))*sin(2*pi*Win*time(i,1)-(2*pi/3))*sin(3*2*pi*Win*time(i,1))];
 AMods(i,3)=(1/3)*[1+(2*supply(i,3)*ATarget(i,1))/(Vin^2)];
 AMods(i,3)=AMods(i,3)+[((4*q)/(9*sqrt(3)))*sin(2*pi*Win*time(i,1)-(4*pi/3))*sin(3*2*pi*Win*time(i,1))];

 AVout(i,1)=[supply(i,1)*AMods(i,1)]+[supply(i,2)*AMods(i,2)]+[supply(i,3)*AMods(i,3)];
 Alout(i,1)=(Vin*q/Z)*cos((2*pi*time(i,1)*Wout)-theta);

% DEFINES STANDARD SEQUENTIAL SWITCHING ORDER
 Standard(i,1)=1;
 Standard(i,2)=2;
```

```
 Standard(i,3)=3;
end

% CALCULATES CONVERTER CONDUCTION LOSS
 Ioutrms=[(Vin*q)/Z]/sqrt(2);                    % per output phase
 Loss(1,1)=[(Vce+(2*Vf))*Ioutrms*(2*sqrt(2)/pi)]+[(Rce+(2*Rd))*Ioutrms^2]; % Diode Bridge Conduction loss

% CALCULATES COMMUTATION LOSS FOR DIODE BREAK-BEFORE-MAKE COMMUTATION
 for i=1:SWF;                                    % Loop through each switching cycle
  Tcom=time(i,1);                                % Determines time of each switching cycle
  for j=1:3;                                     % Loop through each commutation
   SwOut=Standard(i,j);                          % Outgoing Switch of each Commutation
   SwIn=Standard(i+floor(j/3),mod(j,3)+1);       % Incoming Switch of each Commutation
   Tcom=Tcom+AMods(i,SwOut)/SWF;                 % Precise time of Commutation

   SwVoltOut=Vin*cos(2*Win*pi*Tcom-(2*(SwOut-1)*pi/3)); % Outgoing Switch Voltage at Commutation
   SwVoltIn=Vin*cos(2*Win*pi*Tcom-(2*(SwIn-1)*pi/3));   % Incoming Switch Voltage at Commutation
   Vdif=SwVoltIn-SwVoltOut;                      % Voltage Change during Commutation
   IoutINST=(Vin*q/Z)*cos((Wout*2*pi*Tcom)-theta); % Load Current at each commutation
                                                 % Assuming break-before-make
   Eoff=abs(IoutINST*Vdif*eoff);                 % Outgoing Commutation Loss
   Eon=abs(IoutINST*Vdif*eon);                   % Incoming Commutation Loss
   Erec=4*abs(IoutINST*abs(SwVoltOut)*erec);     % Diode Loss, all are reverse-biased
   Loss(1,2)=Loss(1,2)+(Eoff+Eon+Erec)/1e6;      % Calculates total loss for each commutation
  end
 end

Loss(1,3)=Loss(1,1)+Loss(1,2);                   % Determines total converter output loss

disp('-----------------------------------');
disp(Diode-Bridge IGBT Matrix Converter Output Phase Loss');
disp('  Cond(W)    Comm(W)  Total(W)');
disp(Loss)
disp('-----------------------------------');

beep
```

A16 Comparative Matrix Converter Loss Model Data

The loss comparison of a number of matrix converter configurations and combinations of operating strategies was calculated and shown in Figure 130 [p139]. The data was calculated using the detailed loss models created within Matlab, described in the following appendices:

Appendix A14 Anti-Parallel IGBT Matrix Converter Numerical Loss Model [p277]
Appendix A15 Diode-Bridge Matrix Converter Numerical Loss Model [p286]

The loss models employed the following parameters:

Supply Frequency = 50Hz
Supply Voltage = 250V
Output Frequency = 10Hz
Output Amplitude = 0.866
Load: R= 2Ω & L=0.02H

The above models provided the data shown in Table 63, with the data shown in *italics* calculated using the relationships discussed in Section 2.4.3 [p46] (Four step staggered commutation that halves switching loss) and Section 6.7 [p145] (Semi-symmetrical PWM that reduces commutation loss by a third). The above assumptions are considered accurate as the loss model data shows that four-step staggered commutation with semi-symmetrical PWM incurs a third less loss than the four-step staggered strategy alone, agreeing with work published by Wheeler et al [93].

	Diode Bridge	Anti-parallel IGBT			
SWF	Break-Before-Make	Break-Before-Make	Four Step Staggered	SemiSym PWM	Four Step + SemiSym PWM
0	246.99	170.31	170.31	170.31	170.31
1000	291.32	204.32	187.31	192.98	181.53
2000	336.78	239.22	204.76	216.25	193.17
3000	382.15	274.09	222.20	239.50	204.84
4000	427.65	309.08	239.70	262.82	216.45
5000	473.09	344.02	257.17	286.12	228.10
6000	518.48	378.93	274.62	309.39	239.74
7000	563.95	413.89	292.10	332.70	251.39
8000	609.38	448.83	309.57	355.99	263.04

Table 63 - Simulated Loss (W) Model Data from Figure 130

A17 Standard Strategy Supply Current Spectral Waveforms

Venturini	SWF	F_{out}	q	Load
Advanced	4 kHz	10 Hz	0.60	Induction Motor

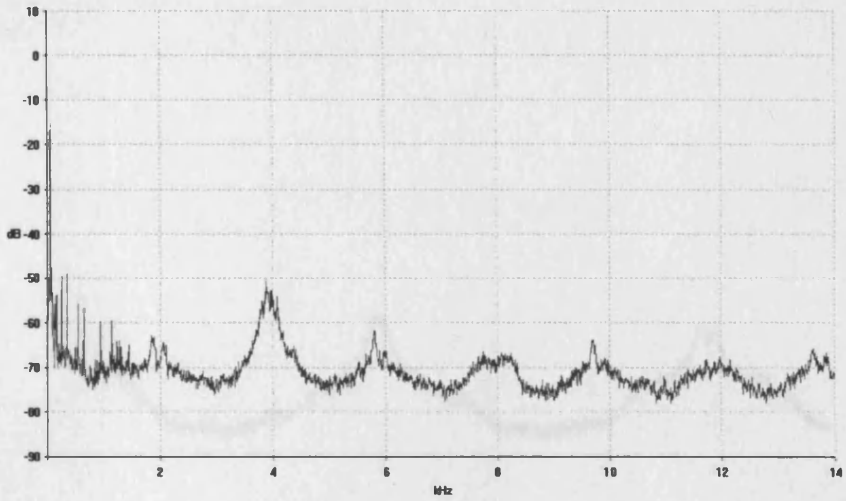

Figure 224 - 'Red' Supply Current Spectrum

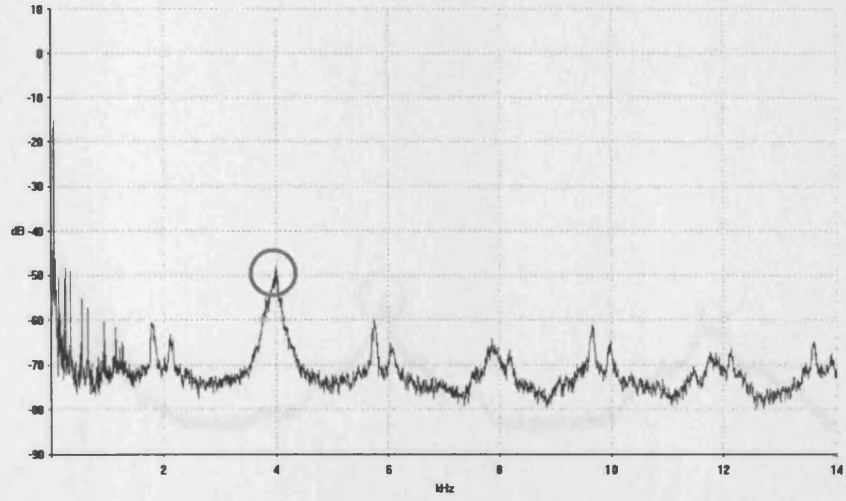

Figure 225 - 'Yellow' Supply Current Spectrum

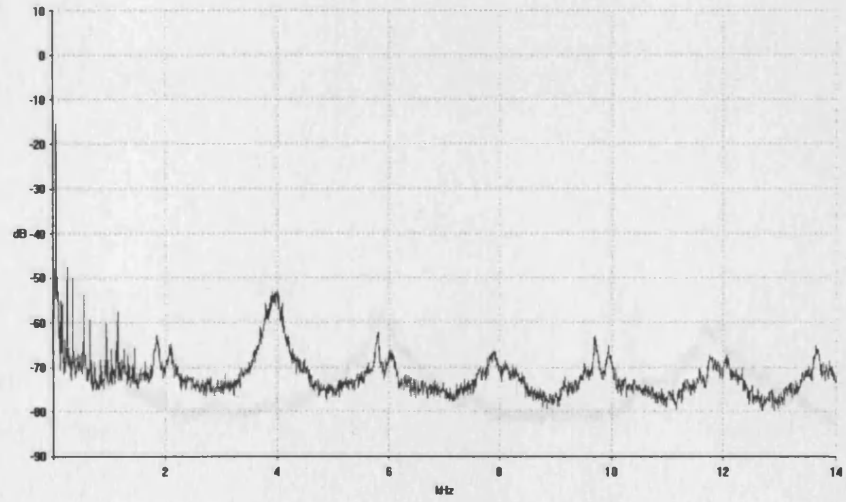

Figure 226 - 'Blue' Supply Current Spectrum

6kHz Supply Current Spectral Analysis:

Venturini	SWF	F_{out}	q	Load
Advanced	6 kHz	10 Hz	0.60	Induction Motor

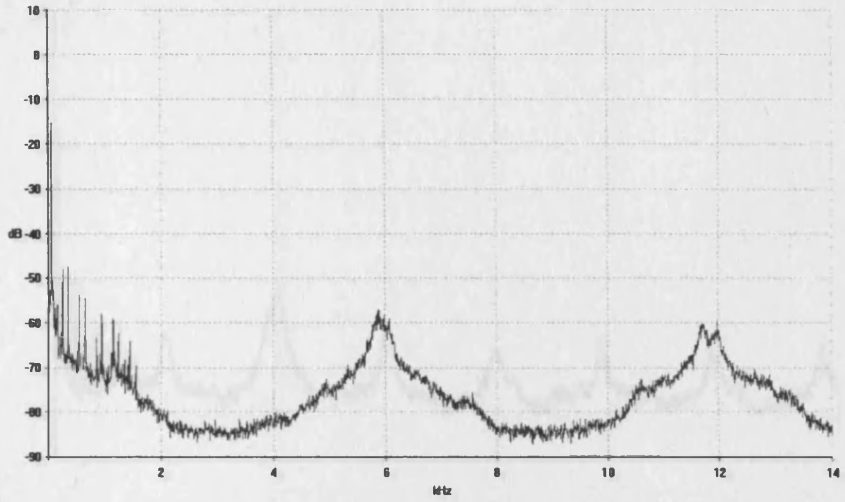

Figure 227 - 'Red' Supply Current Spectrum

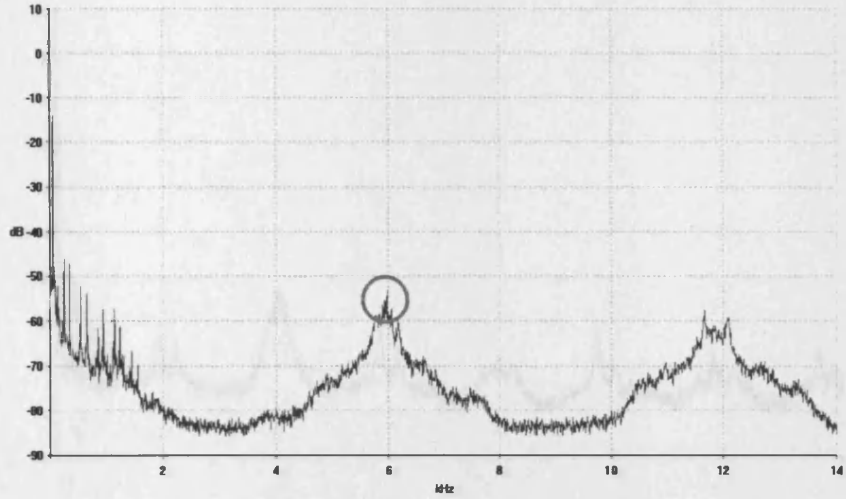

Figure 228 - 'Yellow' Supply Current Spectrum

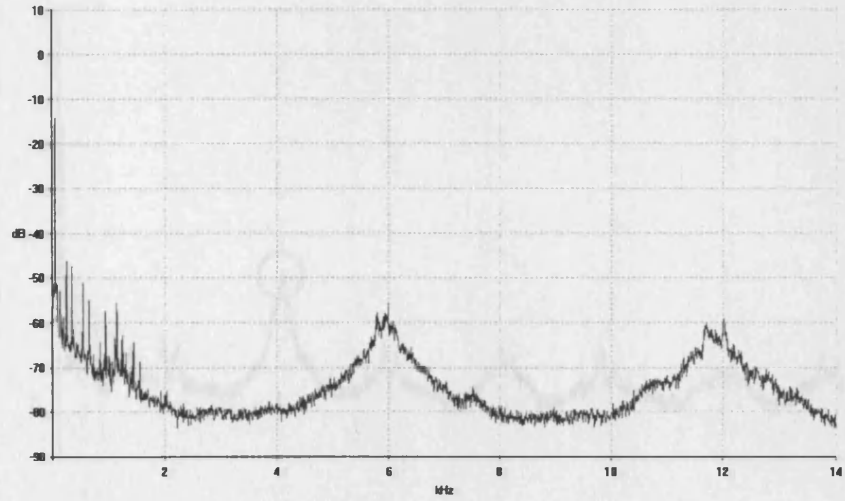

Figure 229 - 'Blue' Supply Current Spectrum

A18 Supply Current Spectral Waveforms: 2 - 3 - 1 Order

Venturini	SWF	F_{out}	q	Load
Advanced	4 kHz	10 Hz	0.60	Induction Motor

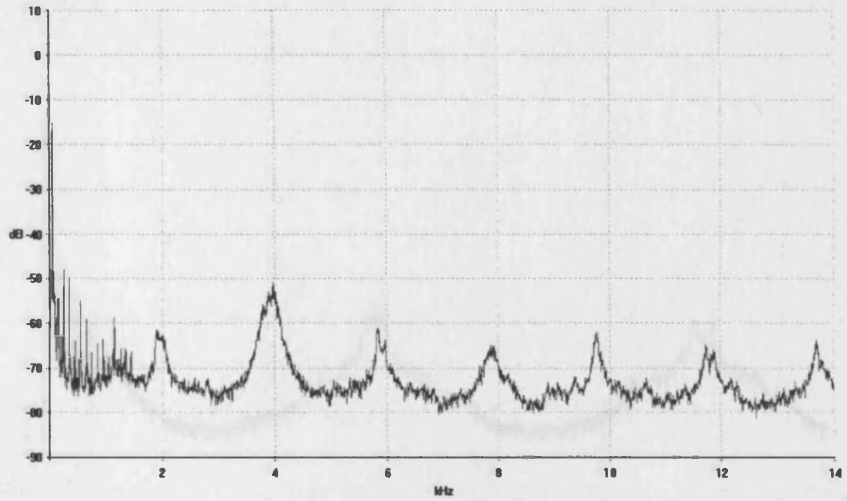

Figure 230 - 'Red' Supply Current Spectrum: 2 - 3 - 1 Order

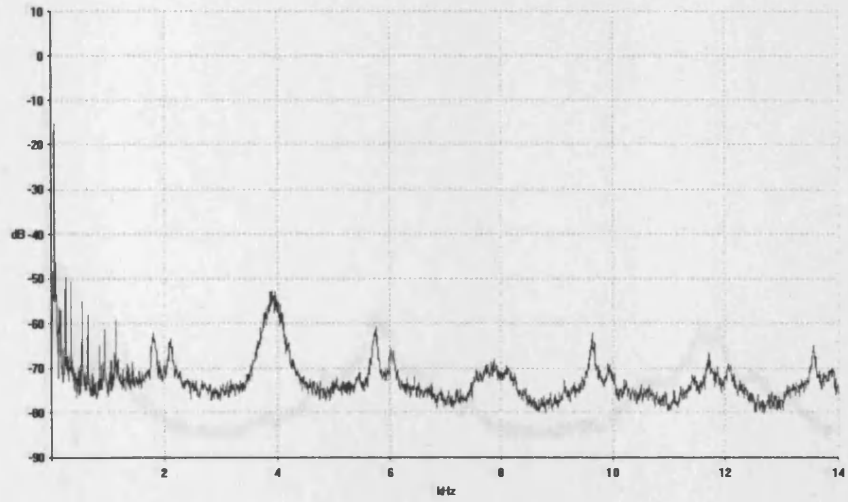

Figure 231 - 'Yellow' Supply Current Spectrum: 2 - 3 - 1 Order

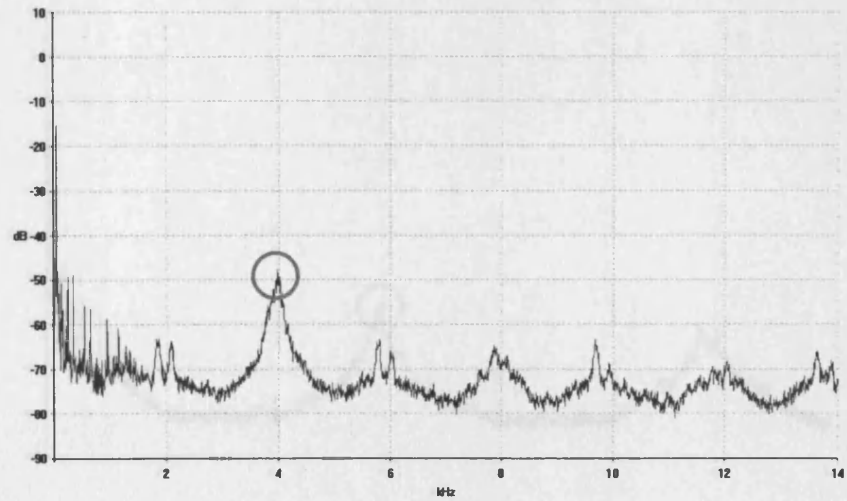

Figure 232 - 'Blue' Supply Current Spectrum: 2 - 3 - 1 Order

6kHz Supply Current Spectral Waveforms: 2 - 3 - 1 Order

Venturini	SWF	F_{out}	q	Load
Advanced	6 kHz	10 Hz	0.60	Induction Motor

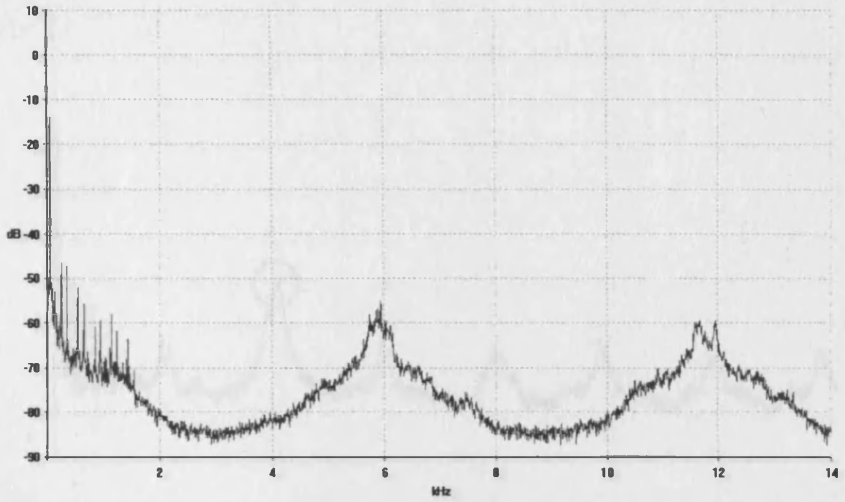

Figure 233 - 'Red' Supply Current Spectrum: 2 - 3 - 1 Order

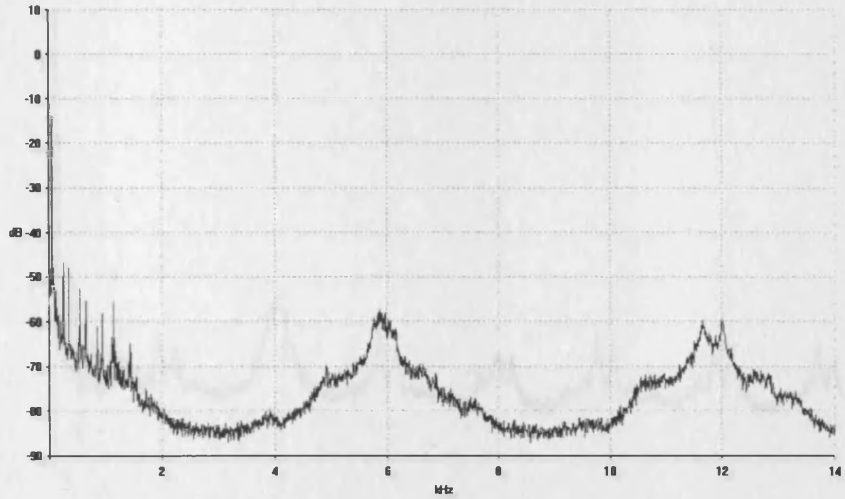

Figure 234 - 'Yellow' Supply Current Spectrum: 2 - 3 - 1 Order

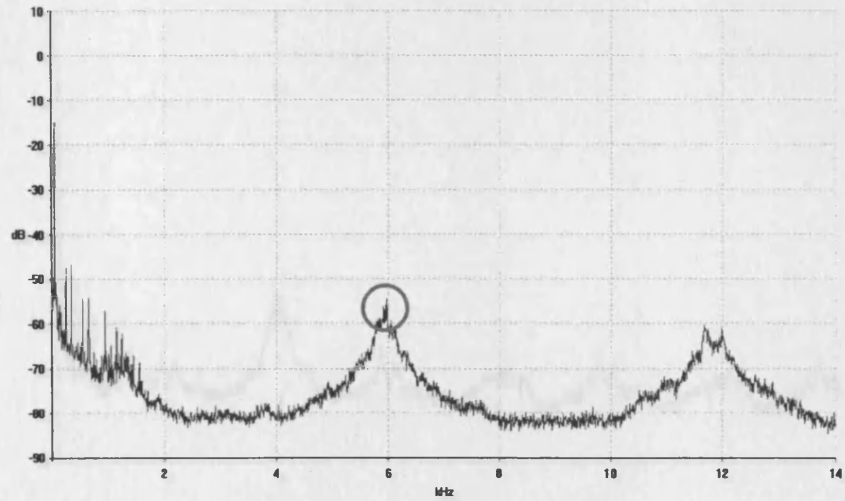

Figure 235 - 'Blue' Supply Current Spectrum: 2 - 3 - 1 Order

A19 Supply Current Spectral Waveforms: 3 - 1 - 2 Order

Venturini	SWF	F_{out}	q	Load
Advanced	4 kHz	10 Hz	0.60	Induction Motor

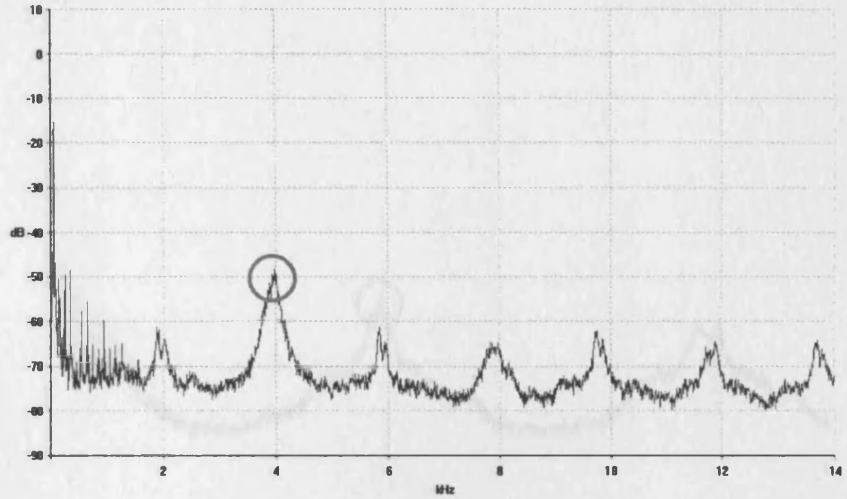

Figure 236 - 'Red' Supply Current Spectrum: 3 - 1 - 2 Order

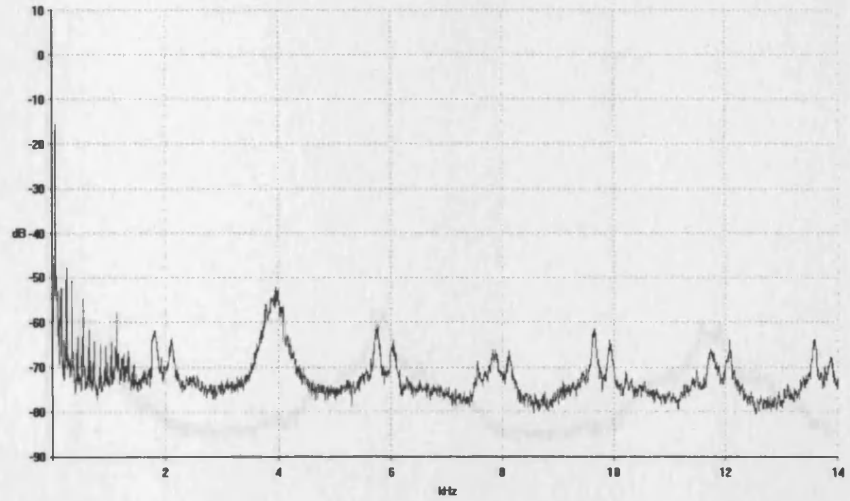

Figure 237 - 'Yellow' Supply Current Spectrum: 3 - 1 - 2 Order

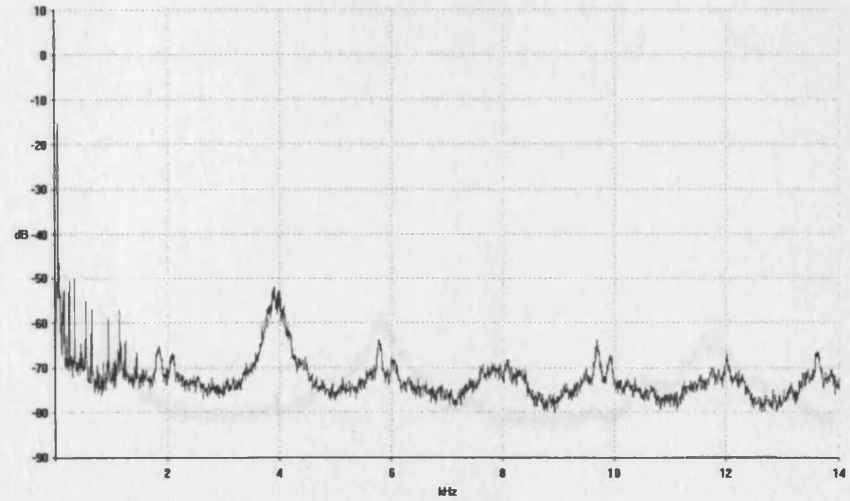

Figure 238 - 'Blue' Supply Current Spectrum: 3 - 1 - 2 Order

6kHz Supply Current Spectral Waveforms: 3 - 1 - 2 Order

Venturini	SWF	F_{out}	q	Load
Advanced	6 kHz	10 Hz	0.60	Induction Motor

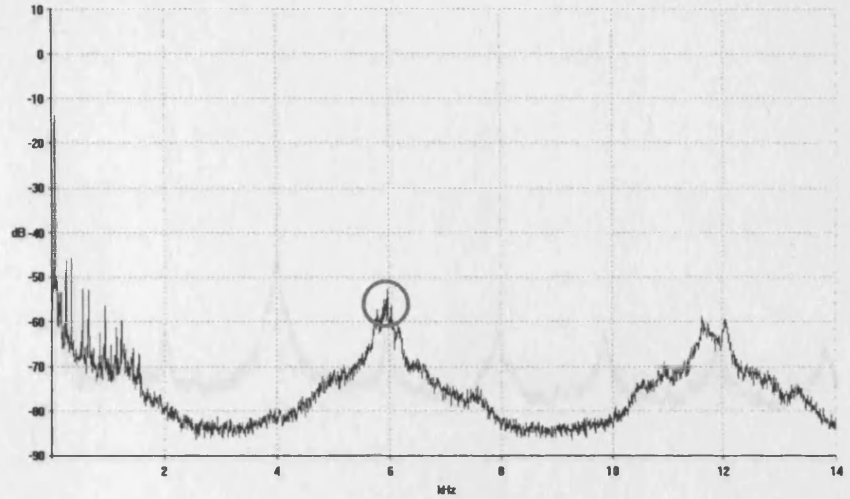

Figure 239 - 'Red' Supply Current Spectrum: 3 - 1 - 2 Order

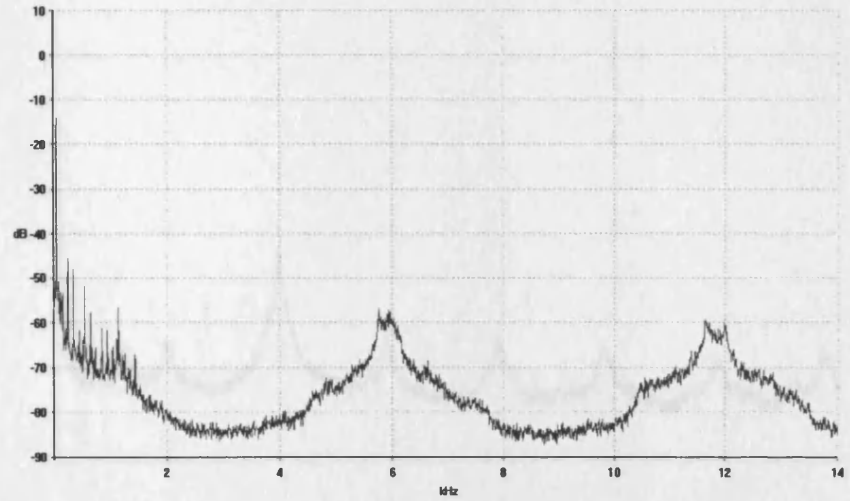

Figure 240 - 'Yellow' Supply Current Spectrum: 3 - 1 - 2 Order

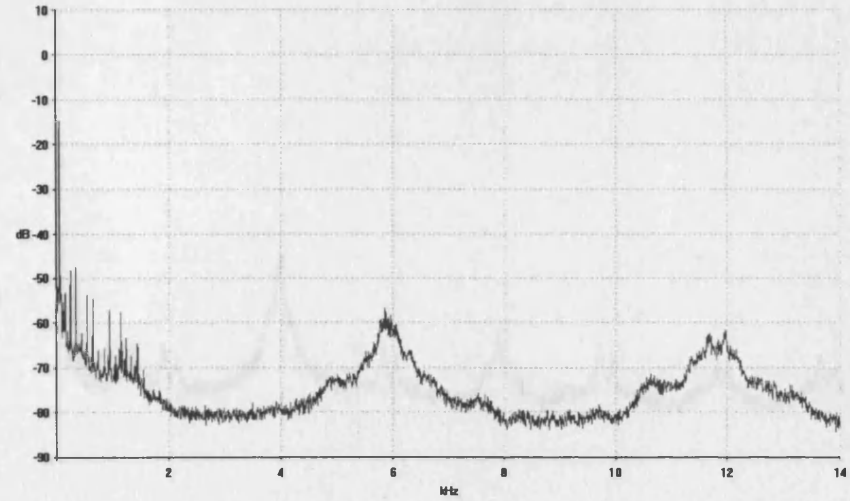

Figure 241 - 'Blue' Supply Current Spectrum: 3 - 1 - 2 Order

A26 Four-Step Staggered Commutation Test Circuit Simulation

A computer model of a pair of anti-parallel bi-directional switches with associated control systems that implement the four-step staggered commutation sequence for safer current commutation was developed. The switches are combined to allow testing and analysis of the behaviour and conditions required for soft commutations when employing staggered commutation. Figure 278 shows the generalised model.

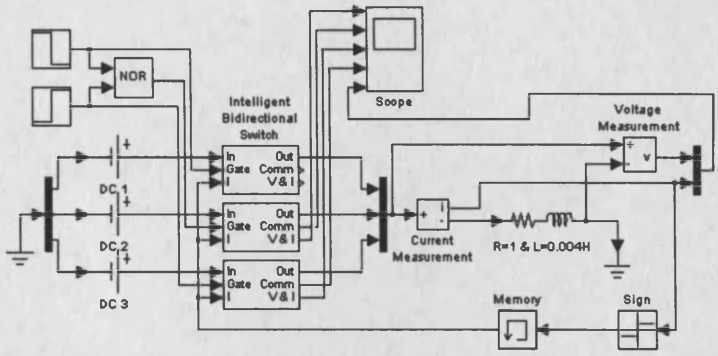

Figure 278 - Generalised Commutation Test Circuit Computer Model

DC voltage sources provide power to the circuit with commutation between alternative voltage levels possible by changing the supply voltages. Control signals are produced by the step blocks (top left), a NOR block ensure only one switch is gated at a time. Figure 279 shows the layout of each bi-directional switch module, including the gate control logic used to manage the staggered commutation strategy.

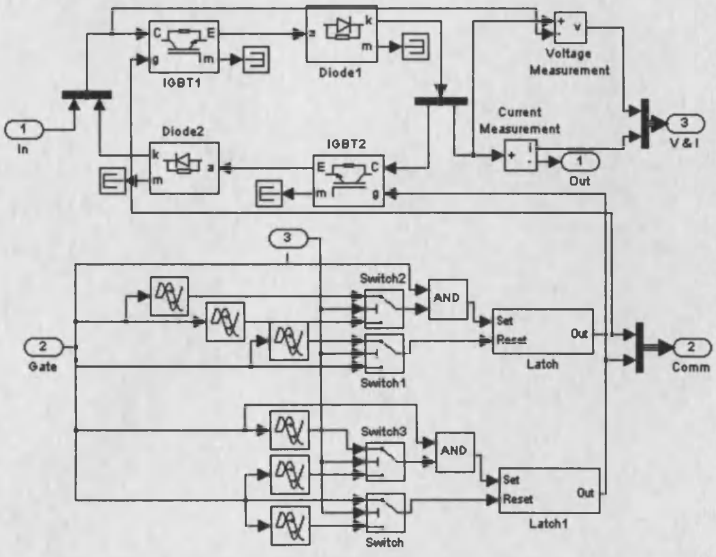

IGBT Parameters
On Resistance = 0.01Ω
On Inductance = 1μH
Forward Voltage = 1V
Current 10% Fall time = 1μs
Current Tail Time = 2μs
Snubber Resistance = 10Ω
Snubber Capacitance = 0.01μF

Diode Parameters
On Resistance = 0.01Ω
On Inductance = 1μH
Forward Voltage = 0.8V
Snubber Resistance = 10Ω
Snubber Capacitance = 0.01μF

Figure 279 - Anti-Parallel Switch Computer Model Subsystem & Model Parameters

In the on state, the IGBT model has a resistance of 0.01Ω, an inductance of 1μH and a forward voltage drop of 1 volt. The IGBT turn off characteristic is approximated by two segments. When the gate signal stops, the collector current falls from Imax to 0.1 Imax during the fall time (Tf = 1μs), and then from 0.1 Imax to 0 during the tail time (Tt = 2μs). An RC Snubber is included across each IGBT and diode.

A27 Single-Phase Output Model with 'Opti-Soft' Commutation

The matrix converter computer model was updated to include the anti-parallel IGBT bi-directional switches, as described in Appendix A26 [p309] to allow natural current commutation and implementation of the 'Opti-Soft' switch sequencing strategy. The standard Venturini control strategy was implemented, albeit in the voltage tracking guise described in Section 2.9.1 [p64] for simplicity. The control system monitored the output supply current to reorder the switching sequence to maximise soft commutation between switches by employing 'Opti-Soft'.

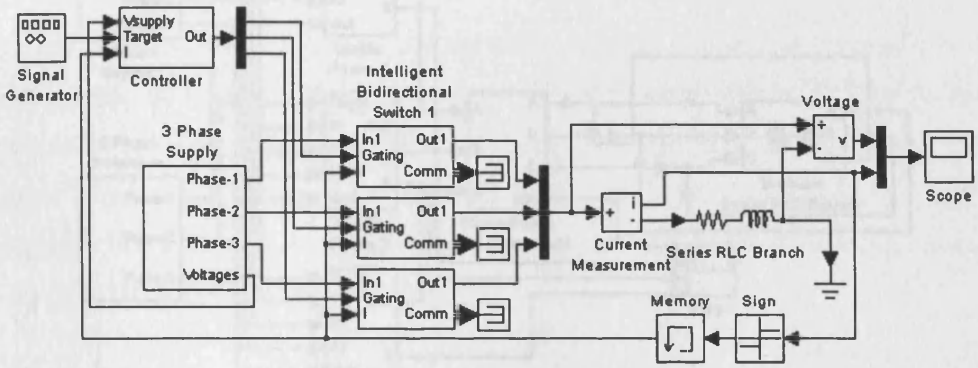

Figure 280 - Single-Phase Output Matrix Converter Model Implementing 'Opti-Soft'

The computer model was operated with a variable ODE solver as recommended by Matlab when implementing models containing elements from the PowerSystem Blockset. The variable step solver, as opposed to a fixed step solver, reduced model execution times while maintaining detail at key points of the simulation. The initial model produced the simulated output currents shown in Figure 145 [p162] and Figure 146 [p162] that contained a disturbance when crossing the zero current threshold. This was traced and the modified 'Opti-Soft' eliminated the disturbance to produce the output currents shown in Figure 148 [p164] and Figure 149 [p164].

A29 Marine Matrix Converter Topology Selection Spreadsheet

A computer spreadsheet was developed to allow comparison between the six marine matrix converter topologies proposed in Section 8.4 [p187]. This considers the differing supply and output phase configurations and the implication of each design when providing the same 20MW power output. Increasing the number of input phases has the benefit of improving supply utilisation, as discussed in Section 2.6 [p51], however, this increases both the number of semiconductor devices necessary and the number of transformers to provide the additional input phases.

Using data from the ABB PP-IGBT datasheets, the spreadsheet estimates the weight and volume of the semiconductor devices required by each topology. The datasheets also provide linearised data for the IGBT & diode forwards voltage drop characteristics. Converter Topologies 1, 2 & 4 employ ABB 20H2500 (2.5kV 2kA) PP-IGBTs, Topologies 3 & 5 use ABB 13H2500 (2.5kV 1.3kA) PP-IGBTs and Topology 6 employs the ABB 10H2500 (2.5kV, 1kA) PP-IGBT.

The mean conduction loss per output phase is calculated with linearised IGBT device loss parameters using the approach widely published [114] and employed by the developed computer loss models, see Section 7.9.3 [p174] :

$$P_{cond,phase} = (V_{ce0} + V_{f0})I_o[(2\sqrt{2})/\pi] + (r_{ce} + r_d)I_o^2(t)$$

V_{ce0} = IGBT collector-emitter drop voltage at zero current
r_{ce} = IGBT on-state resistance for the linearised characteristic
V_{f0} = Diode forward voltage drop at zero current
r_{ce} = Diode on-state resistance for the linearised characteristic

The sinusoidal load current is conducted by a series combination of a diode and IGBT (assuming anti-parallel IGBT bi-directional switches), with an output RMS current of magnitude I_o. This calculates the mean conduction loss per output phase.

The peak load current per phase is calculated using the method described in Section 8.6.5 [p197]:

$$V_{PK} = \frac{\sqrt{2} \times V_{LINE} \times 2}{\sqrt{3}} \quad \& \quad I_{PK}(\text{per phase}) = \sqrt{2} \times \frac{\text{PowerPerPhase}}{V_{pH} \times VTR \times PF}$$

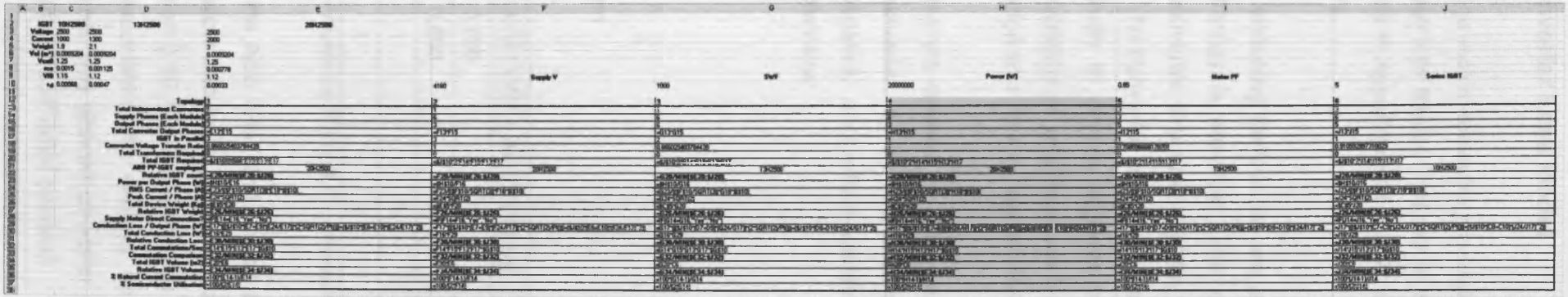

Figure 283 - Marine Matrix Converter Topology Spreadsheet Formula

A30 Marine Matrix Converter Loss Model

The losses in a 20MW marine matrix converter propulsion system were modelled using the following Matlab computer loss model. This model is a development of the previous three-phase model described in Appendix A14 [p277], allowing analysis of any number of supply and output phases.

To achieve representative switching periods for any sized converter configuration, a more simplified control strategy is assumed. The original Venturini strategy was modified for fully variable converter structures, but the limitation of this strategy is the reduced output amplitude. The converter output current was therefore modelled at the maximum allowable amplitude to enable accurate approximation of the converter structure. The approach is considered valid because for equal output amplitudes, there is no difference in commutation loss for the original and advanced Venturini strategies.

The motor R and L parameters depend on the number of motor phases and the voltage provided by the converter. As these values vary significantly for the matrix converter topologies investigated, appropriate values for R and L were calculated assuming the follow characteristics:

- 20MW induction Motor
- 6 pairs of poles
- 0.85 Power Factor
- 180 rpm maximum speed

Converter Type	Converter VTR	Motor Phases	Motor R (Ω)	Motor L (H)
3 X [3inX5out]	0.788	15	5.823	0.0319
[6inX6out]	0.866	6	2.813	0.0154
2 X [6inX3out]	1	6	3.751	0.0206
3 X [6inX3out]	1	9	5.627	0.0308

Calculated Propulsion Motor R & L Characteristics for Model

Device characteristics for the ABB IGBT and Diodes modules were derived from the respective datasheets, to allow calculation of conduction and commutation loss across the power range, see Section 8.10.1 [p209] & Section 8.10.2 [p210]. The model does not consider the losses associated with snubber devices as the selected devices enable snubberless operation. This allowed converter efficiency and power loss to be calculated, using the computer model listed overleaf: